

1. Report No. FHWA/TX-95-1243-5F	2. Government Accession No.	3. Recipient's Catalog No.	
4. Title and Subtitle EVALUATION OF STRESS-WAVE METHODS FOR IMPLEMENTATION INTO A ROLLING SYSTEM TO DETECT PAVEMENT IRREGULARITIES		5. Report Date April 1995	6. Performing Organization Code
7. Author(s) Brent L. Rosenblad, Kenneth H. Stokoe, II, and J. M. Roesset		8. Performing Organization Report No. Research Report 1243-5F	
9. Performing Organization Name and Address Center for Transportation Research The University of Texas at Austin 3208 Red River, Suite 200 Austin, Texas 78712-1075		10. Work Unit No. (TRIS)	11. Contract or Grant No. Research Study 0-1243
12. Sponsoring Agency Name and Address Texas Department of Transportation Research and Technology Transfer Office P.O. Box 5080 Austin, Texas 78763-5080		13. Type of Report and Period Covered Final	
15. Supplementary Notes Study conducted in cooperation with the U.S. Department of Transportation, Federal Highway Administration. Research study title: "Automated Equipment for Characterizing the Properties and Thicknesses of Pavements"		14. Sponsoring Agency Code	
16. Abstract <p>Experimental testing was performed to study the feasibility of implementing two stress-wave techniques, the impact-echo and impulse-response methods, into a rolling system for "on-the-fly" detection of subsurface flaws in rigid concrete pavements. These studies have concentrated on flaws such as delaminations within the rigid surface layer, and on voids and debondings directly under the rigid surface layer. Results from previous finite element studies are presented to demonstrate the effects of parameters associated with the flaw (such as size and depth) and the pavement system (such as surface layer thickness and surface-base impedance contrast). Experimental tests were performed under controlled conditions at three test sites, including two full-scale test pavement facilities. Identical locations were tested using the impact-echo and impulse-response techniques so that the applicability of each technique for detection of various flaw conditions could be directly compared. Successful application of these techniques to detecting voids and debondings is presented.</p> <p>Lastly, experimental studies were performed to evaluate the feasibility of receiving the frequencies of interest for the impact-echo and impulse-response methods with a wheel-mounted receiver. These results, along with the experimental field results and numerical modeling results, are used to illustrate the advantages and limitations of each nondestructive testing technique for implementation into a rolling system for project-level studies.</p>			
17. Key Words Rigid pavements, nondestructive pavement testing, pavement monitoring, pavement irregularities, delamination, debonding, voids, stress wave testing, impact-echo test, impulse-response test		18. Distribution Statement No restrictions. This document is available to the public through the National Technical Information Service, Springfield, Virginia 22161.	
19. Security Classif. (of this report) Unclassified	20. Security Classif. (of this page) Unclassified	21. No. of Pages 188	22. Price

**EVALUATION OF STRESS-WAVE METHODS FOR IMPLEMENTATION
INTO A ROLLING SYSTEM TO DETECT PAVEMENT IRREGULARITIES**

Brent L. Rosenblad
Kenneth H. Stokoe, II
and
Jose M. Roesset

Research Report 1243-5F

Research Project 0-1243
Automated Equipment of Characterizing the Properties
and Thicknesses of Pavements

conducted for the

Texas Department of Transportation
in cooperation with the
U.S. Department of Transportation
Federal Highway Administration

by the

CENTER FOR TRANSPORTATION RESEARCH
Bureau of Engineering Research
THE UNIVERSITY OF TEXAS AT AUSTIN

April 1995

IMPLEMENTATION STATEMENT

The results from the experimental studies conducted for this project have demonstrated the problems associated with implementing stress-wave based methods into a rolling system for "on-the-fly" pavement evaluation. The results have demonstrated the necessity of generating and receiving a broad range of frequencies for effective pavement evaluation. Experimental testing of wheel-mounted receivers has been unsuccessful as a means of receiving the necessary high-frequency energy (1 to 20 kHz) employed in impact-echo testing. Lower frequency energy (10 to 1000 Hz), which is employed in impulse-response testing, was successfully received through a wheel-mounted receiver. The site-specific experimental impact-echo and impulse-response tests that were performed provide valuable information concerning the pavement defects that can be detected with each method, as well as the proper testing methodology for effective pavement evaluation with these methods.

Prepared in cooperation with the Texas Department of Transportation and the U.S. Department of Transportation, Federal Highway Administration.

DISCLAIMERS

The contents of this report reflect the views of the authors, who are responsible for the facts and the accuracy of the data presented herein. The contents do not necessarily reflect the official views or policies of the Federal Highway Administration or the Texas Department of Transportation. This report does not constitute a standard, specification, or regulation.

There was an invention conceived and first actually reduced to practice in the course of this contract, namely, the Rolling Dynamic Deflectometer. This device may be patentable under the patent laws of the United States of America or any foreign country.

NOT INTENDED FOR CONSTRUCTION, BIDDING, OR PERMIT PURPOSES

Kenneth H. Stokoe, P.E. (Texas No. 49095)
Research Supervisor

TABLE OF CONTENTS

IMPLEMENTATION STATEMENT.....	iii
SUMMARY	ix
CHAPTER 1. INTRODUCTION	1
BACKGROUND.....	1
NONDESTRUCTIVE TESTING OF PAVEMENTS	1
PURPOSE OF STUDY	2
ORGANIZATION OF THE REPORT	3
CHAPTER 2. METHODS OF FLAW DETECTION IN CONCRETE SLABS	4
INTRODUCTION.....	4
NON-SEISMIC METHODS OF FLAW DETECTION.....	6
Visual Surveys	6
Ground Penetrating Radar	6
Infrared Thermography	8
Half-Cell Potential	12
DEFLECTION BASED METHODS OF FLAW DETECTION.....	15
Static Deflection Methods.....	15
Dynamic Deflection Methods.....	15
STRESS-WAVE METHODS OF FLAW METHODS.....	21
Manual Sounding Method.....	21
Automated Sounding Device.....	22
Pulse-Echo Ultrasonic Testing	22
Impact-Echo Testing	25
Impulse-Response Testing	26
Spectral-Analysis-of-Surface-Waves (SASW) Method.....	27
SUMMARY	27
CHAPTER 3 METHODOLOGY, EQUIPMENT, AND FACILITIES USED IN IMPACT-ECHO TESTING.....	28
INTRODUCTION.....	28
DESCRIPTION OF IMPACT-ECHO METHOD.....	28
IMPACT-ECHO TESTING METHODOLOGY.....	32
Testing Procedure and Equipment.....	32
Data Reduction Procedures.....	34
Time Records	34
Power Spectrum.....	34
Cross Spectrum.....	36

Frequency Response.....	36
Coherence.....	38
TESTING SITE DESCRIPTIONS.....	38
Site 1: Test Slab in Ernest Cockrell Jr. Hall.....	38
Site 2: Center for Transportation Research (CTR) Test Pavement.....	41
Site 3: Texas Transportation Institute (TTI) Test Pavement	41
SUMMARY	45

CHAPTER 4. ANALYTICAL AND EXPERIMENTAL RESULTS FROM IMPACT-ECHO TESTING.....	46
INTRODUCTION.....	46
EFFECTS OF PHYSICAL CHARACTERISTICS OF PAVEMENT STRUCTURE	46
Effect of Void Size.....	46
Effect of Acoustic Impedance Ratio.....	50
Effect of Size-to-Depth Ratio of the Void	53
Effect of Pavement Debonding	60
EFFECT OF VARIATIONS IN TESTING METHODOLOGY.....	60
Effects of Impact Mechanism and Impact Duration.....	60
Effects of Single versus Multiple Averages of Records.....	66
SUMMARY	72

CHAPTER 5. EXPERIMENTAL FIELD TESTING AND ANALYTICAL RESULTS FROM IMPULSE-RESPONSE METHOD.....	76
INTRODUCTION.....	76
DESCRIPTION OF THE IMPULSE-RESPONSE METHOD	76
IMPULSE-RESPONSE TESTING METHODOLOGY.....	78
Testing Procedure and Equipment.....	78
Data Reduction Procedures.....	80
Dynamic Slab Stiffness.....	80
Average Mobility.....	80
NUMERICAL MODEL RESULTS FOR IMPULSE-RESPONSE TESTING.....	80
Effect of Void Size.....	84
Effect of Void Depth.....	84
EXPERIMENTAL RESULTS FROM IMPULSE-RESPONSE TESTS AT SITE 2	87
Pavement with a Void versus Sound Pavement.....	87
Debonded Pavement versus Sound Pavement	94
EXPERIMENTAL RESULTS FROM IMPULSE-RESPONSE TESTS AT SITE 3.....	101
Test Results from 17.8-cm Thick Slab at Site 3	101
Test Results from 30.5-cm Thick Slab at Site 3	106
HIGHER FREQUENCY FLEXURAL RESPONSE.....	111

SUMMARY	118
CHAPTER 6. RECEPTION OF HIGH-FREQUENCY ENERGY WITH A MOBILE RECEIVER	120
INTRODUCTION	120
ENERGY RECEPTION USING WHEEL MOUNTED RECEIVERS	123
Testing Arrangement and Procedures.....	123
Energy Reception using a Steel Wheel.....	125
Effect of Wheel Type on Energy Transmission.....	128
Test on Aluminum Wheels	141
Effect of Wheel Size and Shape	141
Effect of Tread Material on Energy Reception	146
SUMMARY OF RESULTS FROM WHEEL MOUNTED RECEIVER TESTS	151
ENERGY RECEPTION WITH PIEZOELECTRIC CERAMIC MATERIALS.....	152
Frequency Response of Piezoelectric Ceramic Materials.....	152
SUMMARY	156
CHAPTER 7. RECEPTION OF LOW-FREQUENCY ENERGY WITH A MOBILE RECEIVER	157
INTRODUCTION	157
LOW-FREQUENCY ENERGY RECEPTION USING WHEEL MOUNTED RECEIVERS	157
Testing Arrangements and Procedures.....	157
Wheel Mounted Receiver Tests.....	159
Results from Tests on Wheels of Different Sizes.....	159
Discussion of Results.....	162
Effect of Wheel Mass and Tread Material	162
SUMMARY	170
CHAPTER 8. SUMMARY, CONCLUSIONS, AND RECOMMENDATIONS.....	171
SUMMARY	171
CONCLUSIONS.....	172
RECOMMENDATIONS.....	173
REFERENCES	175

SUMMARY

Experimental testing was performed to study the feasibility of implementing two stress-wave techniques, the impact-echo and impulse-response methods, into a rolling system for “on-the-fly” detection of subsurface flaws in rigid concrete pavements. These studies have concentrated on flaws such as delaminations within the rigid surface layer, and on voids and debondings directly under the rigid surface layer. Results from previous finite element studies are presented to demonstrate the effects of parameters associated with the flaw (such as size and depth) and the pavement system (such as surface layer thickness and surface-base impedance contrast). Experimental tests were performed under controlled conditions at three test sites, including two full-scale test pavement facilities. Identical locations were tested using the impact-echo and impulse-response techniques so that the applicability of each technique for detection of various flaw conditions could be directly compared. Successful application of these techniques to detecting voids and debondings is presented.

Lastly, experimental studies were performed to evaluate the feasibility of receiving the frequencies of interest for the impact-echo and impulse-response methods with a wheel-mounted receiver. These results, along with the experimental field results and numerical modeling results, are used to illustrate the advantages and limitations of each nondestructive testing technique for implementation into a rolling system for project-level studies.

CHAPTER 1.

INTRODUCTION

1.1 BACKGROUND

The development of irregularities in pavements greatly accelerates the deterioration of a pavement system. Often these pavement anomalies have their origin below the surface and are, therefore, not detectable from visual inspection. When these subsurface flaws do become apparent on the surface, the pavement may already be seriously degraded. Two of the most common and damaging subsurface irregularities in pavements are voids and delaminations.

Delaminations typically develop around the reinforcing steel in rigid pavements. The development of delaminations is initiated by the corrosion of the reinforcing steel in the pavement. The volumetric expansion of the corrosion product creates stresses in the pavement that result in horizontally oriented fracture planes within the concrete surface layer. Vertically oriented cracks may develop and propagate towards the surface of the pavement. Under traffic loading, these cracks may create surface spalling of the concrete, commonly termed "potholes". Unchecked, delamination formation can create large areas of deteriorated pavement resulting in expensive repairs.

Unlike delaminations, voids are anomalies that develop below the pavement surface layer. Typically, they occur at joint edges or at pavement corners. Some typical causes of void formation include pumping of subgrade material from under the pavement, the shrinkage of subsurface material, or the decomposition of organic material beneath the pavement. The loss of support due to void formation under the pavement causes increases in stresses within the pavement which leads to decreased life of the pavement. Under repeated traffic loading, the pavement will eventually crack and fail. Voids are easily repaired at early stages of development, but are very costly to repair at later stages of development.

1.2 NONDESTRUCTIVE TESTING OF PAVEMENTS

A variety of nondestructive testing methods have been applied to the problem of detecting subsurface flaws in pavements. These nondestructive methods are based on the ability to detect the deviation of some property of the pavement in order to locate an anomaly below the surface. Examples of properties that are detected using these methods include the sound from an impact,

deflection of the pavement under a dynamic load, infrared radiation from the pavement, electromagnetic-wave propagation through the pavement, and stress-wave propagation through the pavement.

In this research, the use of stress-wave based methods for detecting subsurface anomalies in pavements is investigated. Stress-wave based methods involve generating stress waves in a material and recording the propagation of the waves through the material. The presence of flaws can often be detected from the reflection of waves off the flaw surface. The typical horizontal orientation of delaminations and voids in pavements enhances the detectability of these flaws with stress-wave based nondestructive testing methods. There are several stress-wave based methods that vary both in the means used to detect flaws and in the frequencies that are generated in the pavement. To this point, however, stress-wave measurements have been made at discrete locations. The aim of this research is to study the feasibility of using stress-wave methods in a rolling device capable of continuous measurements for project-level studies.

1.3 PURPOSE OF STUDY

The ability to effectively and rapidly detect subsurface anomalies in pavements is a necessary component of any pavement management program. The purpose of this study is to evaluate the feasibility of implementing stress-wave based nondestructive testing methods into a rolling testing system capable of "on the fly" pavement evaluation. Towards this goal, it was necessary to review several nondestructive stress-wave based methods that could conceivably be applied to this problem. Two methods, the impact-echo and impulse-response methods, were chosen to be investigated both experimentally and analytically. Experimental testing was performed at three test facilities with preformed flaws to mimic actual flaw conditions in pavements. The experimental results were augmented with finite element tests performed by Chine Chung Chiang, as part of Project 1243. The experimental and numerical results were used to evaluate both the effectiveness of the stress wave methods for detecting various flaws in rigid pavements and the feasibility of implementing these methods into a rolling testing system capable of "on the fly" measurements. Experimental testing was then performed to study the feasibility of receiving the frequencies of interest for each test through a receiver wheel so that continuous measurements could be performed for project-level studies.

1.4 ORGANIZATION OF THE REPORT

Chapter Two is a review of nondestructive methods that have been applied or could conceivably be applied to the problem of detecting flaws in rigid pavements. Examples of past applications, as well as a discussion of advantages and disadvantages of each method are included.

Chapter Three is devoted to a description of the principles behind the impact-echo testing method. A description of the testing arrangement that was employed in the experimental tests performed in this work is also included. Lastly, a description of the test facilities at the Center for Transportation Research (CTR) at The University of Texas and the Texas Transportation Institute (TTI) at Texas A&M University that were used for experimental impact-echo testing is included.

Chapter Four contains a presentation of the experimental impact-echo test results obtained from the test facilities. These results are augmented with numerical model results from similar pavement profiles. A discussion of the parameters affecting the reliability and quality of the impact-echo test is also included in this chapter.

Chapter Five contains a description of the impulse-response testing method, including both the principles behind the method and the testing arrangement used for experimental testing. Results from the experimental tests performed at the test facilities described in Chapter Three are also included. Numerical models are again used to augment the results from the experimental tests. Lastly, a discussion of the advantages and limitations of this method is presented.

Chapter Six contains experimental results from high-frequency (1 to 20 kHz) energy propagation tests through mobile receivers, receivers on wheels which are intended to collect data while rolling. Tests were performed to study the feasibility of receiving high-frequency stress wave energy in the range of impact-echo testing through a rolling receiver. Results are presented from tests on several wheels of various materials and sizes.

Chapter Seven contains experimental results from low-frequency (10 to 1000 Hz) energy propagation tests through rolling receivers. Tests were performed to study the feasibility of receiving energy in the range of impulse-response testing through a mobile receiver. Results are presented from tests on several wheels of various materials and sizes. The development of a source wheel was previously studied (Ref 1), and was, therefore, not addressed in this study.

Chapter Eight provides a summary and conclusions of this research. It also contains recommendations for future work.

CHAPTER 2.

METHODS OF FLAW DETECTION IN CONCRETE SLABS

2.1 INTRODUCTION

As discussed in Chapter 1, the ability to detect and delineate subsurface flaws in a pavement system is a vital component of any effective pavement management plan. Presently, there are several nondestructive methods that have been applied, or could conceivably be applied, to the problem of flaw detection in rigid concrete pavement systems. These methods range from simple visual surveys of concrete pavements to more complex systems utilizing radar and infrared testing methods.

In this chapter, various nondestructive methods of subsurface flaw detection in concrete are discussed. These methods include those that have been used in the past on pavements, as well as methods that have been used on concrete slabs and have the potential to be used on concrete pavement systems. The methods are divided into the following three general categories in this chapter:

1. non-seismic methods,
2. deflection based methods, and
3. stress wave methods.

A description of each method and examples of past applications are included as well as a discussion of the advantages and disadvantages of each method for rolling, project-level pavement evaluation.

The discussion of nondestructive testing methods presented herein is limited to the problem of subsurface flaw detection and does not include discussion of methods for detection of vertically oriented surface cracking or surface spalling. The flaws of interest are regions of deterioration within or immediately below the rigid pavement layer as illustrated in Figure 2.1. In this research, these flaws are assumed to be detected at a time early enough so that they show no surface manifestation. Delaminations are defined as horizontally oriented planar separations within the rigid surface layer that usually develop around the reinforcing steel. Voids are generally meant to mean regions below the rigid surface layer where subgrade support is degraded or nonexistent.

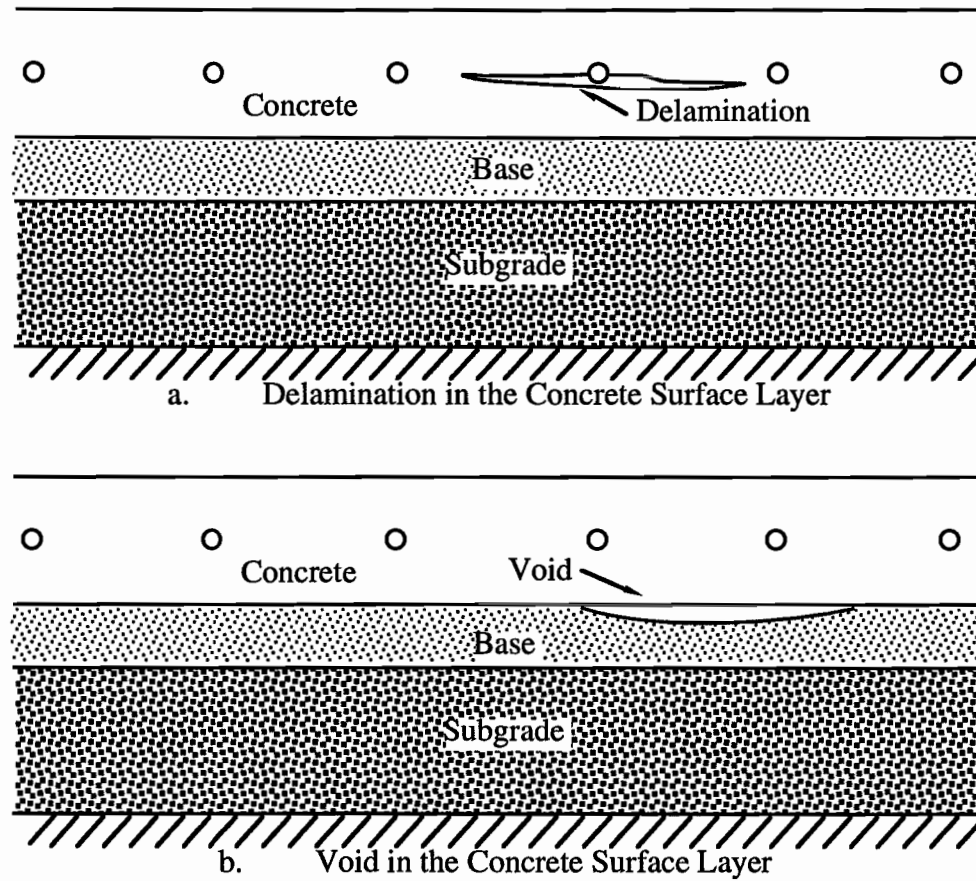


Figure 2.1 Types of Subsurface Flaws in Rigid Pavements which are to be Detected in this Research

2.2 NON-SEISMIC METHODS OF FLAW DETECTION

2.2.1 *Visual Surveys*

Probably the simplest method of evaluating pavements is visual surveying. Surface features such as cracks and spalls are very useful for determining problems below the pavement surface. Surface spalling of concrete, for example, often indicates advanced delamination formation and decay below the surface (Ref 2). Void formation below the pavement is best indicated by visual evidence of edge pumping (Ref 3). Corner cracking and transverse joint faulting also suggest the presence of a void (Ref 4). Visual surveys require no equipment and are generally unaffected by the presence of overlays on the concrete pavement. The method is, however, very slow and tedious and often detects problems after the quality of the road surface has been adversely affected. Secondly, the reliability of this method in many cases is low, with a 50% reported reliability for void detection (Ref 5). Visual surveys are best used as supplements to other methods of pavement evaluation.

2.2.2 *Ground Penetrating Radar*

Ground penetrating radar (GPR) first came into existence in the late 1960's and has been used in a variety of applications. In 1977, the method was applied to problems such as detecting voids and deterioration in masonry walls, and the evaluation of bridge deck deterioration (Ref 6). Since that time, GPR has been shown to be a promising method for many pavement maintenance applications.

GPR is based on the behavioral properties of electromagnetic waves when they encounter an interface between materials with different dielectric constants. Two types of GPR exist, they are swept-frequency GPR and short-pulse GPR. Swept-frequency GPR varies the frequency of the electromagnetic energy and is, therefore, not suited for mobile testing of large areas such as pavements. Short-pulse GPR inputs high-frequency signals, with center frequencies ranging from 80 MHz to 1 GHz, into the pavement. The depth of penetration and resolution is controlled by the frequency of the input signal. High-frequency waves will penetrate shallow depths with high resolution; lower frequencies penetrate to greater depths at the expense of decreased resolution.

The basic operating principle is based on the behavior of the waves at the interface between materials. When the electromagnetic waves encounter materials with different dielectric constants, a portion of the energy is reflected back to the surface. Therefore, any change in dielectric constant, whether it be from pavement layering, reinforcing steel or voids, will reflect energy back to the transmitter. Figure 2.2 illustrates the wave reflections and corresponding receiver output

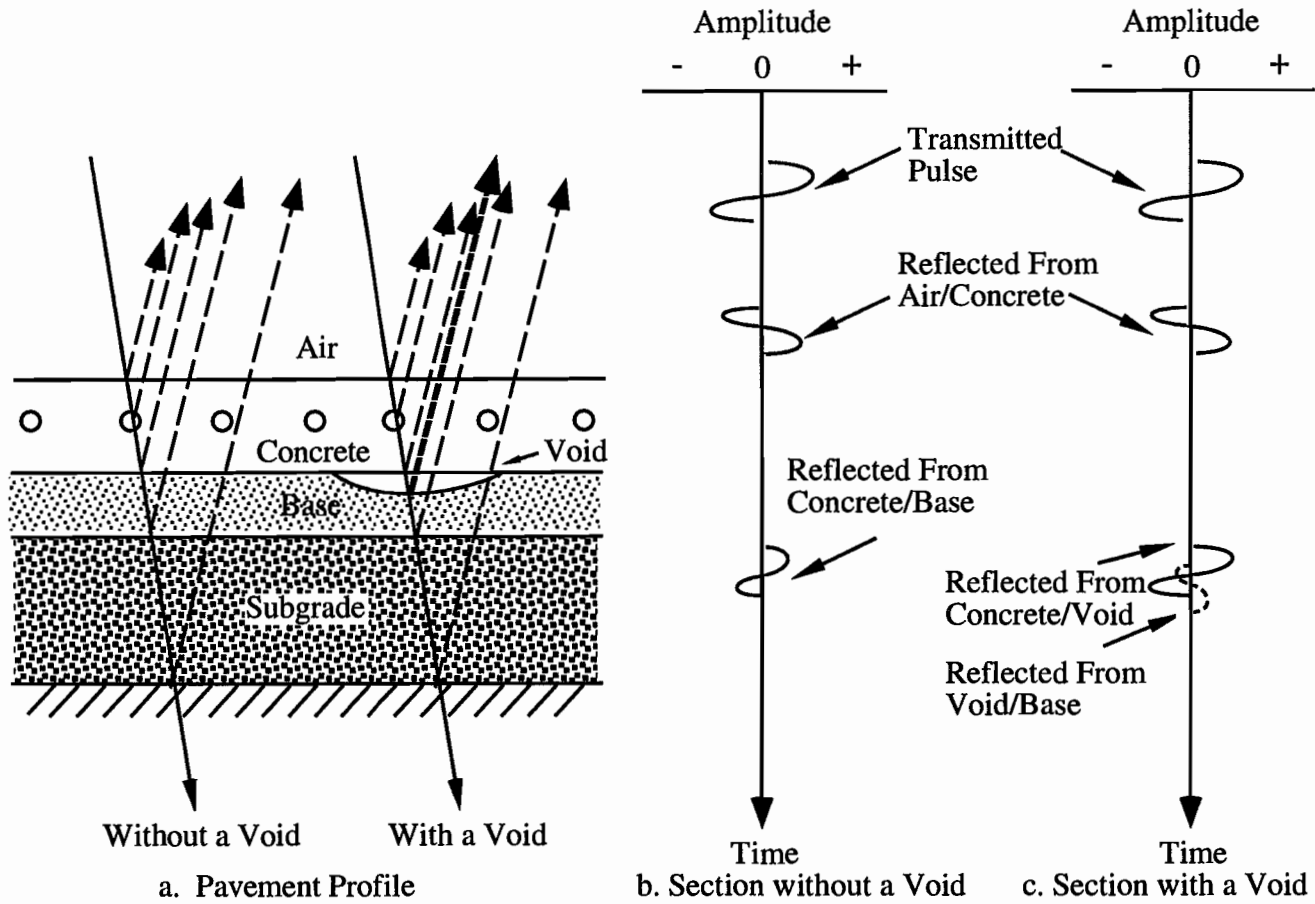


Figure 2.2 Propagation and Reflection of Electromagnetic Energy Through a Concrete Pavement, with and without a Void (after Ref 11)

from pavement systems with and without voids. The received energy is typically amplified and recorded on both magnetic tape and a chart recorder (Ref 7). If the dielectric constant, and hence the velocity of the electromagnetic wave, is known, the depth of the anomaly can be found from the time interval for the reflected wave to arrive. Testing can be repeated at a rate of 50 kHz. Therefore, a continuous record of the pavement can be achieved with a moving radar unit.

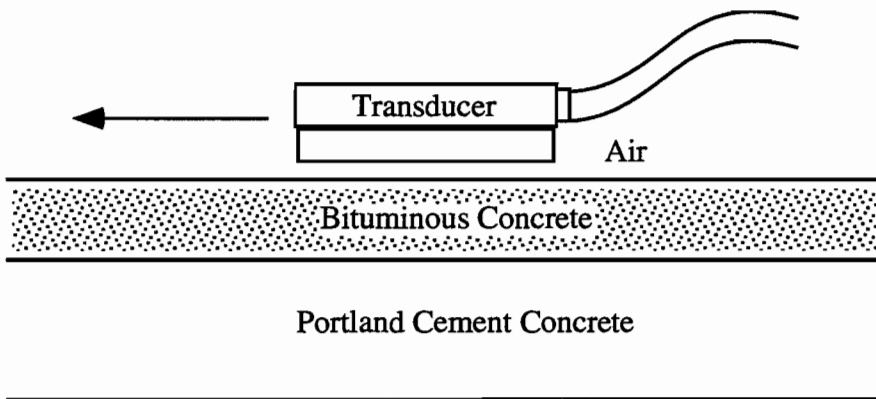
Figure 2.3 shows a typical GPR output from tests performed over a bridge deck. Every interface between materials of differing dielectric constants are visible in the output. One of the important advantages of GPR, therefore, is that the quality of the test is unaffected by the presence of an asphalt surface layer (Ref 8). A surface layer will appear only as another interface in the pavement and will not adversely affect the quality of the test. GPR also is virtually unaffected by environmental factors with the exception of wet pavement effects on high-frequency testing.

GPR also has the advantage of easy mobility. The transmitter / receiver units do not have to touch the ground, thereby increasing the speed of the test. Testing rates of approximately 3 mph are typical for pavement evaluations, so a moving lane closure is still required (Ref 9). GPR units are typically mounted over wheel tracks, so only a portion of the pavement can be evaluated. Multiple passes are required if the entire width of the pavement section is to be scanned. GPR has shown to be effective as a means of evaluating joint deterioration in rigid pavements (Ref 9). The method has also been effective as a means of void detection (Ref 9), but has had only limited success as a means of detecting delaminations. Clemena (1983) reports inconsistent detection of voids that are less than 0.3 m (12 in.) in extent (Ref 10). Difficulty in detecting thin voids was also observed with an accuracy of only about 54% (Ref 11).

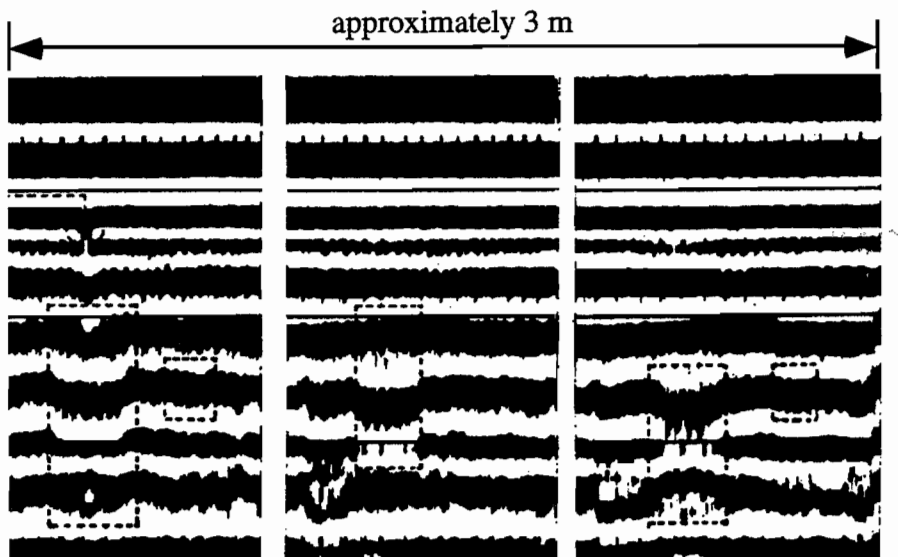
One of the most common criticisms of GPR is the complexity of the data interpretation. The detection and identification of flaws in radar records is often difficult for the untrained observer. Much experience in this area is required for accurate identification of flaw features in the pavement. This may be one reason why GPR has not been used more extensively for pavement evaluations in the past. Further development of computer software to analyze radar records should help to improve this aspect of the test method.

2.2.3 Infrared Thermography

Infrared thermography is another non-seismic based method that has shown promise as a means of locating flaws in pavements. The method is based on the differential heating that occurs around defects in the upper portion of a pavement system. Defects in the pavement will tend to cause the surface temperature of the pavement near the anomaly to increase above the temperature



a. Pavement Profile



b. Example GPR Reflection Profile

Figure 2.3 Sample GPR Reflection Profile from Test over a Concrete Bridge Deck (after Ref 10)

of adjacent sound pavement. Under ideal testing conditions, infrared thermography has shown to be a useful and fairly accurate tool for locating delaminations in rigid pavements and bridge decks, with and without asphalt overlays.

The test is typically performed with a scanner that detects the infrared radiation emitted from the pavement or bridge deck. The scanner is a non-contacting device that can scan an entire road width with one pass. The scanning width is a tremendous advantage of this method over other testing techniques that are limited in the lateral extent of single-pass testing. The scanner can be mounted on a moving vehicle from which the output of the infrared scanner and a video record of the actual pavement surface are recorded. The scanner should be located about 4.5 to 6.0 m above the pavement surface to minimize distortion from surface reflections (Ref 12).

Holt and Eales (1987), report two case studies of infrared thermography used in practical applications (Ref 9). The first application involved surveying 29.8 km of the Dan Ryan expressway in Chicago. Using a van mounted infrared scanner and video recorder, the 29.8-km length was scanned in 5 days, and delaminations as small as 10.2 cm were detected. In a second case study, 127 km of pavement were scanned in 8 days. The pavement types included continuously reinforced concrete pavements and asphalt overlaid jointed reinforced concrete pavement. A series of cores at this site showed the infrared data to be accurate 99 percent of the time. In both cases, the testing required moving lane closures of the road.

The infrared thermography method does have several drawbacks that have limited its use in practice. Manning and Holt (1983) report that the maximum temperature difference between flaws and sound pavement is typically 2 to 3 degrees C (Ref 13). To detect differences this large, tests must be performed between approximately 11:00 AM and 2:00 PM. During other parts of the day, the temperature differences are greatly reduced and accurate detection is difficult. Figure 2.4 illustrates the effect of the time of day on infrared testing effectiveness. Further restrictions are that temperatures above 18 degrees C, wind speed less than 40 km/hr, humidity less than 50%, and cloud cover less than 40% are all necessary for effective and accurate testing. Therefore, the great advantage of rapid single-pass testing is largely mitigated by limitations on allowable testing times. Even under ideal testing conditions, there are limitations on the effectiveness of infrared thermography. Local surface features such as tire marks or asphalt patches may be interpreted as delaminations if proper visual correlation of video and infrared records is not performed (Ref 12). Secondly, voids beneath the pavement and debonding between layers will generally not be detected with infrared thermography. Knorr et al (1983), also found difficulty in determining the lateral extent of many delaminations (Ref 12). This along with the fact that the depth to the delamination can not be detected severely limits this method for use in calculating contract repair figures.

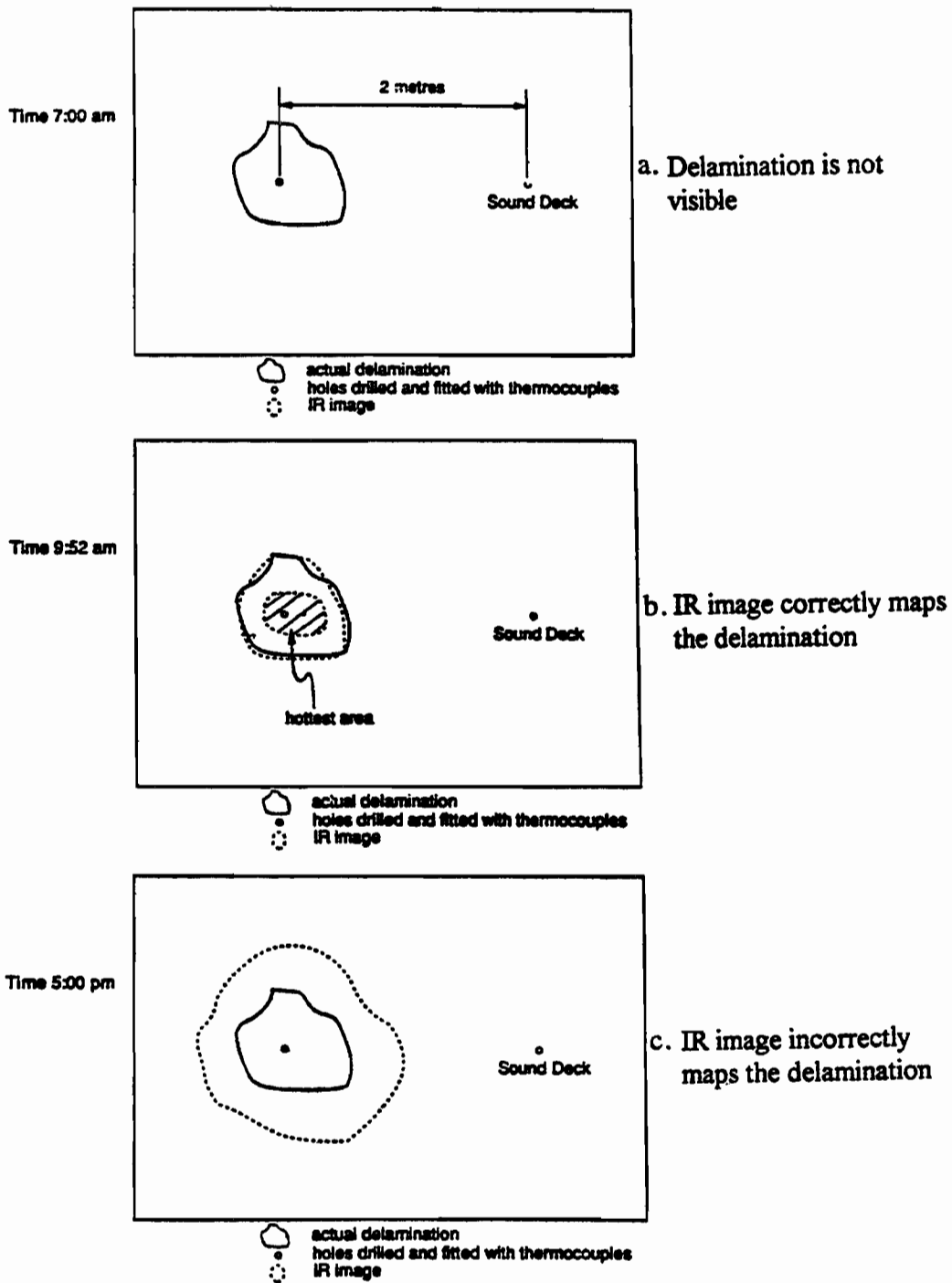


Figure 2.4 Effect of Time of Day on Infrared Thermography Results (Ref 35)

Under the right weather conditions, the infrared thermography method can be an effective means of rapidly scanning pavements for regions of poor concrete. However, for accurate measurement of size and extent, other more localized methods may need to be employed.

2.2.4 Half-Cell Potential

Half-cell potential measurements are used only for monitoring conditions favorable for delamination development in bridge decks (Ref 2). This method relies on measurements indicating deterioration of the steel reinforcement as a means of detecting conditions that may create delaminations in the pavement or bridge deck. Delaminations develop due to stresses created in the concrete from the volumetric expansion of corroding reinforcing steel and are, therefore, typically located at the same depth as the top layer of reinforcing steel. By monitoring the corrosion potential of the reinforcing steel, one can also monitor the conditions for development of delaminations in the pavement.

The half cell tests are typically performed using the arrangement shown in Figure 2.5. A positive connection to the reinforcing steel is required along with a reference cell that usually consists of copper in a copper sulfate solution. A moisture junction must also be provided through the concrete between the copper rod and the reinforcing steel. A voltmeter is placed in the circuit to measure the potential difference. Van Daveer (1975) and Manning and Ryell (1981) report that readings more negative than -0.35 volt indicate a 95% probability that the steel is corroding (Refs 2, 14). Figure 2.6 shows an equipotential map of values obtained from tests on a bridge deck. A study of half-cell potentials conducted in 1970 indicates a strong correlation between high potential differences and severe deck deterioration (Ref 2).

By monitoring the conditions that create physical distress in the pavement, the half-cell potential method has the great advantage of predicting problem areas before physical distress has occurred. There are, however, problems associated with this testing method. Manning and Ryell (1981) point out that half-cell readings measure the presence of corrosive activity, not the rate of corrosion (Ref 14). Therefore, the pavement may be functioning very well with no actual physical distress for many years after these tests have indicated negative performance. Secondly, the half-cell method is not suited for rapid testing of pavements. Good contact with the pavement is required for accurate tests. For decks overlaid with asphalt, holes must be drilled through the asphalt to provide good contact with the rigid pavement layer (Ref 13). Lastly, this method is only good for detecting one type of pavement problem, delaminations caused by steel corrosion, and is, therefore, not useful for detecting other problems associated with bridge decks and pavements.

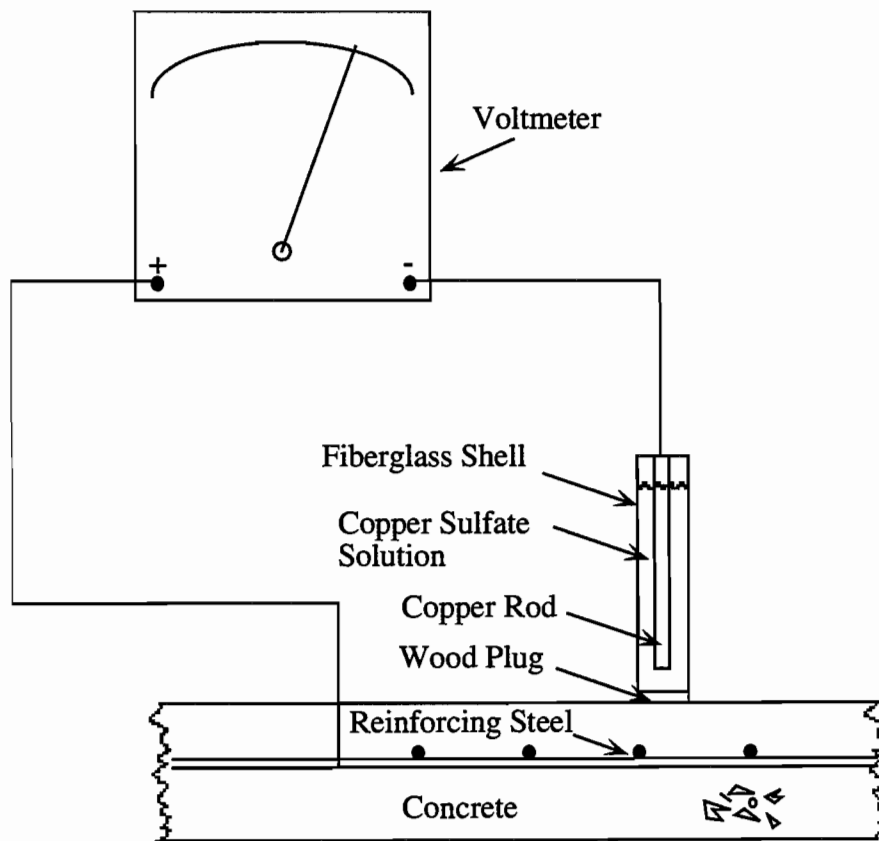


Figure 2.5 Testing Arrangement for Half-Cell Potential Test (after Ref 2)

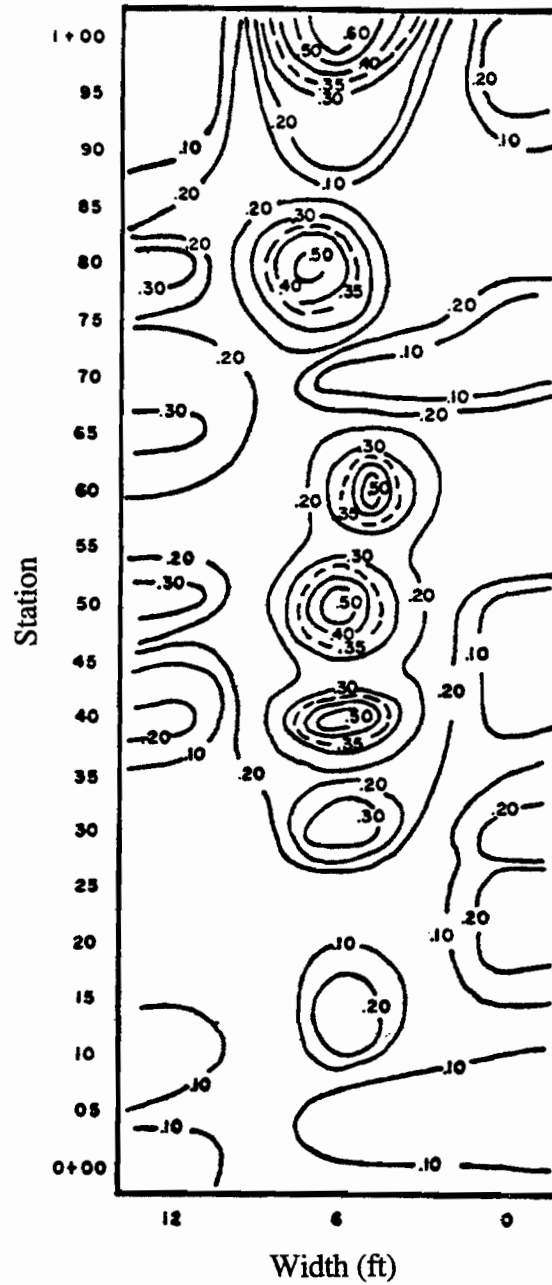


Figure 2.6 Contour Plot of Potential Readings (in Volts) from Half-Cell Potential Test Performed over a Concrete Bridge Deck (Ref 2)

2.3 DEFLECTION BASED METHODS OF FLAW DETECTION

Deflection methods are based on the deformational characteristics of a pavement under an applied load. The measured deflection is then compared to an established specification to evaluate the condition of the pavement. Large areas of voids or subgrade support loss will exhibit higher deflections and can, therefore, be delineated from sound pavement. Deflection based methods are divided into two categories, static and dynamic. This classification is based on the nature of the load applied to the pavement.

2.3.1 Static Deflection Method

Static deflection methods are based on the displacement of a pavement under an applied static load. Typically, a standard 8172-kg single axle is applied to the pavement and the displacements are measured with a Benkelman Beam or similar device. The measured displacements are compared to specified allowable values to evaluate the pavement. Static load displacements are local tests that require fairly long equipment set-up times and are, therefore, not well suited for rapid evaluation of pavements.

2.3.2 Dynamic Deflection Surveys

Some of the practical problems associated with static tests are overcome by dynamic deflection tests. A dynamic deflection test differs from a static test in the method of deforming and measuring the deformation of the pavement. Loads for the dynamic tests are typically applied through rotating wheels, hydraulic actuated masses, or dropped weights. The pavement response is usually measured with a velocity transducer such as a geophone.

There are several dynamic deflection systems available for pavement evaluation. One of the most common methods is the Falling Weight Deflectometer (FWD) testing system. The FWD testing arrangement is shown in Figure 2.7. The load is applied from weights dropped onto the pavement surface. The magnitude of the weight and the height of the weight drop can be varied. More weight and a higher drop will generate lower frequencies and higher magnitudes for deeper sampling of the pavement system. Typically, peak loads range from 6.7 to 107 kN. An array of 7 geophones is used to measure the motion of the pavement surface. The peak deflections measured at each geophone are used to form the deflection basin at that location. Linear elastic

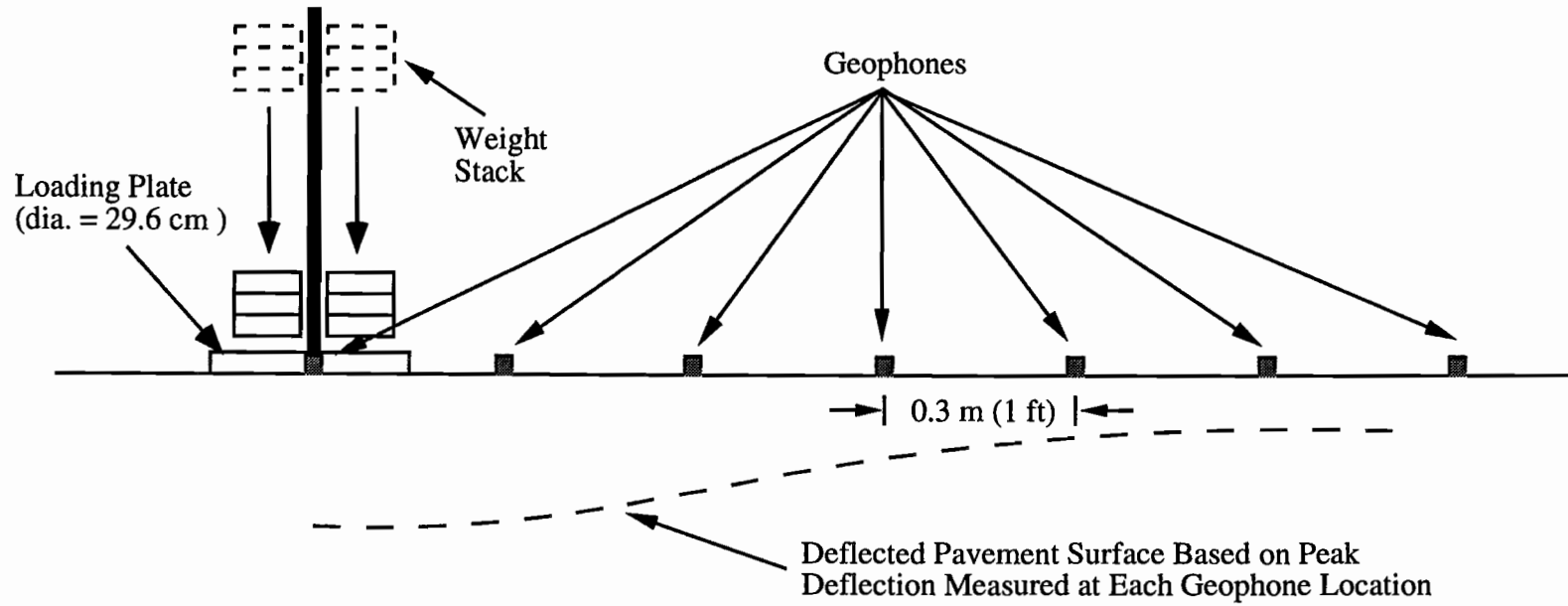


Figure 2.7 Falling Weight Deflectometer (FWD) Testing Arrangement (after Ref 36)

layered theory is then used to analyze the data. A set of Young's modulus values are assumed and adjusted through trial and error to match the theoretical result to the experimental measurement.

One of the problems with the FWD is that the programs used to generate the theoretical deflection basins usually are based on a static analysis (replacing the actual dynamic force with an equivalent static force). This approach is fine if no shallow reflecting layer exists below the test location. However, if bedrock is shallow, the results from the FWD test can be adversely affected (Ref 15). Another drawback of the FWD is that it is a discrete testing system, meaning individual tests are performed at specific locations. As such, the method can be fairly slow for evaluating long stretches of pavement.

A device which has recently been developed at the Center for Transportation Research (CTR) as part of Project 1243, allows continuous profiling of pavements (Ref 16). This device is called the Rolling Dynamic Deflectometer (RDD). The RDD consists of a large " Vibroseis " truck, typically used for geophysical applications, retrofitted with two rolling wheels under the large vibrating mass, as shown in Figure 2.8. A function generator is used to input any fixed sinusoid or multi-frequency signal between about 1 and 20 Hz to the hydraulic system that drives the mass and loading wheels. Loads up to 156 kN can be generated by the RDD. A single receiver is mounted on two wheels between the loading wheels. The "receiver wheel" is used to measure the pavement response, as shown in Figure 2.9. The pavement response to the vibrating load can be determined "on the fly", allowing continuous evaluation of the pavement. Initial testing of this system has been successful (Ref 16), and various tests are already planned for the future.

The deflection methods outlined above, are used for finding large areas of support loss. Small areas of deterioration of the concrete or the base would probably not be detected by these methods. A smaller scale dynamic deflection method developed in France is the Collograph machine (Ref 17). This system consists of counter-rotating wheels that generate a cyclic force. The force cycles from 1 to 5 kN, thereby generating deflections in the pavement. The deflections are measured "on the fly" by a moving oil filled wheel with an hydrophone mounted inside the wheel. The voltage output of the hydrophone corresponds to the vertical displacement of the pavement. Cracks and delaminations are identified by characteristic responses as shown in Figure 2.10. The performance of the Collograph and details concerning the size and depth of flaws that can be located are not well documented in the literature.

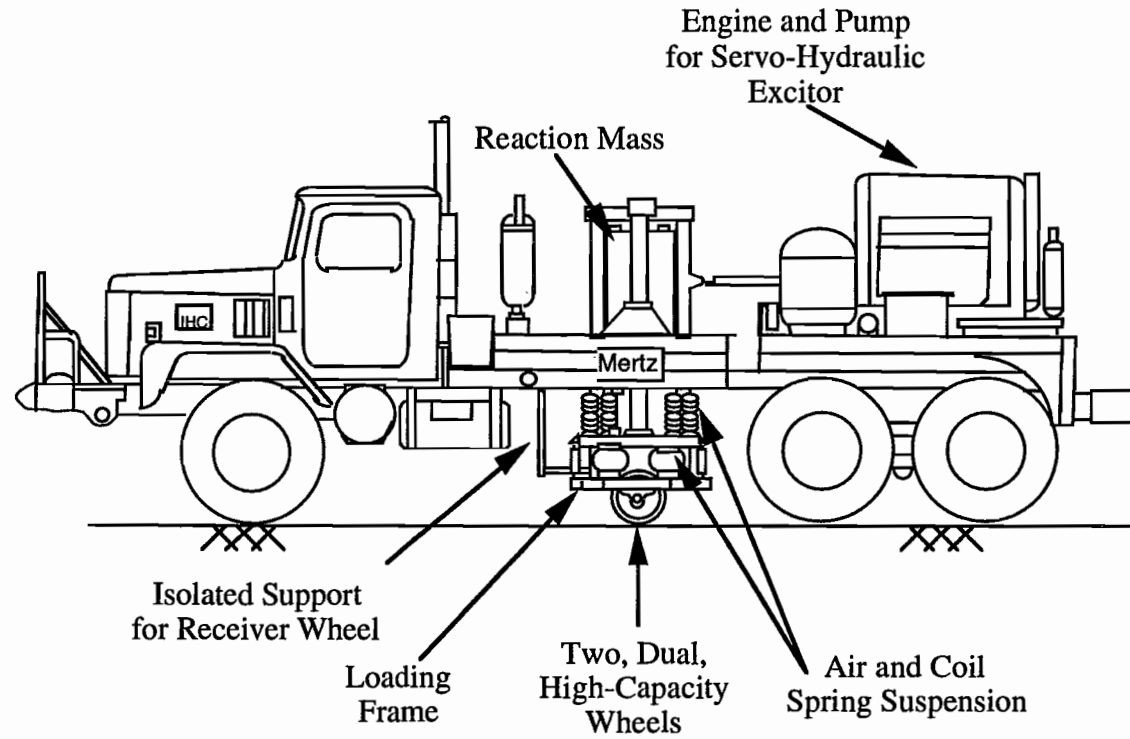


Figure 2.8 Profile View of Rolling Dynamic Deflectometer (RDD) (from Ref 16)

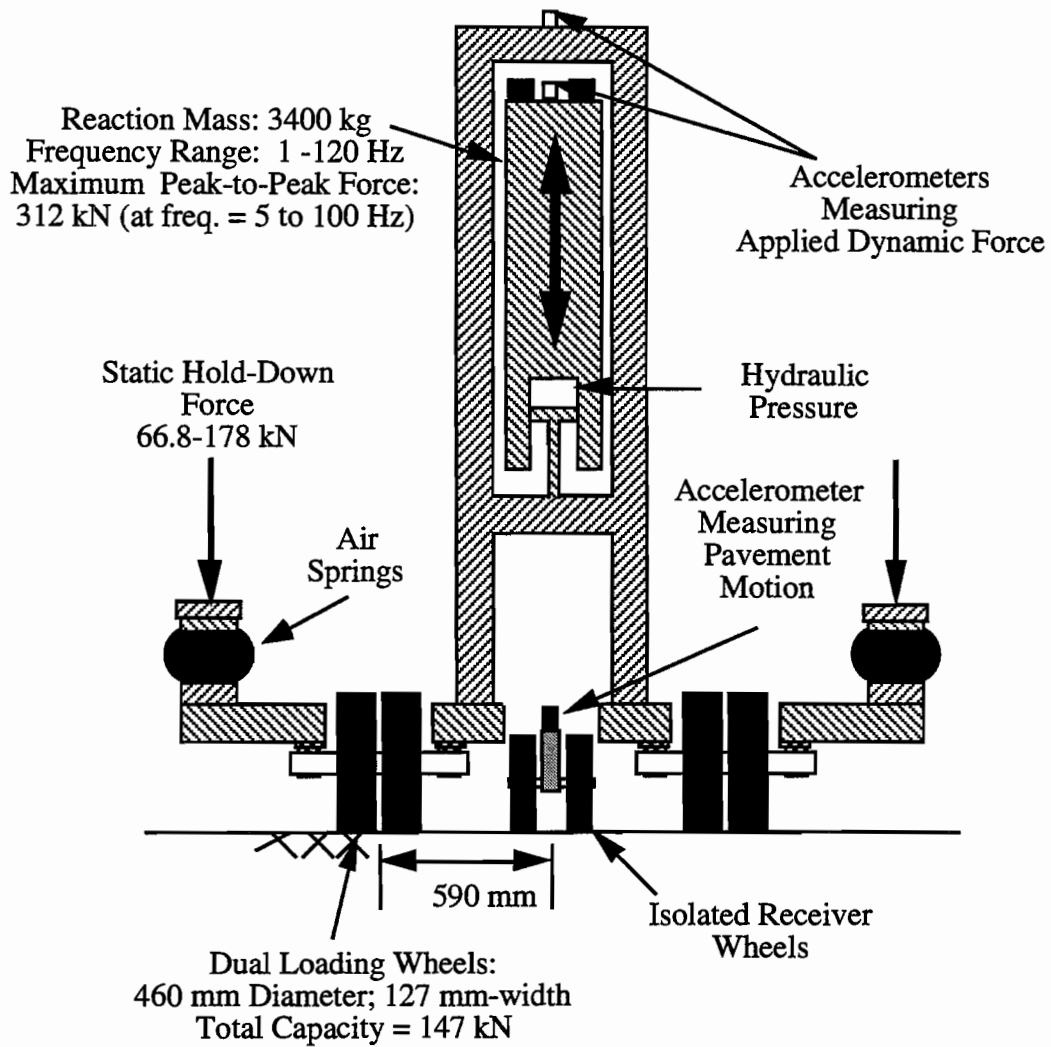


Figure 2.9 Front Cross-Sectional View of Dynamic Loading and Monitoring Systems of the Rolling Dynamic Deflectometer (from Ref 16)

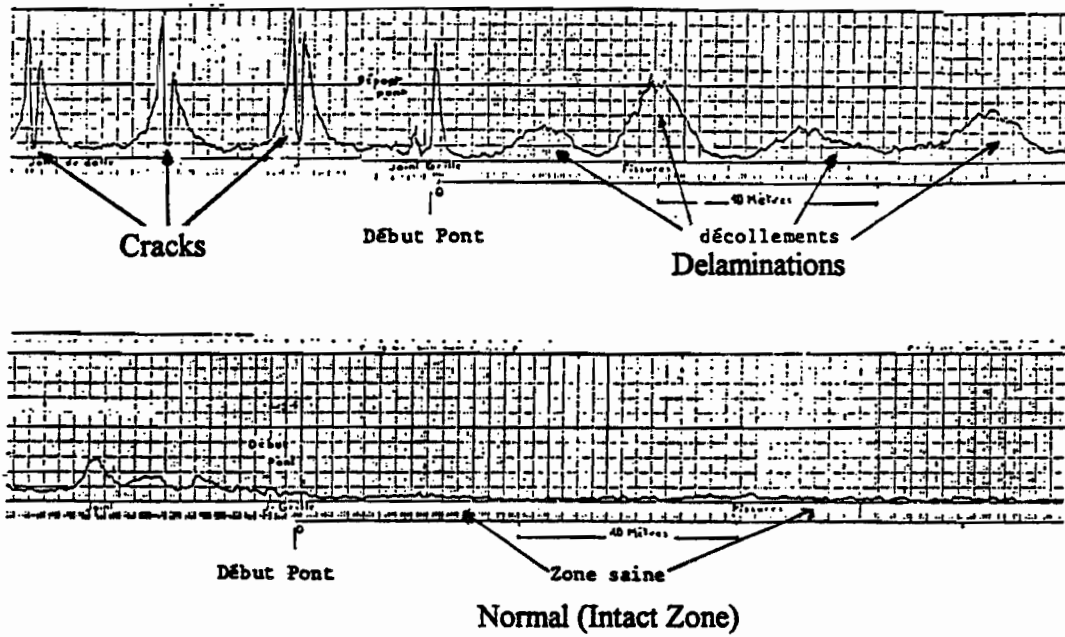


Figure 2.10 Sample Output from Collograph Testing System (from Ref 17)

2.4 STRESS WAVE METHODS OF FLAW DETECTION

The methods that have been outlined above are based on the ability to measure deviation in the properties of the pavement - such as infrared radiation, electromagnetic reflection, electric potential, and surface deflection - when a flaw or anomaly of interest is encountered. In much the same way, seismic (stress-wave) measurements are used to observe the deviation of propagating stress waves when flaws are encountered. Generally, the following three fundamental types of stress waves are generated when an elastic material is excited: compression (P waves), shear (S waves) and surface or Rayleigh waves (R waves). Shear waves can further be divided into vertically (SV) and horizontally (SH) propagating shear waves. Several methods exist that utilize these various stress waves to infer conditions below the pavement surface. Stress-wave based methods, sometimes termed acoustic methods, can also be divided according to the frequencies generated by the test. Tests that involve frequencies that can be detected by the human ear (20 Hz to 20 kHz) are termed sonic tests, while tests performed with frequencies outside of the human audible range are called ultrasonic tests.

2.4.1 Manual - Sounding Method

The simplest and most commonly used stress-wave method for flaw detection in pavements is the manual sounding method. This method, which can be categorized as a sonic method, involves a person listening for flexural resonances in the pavement. Much as one detects solid wooden members behind a wall by tapping on the wall, voids and delaminations are detected by striking the pavement and listening to the response. To generate the required response, the pavement must be excited with a source that generates significant energy in the required frequency range. The ideal source, therefore, must input a broad range of high-energy frequencies. Also, the source itself must not exhibit high-amplitude resonances in the audible frequency range that could overshadow the pavement response. Based on practical experience, the sources which have been used to test pavements are falling rods and dragged chains. The chain arrangement usually consists of 4 to 5, 0.5-m long chains made up of 2.54-cm long links. These chains are attached to a T-shaped piece of tubing that is dragged from side to side over the pavement (Ref 8). An operator listens to the sound generated by the dragging chains. When a flaw is encountered, a hollow or dull sound is created. The chain is shortened, and the limits of the flaw are marked off. Despite its primitive and simplistic nature, this is a method commonly used to detect flaws in rigid pavements.

This method, however, has several shortcomings. The flexural vibration frequency and amplitude of the pavement over a delamination are a function of the depth to the delamination and the lateral extent and shape of the flaw. Small, deep flaws, for example, will resonate at very high frequencies and low amplitudes. The dragging chain will not excite the high frequencies and high amplitudes that are necessary for audible detection of these flaws. Many subsurface problems, therefore, would go undetected by this method. Furthermore, the method is tedious, time consuming and depends on the subjective evaluation of an operator. To overcome some of these problems, a mechanical device was developed to automate the procedure.

2.4.2 Automated Sounding Device

An automated device to perform the sounding test on pavement was developed at Texas A&M University (Ref 18). The device, shown in Figure 2.11, consists of a rolling source and receiver system. The source is a pair of rigid steel wheels spaced 0.15 m apart that are excited by a vertical, solenoid-driven plunger. The plunger oscillates at 60 Hz as the device rolls along the pavement. The receivers are two oil-filled wheels with vertical hydrophones that are spaced 0.3 m apart, with the source wheel arrangement centered between them. The system, therefore, consists of two channels that survey two 7.62-cm wide paths that are spaced 0.15 m apart. The output of the receivers are filtered such that only frequencies between 300 to 1200 Hz are passed. The signals are then passed to a DC rectifier, and the voltage output is plotted on a pen recorder. Since the plunger is impacting 60 times a second, voltage values are plotted at intervals of 16.7 ms. Figure 2.12 shows sample output of the two wheels over a solid deck and over a delaminated deck (Ref 18). Based on these results, the device appears to perform well. Subsequent field testing of the mechanical device, however, has shown it to be less effective than the chain drag method for detecting delaminations (Ref 8).

2.4.3 Pulse-Echo Ultrasonic Testing

Another approach for detecting flaws in concrete is to propagate ultrasonic waves through the material and detect reflections off of subsurface anomalies. Active sonar in water is an analogous method where objects in a fluid are located by measuring the time for stress waves to travel from the source, reflect off the object, and return to the source. In a fluid such as water, only compression waves are generated. In solids the detection of reflections becomes more difficult due to the generation of shear and Rayleigh waves. This method can be used successfully in homogeneous solids as a means of high resolution detection of flaws. The successful

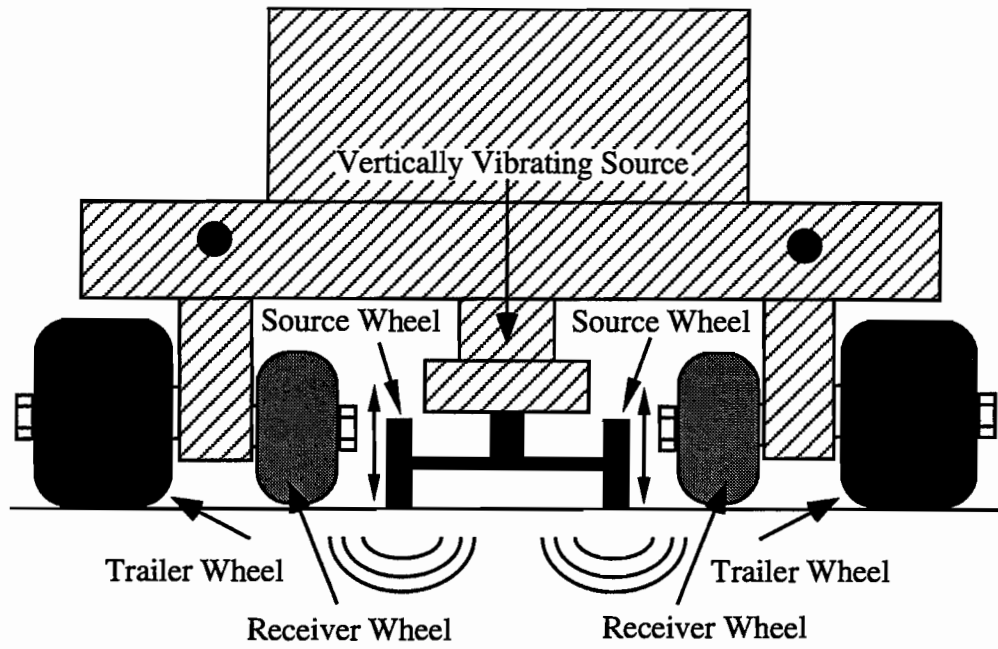
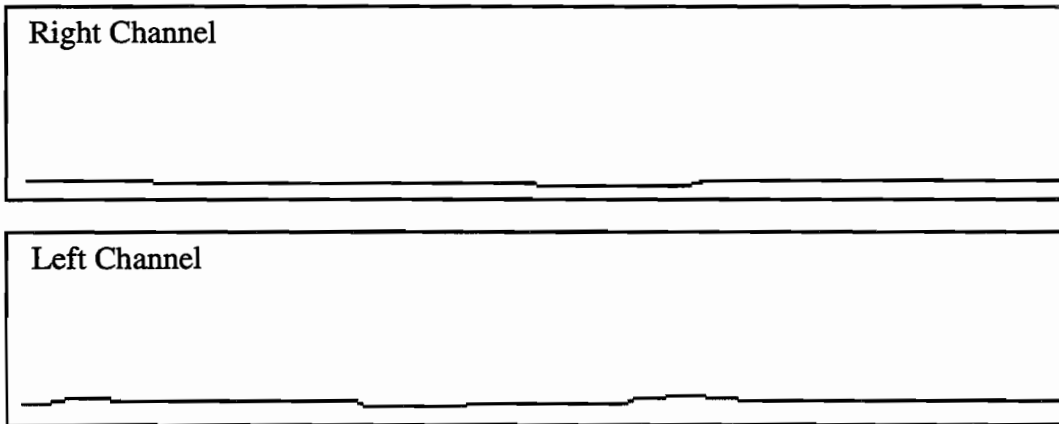
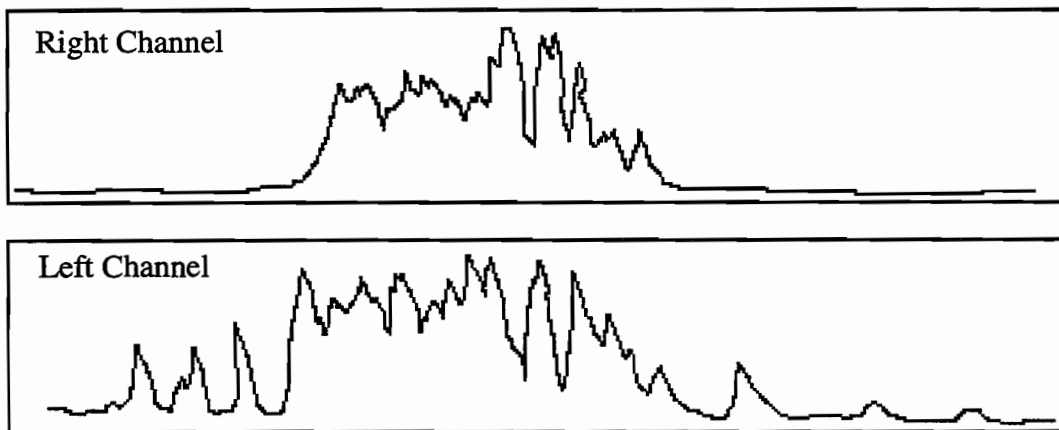


Figure 2.11 Rear View of Delamtect Automated Sounding Device (after Ref 18)



a. Output Over Sound Pavement



b. Output Over Delaminated Pavement

Figure 2.12 Sample Output from Delamtect Over Sound and Delaminated Pavement (after Ref 18)

application of such a method in concrete would allow for detection of the depth and size of subsurface flaws. However, the heterogeneous nature of concrete greatly complicates the successful application of this method.

The pulse-echo method typically involves using a single transducer which is used to both propagate waves into a solid and detect the reflections of the waves off subsurface flaws. The transducer, therefore, acts in two modes: a "talking" mode when it emits a signal, and a "listening" mode when it detects reflected signals. The "talking" of the transducer and any subsequent internal ringing in the transducer must be completed before reflected waves arrive (Ref 19). Therefore, very high frequency or short-pulse durations from the source are desirable for this type of testing. In homogeneous materials, the high frequencies are also desirable because they will reflect off small defects and provide better resolution. However, in heterogeneous materials, such as concrete, the high-frequency waves will reflect off coarse aggregate and scattering of the wave will result. Therefore, there is a limited range of acceptable frequencies that can be used successfully in concrete. Some of these problems can be eliminated by using a modified version of the pulse-echo method called the pitch-catch method. The pitch-catch method uses a separate transducer to receive the signal. When this method is used, very short impact durations are needed so that interfering Rayleigh waves do not mask echo patterns from voids (Ref 20).

Alexander and Thornton (1988) and Carino et al. (1986) have reported success in detecting flaws and the thickness of concrete slabs (Ref 19, 20). The very high frequencies required and the special considerations for receiver design have limited the use of this method. This method, therefore, was not investigated experimentally for implementation into a mobile testing system.

2.4.4 Impact-Echo Testing

The impact-echo method is an ultrasonic stress-wave based method that has been developed for the detection of flaws in concrete. The impact-echo method is used to detect flaws by measuring the compression-wave resonant condition that develops over reflecting surfaces in the pavement. For the case of an air-filled void or delamination, the difference in acoustic impedance values is so large that the concrete/air interface can be considered a total reflector. Therefore, the void interface and the air interface at the top of the pavement result in two, stress-free boundary conditions. First-mode resonance of a free-free system occurs when the wavelength equals twice the depth (d) to the void. Therefore, if the velocity (v) of the material is known and the resonant frequency (f) is measured, the depth to the void can be calculated from:

$$d = v / (2 * f) \tag{2.1}$$

Because the impact-echo method does not require the detection of arrival times, many of the problems associated with pulse-echo testing are overcome. However, the ability to determine the resonant frequency from the time record may be difficult due to overshadowing effects of surface and shear arrivals. For this reason the data from the impact-echo test are viewed in the frequency domain so that dominant vibration frequencies can be easily identified. More details of the testing procedure are provided in Chapter 3.

The impact-echo method has shown to be a very useful method for detecting many types of flaws in concrete. Research on concrete slabs has shown the ability to detect the depth and location of voids and delaminations within a concrete slab (Ref 21, 22). The method has also been used to measure the depth of vertically oriented surface cracks and to detect simulated honeycombing in concrete (Ref 23). In practice, the method has been used to locate areas of freeze-thaw damage in a thin-arch concrete dam (Ref 24). The impact-echo method has shown to be an effective means of detecting many flaws commonly found in concrete pavements. However, no project-level, mobile system has been developed to utilize this method for testing large pavement areas. The impact-echo method was chosen as one of the seismic methods to be investigated analytically and experimentally to determine the feasibility and effectiveness of this method for project-level pavement evaluations.

2.4.5 Impulse - Response Method

The impulse-response method is a nondestructive testing technique originally used for integrity testing of piles that has been adapted for integrity testing of pavements. The impulse-response method detects subsurface flaws by utilizing low-frequency, high-amplitude, flexural vibrations that develop over large void regions. Like the sonic methods described in Section 2.4.1, the impulse-response method is performed by exciting vibrations in the pavement with a low-frequency generating impact. The response of the pavement is recorded with a velocity transducer coupled to the pavement surface. The difference between this method and other sonic methods is that the results are analyzed in terms of the frequency components. Detailed discussions of the testing method and data interpretation are included in Chapter 5, which deals with the experimental and analytical results of impulse-response testing.

The impulse-response method has been used effectively by the Oklahoma Department of Transportation to locate voids and delaminations in pavements (Ref 25). It also served to evaluate the effectiveness of stabilization methods used to improve pavement support. The method was also used effectively to locate regions of support loss under a concrete slab that had been uplifted

by water pressure (Ref 26). Based on these results, the impulse-response method was investigated experimentally and analytically to evaluate the applicability of this test for mobile testing of pavements. The results and discussion of these investigations are included in Chapter 5.

2.4.6 Spectral-Analysis-of-Surface-Wave (SASW) Method

Unlike the stress wave methods discussed previously, the SASW method uses surface waves (R waves) to investigate subsurface conditions. The test is performed with two surface receivers and one impacting device, all equally spaced along a straight line on the surface of the material being tested. Based on the receiver spacing and the difference in phase of the propagating waves, the velocity of the material as a function of wavelength can be determined. The depth that is sampled is related to the wavelength of the wave that is being propagated. Therefore, a profile of the velocity of a material at various depths can be determined. Areas that contain a void, therefore, would likely be detected by low velocity regions in the pavement. The most common use of this method on pavements is for evaluating stiffness profiles (Ref 27)

Past applications of the SASW method have shown it to be a valuable instrument for in-situ testing of soils (Ref 28). It has also been investigated as a means of determining in situ stiffness of curing concrete (Ref 29), and it was successfully used to quantify and locate damaged concrete in a highway bridge beam (Ref 30). Currently testing of this method for pavement profiling is being performed through a joint CTR and University of Texas at El-Paso project as part of project 1243. The SASW method was, therefore, not investigated as part of this study.

2.5 SUMMARY

Based on a literature review of available methods for pavement evaluation, it appears that no single method is ideally suited for rapid and effective detection of subsurface flaws. Several stress-wave based methods have been shown to be effective for site-specific detection of pavement and concrete slab flaws. Two stress-wave based methods, impact-echo and impulse-response, have been chosen to be evaluated for effectiveness and applicability for implementation into a rolling system of flaw detection for project-level investigations.

CHAPTER 3.

METHODOLOGY, EQUIPMENT, AND FACILITIES

USED IN IMPACT-ECHO TESTING

3.1 INTRODUCTION

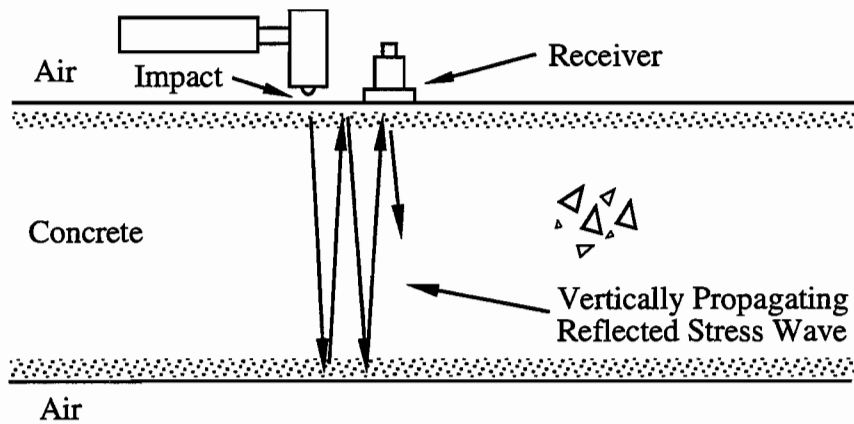
The impact-echo test is a nondestructive stress-wave based method that has been used successfully in many site-specific applications for detecting various subsurface flaws in concrete structures. The method makes use of the resonant condition that develops over a flaw to infer the subsurface condition of the concrete structure. This method became viable with the advent of algorithms to rapidly convert waveforms to their frequency components.

As discussed in Chapter 2, the impact-echo method avoids many of the problems associated with other stress-wave based systems for testing concrete. In many ways, the impact-echo test appears to be ideally suited for providing the necessary information for effective pavement evaluation. However, due to the site-specific nature of the test in its present form, the method has never been implemented into a rolling system that could be used for project-level studies of pavements.

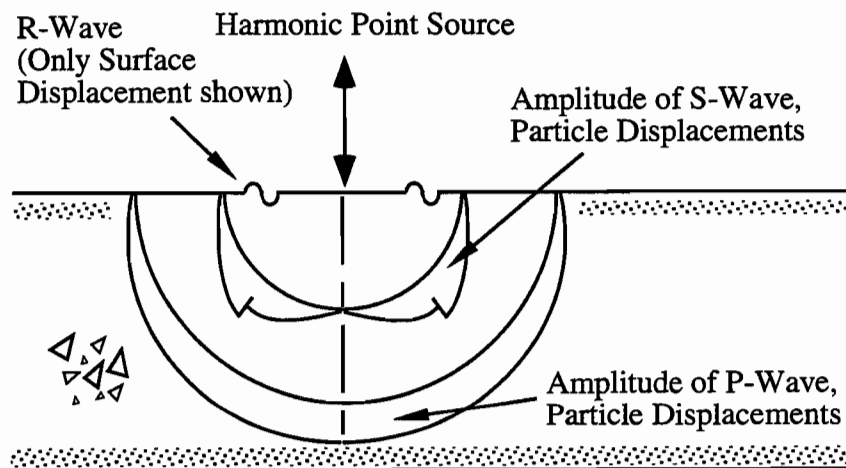
The purpose of this chapter is to evaluate the effectiveness and suitability of the impact-echo test for project-level testing of pavement systems. Included herein is a description of the impact-echo method, the testing methodology and equipment used, data reduction procedures, and experimental test sites.

3.2 DESCRIPTION OF THE IMPACT-ECHO METHOD

The impact-echo test is typically performed with a single source and a single receiver mounted on one surface of the structure. The source is typically an impacting device such as a small hammer or a steel ball. The receiver may be an acceleration transducer. However, a special displacement transducer has also been developed that is commonly used for this purpose (Ref 31). The source is used to impart a transient stress wave to the structure by impacting the surface, as shown in Figure 3.1a. The following three types of waves are generated in a solid material:



a. Idealized Compression Wave Propagation for Impact-Echo Testing



b. Wave Types and Amplitudes Created from Harmonic Point Source (after Ref 37)

Figure 3.1 Stress Wave Propagation Behavior in Solid

compressional waves, shear waves, and surface or Rayleigh waves, as shown in Figure 3.1b. Each of these wave types travels through the material at a different velocity that depends on the material properties of the structure.

The impact-echo test utilizes vertically propagating compression waves to infer subsurface conditions in the pavement. The velocity at which compression waves propagate depends on the dimensions of the material being tested. In a test cylinder with an aspect ratio of 2:1, for example, the waves will first propagate as constrained compression (P) waves before evolving into slower velocity unconstrained compression waves. The velocity of these unconstrained waves (v_c) can be calculated according to the following equation:

$$v_c^2 = E / \rho \quad (3.1)$$

where E = Young's Modulus, and
 ρ = mass density.

If, however, the material is constrained, such as in a uniform half space, the waves will propagate at a faster velocity (v_p) according to the following equation:

$$v_p^2 = M / \rho \quad (3.2)$$

where M = constrained modulus.

The constrained modulus (M) is related to Young's modulus (E) according to the following equation:

$$M = E (1 - \nu) / [(1 + \nu) (1 - 2\nu)] \quad (3.3)$$

where ν = Poisson's ratio.

Therefore, if the mass density and Young's modulus of a material are known, the unconstrained compression wave velocity can be determined. If Poisson's ratio is known or assumed, then the constrained modulus and v_p can also be determined.

Two other terms used to describe waves in a material are frequency (f) and wavelength (λ). The frequency of the wave refers to the number of waves that pass by a fixed point per unit time (Hz). The frequency expressed in terms of radians is called the angular or circular frequency (ω). The values of f and ω are related by:

$$\omega = 2\pi f \quad (3.4)$$

The wavelength is defined as the distance a wave travels in one cycle. The frequency, velocity and wavelength of a wave in a material are related to one another by the following equation:

$$v = f * \lambda \quad (3.5)$$

The impact-echo test is used to determine the frequency components of the vibrating material. In a uniform, infinite half-space containing no reflecting interfaces, only waves propagating along the surface create particle motions at the surface. However, in a system with finite boundaries and layers, such as a pavement, some energy from incident waves reflects off interface boundaries within the solid and creates additional motion on the surface. The magnitude of the reflected energy depends on the ratio of the acoustic impedance values of the two materials. The acoustic impedance is defined as the product of the material mass density (ρ) and the wave velocity (v). If the values of acoustic impedance are equal, no energy is reflected. But if the values are different, some of the incident energy is reflected from the interface. It is this property that is often utilized in stress wave testing of materials.

Ideally, one could measure the time it takes the wave to reflect from the interface and return to the surface. However, as discussed in Chapter 2, this is very difficult and ineffective in heterogeneous materials such as concrete. Furthermore, single-mode waves that reflect off an interface generate reflected and refracted waves in other modes. For example, a P wave can generate reflected and refracted, vertically and horizontally oriented shear waves (S waves) at every interface the wave encounters. Each of these newly generated waves can likewise generate new modes of waves when other interfaces are encountered. Rayleigh waves (R waves) that propagate along the surface from the impact generate P and S waves as well as a reflected R wave at the lateral boundaries of the surface. Therefore, the waveform that is recorded by the receiver can be very complicated and contains many frequencies that are not easily identified in the time domain. However, by using a Fourier transformation procedure, the time record can be viewed in terms of the magnitudes of the frequencies present in the time record trace. It is from viewing this frequency response that information about the subsurface of the pavement can be inferred.

When the frequency response from a test performed over a fairly uniform material is examined, the magnitude of the response at each frequency is fairly constant. However, when the frequency response is examined from a test performed over a flaw or layer boundary within the solid structure, a dominant peak is observed at one frequency. This peak corresponds to the

compressional resonant frequency that develops over the planer flaw (typical records illustrating resonance conditions are presented in Section 4.2.1, see Figure 4.2 for instance). The frequency and magnitude of the P-wave resonance depends on both the depth to the reflecting interface and the acoustic impedance ratio of the interface materials. For the case of pavements, the depth to the flaw is unknown. Typically, however, flaws that develop will be air-filled voids or delaminations that act virtually as total reflectors of incident wave energy. The boundary conditions, therefore, are such that there is no stress at either interface and the pavement acts as a " free-free" system. For a "free-free" system, the wavelength at first-mode resonance is related to the depth to the interface (d) by the following equation:

$$\lambda = 2d \quad (3.6)$$

Therefore, not only can the presence of a flaw in the pavement be detected with the impact-echo method, but the depth to the flaw can be calculated from combining Equations 3.5 and 3.6 to give:

$$d = v / (2 * f) \quad (3.7)$$

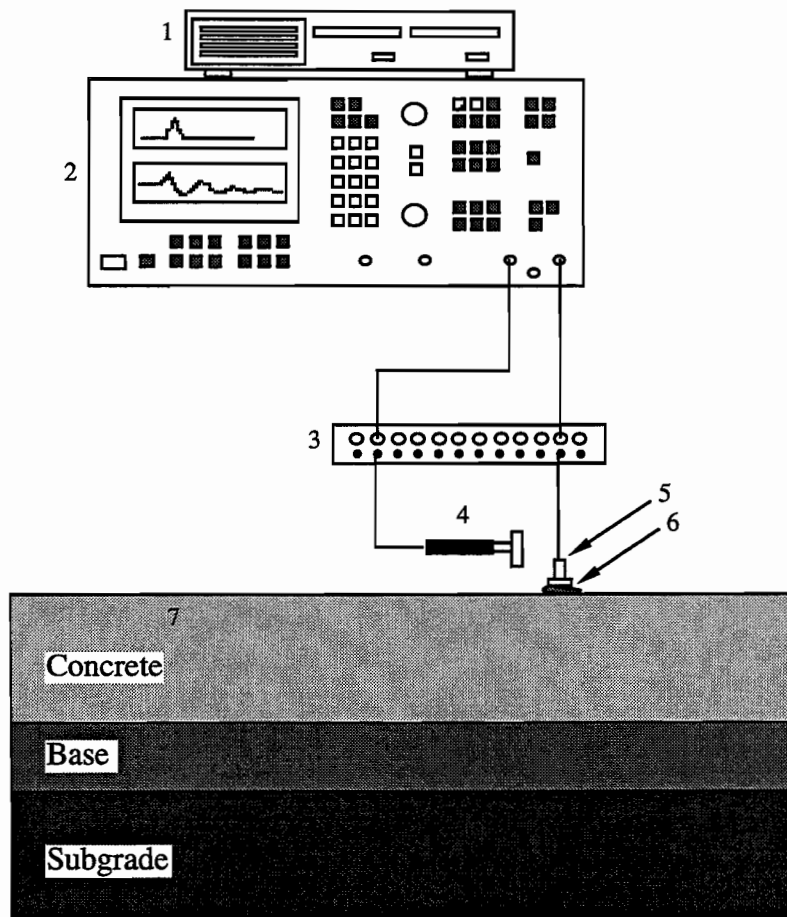
Evaluation of the depth to the flaw - in addition to detecting the flaw - is a strong attribute of the impact-echo method. However, accurate evaluation of the flaw depth requires that the compression wave velocity in the concrete (v_p) at that location be known or assumed. The velocity in the concrete may vary from one location to the next depending on concrete strength, age and deterioration.

3.3 IMPACT-ECHO TESTING METHODOLOGY

Field testing using the impact-echo method was performed at the four locations described in Section 3.4. Discussions of the experimental arrangement, equipment used and data reduction procedures are included in this section.

3.3.1 Testing Procedure and Equipment

The general testing arrangement and equipment for the impact-echo test is shown in Figure 3.2. Several devices were used as sources for the impact-echo tests performed herein. Two instrumented PCB hammers were used for the majority of the tests. The PCB 086 B01 hammer weighs approximately 0.1 kg and has an aluminum head with a diameter of 1.52 cm. This hammer



1. Hewlett Packard 9122 Disk Drive
2. Hewlett Packard 3562A Dynamic Signal Analyzer
3. PCB 483A07 Multi-Channel Power Unit
4. PCB 086B01 Instrumented Impact Hammer or
PCB 086C80 Instrumented Impact Hammer
5. PCB 303A12 Accelerometer
6. PCB 080A24 Mounting Wax
7. Portland Cement Concrete Slab

Figure 3.2 Impact-Echo Test Arrangement and Equipment

is capable of exciting vibrational frequencies that range to approximately 10 kHz. The hammer is instrumented with a load cell with a sensitivity of 12 mV/N to transform the force of the hammer to an electrical signal. The output from this load cell is used to determine the frequencies that were generated by the hammer impact. The resonant frequency of the hammer is 31 kHz. The smaller PCB 086 C80 hammer has a weight of 0.002 kg and a steel head with a diameter of 0.64 cm. This hammer will excite frequencies that range to approximately 20 kHz. The load cell in this hammer has a sensitivity of approximately 23 mV/N. In some cases steel ball bearings with diameters ranging from 0.32 to 2.54 cm were also used as sources. A PCB 303A12 accelerometer with a weight of 3.5 g, a diameter of 7.1 mm, a sensitivity of approximately 100 mV/g, and a resonant frequency of approximately 75 kHz was used as the receiver in all cases. The output from the source (if an instrumented hammer was used) and the receiver were passed through a PCB 483A07 multi-channel power unit. The output from each channel of the power unit was recorded with a Hewlett Packard 3562A Dynamic Signal Analyzer.

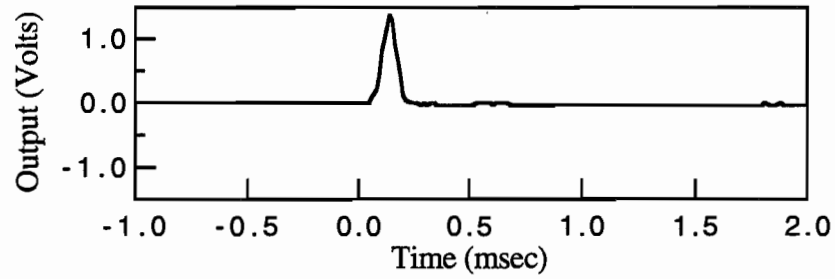
3.3.2 Data Reduction Procedures

The data from each test was collected using the Hewlett Packard 3562A Dynamic Signal Analyzer. This analyzer is capable of single or dual-channel measurements, with a measurement frequency range of 64 μ Hz to 100 kHz. The analyzer samples 2048 points in each time window and is equipped with a Fast Fourier Transform (FFT) algorithm to convert time-domain representations of records to frequency-domain representations. Results from the impact-echo test are interpreted using the frequency-domain representation of the data.

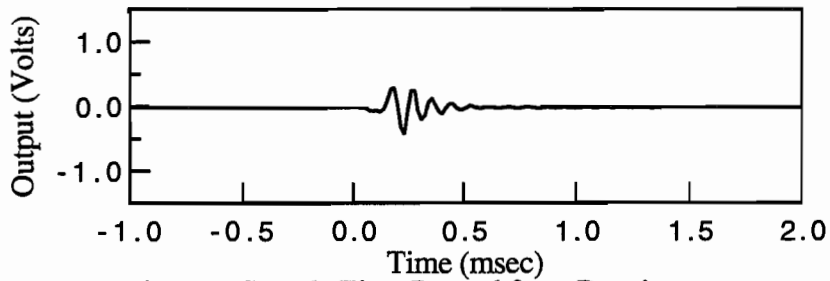
The following is an explanation of the five representations of data that are used throughout this work. The data were generated for testing performed on concrete pavements using the testing arrangement shown in Figure 3.2.

3.3.2.1 Time Records: Time records are plots of the voltage output from a transducer - either source or receiver - as a function of time. Typical time plots from an impact hammer and receiver are shown in Figure 3.3 a and 3.3b.

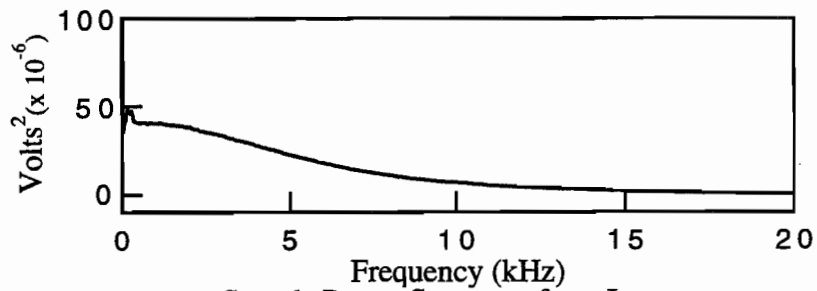
3.3.2.2 Power Spectrum: The power spectrum is the frequency domain representation of a time record displayed in terms of voltage output versus frequency. The power spectrum is defined as the following:



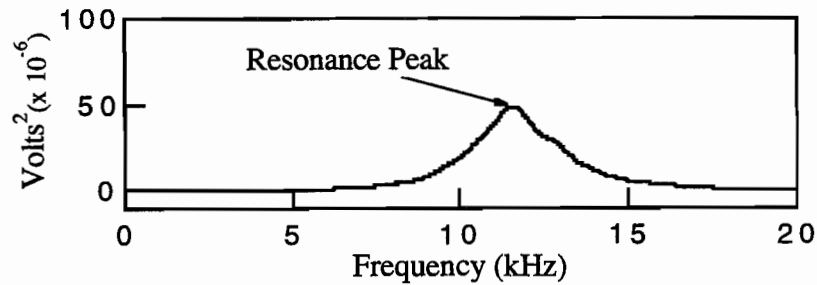
a. Sample Time Record from Impact Hammer



b. Sample Time Record from Receiver



c. Sample Power Spectrum from Impact



d. Sample Power Spectrum from Receiver

Figure 3.3 Sample Records from an Impact-Echo Test

$$G_{xx} = F_x F_x^* \quad (3.8)$$

where F_x = linear spectrum (FFT of time record), and
 F_x^* = complex conjugate of the linear spectrum.

Because the power spectrum is the product of the linear spectrum with its complex conjugate, the imaginary term in the record is lost, and the power spectrum contains only amplitude information and no phase information. The power spectra of the time records shown in Figures 3.3a and 3.3b are shown in Figures 3.3c and 3.3d. The primary use of the power spectra is to show the energy distribution of a record as a function of frequency to identify any resonance peaks, as shown in Figure 3.3d.

3.3.2.3 Cross Spectrum: The cross spectrum, G_{xy} , shows the amplitude product of two spectra (i.e. channels 1 and 2) and the phase difference between them. It is computed from:

$$G_{xy} = F_x^*(F_y) \quad (3.9)$$

where F_x^* = Channel 1 linear spectrum complex conjugate, and
 F_y = Channel 2 linear spectrum.

One of the primary uses of the cross spectrum is to show the phase relationships between two receivers. Figure 3.4c shows the phase relationship between two receivers obtained from the time records shown in Figures 3.4 a and 3.4b.

3.3.2.4 Frequency Response: The frequency response, $H(f)$, is the ratio of the linear spectra of two signals. It is calculated as:

$$H(f) = G_{xy} / G_{xx} \quad (3.10)$$

where G_{xy} = cross spectrum, and
 G_{xx} = Channel 1 power spectrum.

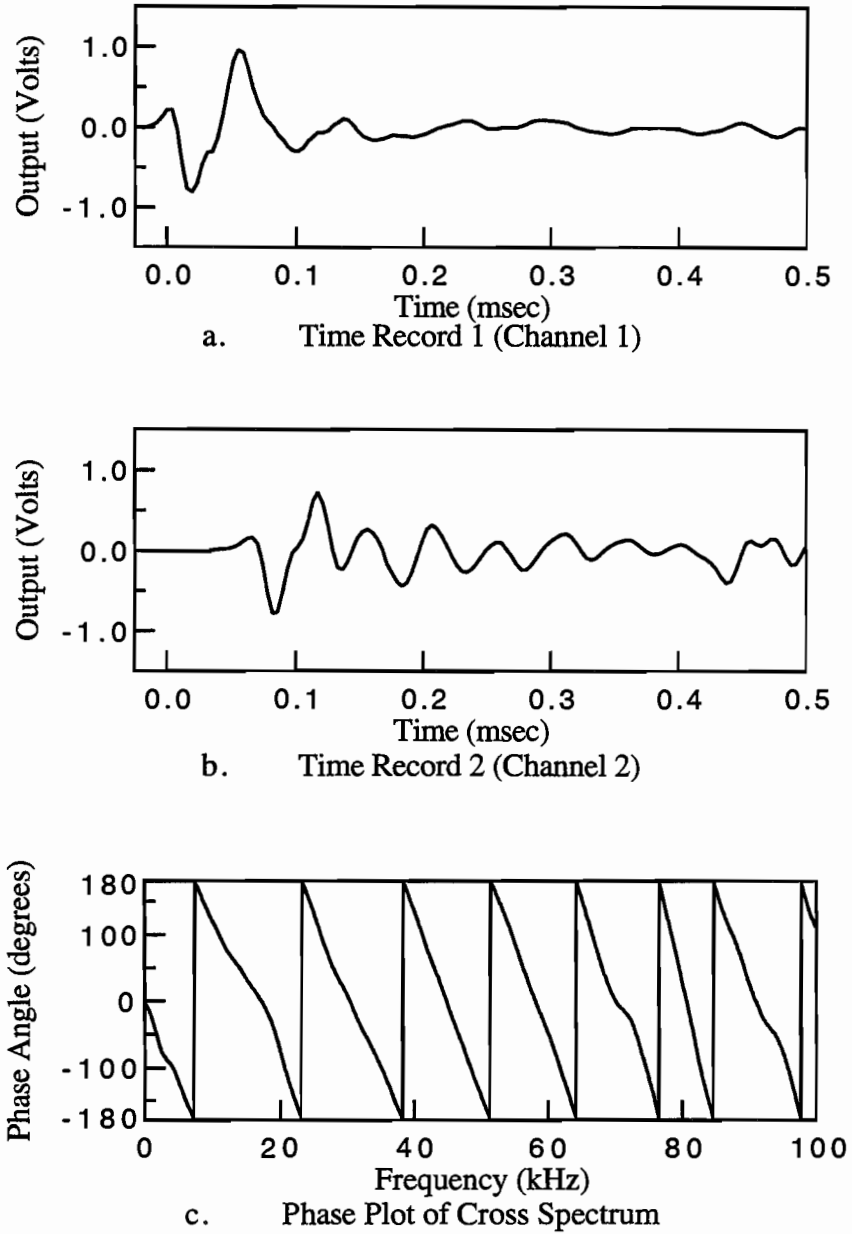


Figure 3.4 Sample Time Records and Cross Spectrum

The frequency response representation of data is useful as a means of normalizing the output of a receiver to the input from a source. Figure 3.5a shows the frequency response of the time records shown in Figures 3.3a and 3.3b. The received signal is normalized with respect to the energy content of the impact.

3.3.2.5 *Coherence*: The coherence spectrum shows the portion of the output power spectrum that is related to the input spectrum. It is calculated from:

$$\gamma^2 = G_{xy} G_{xy}^* / G_{xx} G_{yy} \quad (3.11)$$

where G_{xy} = cross spectrum,
 G_{xy}^* = complex conjugate of cross spectrum,
 G_{xx} = Channel 1 power spectrum, and
 G_{yy} = Channel 2 power spectrum.

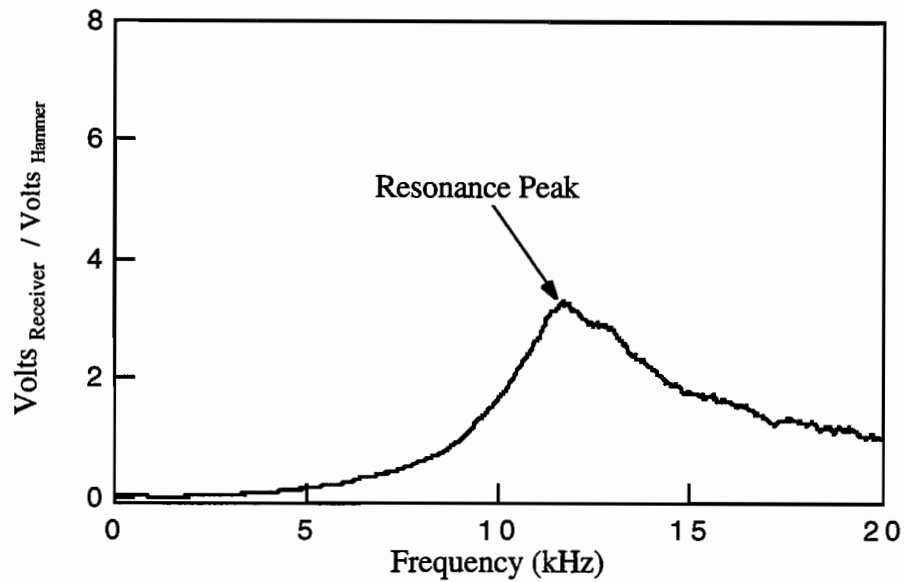
Coherence is measured on a scale of 0 to 1.0, where 1.0 indicates perfect coherence. Low coherence values are caused by extraneous noise, system non-linearities and uncorrelated input signals. The coherence record for the frequency response shown in Figure 3.5a is shown in Figure 3.5b.

3.4 TESTING SITE DESCRIPTIONS

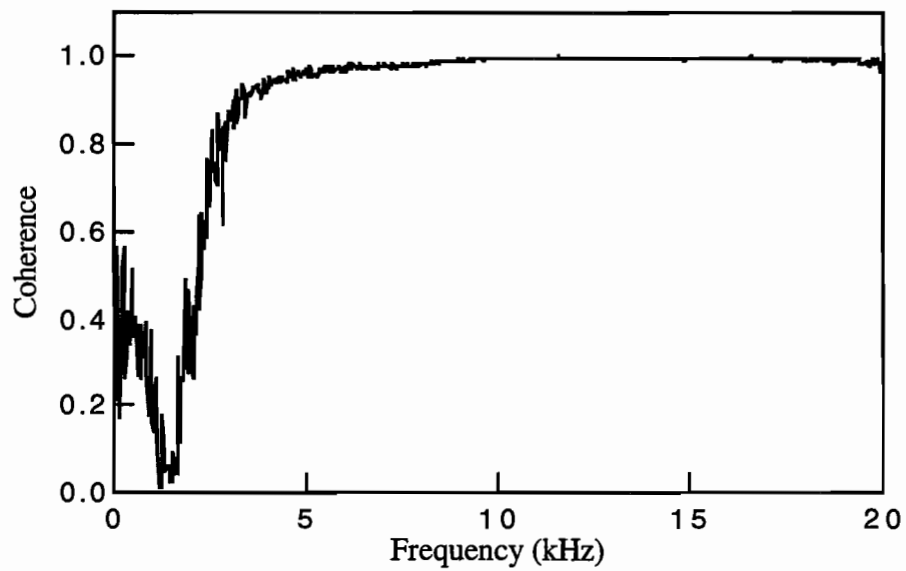
Three sites were used for experimental stress wave testing on concrete pavements. All of the experimental results presented in this report are from these three sites which are described below.

3.4.1 Site 1: Test Slab in Ernest Cockrell Jr. Hall (ECJ)

Impact-echo testing was performed on a Portland cement concrete slab located in the basement of Ernest Cockrell Jr. Hall at The University of Texas at Austin. The test slab, shown in Figure 3.6, is 3.05 m long, 1.22 m wide, and 50.8 cm thick. The test slab was constructed for use in evaluating test methods employing stress waves. Two, 5.08-cm square "tunnels" with crown depths of 2.54 cm and 7.0 cm were constructed in the slab, with their exposures on the east

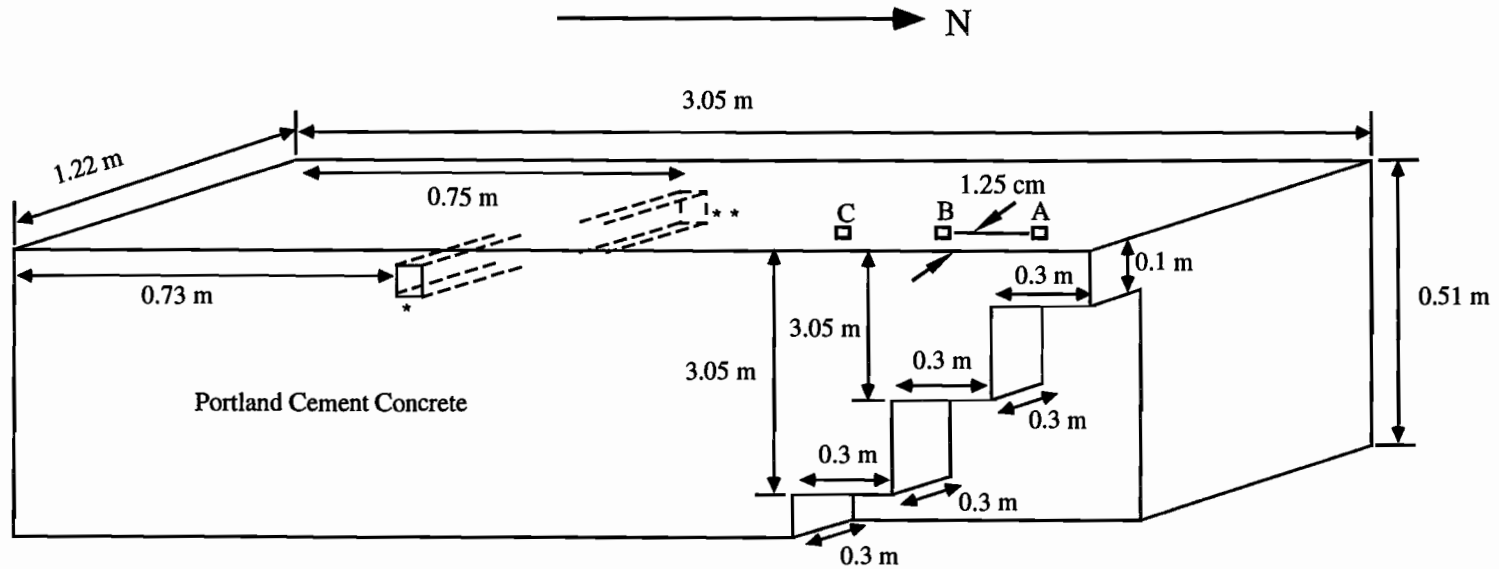


a. Frequency Response



b. Coherence

Figure 3.5 Sample Frequency Response and Coherence Plots



- * 5.0 cm Square Tunnel Extending 0.61 m into Slab from East Edge
Crown Depth = 2.54 cm
Center at 0.72 m from South End of Slab
- ** 5.0 cm Square Tunnel Extending 0.61 m into Slab from West Edge
Crown Depth = 7.0 cm
Center at 0.74 m from South End of Slab

Figure 3.6 Site 1, Concrete Test Slab in Basement of ECJ

and west ends of the slab, respectively. Each tunnel is located approximately 76.2 cm from the south end of the slab, and extends to approximately 1/2 the width of the slab. On the north-east corner of the slab, three stepped sections were formed in the slab as shown in Figure 3.6. The stepped sections are each 0.305-m square, with depths of 10.2 cm, 25.4 cm, and 40.0 cm. The entire slab is underlain with a layer of plywood.

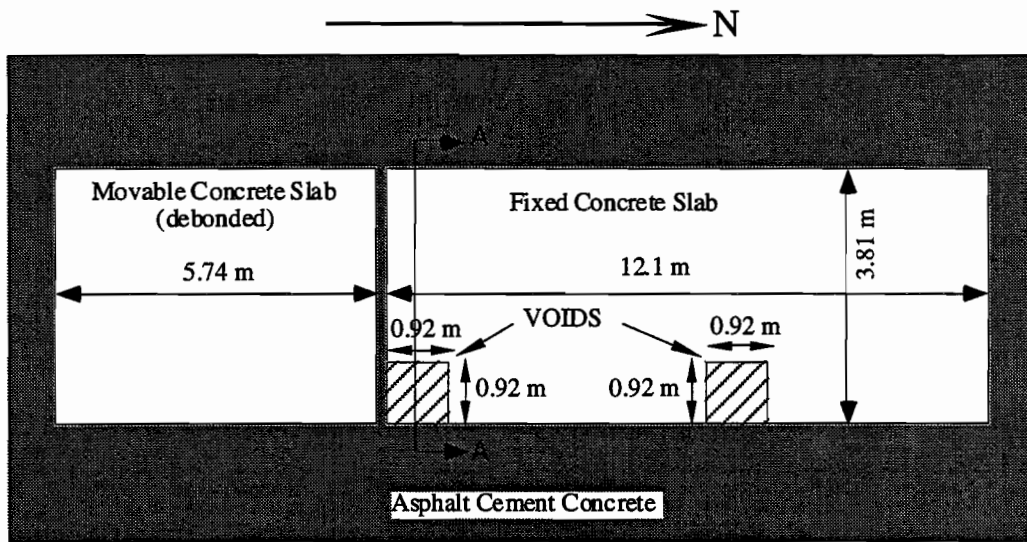
3.4.2 Site 2: Center for Transportation Research (CTR) Test Pavement

Testing was performed on a Portland cement concrete test pavement at the Pickle Research Center at the University of Texas at Austin. The pavement area was constructed by CTR and consists of a movable slab that is 5.75 m long and 3.81 m wide, and a fixed slab that is 12.15 m long and 3.81 m wide, as shown in Figure 3.7a (Ref 32). The pavement profile for both slabs consists of 25.4 cm of Portland cement concrete, 7.62 cm of asphalt, and 15.24 cm of crushed stone subbase, as shown in Figure 3.7b. The concrete layer in the movable slab is underlain by a thin layer of plastic to represent debonding of the pavement. A 0.92-m square void was created below the rigid pavement layer in the fixed slab. The void was created by placing foamed styrene into a preformed void. After the surface layer was placed and set, the styrene was dissolved with a solvent. The void was 2.54 cm thick. Because the void is below the surface layer, the depth to the void interface is the same as the thickness of the surface layer, 25.4 cm.

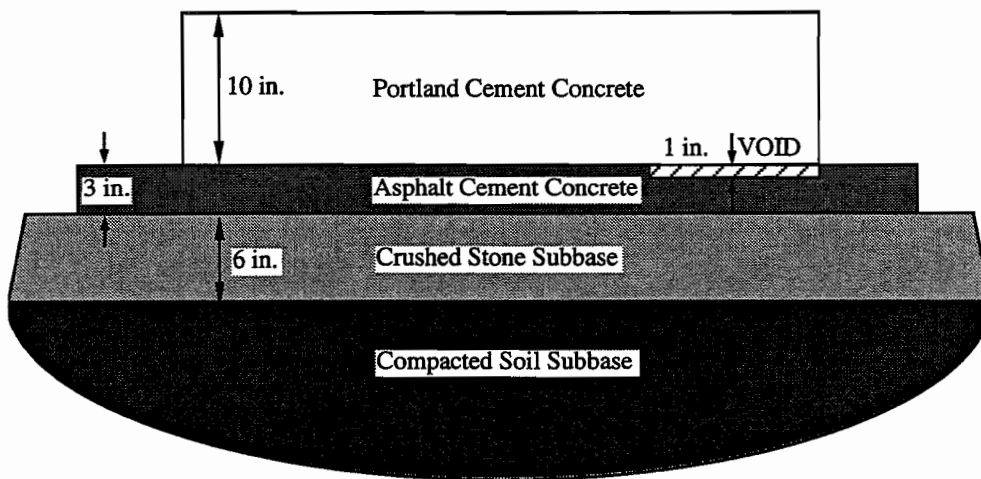
3.4.3 Site 3: Texas Transportation Institute (TTI) Test Pavement

The TTI test facility is located at Texas A&M University on the Riverside campus. The test facility consists of two rigid pavement sections. The first section consists of 17.8 cm of Portland cement concrete, 10.2 cm of cement treated base, and 15.2 cm of lime stabilized subgrade, as shown in Figure 3.8. The rigid surface layer in this case is debonded from the underlying cement-treated base.

The second pavement consists of 0.305 m of Portland cement concrete underlain by 10 to 13 cm of asphalt, as shown in Figure 3.9. In both slabs, a 0.92-m square void was constructed at the midpoint of one edge of the pavement. The void in both cases is 1.27 cm thick and was cast into the bottom of the surface layer. The thicknesses of the pavement over the void in these cases are 16.5 and 29.2 cm, respectively. A 1.22-m square void was also constructed in each pavement into the bottom of the concrete surface layer. These voids are 2.54 cm thick and filled with styrofoam. The thicknesses of the pavement over these voids are 15.2 and 25.4 cm, respectively.

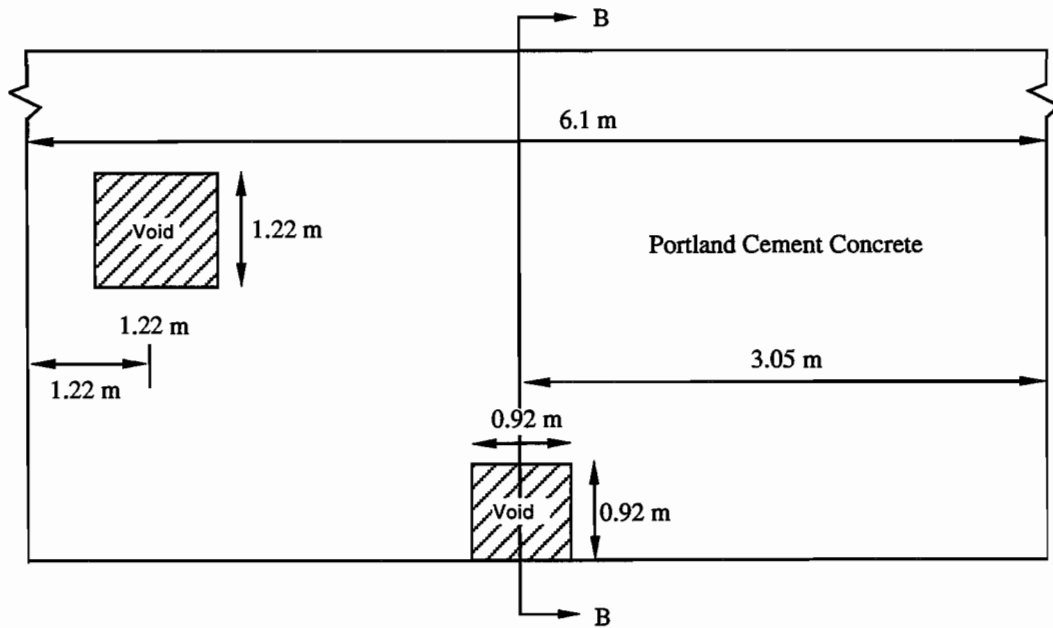


a. Plan View

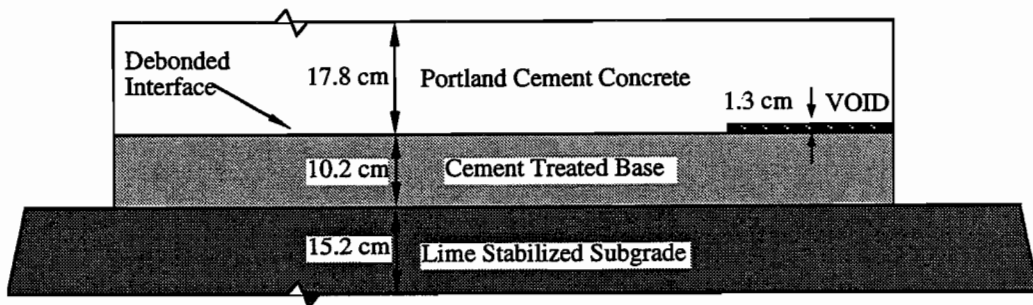


b. Cross-Section AA

Figure 3.7 Plan and Cross-Sectional Views of Site 2, CTR Test Pavement

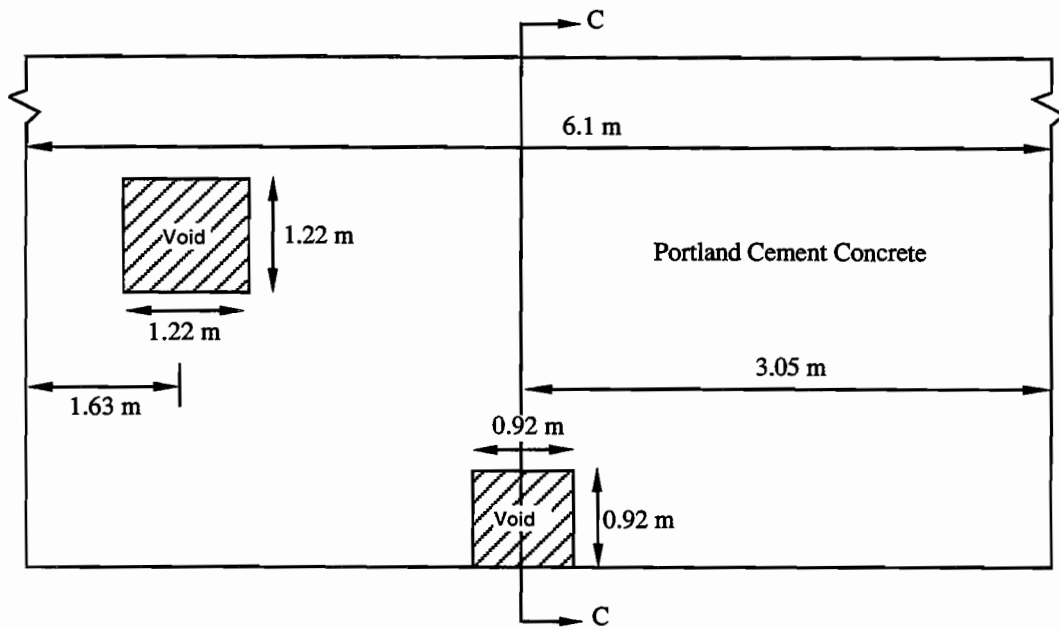


a. Plan View

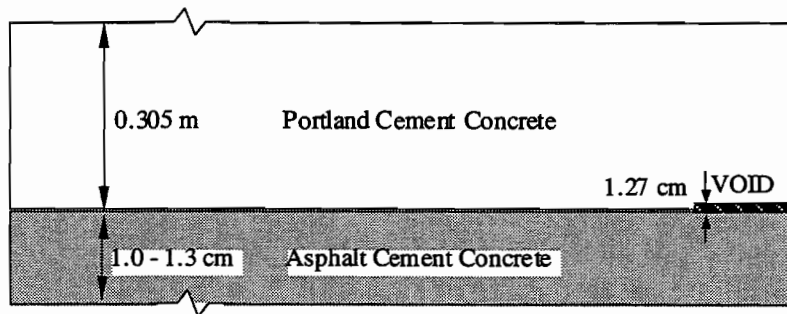


b. Cross-Section BB

Figure 3.8 Plan and Cross-Sectional Views of 0.178-m Thick Concrete Test Pavement at TTI



a. Plan View



b. Cross-Section CC

Figure 3.9 Plan and Cross-Sectional Views of 0.305-m Thick Concrete Test Pavement at TTI

In both slabs, the voids are located with the center of the void at a distance greater than 1.2 m from the edge of the slab. Plan views of both slabs with the void locations shown are presented in Figures 3.8 and 3.9 for the 17.8-cm and 30.5-cm thick slabs, respectively.

3.5 SUMMARY

The impact-echo method is a nondestructive stress-wave based method that utilizes compression wave resonance to detect flaws in a concrete structure. The impact-echo method has been used successfully to detect many irregularities in concrete slabs. Therefore, it was considered for implementation into a rolling device for project-level rigid pavement testing. If the velocity of the compression wave in the material is known or assumed, the depth to the flaw can be calculated from the resonant frequency. The resonant frequency is determined from the peak in the power spectrum or frequency response plots. The test is performed with an impact source and an accelerometer or displacement receiver to measure vibrations. Experimental impact-echo tests were performed at three test sites. Each of these sites is described in this chapter. The experimental results along with results from finite element models are presented in Chapter 4.

CHAPTER 4.

ANALYTICAL AND EXPERIMENTAL RESULTS FROM IMPACT-ECHO TESTING

4.1 INTRODUCTION

Experimental impact-echo tests were performed at the three sites described in Section 3.4. These tests were site-specific and were performed with a stationary source and receiver. The tests were performed in order to study the factors affecting the vibrational response of the pavement over various flaws. This study was needed before the impact-echo method could be integrated into a rolling system. The factors affecting the impact-echo testing on pavements can be divided into two general categories: physical characteristics of the pavement system, and testing procedures and methodology. Experimental testing allowed for evaluation of important factors affecting the impact-echo results. Numerical modeling was used for both comparison and augmentation of the experimental results.

4.2 EFFECTS OF PHYSICAL CHARACTERISTICS OF PAVEMENT STRUCTURE

The reliability and effectiveness of impact-echo testing is greatly dependent on the physical characteristics of the pavement structure. Variables such as flaw depth, flaw size, and pavement characteristics affect the impact-echo results. The following is a discussion of the conditions within a pavement that affect the results of the impact-echo test.

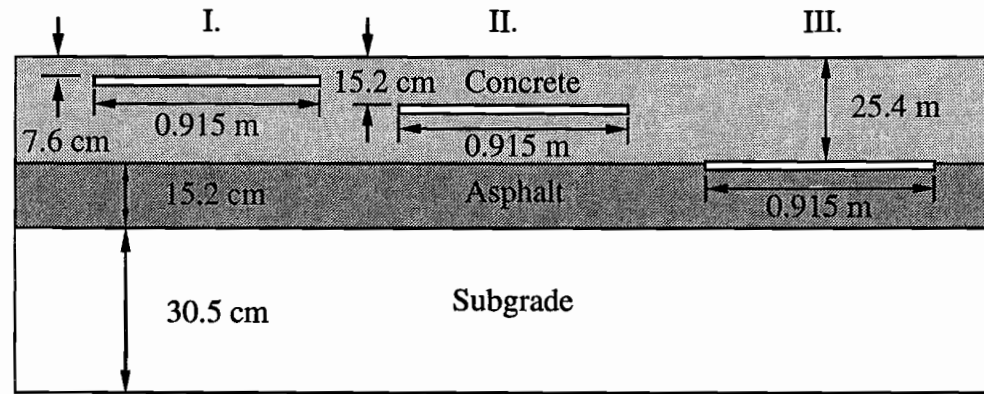
4.2.1 Effect of Void Depth

Flaws in pavements may occur at any depth in the pavement system. Typically, however, voids develop directly below the rigid surface layer and delaminations develop at a depth near the reinforcing steel, as discussed in Chapter 2. From Equation 3.7, it is observed that the resonant frequency is a function of both the depth to the void and the wave velocity through the propagating medium. One of the assumptions that is employed for the impact-echo test is that the

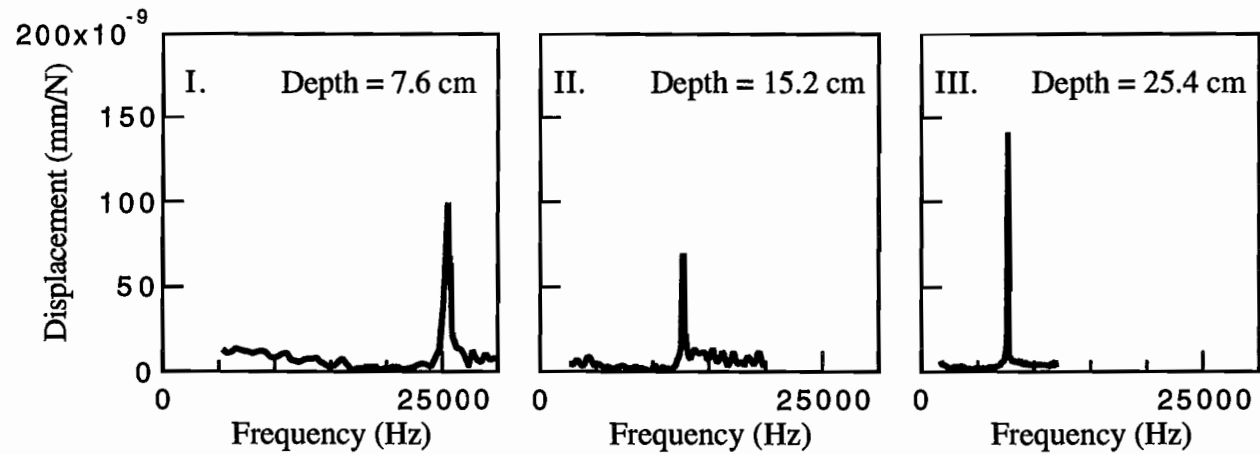
compression wave velocity of the pavement is known. The actual compression wave velocity may vary within a pavement. Except for the case of deteriorated concrete, the compression wave velocity can generally be approximated in the range of 3600 to 4270 m/s. Therefore, using Equation 3.7, the approximate expected resonant frequency in Hz can be calculated as: 4000 m/s divided by twice the depth to the void. For example, a 25.4-cm thick slab will resonate at a frequency between 7.2 to 8.4 kHz.

The results of finite element tests performed for three identical voids at three different depths in a typical pavement system are shown in Figure 4.1. The results are presented in terms of the frequency response, as defined in Section 3.3.2.4. The y-axis in these plots is shown in terms of displacement per unit of applied force, which is typically termed flexibility. It is observed that the results from the finite element model demonstrate the behavior described by Equation 3.7. If no reflecting interfaces were present in the material, the frequency response would contain no dominant frequency, and the response would be flat across the entire spectrum. When voids or flaws are present, a dominant frequency represented by a distinct peak is observed in the frequency response plot. Shallow voids, such as void I, are identified by a high-frequency resonance peak. As the depth to the void increases, however, the resonant frequency decreases proportionally. This behavior is one of the benefits of the impact-echo method, in that based on a measured frequency and an assumed or measured compression wave velocity of the concrete (v_p), the depth to a flaw can be determined.

Experimental impact-echo tests were performed in the field at Sites 1, 2 and 3, described in Section 3.4. Each test facility contained a flaw interface that reflected some of the incident energy. The depths to the interface in these cases varied from 16.5 cm to 50.8 cm. Figures 4.2a through 4.2c show the frequency responses obtained from tests performed directly over reflecting surfaces at Sites 1 through 3, respectively. As described in Section 3.3, the surface movements were measured in terms of acceleration. To present the data in units of flexibility, the output of the accelerometer was integrated twice to obtain displacement, and the source and receiver were multiplied by the appropriate calibration factors to get units of force and displacement, respectively. The displacement spectrum was then divided by the force spectrum. As expected, the resonant frequencies that were measured were generally consistent with the resonant frequencies predicted by Equation 3.7. The deepest interfaces produced resonances that were at lower frequencies than the interfaces that were closer to the surface. Although the values of the resonant frequencies were as predicted, the magnitude of the resonant peaks varied greatly from one test to another. Several other factors, in addition to the depth to the interface, help to explain the difference in amplitude, as discussed in the following sections.



a. Rigid Pavement Model with Voids at Three Different Depths



b. Frequency Response from Impact-Echo Tests

Figure 4.1 Results from Numerical Modeling of Impact-Echo Testing of a Void at Various Depths in a Rigid Pavement (Ref 33)

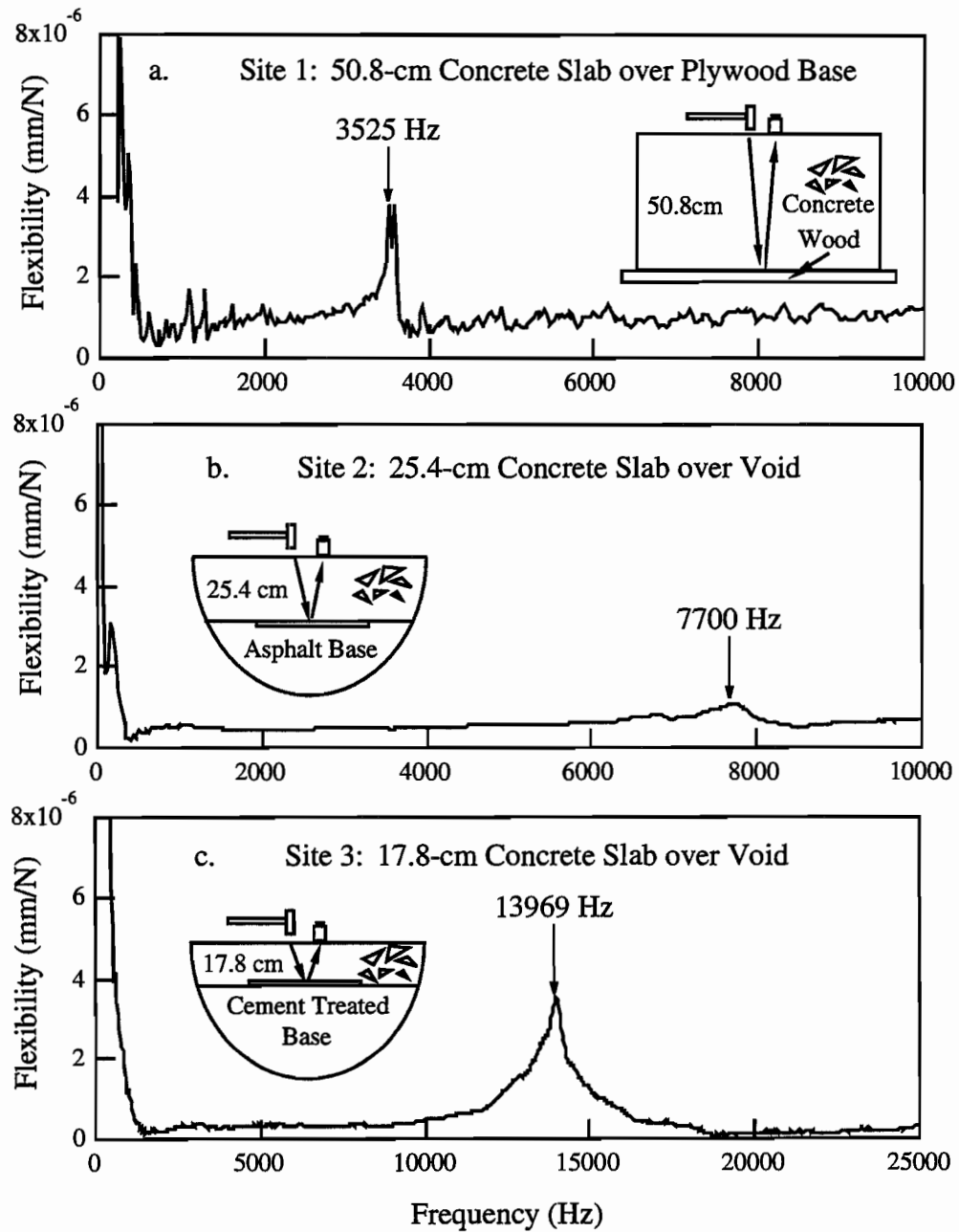


Figure 4.2 Frequency Responses from Impact-Echo Tests of Concrete Slabs with Reflection Interfaces at Different Depths

4.2.2 Effect of Acoustic Impedance Ratio

When a stress wave propagating in a material contacts an interface with another material, a reflected wave and a transmitted wave are created, as illustrated in Figure 4.3. The amount of energy that is reflected from the interface is a function of the acoustic impedance ratio between the two materials. The acoustic impedance of a material is defined as the product of the mass density (ρ) and the stress wave propagation velocity (v). For a one-dimensional wave, the magnitude of the reflected wave, $r(t)$, as a function of the incident wave, $i(t)$, is:

$$r(t) = [(1-K)/(1+K)] i(t) \quad (4.1)$$

where $K = \rho_2 v_2 / \rho_1 v_1$.

When the acoustic impedance of the second material is small relative to the impedance of the first material, virtually all of the energy from the incident wave is reflected back into the material, as indicated by Equation 4.1. An air interface in a concrete slab ($K=0$) is an example of such a condition. On the other hand, at an interface between two materials with the same value of acoustic impedance ($K=1$), Equation 4.1 shows that all of the wave energy will be transmitted into the second material. Interfaces between pavement layers represent a case between the two extremes described above. For this case some portion of the energy is transmitted and some of the energy is reflected towards the surface. Figure 4.4 shows results from a finite element model of impact-echo testing on a concrete slab with three different conditions of acoustic impedance ratios. Figure 4.4a shows the results for the case where the ratio of acoustic impedance is approximately 0.73 (this contrast can be considered to represent a concrete surface layer over a cement treated base). In this case, no resonant peak is observable and the frequency response is fairly flat across the entire frequency range. In Figure 4.4b, the K value has been decreased to approximately 0.47 (this contrast can be considered to represent a concrete surface layer over an asphalt base). In this case, enough incident energy is reflected such that a small broad peak is observed around 11,000 Hz. Figure 4.4c shows the response for the case of an air void under the surface layer. In this case, a clear, high-magnitude, resonant peak is observed at a frequency of 12,000 Hz. This model illustrates how an air void under a pavement can be detected using the impact-echo method.

To use the impact-echo method to differentiate air voids under a concrete pavement from a sound pavement system, the acoustic impedance ratio between the concrete and the base material must not be too small. If the ratio is very small, the difference in magnitude between reflections

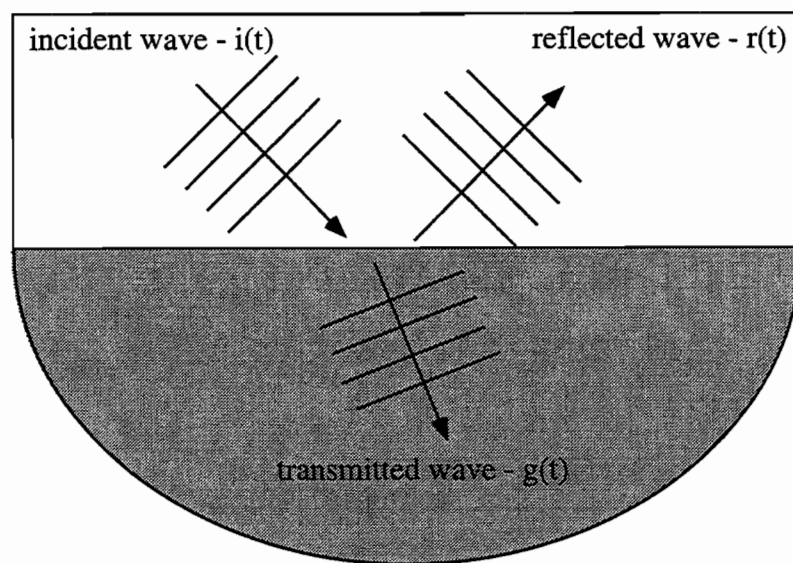


Figure 4.3 Behavior of a Stress Wave at an Interface of Two Materials with Different Acoustic Impedances

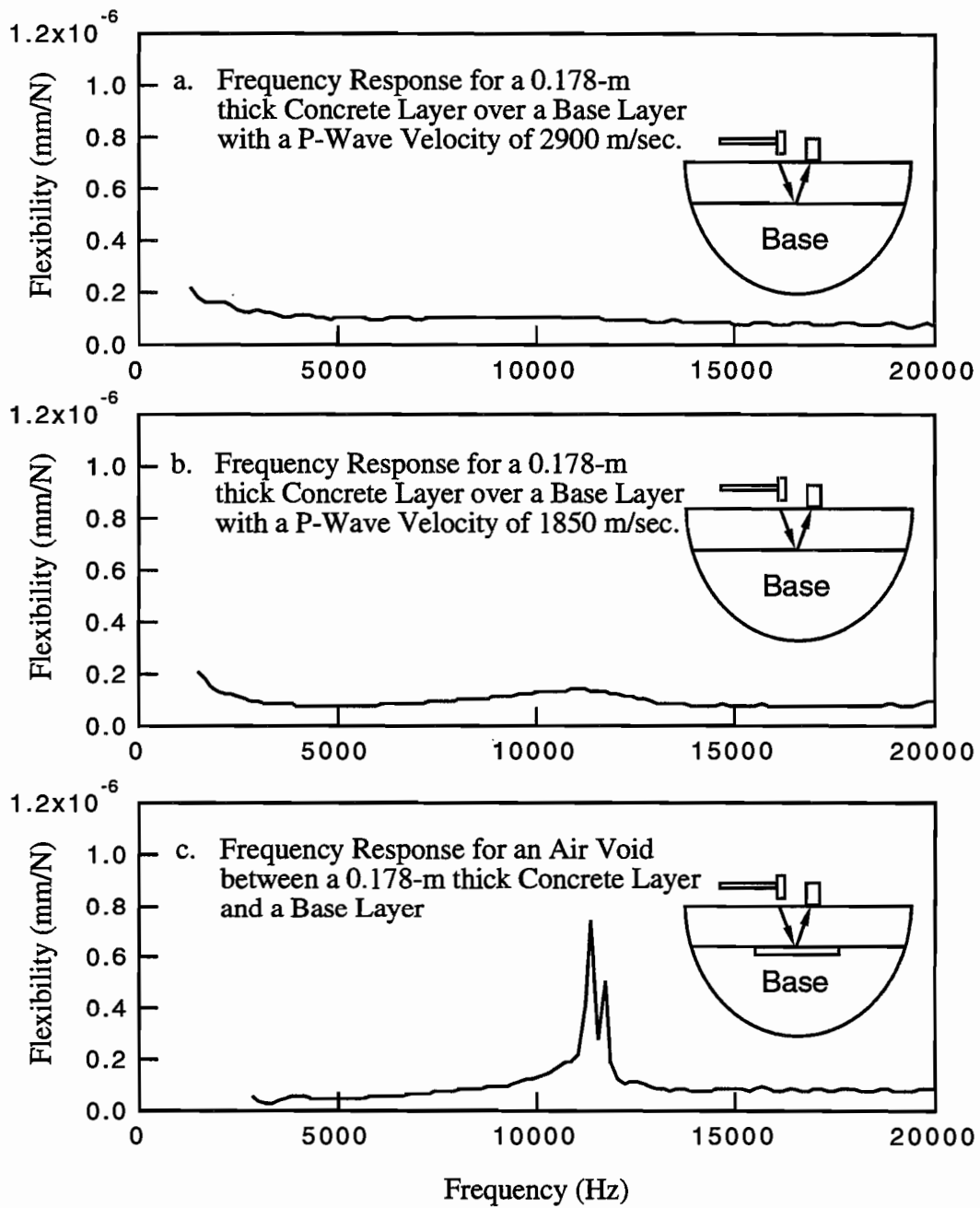


Figure 4.4 Effect of the Stiffness Properties of the Base Layer on Impact-Echo Testing of a 0.178-m Thick Concrete Surface Layer (after Ref 33)

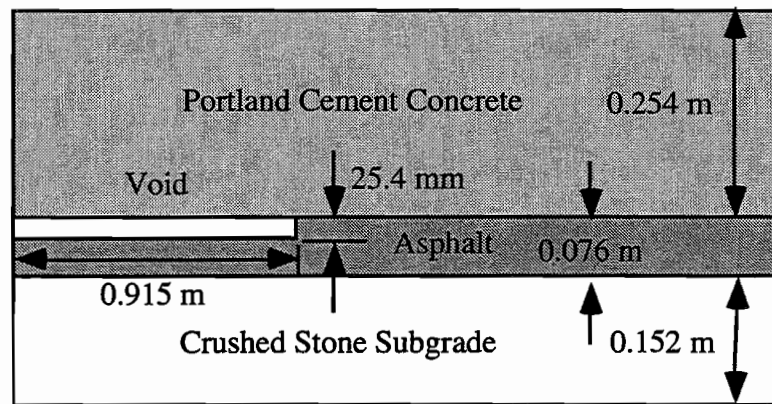
from a sound base material and from a void under the surface layer may not be large enough to be detected.

Experimental tests were performed at several locations on the 25.4-cm thick slab at Site 2. Tests were performed over areas of sound pavement and over the corner void in the pavement, as shown in Figure 4.5. The sound pavement and the void region represented two conditions of acoustic impedance ratio values. Figures 4.6a and 4.6b show the results from two tests, one over the center of the void (location C2), and one over the sound pavement (location I2). The frequency response from the test over the sound pavement is fairly flat with no dominant frequency peak. This flat response is due to the similarity of acoustic impedance values of the two materials which allows little energy to reflect to the pavement surface. Over the void, which is a strong reflector, a peak is measured at 7500 Hz, corresponding to the void depth of 25.4 cm, assuming a compression wave velocity of 3810 m/sec. Figure 4.7 shows a waterfall plot of frequency responses from a series of tests performed along the array A2-I2 (see Figure 4.5) which covers both the sound pavement and the region over the void. This plot demonstrates how the impact-echo method can be used to detect flaws under the rigid surface layer and to delineate their extent.

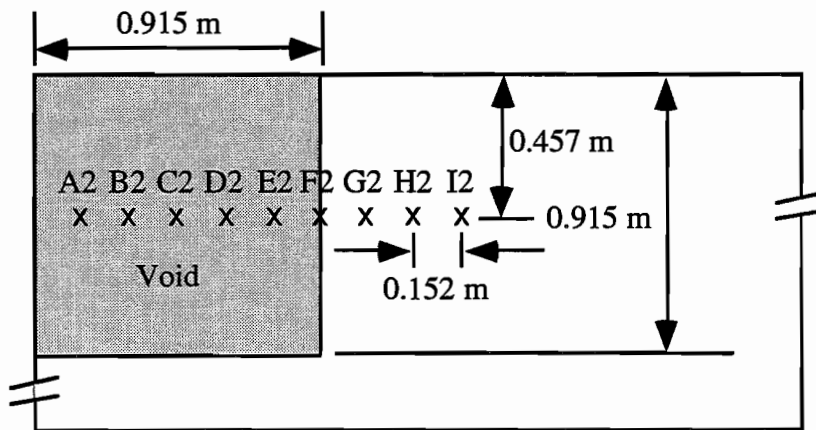
4.2.3 Effect of Size-to-Depth Ratio of the Void

The magnitude of the peak of the resonant frequency recorded from an impact-echo test over a flaw is also a function of the ratio of the lateral size of the void to the depth to the top of the void. As explained previously, the wavelength at first-mode resonance of a "free-free" system is equal to twice the depth to the reflecting interface. Therefore, deeper voids will resonate with longer wavelengths than shallow voids. Sansalone and Carino (1989) report that strong reflections occur only if the incident wavelengths are on the order of the size of the void, or smaller (Ref 22). Therefore, for deep voids to be detected, the void size must be large enough to reflect much of the incident energy at the resonant frequency.

To study the effect described above, tests would need to be performed on several voids of different sizes at the same depth within a concrete slab. Such a facility was not available for experimental testing. Experimental results were obtained for impact-echo tests performed on the three stepped sections located at Site 1. Each step has a bottom reflecting surface of 0.305-m square. The depth of steps A, B and C were 10.2 cm, 25.4 cm, and 40.0 cm, respectively. The ratios of the void size to void depth for steps A, B, and C, therefore, were 3, 1.2, and 0.76, respectively. Figure 4.8 is a plot of the frequency responses from tests performed at locations A, B and C shown in Figure 3.6. Based on Equation 3.7, resonant frequencies of 18.3, 7.3, and 4.6

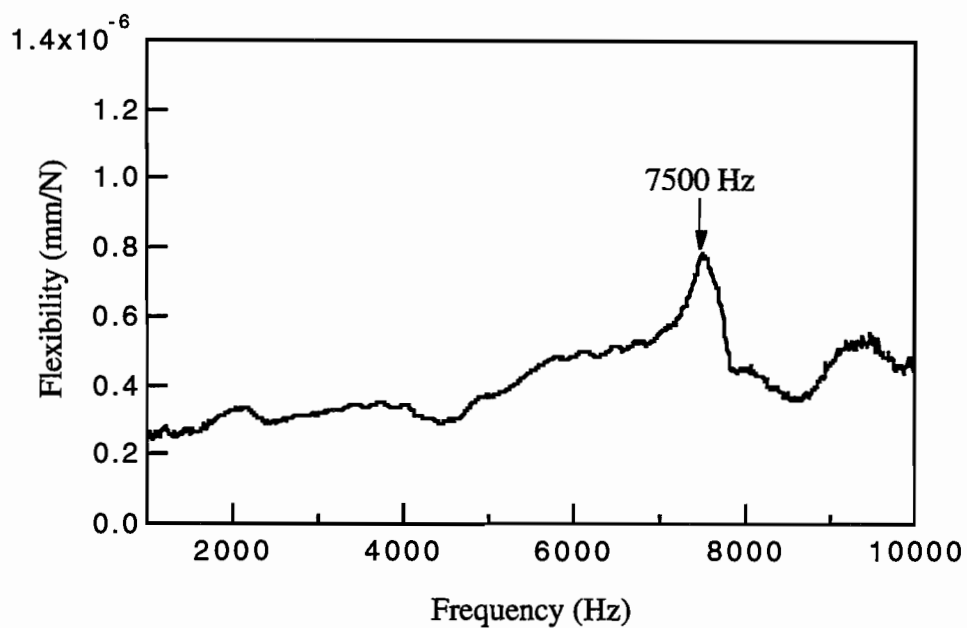


a. Profile View

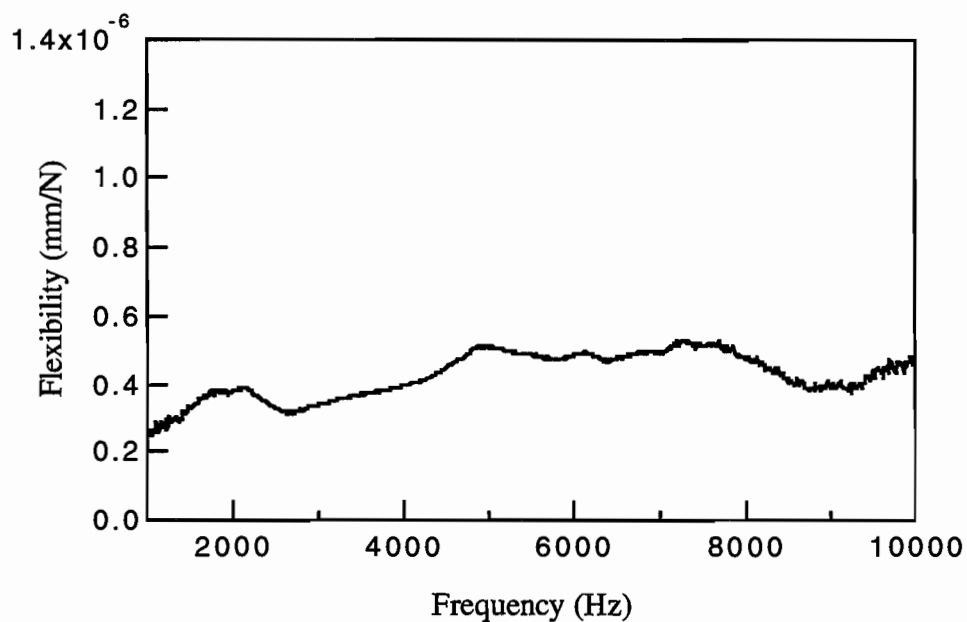


b. Plan View

Figure 4.5 Plan and Profile Views of Site 2 Test Pavement Facility at the CTR



a. Response over Location C2, as shown in Figure 4.5



b. Response over Location I2, as shown in Figure 4.5

Figure 4.6 Comparison of Frequency Responses from Tests over a Void and over Sound Pavement at Site 2

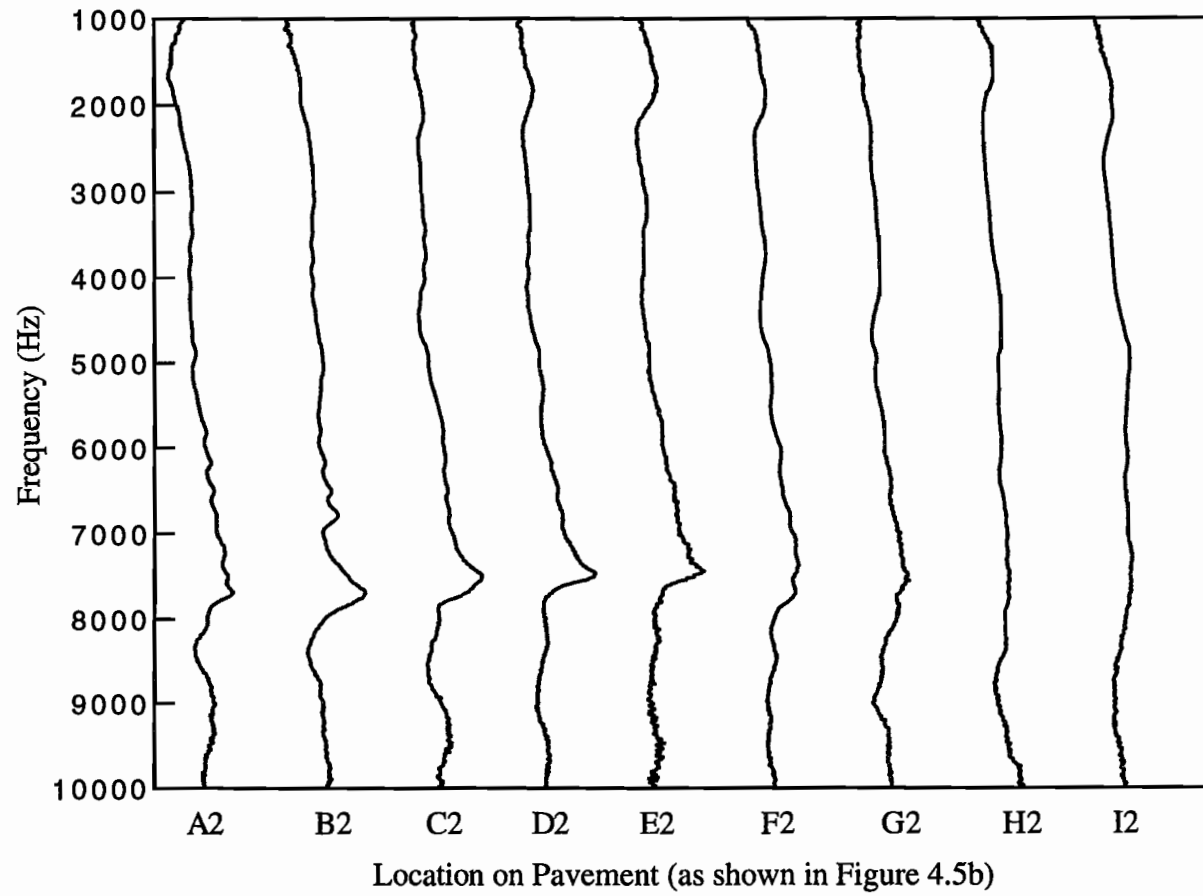


Figure 4.7 Composite Plot of Impact-Echo Testing along Array A2-I2 at Site 2, as shown in Figure 4.5

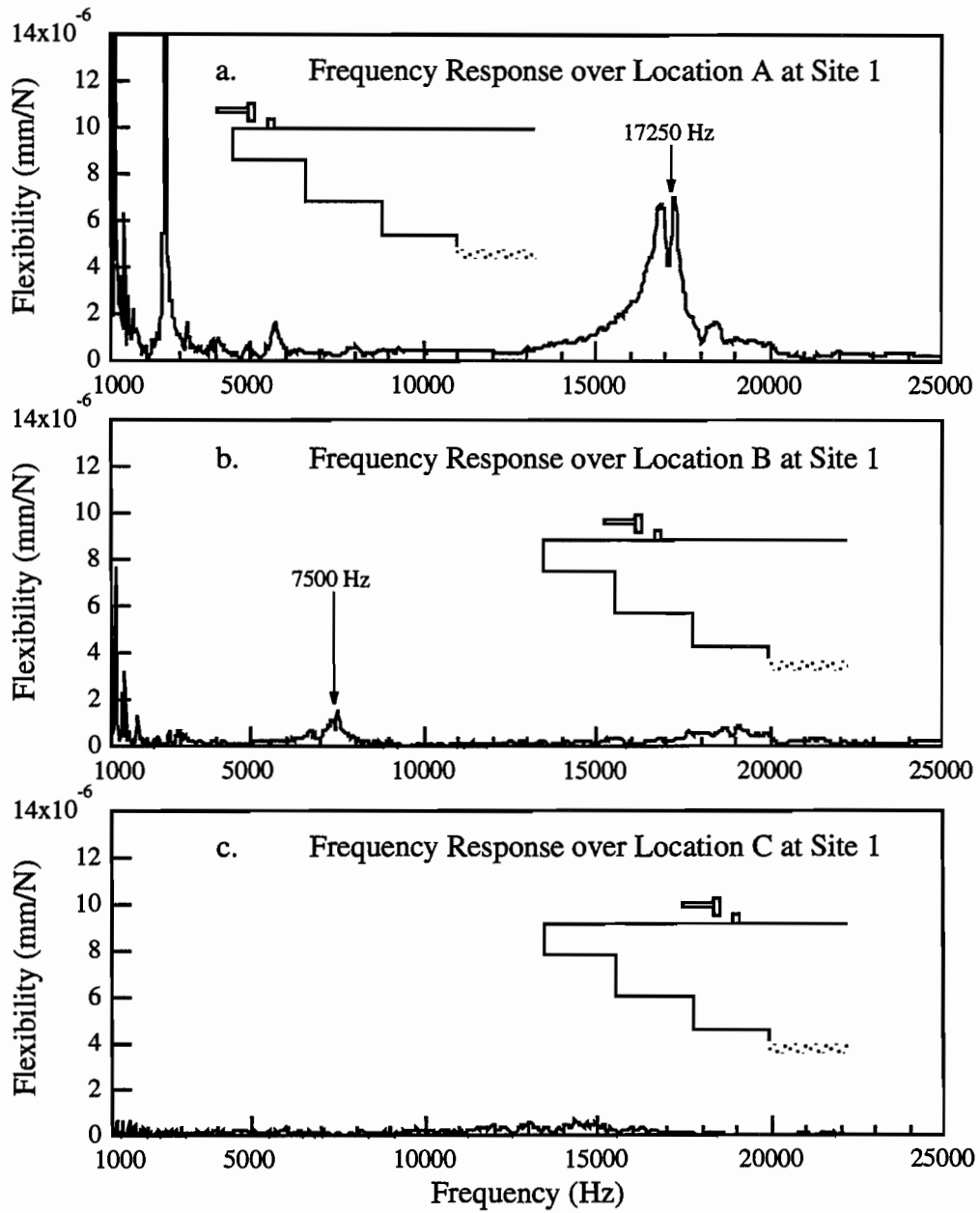


Figure 4.8 Frequency Responses from Impact-Echo Tests over Locations A, B, and C at Site 1

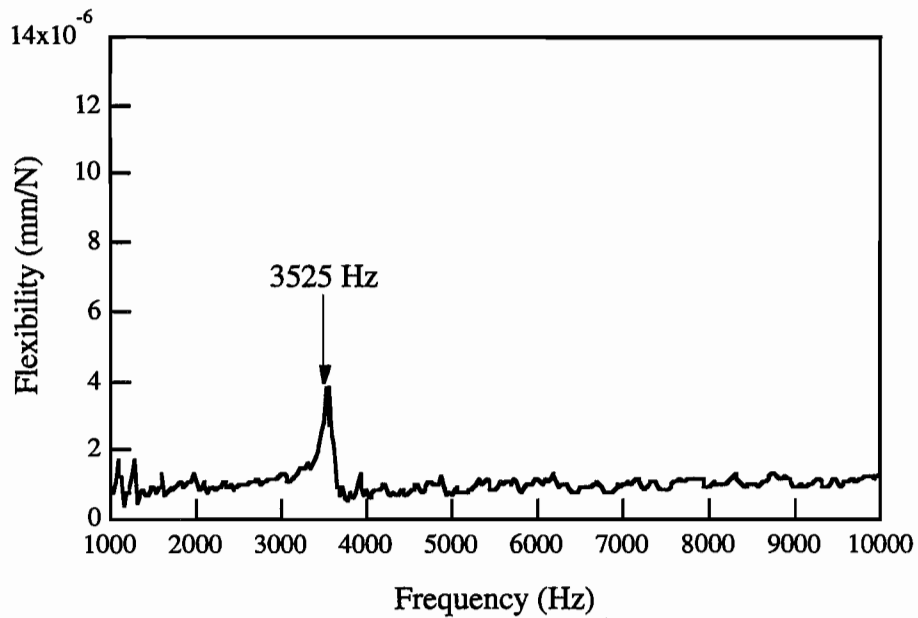
kHz are expected for steps A, B and C, respectively, assuming a P-wave velocity of 3720 m/sec. (from direct travel time measurements in the slab).

Figure 4.8a shows a resonant peak at a frequency of 17.25 kHz which is 5.7% less than the expected value of 18.3 kHz. In Figure 4.8b, a peak is present at 7.5 kHz which is within 2.4% of the expected value of 7.3 kHz. Although the frequency of the peaks agrees fairly well with the expected values, the magnitude of the peaks changes significantly. In Figure 4.8b, the magnitude of the peak is much less than the magnitude of the peak shown in Figure 4.8a. Furthermore, the response over location C, shown in Figure 4.8c, shows no clear peak at the predicted frequency of 4.6 kHz.

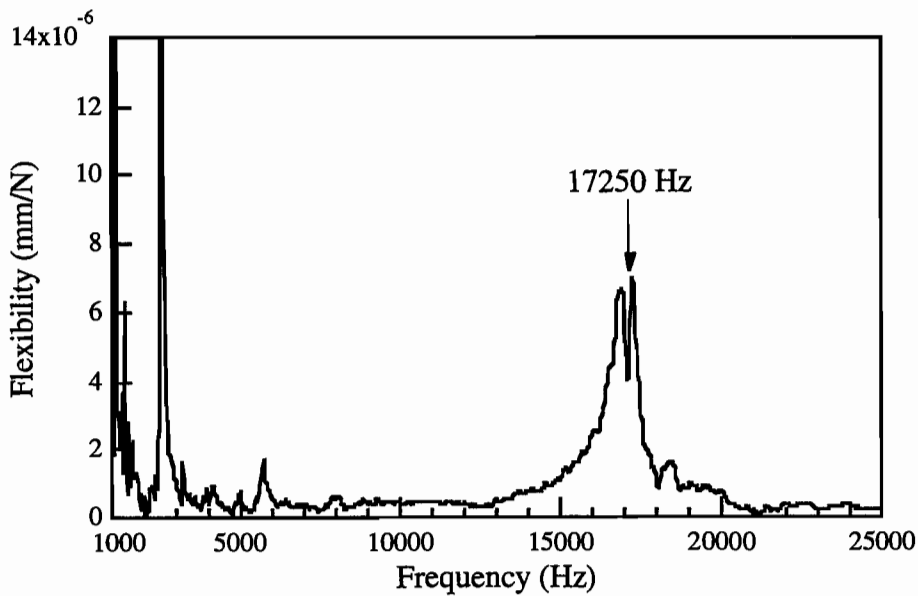
There are two factors that explain this trend. First, as the depth to the void increases, regardless of the size of the void, the magnitude of the resonant peak should decrease due to the larger volume of stressed material. This effect appears to be small based on a comparison of frequency responses from the test at location A and from a test performed over the full 50.8 cm thickness of the slab. This comparison, shown in Figure 4.9, shows that the magnitude of the resonance peak decreased only slightly (less than a factor of 2). The second factor is the ratio of the void size to the void depth. For location A, the ratio is 3, meaning that the void size was 1.5 times greater than the wavelength at resonance. Most of the energy, therefore, was reflected from the interface and a significant peak was observed. For location B, the ratio decreased to 1.2, meaning that the interface dimension was now only 60% as long as the wavelength at resonance. For step location C, the interface dimension was only 38% as long as the wavelength at resonance. Because the length of the wave exceeded the dimensions of the reflecting interface for steps B and C, the amount of energy reflected at resonance was reduced and the magnitude of the measured peak was diminished.

Interestingly, the ratio of void size to void depth for testing over the full depth of the slab could be approximated as 2.4, if the width of the slab is used as the void size. Hence, the void size was 1.2 times greater than the wavelength at resonance and a clear resonance peak was observed, as shown in Figure 4.9a.

The behavior described above of limited energy reflection off of small, deep voids is one limitation of the impact-echo test. Voids that are located deep within the pavement may not be detected if the lateral extent of the void is too small. More extensive experimental and analytical work must be performed to quantify the limitations associated with void size and void depth in impact-echo testing.



a. Frequency Response from Test over 50.8-cm Thick Slab



b. Frequency Response from Test over 10.2-cm Thick Step

Figure 4.9 Comparison of Frequency Responses from Impact-Echo Tests over Concrete of Different Thicknesses

4.2.4 Effect of Pavement Debonding

The 17.8-cm thick pavement at Site 3 is a case where the rigid concrete surface layer is debonded from the underlying cement-treated base material. Figure 4.10 shows the comparison of experimental and analytical impact-echo results from tests over debonded pavement and over the void, locations A3 and E3 respectively, as shown in Figure 4.11b. In the numerical model, the debonding and the void were both modelled as complete reflectors of energy (Ref 33). The comparison of these results to the measured experimental values shows similar changes in relative amplitudes of the peaks. This indicates that the debonded pavement behaves very much like a void in the pavement when tested with the impact-echo method.

Both the experimental and analytical results shown in Figure 4.10 exhibit two or more closely spaced peaks. This response is different than the single resonant peak shown in Figures 4.6 and 4.7, but is similar to the response shown in Figure 4.9b. The reason for the multiple, closely-spaced peaks is unknown. However, a resonant condition, even with multiple, closely-spaced peaks is clearly evident.

Figure 4.12 is a plot of the frequency responses measured by "marching" along array A3-I3, shown in Figure 4.11. In this case, the void is differentiated from the debonded pavement by an increase in both magnitude and frequency of the resonant peak. The numerical results indicate that this is due primarily to the increased depth to the reflecting surface. If the void and debonding were at the same depth, it is unlikely that they could be differentiated from one another.

4.3 EFFECT OF VARIATIONS IN TESTING METHODOLOGY

The testing arrangement, equipment and methodology that are used for impact-echo testing may also have an effect on the reliability of the test results. The following sections present a discussion of various testing parameters that may adversely affect the quality of the impact-echo test.

4.3.1 Effects of Impact Mechanism and Impact Duration

The impact-echo test is performed by introducing a transient stress pulse into the pavement system and recording the response of the pavement. As discussed in Section 4.2.1, the

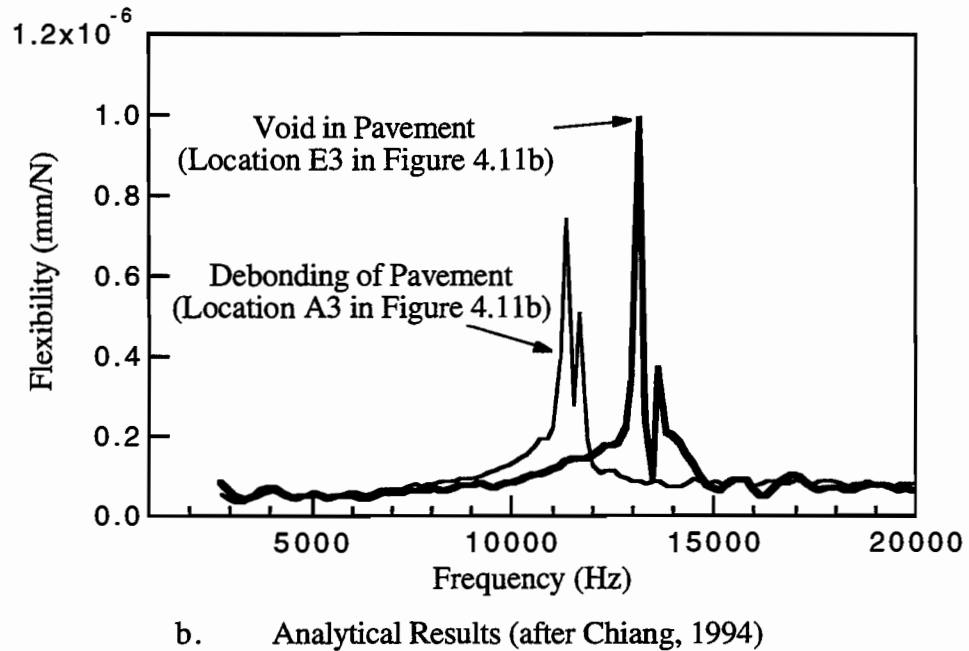
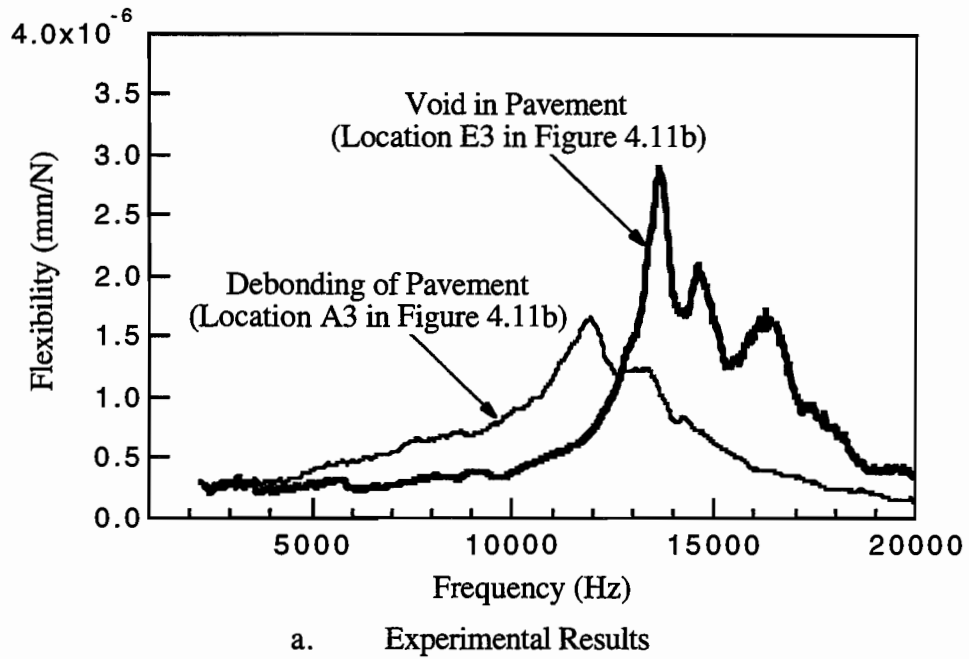
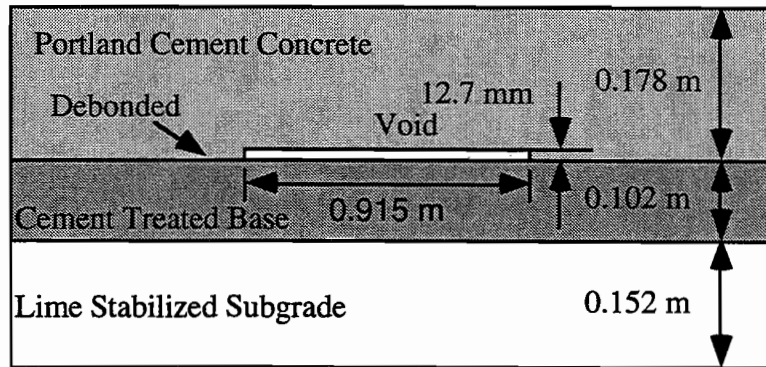
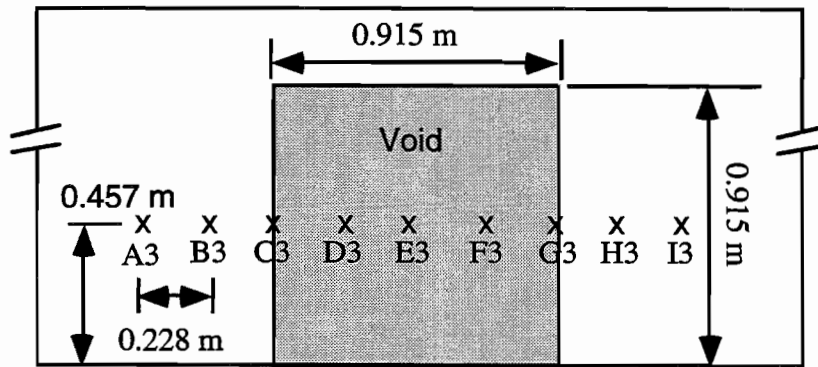


Figure 4.10 Experimental and Analytical Results of Impact-Echo Tests Performed at Site 3 over Locations A3 and E3 shown in Figure 4.11



a. Profile View



b. Plan View

Figure 4.11 Plan and Profile Views of 17.8-cm Thick Test Pavement at Site 3

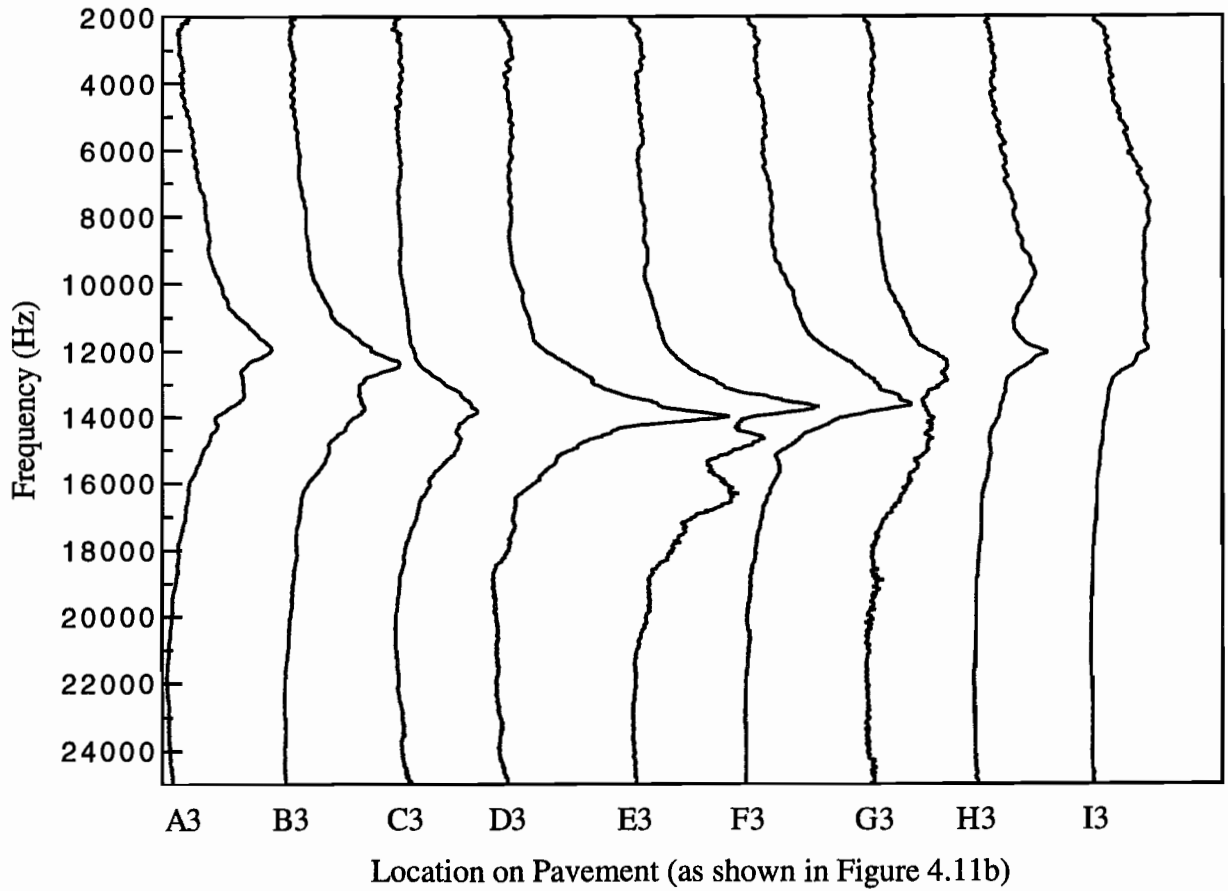


Figure 4.12 Composite Plot of Impact-Echo Testing along Array A3-I3 at Site 3, as shown in Figure 4.11

resonant frequency that is measured in impact-echo testing can vary greatly, depending on the depth to the reflecting interface. Since the locations of flaws in the pavement are not known prior to testing, a broad range of frequencies must be generated in the pavement to evaluate effectively the subsurface condition. For example, to detect voids directly beneath a 25.4-cm thick concrete pavement surface, frequencies around 7500 Hz must be generated in the pavement. For shallow voids that exist within the surface layer, the frequencies that are necessary for void detection are much higher. For example, detection of voids at depths of 2.54 cm below the surface with the impact-echo method requires frequencies in the range of 75,000 Hz.

The range of frequencies that are generated in the pavement is related to the duration of the impact. Short duration impacts will provide a broad range of low-amplitude, high-frequency energy. A longer duration will generate a narrower band of high-amplitude, low-frequency energy. The impact duration is primarily a function of the mass and stiffness of the impacting device, and the stiffness of the material being tested. The highest frequencies, therefore, will be generated when a stiff impacting device with a small mass strikes a smooth, stiff material. One common source used to generate high frequencies for shallow-void detection in concrete is small steel ball bearings (Ref 22). When tests are performed in this manner, no time record of the impact is available, so the resonant peak is determined from the power spectrum of the receiver rather than the frequency response determined from the source and receiver. The highest frequency that is generated by a ball bearing impact is inversely related to the mass of the ball bearing. For site-specific testing of structures, a series of tests may be performed at the same location with incremental increases in the mass of the impacting device. A self-contained hand-held device using this method of energy generation has been developed and successfully used (Ref 34).

Testing with several sizes of ball bearings allows a broad range of frequencies to be examined at one location. The results from each individual test, however, may be misleading if analyzed alone. Figure 4.13 shows the power spectra measured at a single location (location A at Site 1) using three different sized ball bearings. The power spectra that are measured differ significantly from one another. Impacts with longer durations, such as shown in Figure 4.13a and 4.13b emphasize the low-frequency resonance at 2.5 kHz. This peak is likely the dominant flexural resonance of the step. The higher frequency P-wave resonance is not detected because the energy at these frequencies is not generated by the impact. Testing with shorter duration impacts from smaller ball bearing sources, as shown in Figure 4.13c, emphasizes the higher frequency peak at around 17.5 kHz. However, for the impact-echo test to be implemented into a rolling, "on the fly" testing system, a single impact must generate all frequencies of interest. This requirement forms a severe limitation in implementing the impact-echo test into "on-the-fly" measurements.

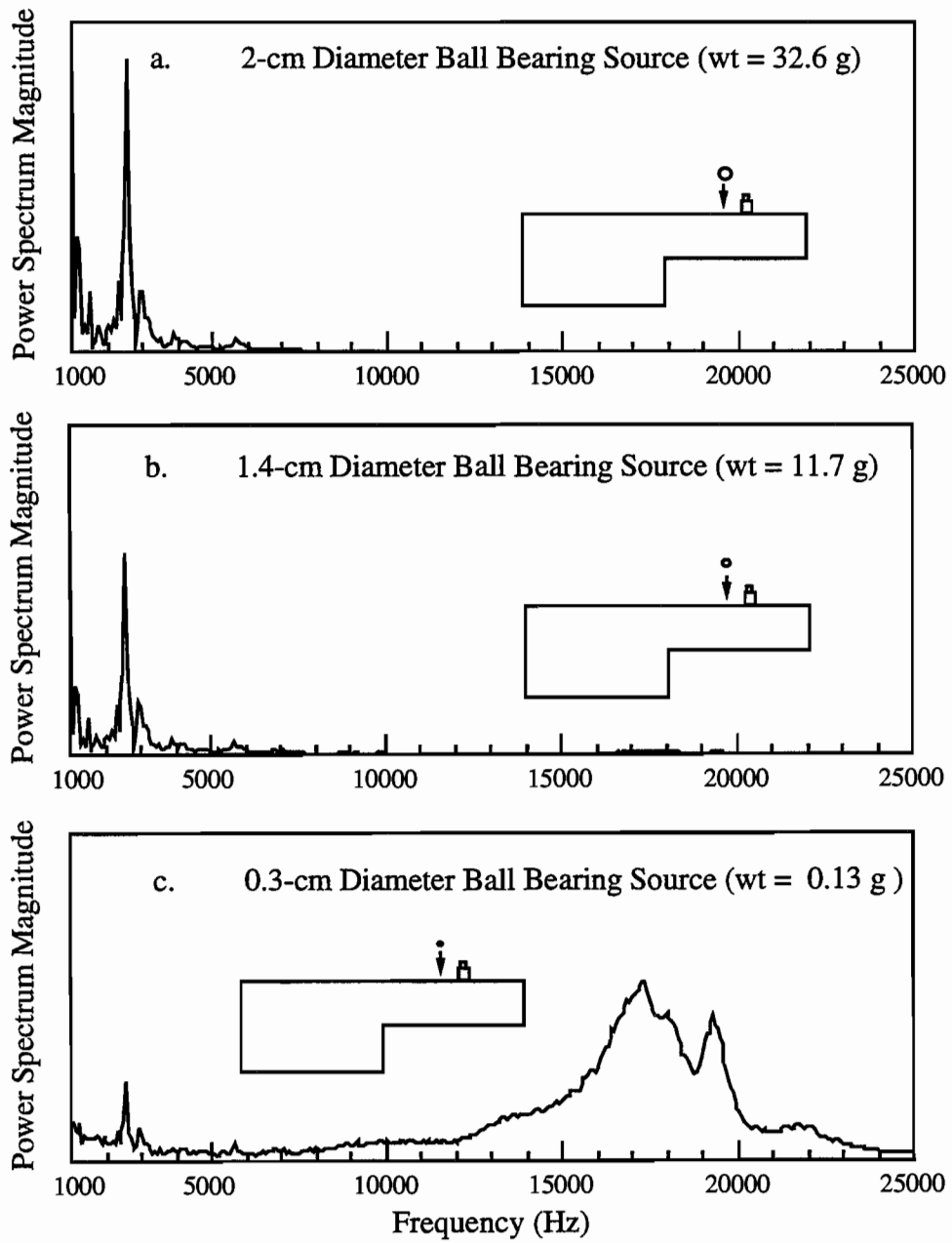


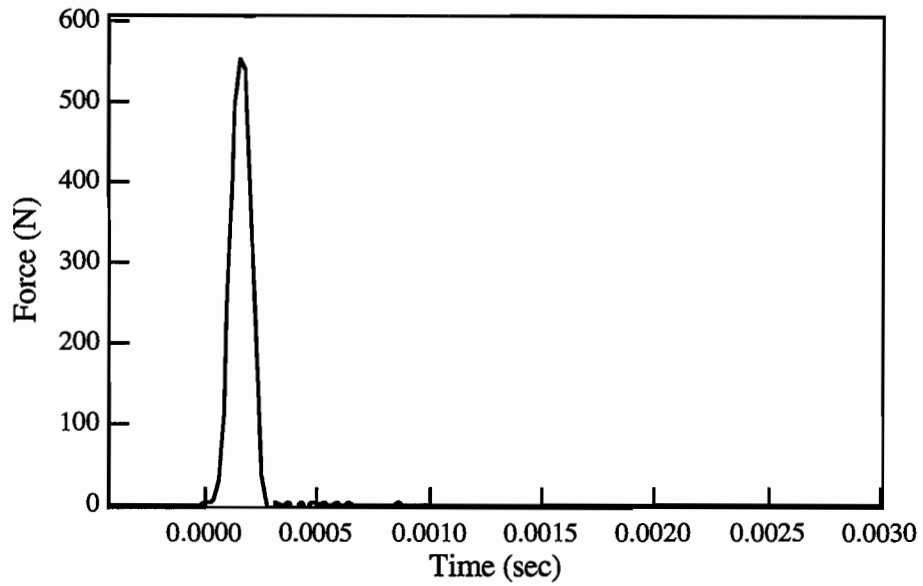
Figure 4.13 Power Spectra from Impacts over Location A Site 1 (Figure 3.6) with Different Sized Ball Bearings

One way to extend the useful frequency range from a single impact is to normalize the output of the receiver with respect to the impact energy. To do this normalization, the source must be instrumented with a load cell. Figures 4.14a and 4.14b are plots of the impact duration and power spectrum, respectively, from the impact of the PCB B01 hammer (0.1 kg) on a concrete pavement. Figures 4.15a and 4.15b are plots of the same information from the impact of the PCB C80 hammer (0.002 kg) on the same concrete surface. From these plots, it is observed that the magnitude of the energy falls off at higher frequencies, with the PCB B01 hammer generating energy to 10 kHz, and the PCB C80 hammer generating energy to 20 kHz.

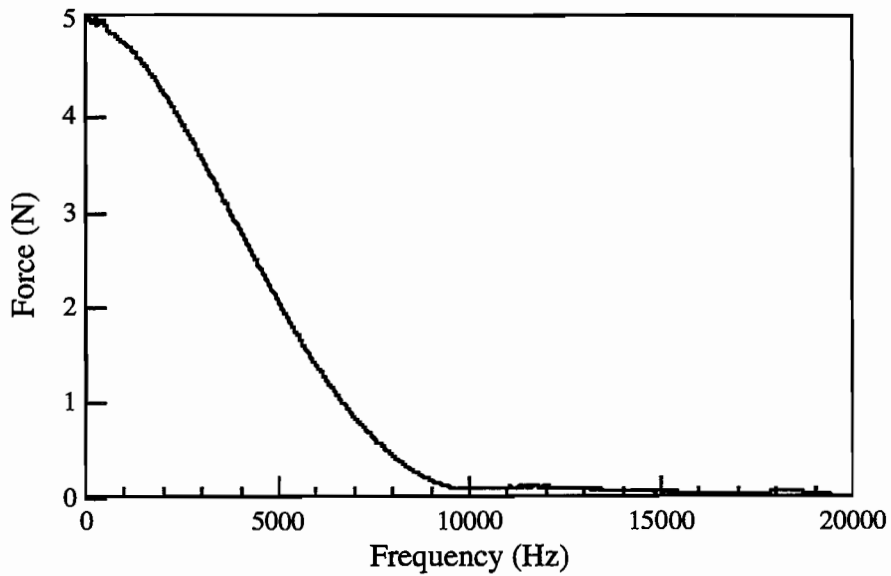
The frequency response can be determined from the impact-echo measurements, as described in Section 3.3.2.4. The output can, therefore, be viewed as the motion of the surface per unit force. Figure 4.16a shows the power spectrum from a test performed over location A at Site 1 using the PCB C80 impact hammer. In this record, the higher frequency peak is visible, but the record is dominated by the low-frequency resonance at about 2.5 kHz (assumed to be a flexural resonance). Figure 4.16b shows the frequency response of the same test, in which the output from the receiver has been normalized with respect to the input. By normalizing the output, the entire range up to 20 kHz can be determined from a single impact, and the relative magnitudes of the low-frequency and high-frequency peaks can be determined. The frequency range of 20 kHz that is shown is the limit of the response of the instrumented hammer. In concrete members, this limits the use of this instrumented hammer to detection of voids located at depths of approximately 9 to 10 cm or greater. Voids that are shallower than this can be detected in other ways, as discussed in Chapter 5.

4.3.2 Effects of Single versus Multiple Averages of Records

Experimental tests were performed at several locations to compare the response from a single impact with the averaged response from multiple impacts. Figure 4.17 shows the frequency response from 5, single impacts performed at location C2 at Site 2. Four of the five records are consistent in shape and show only minor differences in magnitude. For these cases, little is gained from averaging the data. However, one of the impacts, shown in Figure 4.17c, produced a frequency response that includes an erroneous peak at 8.6 kHz. If this single impact was considered alone, one might interpret the bogus peak as a flaw in the pavement. To minimize the effect of the aberrant result, the data may be averaged. Figure 4.18 shows the average frequency response from the same five impacts shown in Figure 4.17. The erroneous peak has been reduced and is not as likely to be misinterpreted when the data is averaged.

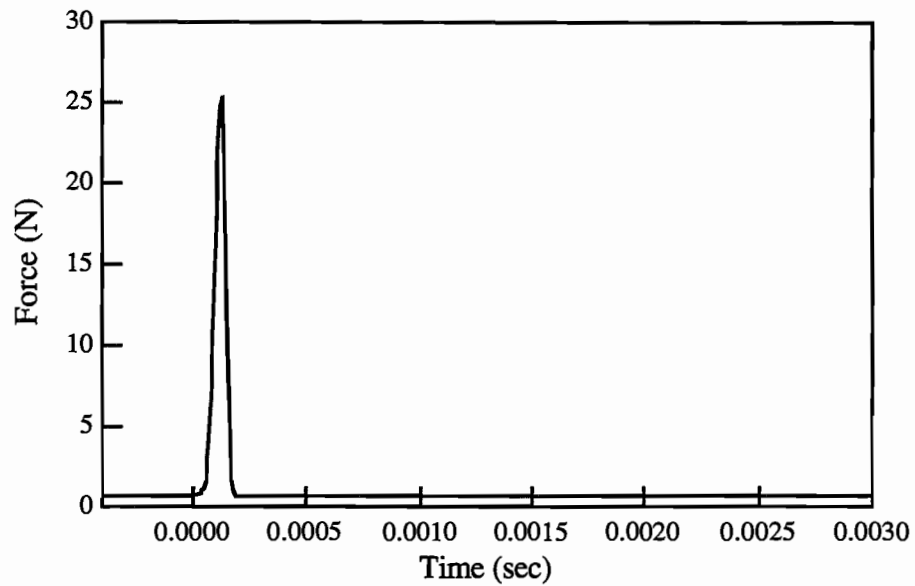


a. Time Record of Impact

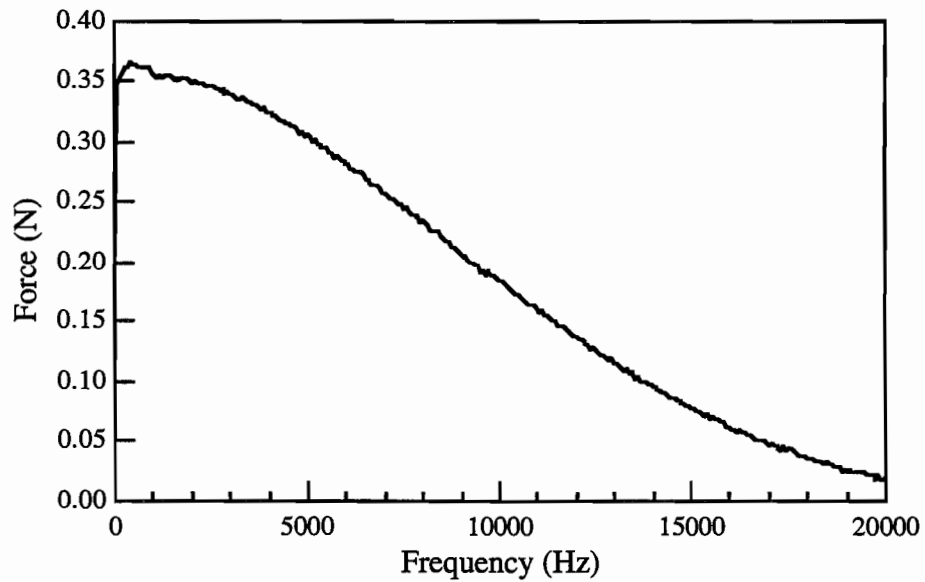


b. Power Spectrum of Impact Energy

Figure 4.14 Time Record and Power Spectrum from Impact of PCB B01 Impact Hammer on the Concrete Pavement at Site 2

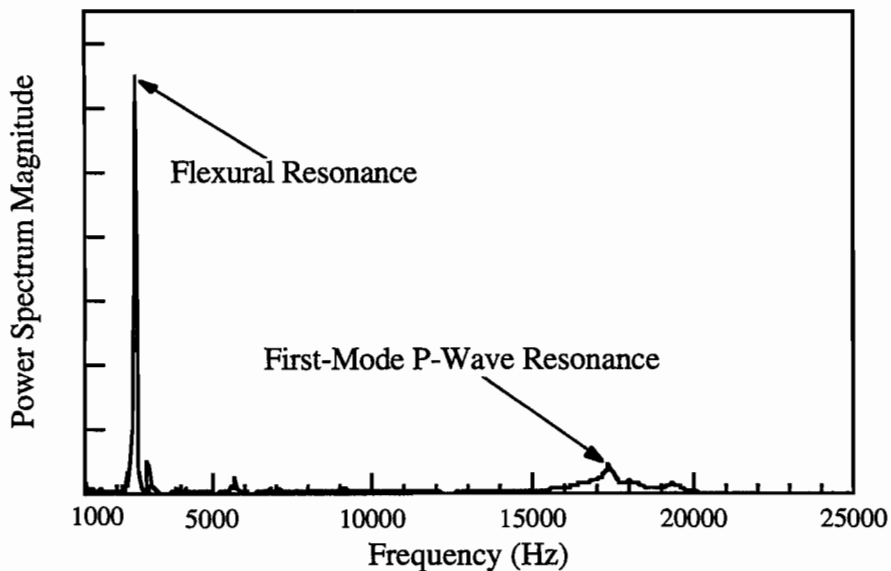


a. Time Record of Impact

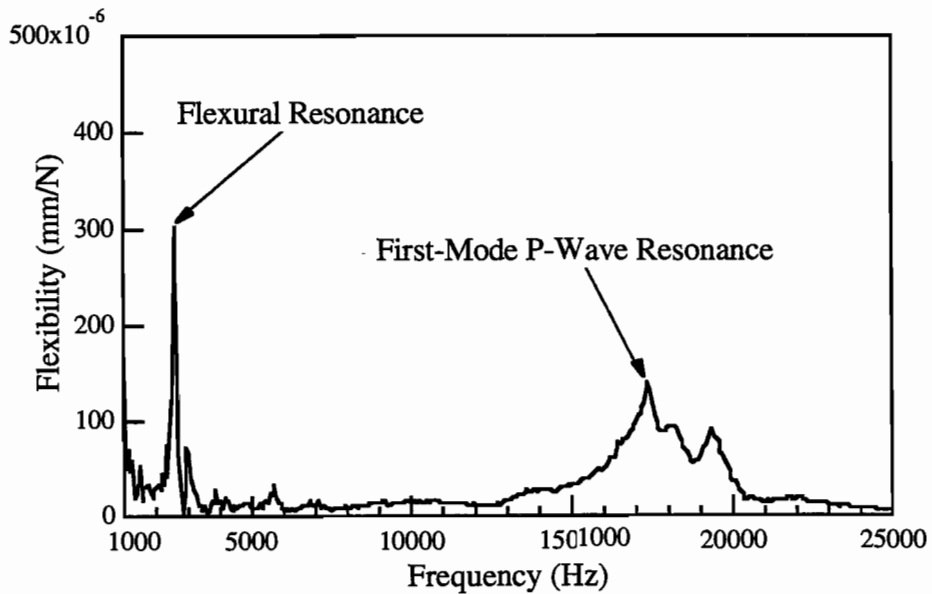


b. Power Spectrum of Impact Energy

Figure 4.15 Time Record and Power Spectrum from Impact of PCB C80 Impact Hammer on the Concrete Pavement at Site 2



a. Power Spectrum of Receiver from Impact with PCB C80 Hammer



b. Frequency Response from Impact with PCB C80 Hammer

Figure 4.16 Power Spectrum and Frequency Response from Impact over Location A at Site 1 using the PCB 086 C80 Impact Hammer

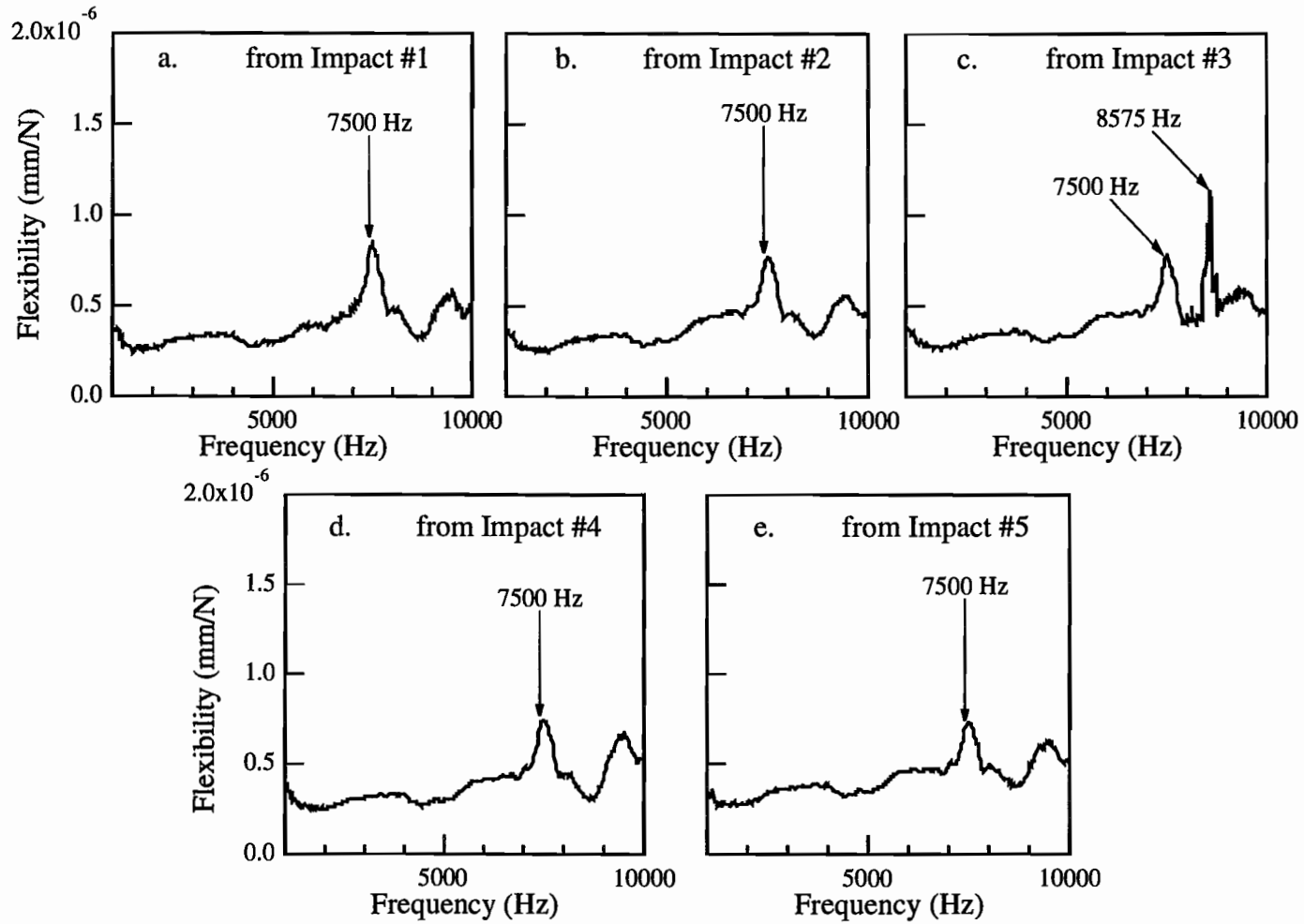


Figure 4.17 Frequency Responses from Individual Impacts over Location C2 at Site 2, as shown in Figure 4.5

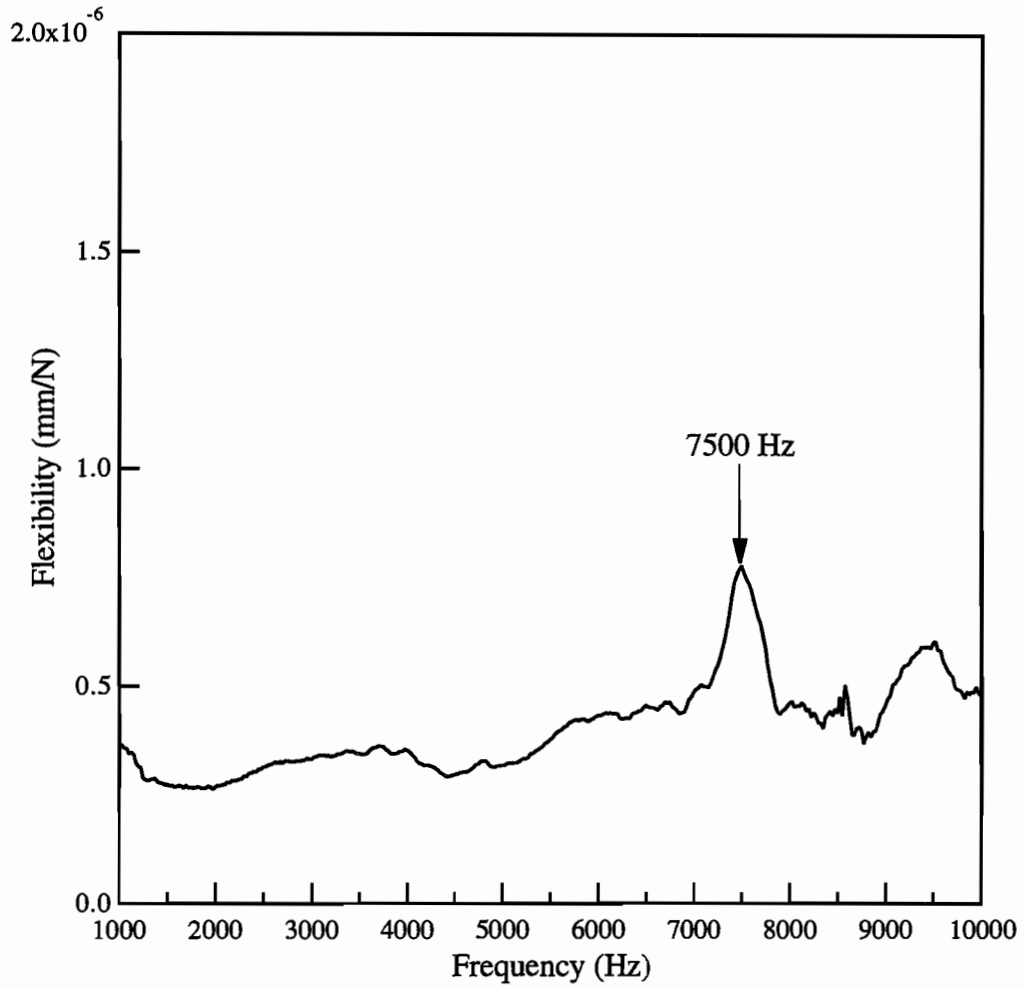


Figure 4.18 Frequency Response Determined from the Average of Tests Performed at Location C2 at Site 2, as shown in Figure 4.5

The reason for the false peak in Figure 4.17c has to do with the impact on the concrete surface. As discussed previously, to generate high frequencies, small impact devices must be used. The size of the impactor may be such that surface features and roughness on the pavement affect the response of the load cell when the impact is applied. Figures 4.19 and 4.20 show the time records and corresponding power spectra from each of the impacts shown in Figure 4.17. Impact #3 (Fig. 4.19c) shows a discontinuity in the time trace, and a null point at 8.6 kHz in the power spectrum (Fig. 4.20c). The false peak is, therefore, an effect of dividing the response of the receiver by an input spectrum that does not accurately reflect the energy input in the pavement (a false or unrepresentative low point). In some cases, this effect may be so pronounced that multiple averaging may not significantly reduce the erroneous result.

Impacting on a concrete surface that is cracked or damaged may increase the duration time of the impact, and hence decrease the range of frequencies generated in the pavement. For site-specific cases, these problems can be overcome by monitoring the location of the impact and the frequency response from the impact. Erroneous data can be disregarded, and the location can be retested. Furthermore, measures such as using strike plates or grinding on the surface may be employed to improve the results. However, for a rolling unit making "on the fly" measurements, these remedies can not be applied and this requirement forms a severe limitation for implementation of the impact-echo method into a rolling system. The use of a small instrumented impactor in a rolling system is unlikely to yield desirable results. Therefore, other systems of energy input, such as introducing band-limited noise, need to be developed.

4.4 SUMMARY

The results from the impact-echo tests performed in this chapter demonstrate the effectiveness of the impact-echo method for site-specific testing of pavements. Many of the flaws of interest in pavements can be effectively delineated using this method. Secondly, the impact-echo method has the added benefit of predicting the depth to the void based on the measured frequency and assumed or measured wave velocity of the concrete.

There are, however, several limitations of this method when applied to testing concrete pavements. The detection of small, deep flaws is difficult using this method due to the small amount of reflected energy from the flaw. Secondly, in order for the impact-echo method to evaluate the pavement completely, a broad range of frequencies must be generated in the pavement. This requires, therefore, that in some cases multiple impacts of different sources be used to cover

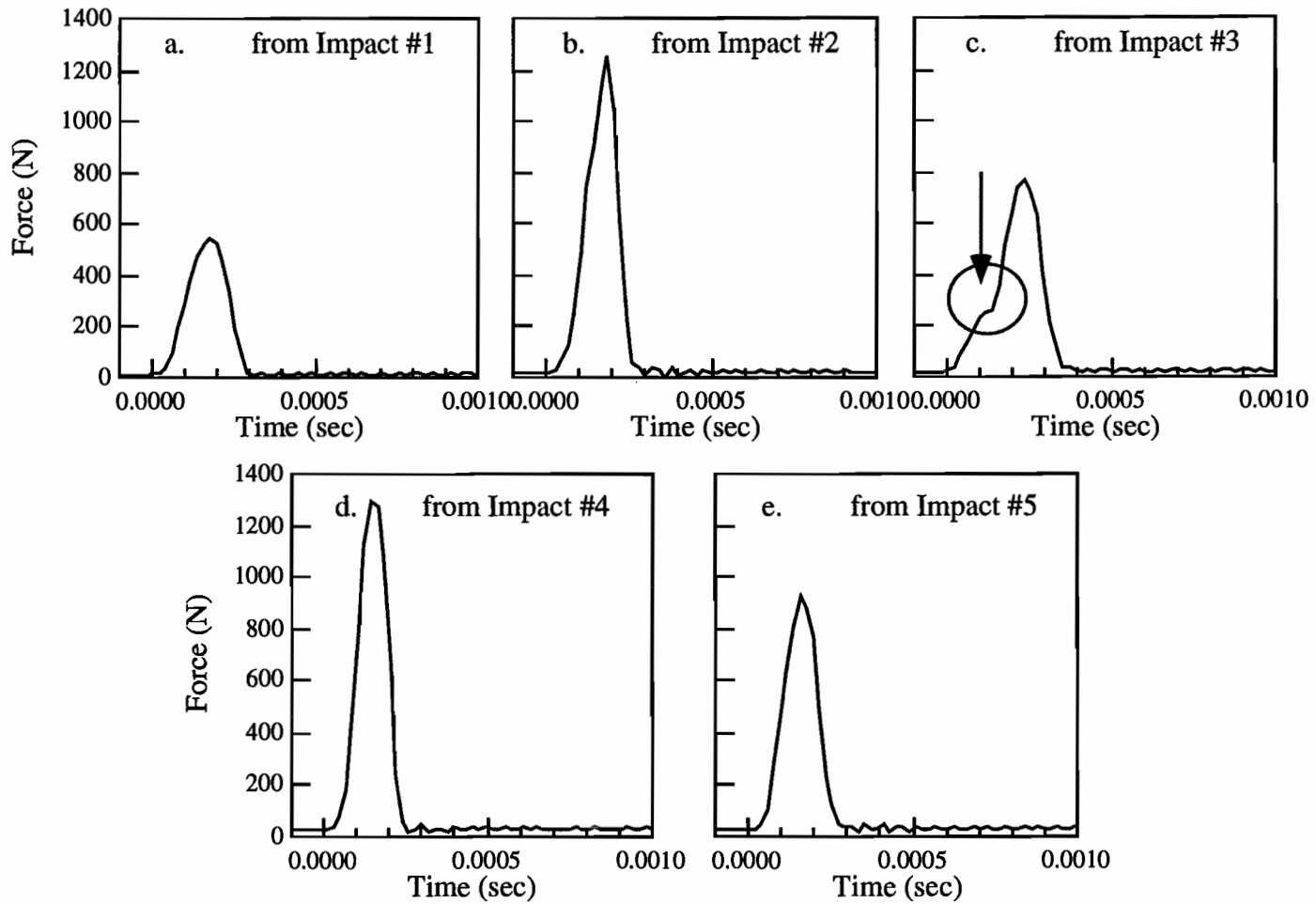


Figure 4.19 Time Records from Individual Impacts over Location C2 at Site 2, as shown in Figure 4.5

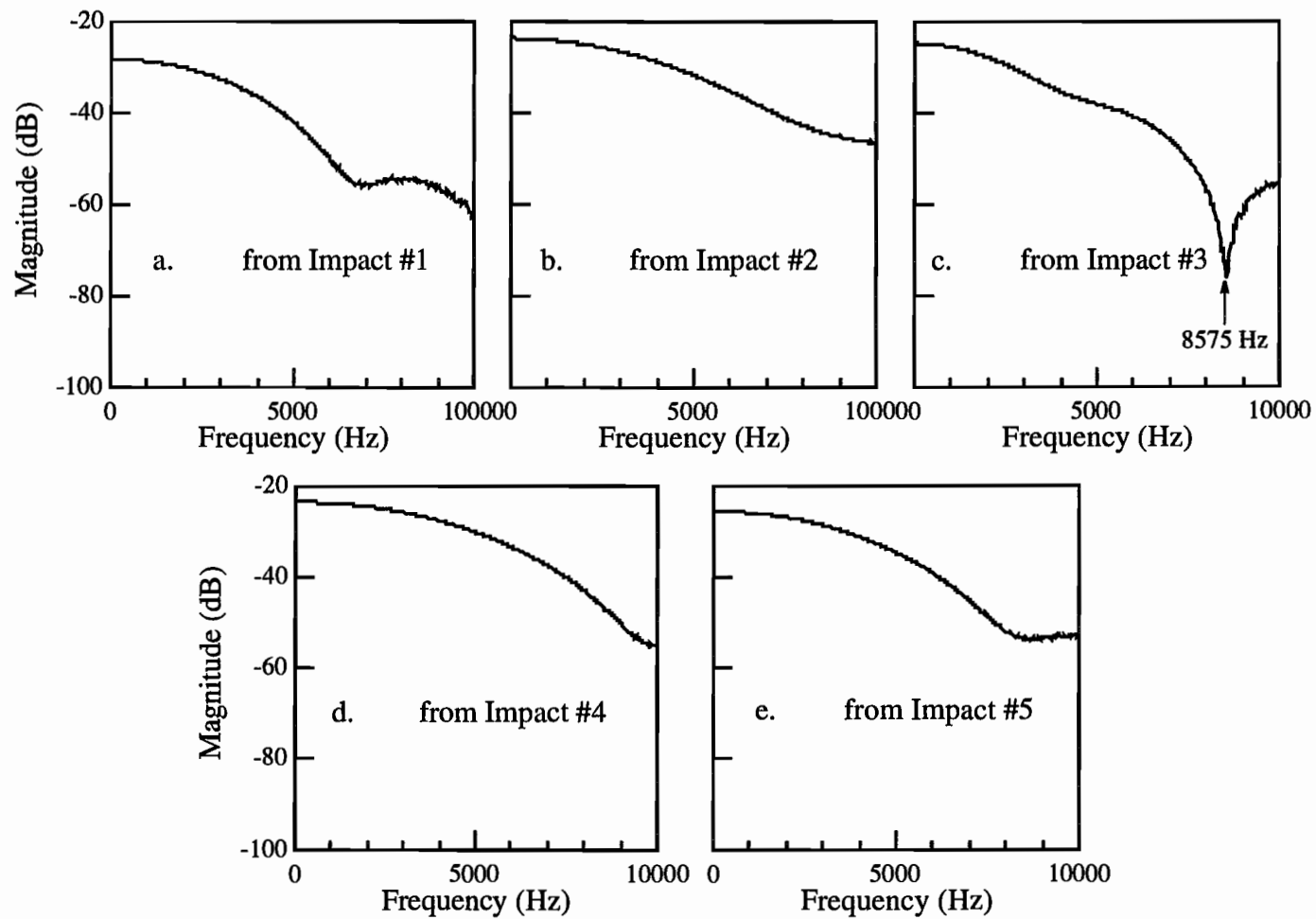


Figure 4.20 Power Spectra from Individual Impacts over Location C2 at Site 2, as shown in Figure 4.5

the entire frequency range. Also, shallow voids in the pavement require very high frequencies for detection, on the order of 75 kHz. The difficulty in effectively generating and receiving these high frequencies is a serious consideration in using the impact-echo method.

Although these problems can be dealt with for site-specific testing, they are serious limitations for implementing the impact-echo method into a mobile, "on the fly" testing system. For such a rolling system, all energy must be consistently generated from a single impact. Surface features of the pavement, such as roughness or damage can adversely affect the frequencies generated from the impact. Secondly, the range of frequencies - and hence the depth range of detectable flaws - that can be generated from a single impact is limited. Using a small, instrumented hammer and normalizing the response of the receiver with respect to the source, a range of 1 to 20 kHz can be tested. This range limits the detection of flaws to those at depths of approximately 7.6 cm or greater. For these reasons, the development of a more consistent source, such as a piezoelectric shaker generating band-limited noise is probably necessary for the impact-echo method to be effectively implemented into a rolling system.

CHAPTER 5.

EXPERIMENTAL FIELD TESTING AND ANALYTICAL RESULTS

FROM IMPULSE - RESPONSE METHOD

5.1 INTRODUCTION

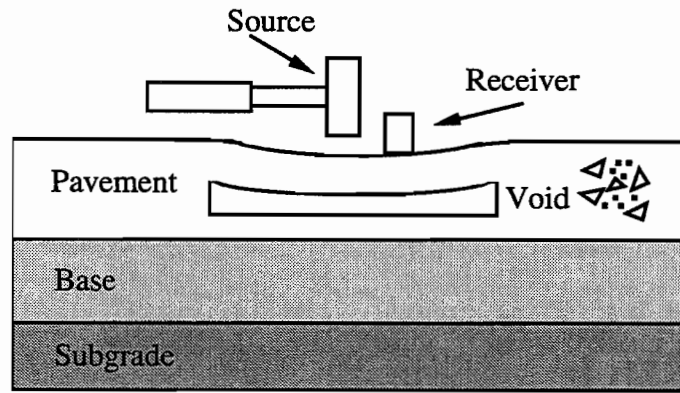
The impulse-response method is a stress-wave based method that has been successfully used to detect regions of poor support under concrete slabs (Ref 26). Unlike the impact-echo method which utilizes P-wave resonance measurements to detect flaws within the pavement, the impulse-response method detects flexural mode motions to infer conditions within the pavement. The low-frequency flexural response that is measured is generally easier to generate and receive as compared to the frequencies needed for the impact-echo method. For this reason, the impulse-response method seems well suited for implementation in a rolling testing system.

In this chapter, a description of the impulse-response method is presented, and the testing methodology, equipment, and data reduction procedures are discussed. Results from analytical and experimental tests are presented and discussed to demonstrate the advantages and limitations of the impulse-response test for implementation into a mobile testing system.

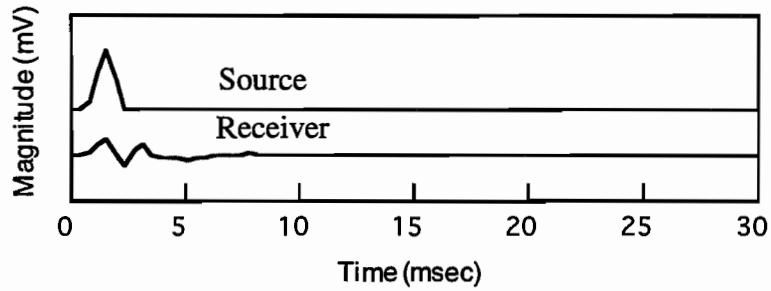
5.2 DESCRIPTION OF THE IMPULSE-RESPONSE METHOD

The impulse-response test is performed with a single source and single receiver mounted on the surface of a pavement or slab, as shown in Figure 5.1a. The source is typically an instrumented hammer that is capable of exciting low-frequency flexural motion in the slab. The low-frequency vibrations are measured with a velocity transducer (geophone) that responds linearly to frequencies in the range from 10 to 1000 Hz. The test is performed by placing the geophone on the pavement, and then impacting near the receiver with the instrumented hammer. The vibration of the pavement is detected with the geophone and displayed on a recorder or waveform analyzer. Typical time records from the source and the receiver are shown in Figure 5.1b.

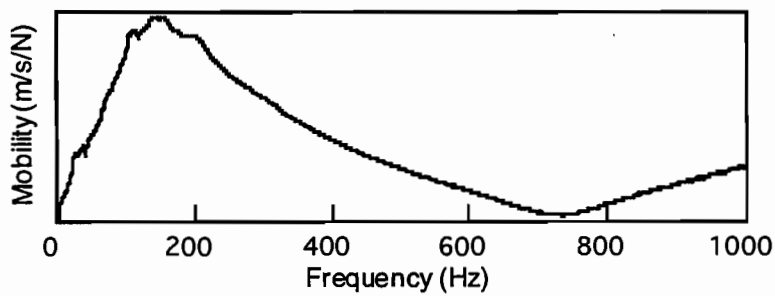
The output from the source and receiver are then transformed into the frequency domain to obtain the frequency response (defined in Section 3.3.2.4), as shown in Figures 5.1c. Frequency



a. Impulse-Response Testing Arrangement



b. Sample Time Record from Impulse-Response Testing



c. Sample Frequency Response from Impulse-Response Testing

Figure 5.1 Testing Arrangement and Sample Data for Impulse-Response Testing

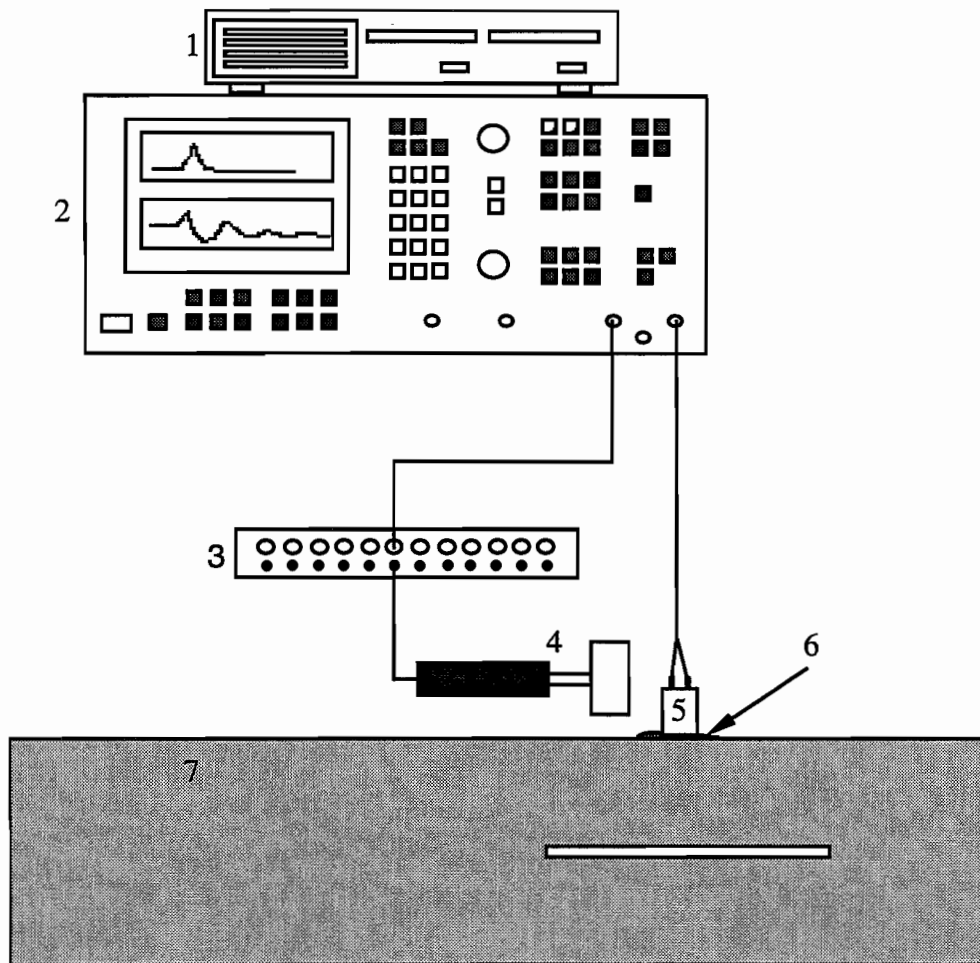
and magnitude characteristics of the pavement vibration obtained from the frequency response can be used to infer conditions below the pavement surface. The frequency and magnitude of the flexural vibrations of the concrete surface layer depend on the integrity and support of the slab. For a pavement with a flaw within or directly beneath the slab, the response is affected by the following four factors: (1) the lateral extent of the flaw, (2) the shape of the flaw, (3) the depth to the flaw, (4) the edge support of the concrete over the flaw. Shallow flaws that are unsupported over a large lateral extent, for example, will resonate at low frequencies and high magnitudes; while deeper, smaller flaws will resonate at higher frequencies and lower magnitudes. Also, the magnitude will increase and the frequency will decrease when tests are performed at the edges or corners of pavements where the concrete surface layer is unsupported along one or more edges.

5.3 IMPULSE-RESPONSE TESTING METHODOLOGY

Experimental impulse-response testing was performed at Sites 2 and 3 described in Section 3.4. Descriptions of the experimental testing arrangement, equipment, and data reduction procedures are included in this section.

5.3.1 Testing Procedure and Equipment

The general testing arrangement and equipment for the impulse-response testing performed in this study are shown in Figure 5.2. The source hammer used in all cases was a PCB 086B20 instrumented impact hammer with a mass of 1.4 kg and a tip diameter of 5 cm. The hammer has a range to 1 kHz, a sensitivity of 0.23 mV/N, and a resonant frequency of 12 kHz. A rigid plastic tip was used on the end of the hammer to impact the pavement. Pavement vibrations were measured with a model L-15B geophone from Mark Products with a natural frequency of 4.5 Hz, a damping ratio of 0.70, and a calibration factor of 55 V/m/sec at frequencies above 7 Hz. The geophone was coupled to the pavement with a poster hanging material that is available at any local hardware store. The output from the instrumented hammer was passed through a PCB 483A07 power unit and into channel 1 of a Hewlett Packard 3562A Dynamic Signal Analyzer. The geophone output was passed directly into channel 2 of the analyzer. Three impacts were performed at a distance of approximately 7.62 cm from the receiver. The responses from the three impacts were averaged to obtain a single frequency response for each location.



1. Hewlett Packard 9122 Disk Drive
2. Hewlett Packard 3562A Dynamic Signal Analyzer
3. PCB 483A07 Power Unit
4. PCB 086B20 Instrumented Impact Hammer
5. L-15B, 4.5-Hz Mark Products Geophone
6. Wall Tack Material
7. Portland Cement Concrete Slab

Figure 5.2 Experimental Arrangement and Equipment for Impulse-Response Testing

5.3.2 Data Reduction Procedures

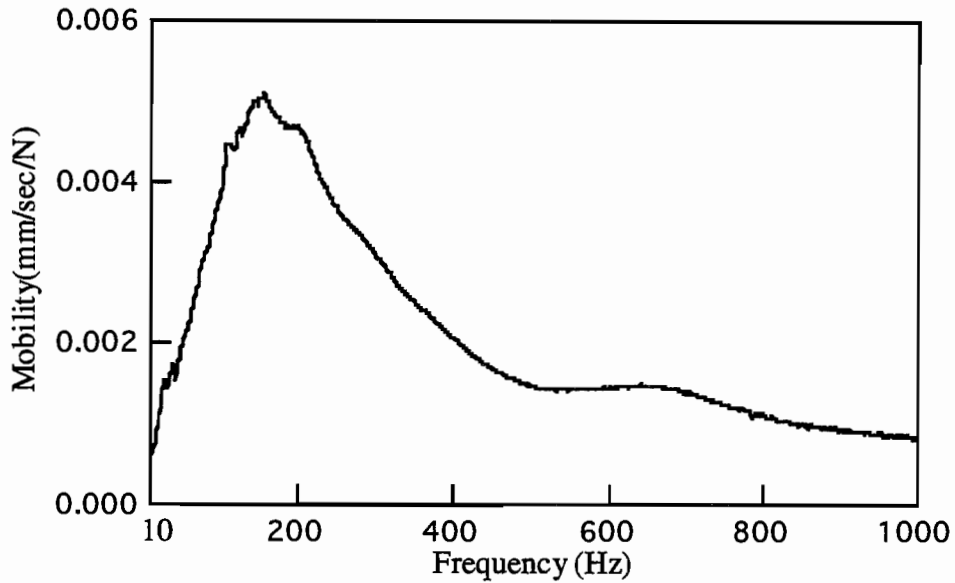
The data from each test was collected using the Hewlett Packard 3562A Dynamic Signal Analyzer and saved using an Hewlett Packard 9122 disk drive. The time records that were obtained from the geophone and the instrumented hammer were transformed into the frequency domain using the FFT algorithm in the analyzer and displayed in terms of frequency response, as explained in Section 3.3.2.4. The appropriate calibration constants for the hammer and geophone were applied to the frequency response. The frequency response was, therefore, displayed in terms of velocity in mm/sec per unit force in newtons and is termed the mechanical admittance or mobility. For each test location a plot of mobility versus frequency from 10 to 1000 Hz was obtained. The results from these tests were presented in terms of dynamic slab stiffness, and average mobility, as discussed below.

5.3.2.1 Dynamic Slab Stiffness: The dynamic stiffness of the slab can be obtained from the mobility plots. The slope of the mobility plots at frequencies below approximately 100 Hz is a measure of the flexibility of the slab (displacement/force). The dynamic stiffness of the slab (force/displacement) is the inverse of this value. To calculate the stiffness, the mobility plots were integrated once to obtain plots of flexibility versus frequency. An average flexibility value was obtained from the flat portion of the flexibility plots in the range of approximately 10 to 100 Hz (Fig. 5.3). This average value of the flexibility from 10 to 100 Hz was then inverted to give the dynamic slab stiffness.

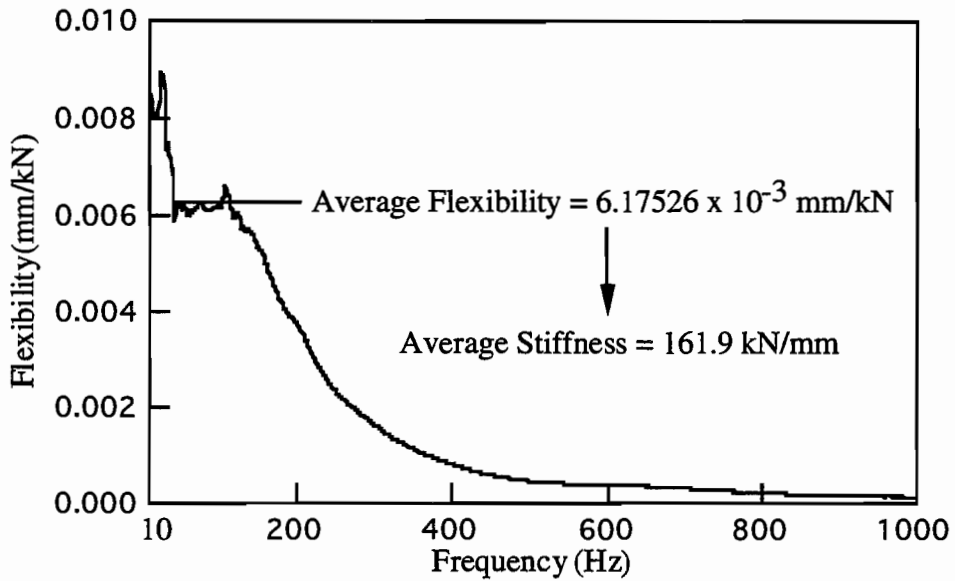
5.3.2.2 Average Mobility: The second method of data reduction was to present the results from each impulse-response test in terms of average mobility. In this case the averaging was performed over the frequency range of 10 to 800 Hz (Fig. 5.4). An average value of mobility was calculated from the frequency response obtained at each location.

5.4 NUMERICAL MODEL RESULTS FOR IMPULSE-RESPONSE TESTING

Finite element studies were performed as part of Project 1243 to simulate impulse-response tests over voids of various sizes and depths for two pavement profiles (Ref 33). Figures 5.5 a and 5.5b show profiles A and B that were used for the finite element studies. Profile A is similar to the

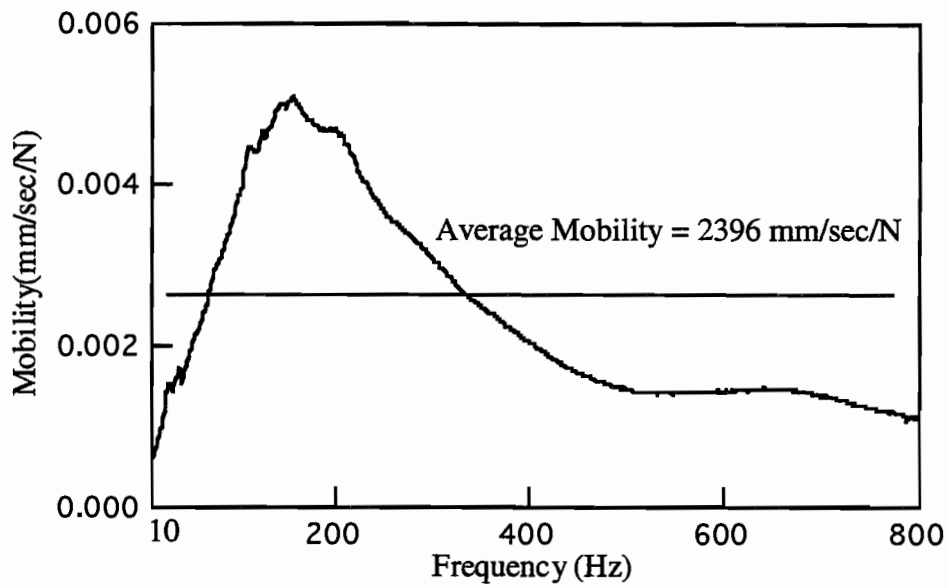


a. Mobility Plot from Impulse-Response Test

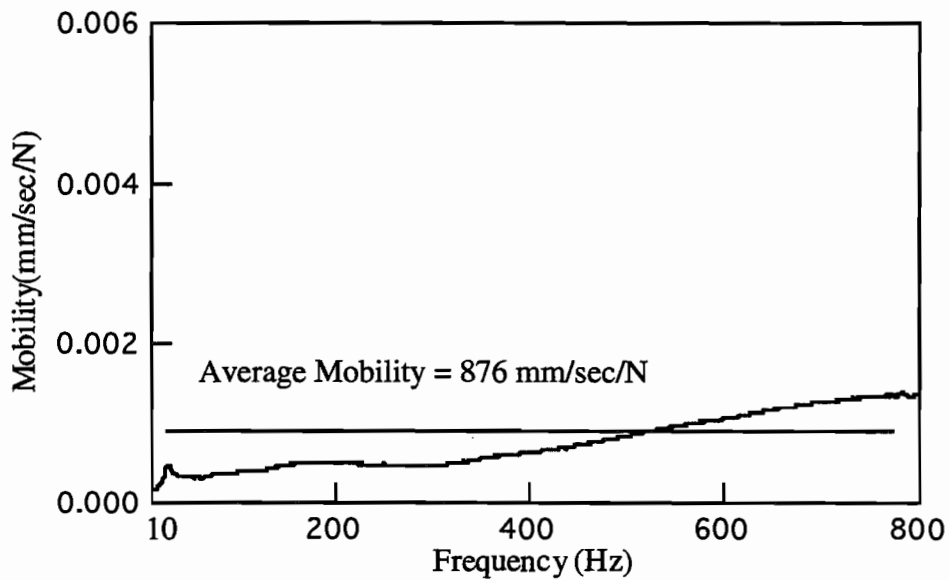


b. Flexibility Plot obtained from Integrating Mobility Plot shown in Figure 5.3a

Figure 5.3 Sample Impulse-Response Results Demonstrating the Determination of Dynamic Slab Stiffness from Mobility Plots

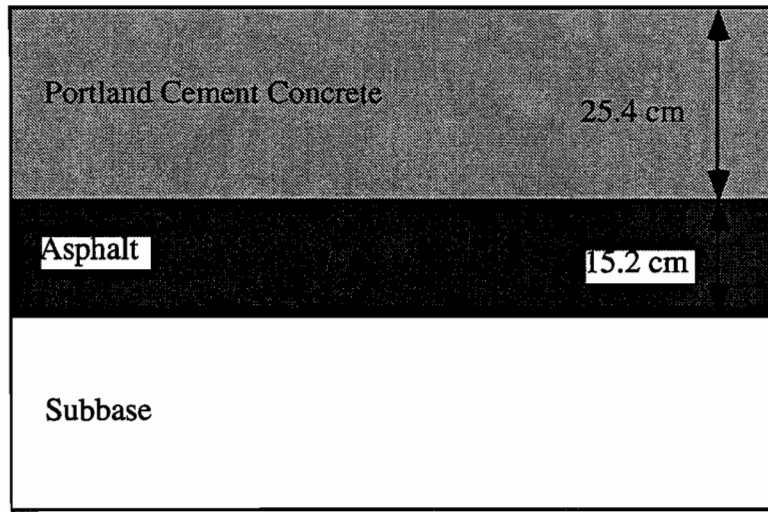


a. Mobility Plot from Test over a Void

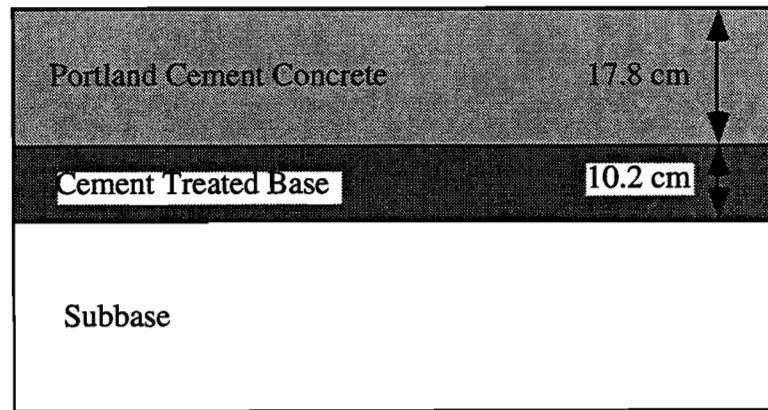


b. Mobility Plot from Test over Sound Pavement

Figure 5.4 Sample Mobility Plots and Average Mobility Values from Tests over a Void and over Sound Pavement



a. Pavement Profile A



b. Pavement Profile B

Figure 5.5 Pavement Profiles used in Numerical Models of Impulse-Response Testing

pavement profile at Site 2 (Fig. 3.7) used for experimental studies, and profile B is the same profile as is found at Site 3 (Fig. 3.8) used for experimental studies.

5.4.1 Effect of Void Size

The flexural response of a pavement over a void depends greatly on the lateral extent of the flaw. Much like vibrating drums, large voids will vibrate at higher magnitudes and lower frequencies than smaller voids. The numerical model results presented in Figure 5.6 demonstrate the expected frequency responses of the pavement in the frequency range of interest (10 to 1000 Hz) for the impulse-response test. Figures 5.6a through 5.6c show a comparison of the frequency responses from impulse-response tests on profile A, shown in Figure 5.5a, performed over three different voids. All voids are located at a depth of 0.076 m below the slab surface. The voids have diameters of 0.915 m, 0.610 m, and 0.305 m. Figure 5.6d shows the expected frequency response over profile A when no void or flaw is present in the slab.

A comparison of the frequency responses in Figure 5.6 shows that the flexural response of the pavement from 10 to 1000 Hz over the 0.610-m and 0.915-m diameter voids is different from the response when no void is present. However, a 0.305-m diameter void at this depth can not be differentiated from sound pavement in the frequency range tested. In this case, the flexural response is at a higher frequency and does not, therefore, affect the low frequencies modelled in the impulse-response method. For this void to be detected, instrumentation measuring higher frequencies would need to be used. These results demonstrate a possible limitation of the impulse-response method; namely that for a given depth, the voids that can be detected with the impulse-response method are directly limited by the lateral extent of the void and the frequency range used in the measurement.

5.4.2 Effect of Void Depth

The results from impulse-response tests also depend on the depth to the void in the pavement. Figures 5.7a through 5.7c show plots of frequency responses from impulse-response tests performed over a 0.610-m (2-ft) diameter circular void at depths of 0.076 m, 0.152 m, and 0.254, respectively, in pavement profile A. At a depth of 7.6 cm, the presence of the void is detected by the large flexural resonance peak at approximately 950 Hz. When the depth is increased to 15.2 cm, the response in the frequency range of impulse-response testing is greatly reduced. The response is further reduced when the depth is increased to 25.4 cm. This reduction

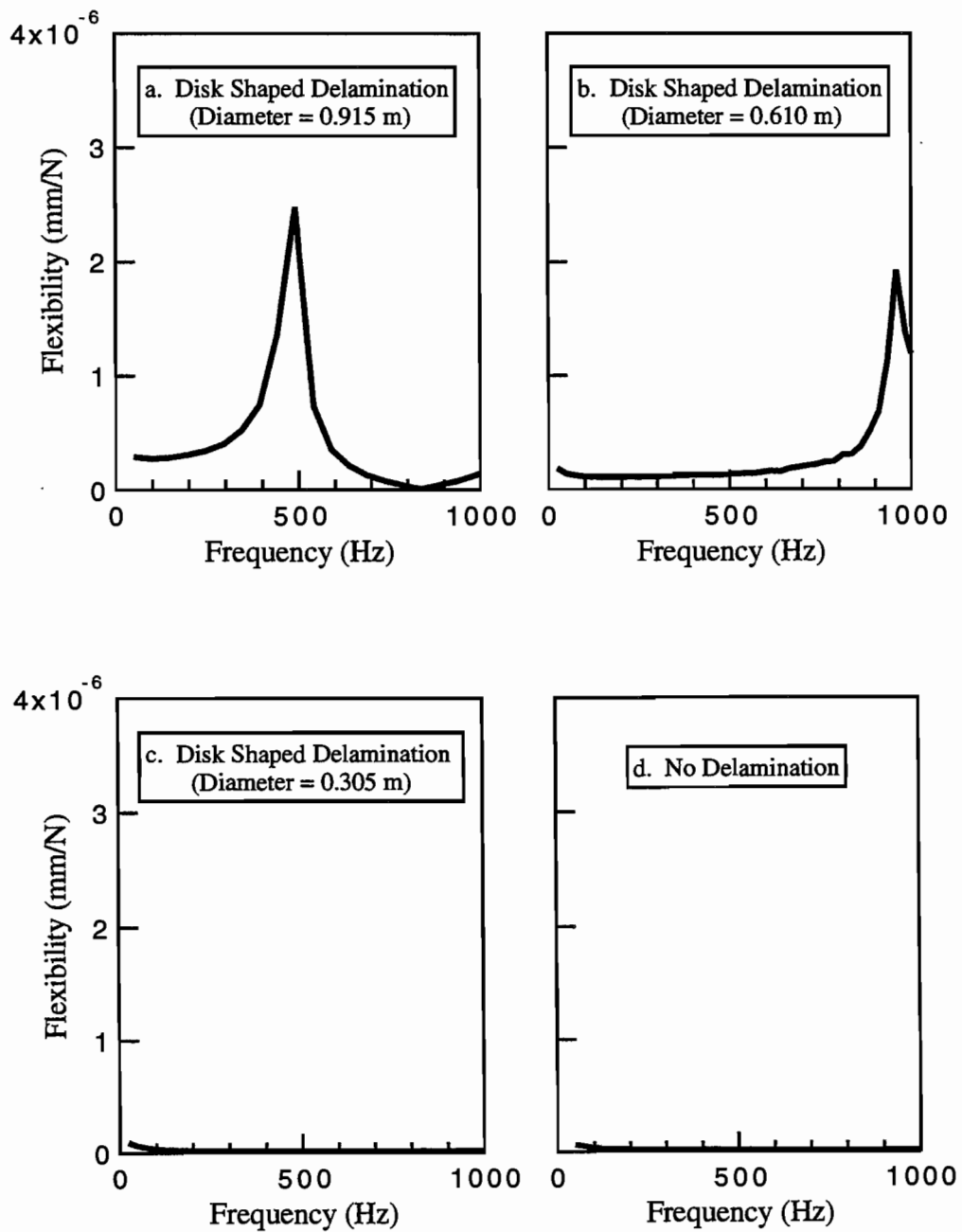


Figure 5.6 Results from Numerical Modeling of Impulse-Response Tests over Circular Voids of Various Diameters (after Ref 33)

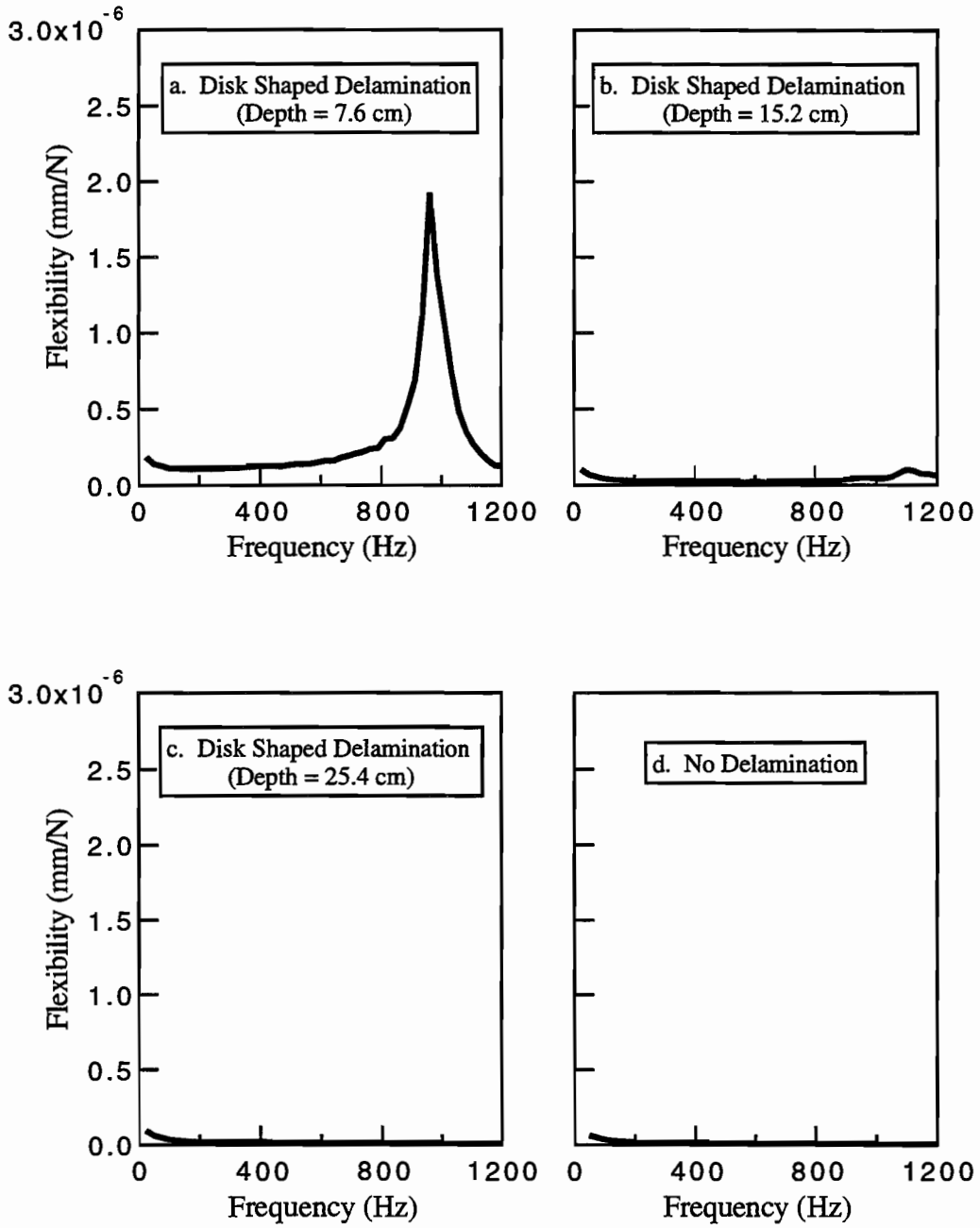


Figure 5.7 Results from Numerical Modeling of Impulse-Response Tests over Circular Voids at Various Depths (after Ref 33)

is again due to the higher frequency flexural response of the thicker and, therefore, stiffer concrete layer over deep voids. Figures 5.8a and 5.8b show rescaled plots of the frequency response over the voids at depths of 15.2 cm and 25.4 cm. When these plots are compared to the frequency response of intact pavement, it is observed that the response over the 15.2-cm deep void can be differentiated from sound pavement by slightly higher mobility values in the range of 10 to 1000 Hz. Because the response is shown up to a frequency of 1200 Hz, the flexural peak is now visible at a frequency of 1100 Hz. The void at a depth of 25.4 cm, however, can not be detected from the frequency responses shown. These results illustrate the effect of void depth on the ability to detect voids of various sizes using the impulse-response method.

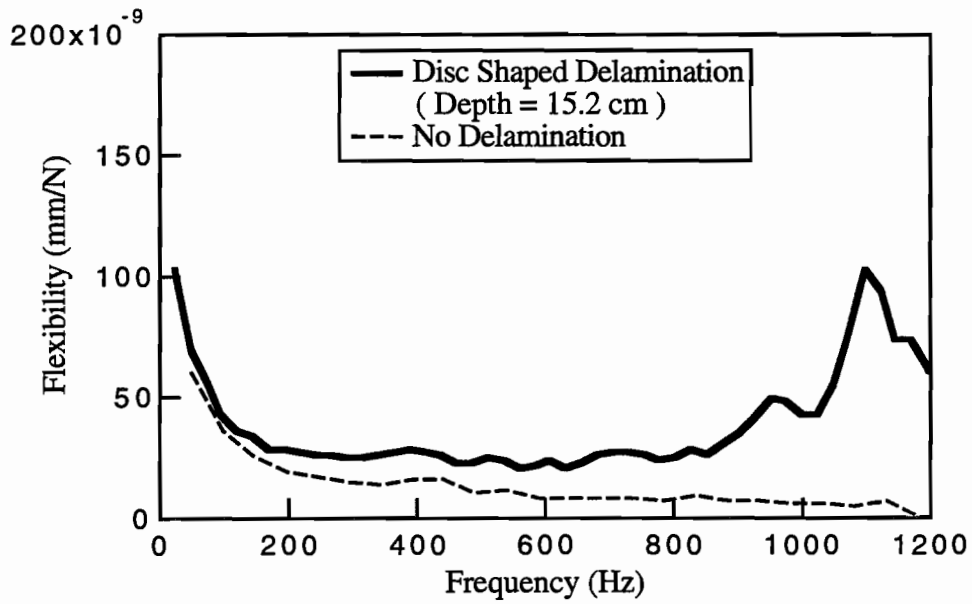
5.5 EXPERIMENTAL RESULTS FROM IMPULSE-RESPONSE TESTS AT SITE 2

5.5.1 Pavement with a Void versus Sound Pavement

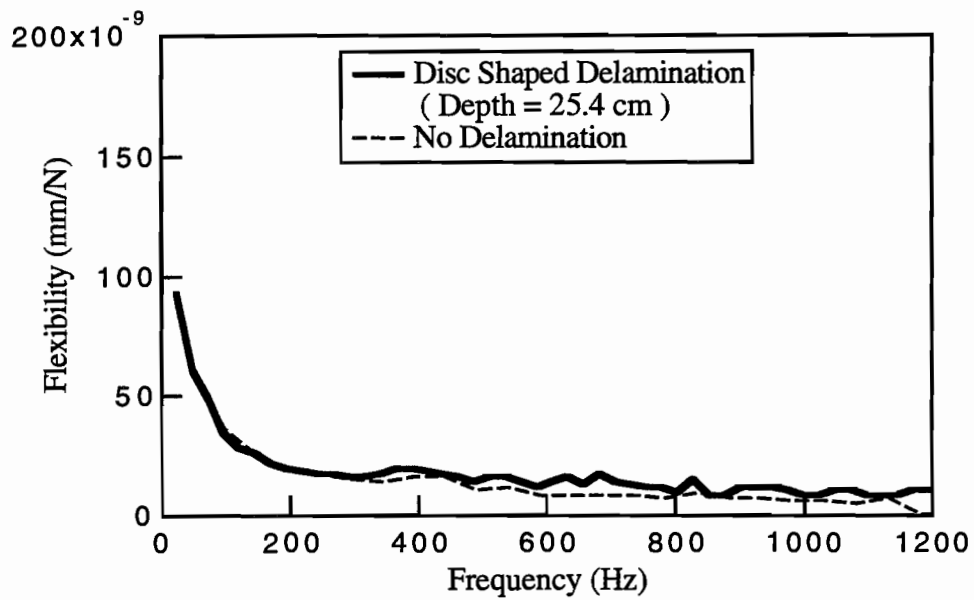
The profile and plan views of the test pavement at Site 2 are shown in Figure 3.7. Impulse-response testing was performed over four regions of this pavement. Region 1 is located over the 0.915-m square corner void under the south-east corner of the fixed slab shown in Figure 3.7. A 1.4-m square area, which included the 0.915-m square corner void, was tested on a grid spacing of 15.2 cm, as shown in Figure 5.9a. Figures 5.10a and 5.10b show a comparison of the mobility plots obtained over the void (grid location A3) and over sound pavement (grid location H3). The void is differentiated from the sound pavement by a mobility plot that is more undulated and higher in magnitude.

A series of mobility plots along the array A3 - H3 in Region 1 is shown in Figure 5.11. As the interior edge of the void is approached, the magnitude and undulations in the plot decrease. Over the sound pavement, the mobility plot is low in magnitude and fairly flat. To simplify data presentation, the average mobility from 10 to 800 Hz is plotted for each location, as shown in Figure 5.12. Using this data presentation method, the void is delineated from sound pavement by higher average mobility values over the void. Figure 5.13 is a contour plot of average mobility values over the entire 1.4-m grid area. The size and location of the void is fairly well delineated by higher average mobility values.

To study the effect of the corner location alone on the average mobility plots, the same test with identical grid spacings was performed over a fully supported corner. Region 2 is located at

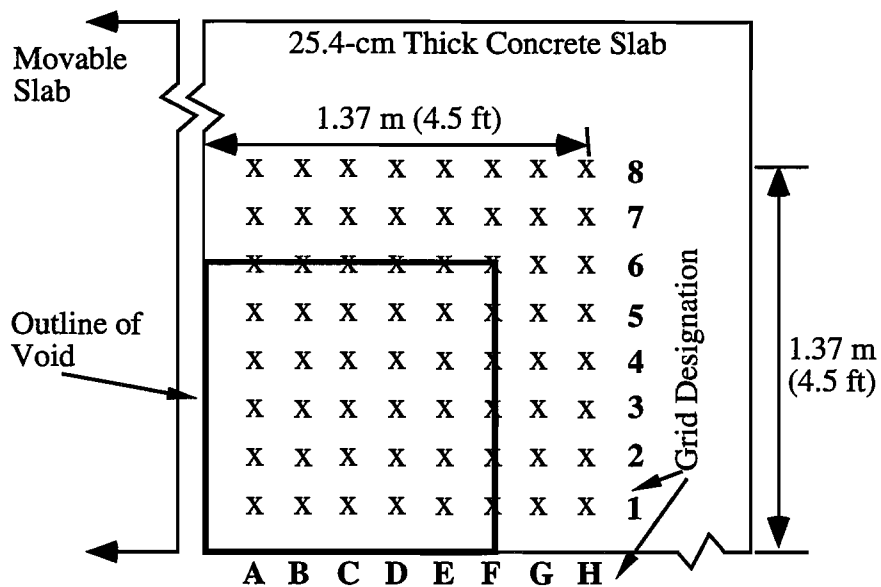


a. Comparison of Pavement Response over 15.2-cm Deep Void to Sound Pavement

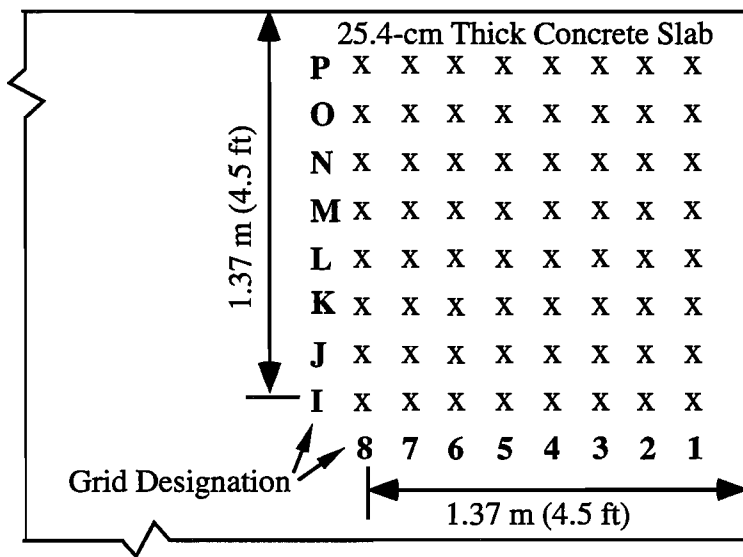


b. Comparison of Pavement Response over 25.4-cm Deep Void to Sound Pavement

Figure 5.8 Comparison of Pavement Response over Voids to the Response over Sound Pavement (Ref 33)

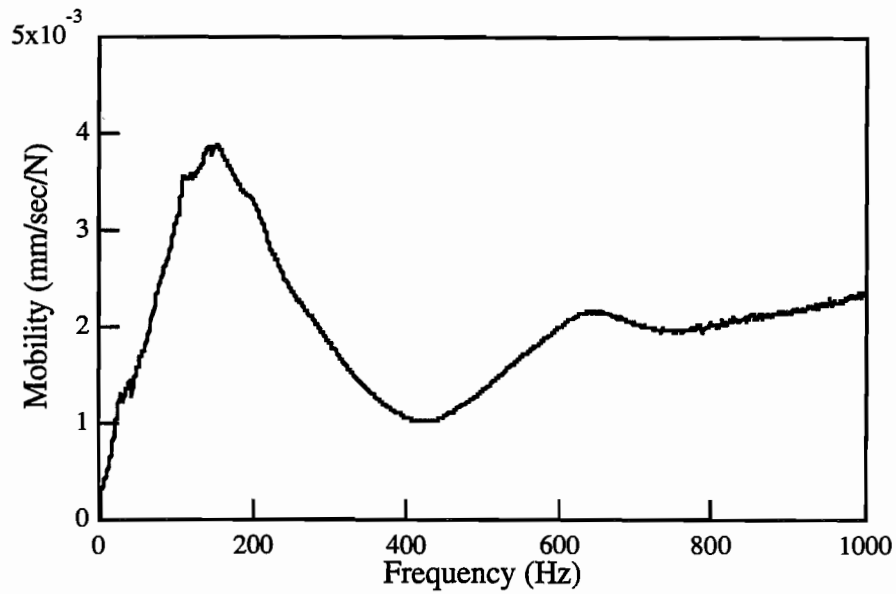


a. Testing Locations in Region 1 over Corner Void

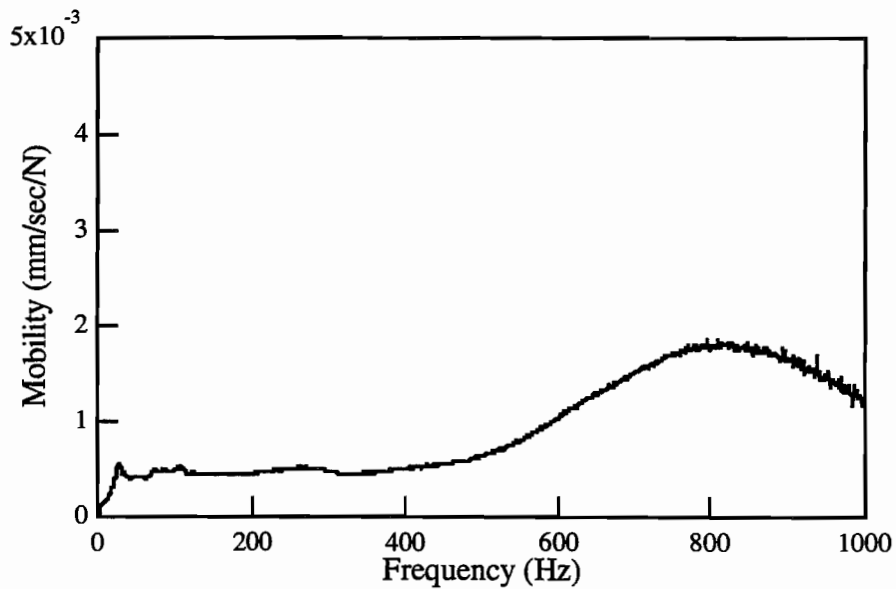


b. Testing Locations in Region 2 over Fully Supported Corner

Figure 5.9 Testing Regions 1 and 2 at Site 2 Test Facility



a. Mobility Plot From Impulse-Response Test
over Location A3 at Site 2



b. Mobility Plot From Impulse-Response Test
over Location H3 at Site 2

Figure 5.10 Comparison of Impulse-Response Tests Performed over a Void and over Sound Pavement at Site 2

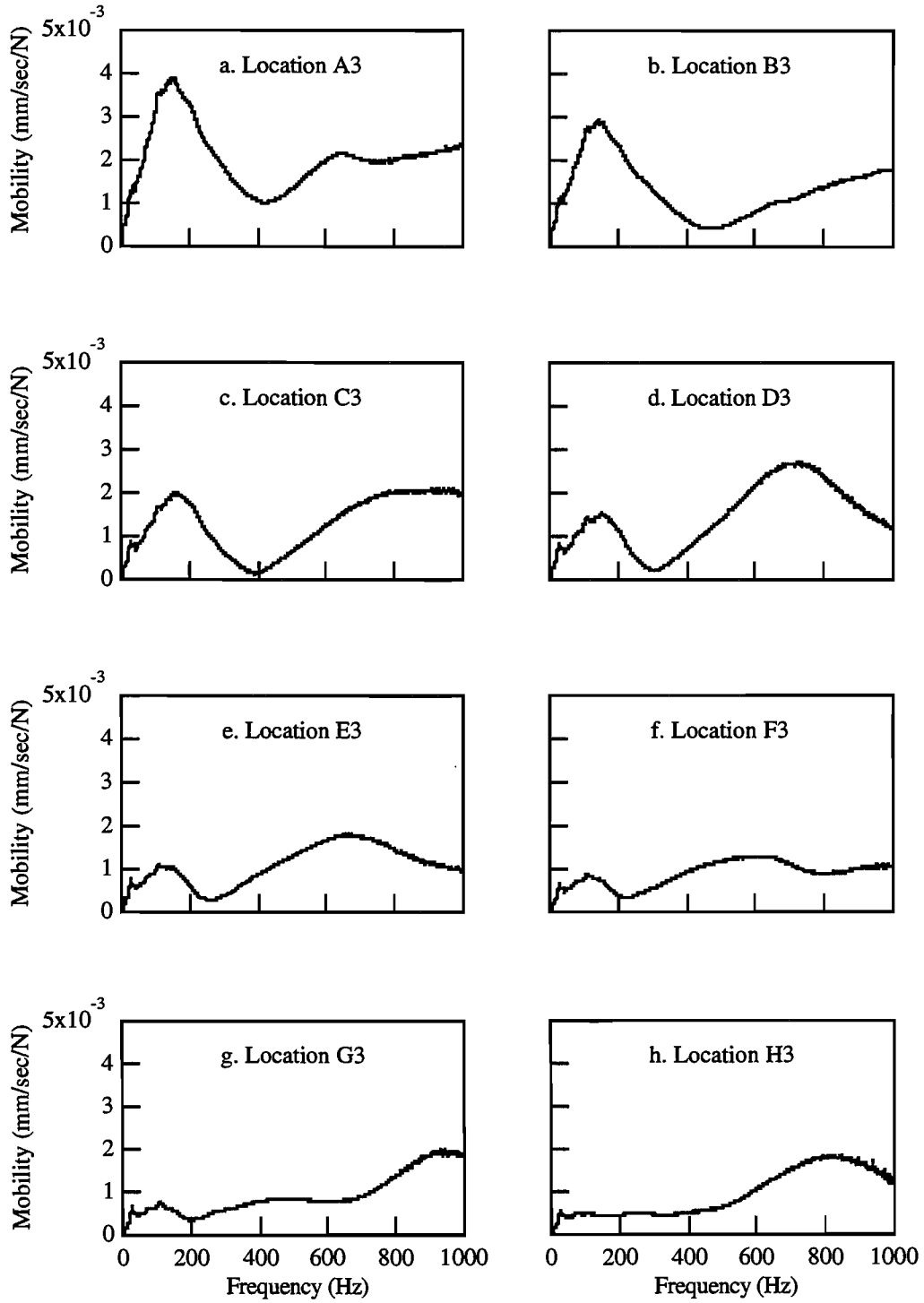


Figure 5.11 Mobility Plots from Impulse-Response Tests along Array A3 - H3 at Site 2

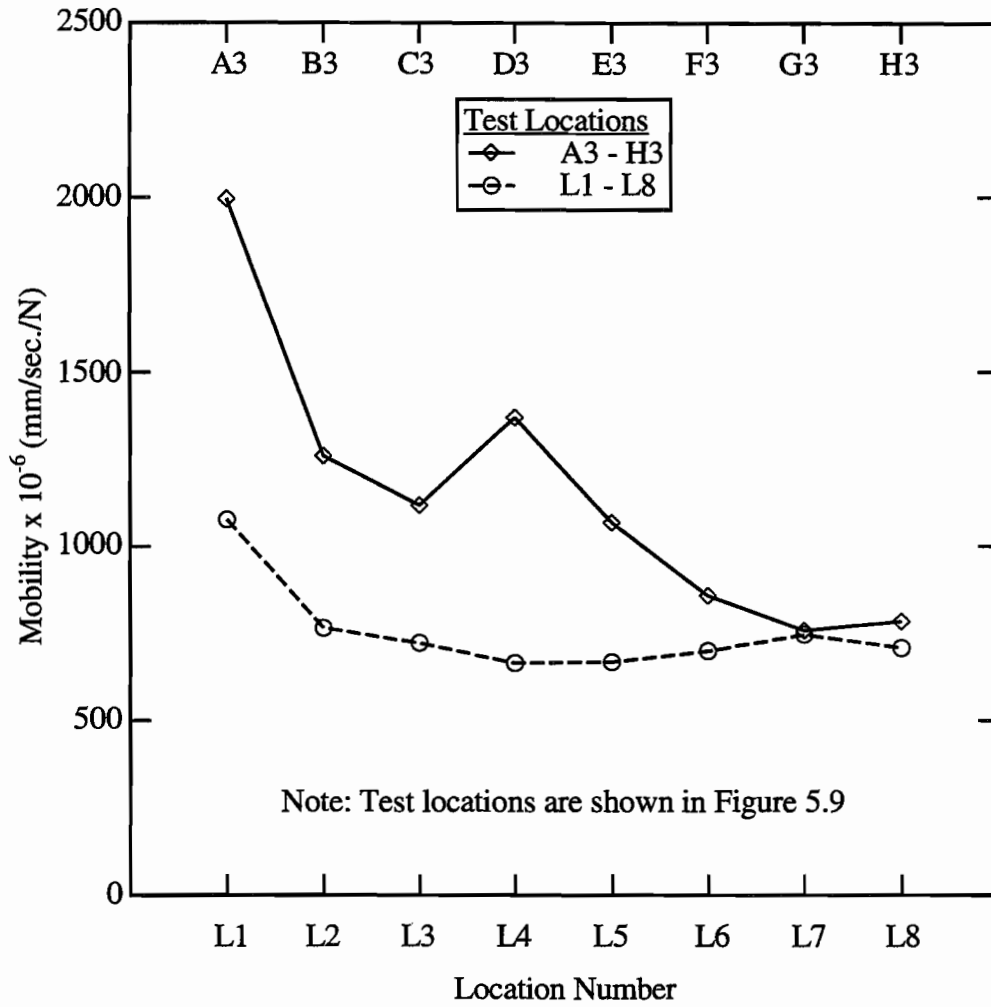


Figure 5.12 Comparison of Average Mobility Values obtained over a Void (A3-H3) and over Sound Pavement (L1-L8), at Site 2

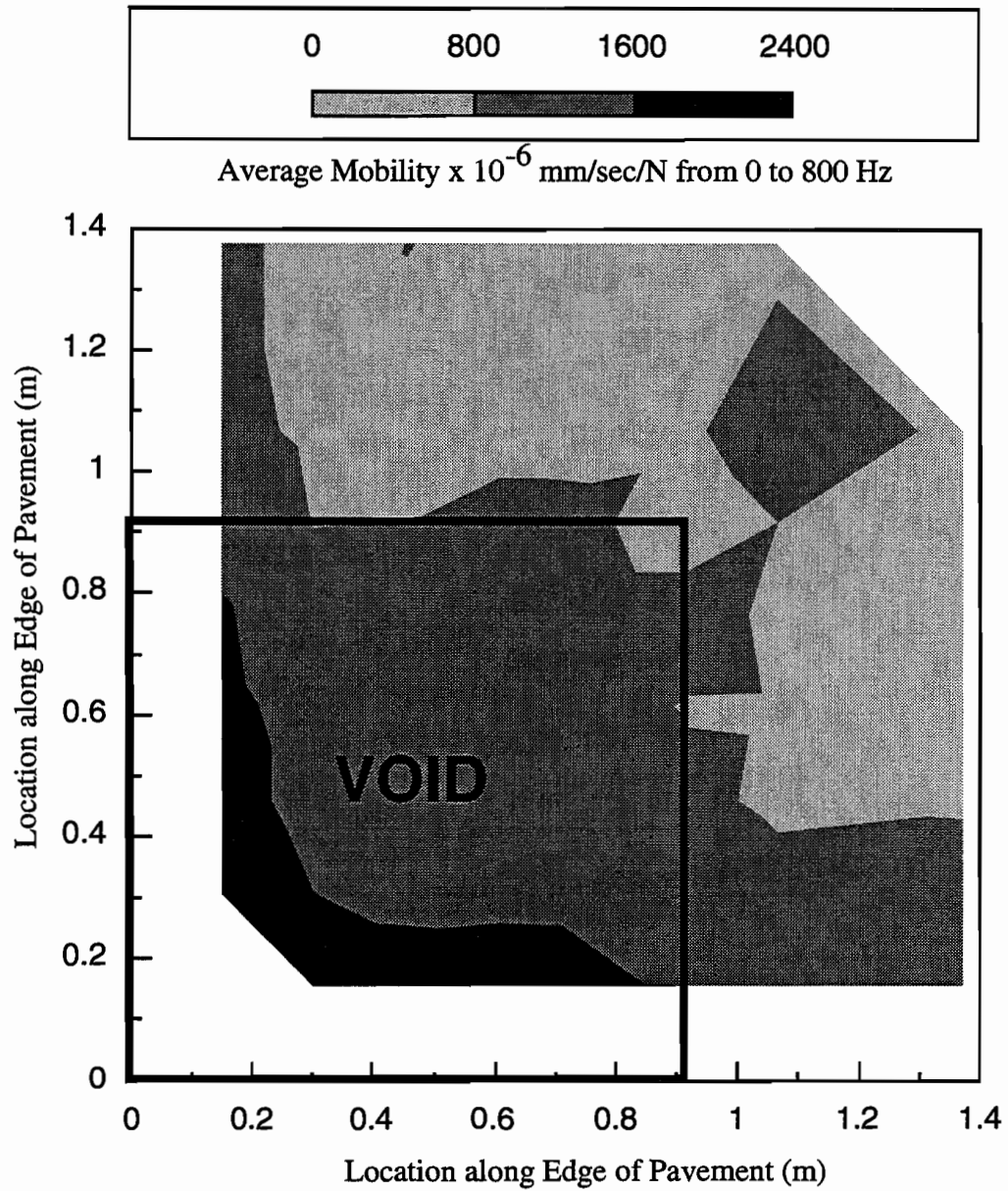


Figure 5.13 Contour Plot of Average Mobility Values from Impulse-Response Tests over Region 1 (Void) at Site 2

the north-west corner of the fixed concrete slab shown in Figure 3.7. An identical 1.4-m grid, shown in Figure 5.9b, was tested at this location. Figure 5.14 is the contour plot of average mobility values from these tests over the fully supported corner at Region 2. In this case, the average mobility values were fairly constant over the grid area, with the exception of higher mobility values near the edge of the slab. The response over the corner with sound pavement is, therefore, easily differentiated from the mobility response over the void.

The results from Regions 1 and 2 were also examined in terms of dynamic stiffness values. Dynamic slab stiffness was calculated as explained in Section 5.3.2.1. Figure 5.15 is a contour plot of dynamic slab stiffnesses obtained from tests in Region 1. A contour plot of dynamic stiffness values obtained in Region 2 is shown in Figure 5.16. A comparison of these plots shows that the stiffness values over the corner with the void are less than those obtained over the well supported corner. However, the size and location of the void are not apparent from the stiffness contours. Based on these results, it appears that presenting the data in terms of the average mobility is a better means of indicating void location and extent.

5.5.2 Debonded Pavement versus Sound Pavement

Lastly, impulse-response testing was performed along arrays over the sound concrete slab to the north (Region 3), and the debonded concrete slab to the south (Region 4), at Site 2. The testing arrays X1-X5 and Y1-Y5 are shown in Figure 5.17. The pavement profiles under these arrays are identical except for the addition of a plastic interface between the concrete and asphalt below array Y1-Y5. Figure 5.18 is a comparison of the mobility plots obtained from locations X1 and Y1. These locations are both at a distance of 0.68 m from the joint between the slabs. The response of the pavement over the debonded slab (location Y1) is differentiated from the response over the sound pavement (location X1) by several peaks spaced 125 Hz apart in the mobility plot. The cause of these peaks is unclear. Figure 5.19a shows a plot of the average mobility values along the same arrays. In both cases the joint location greatly affects the average mobility values. Away from the joint, the average mobility was slightly higher over the debonded slab than over the sound slab. Figure 5.19b is a comparison of dynamic stiffness values obtained over arrays X1-X5 and Y1-Y5. As expected, the stiffness values decreased as the distance away from the joint decreased. The debonded pavement was differentiated from the sound pavement by a decrease in stiffness values.

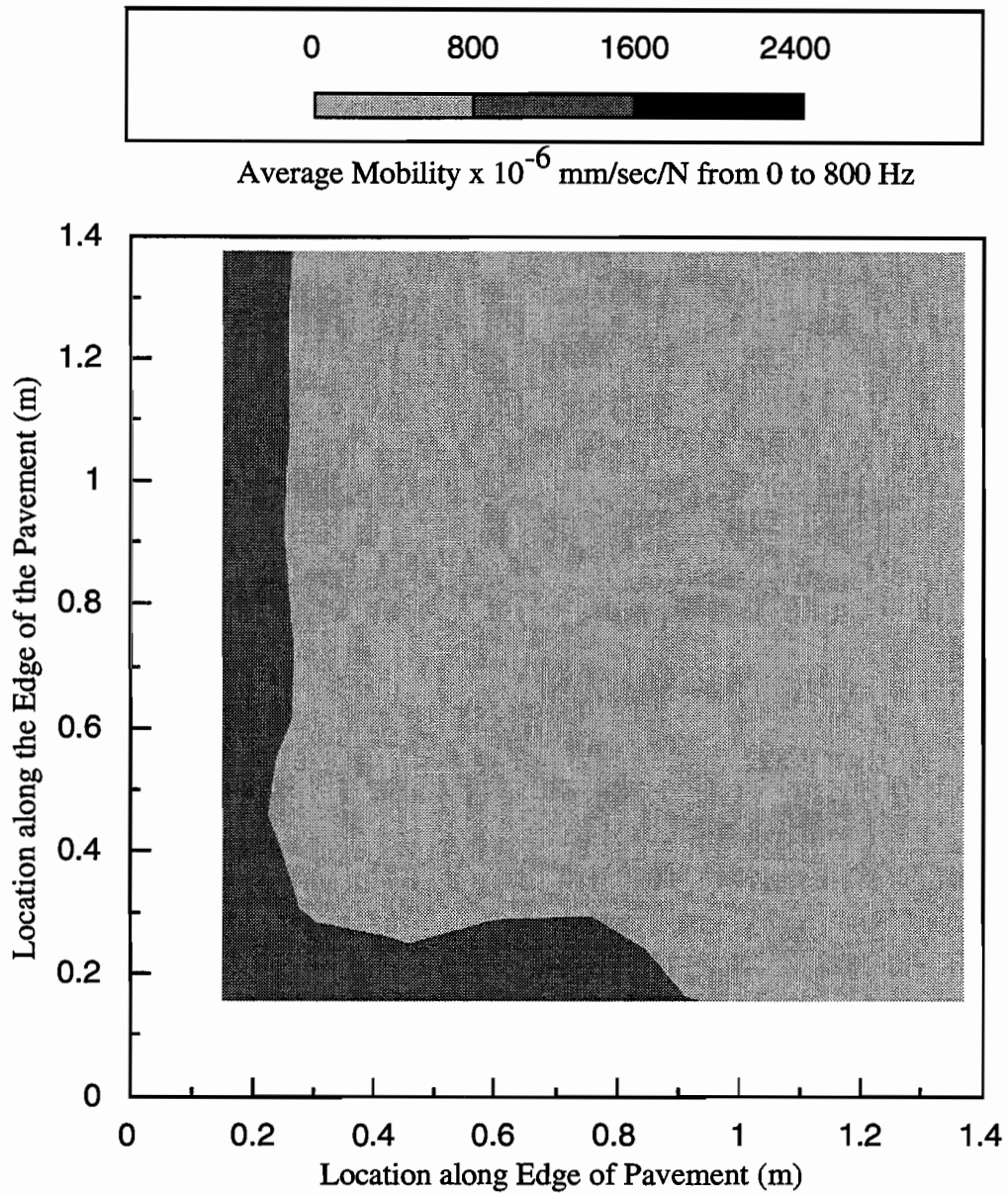


Figure 5.14 Contour Plot of Average Mobility Values from Impulse-Response Tests over Region 2 (No Void) at Site 2

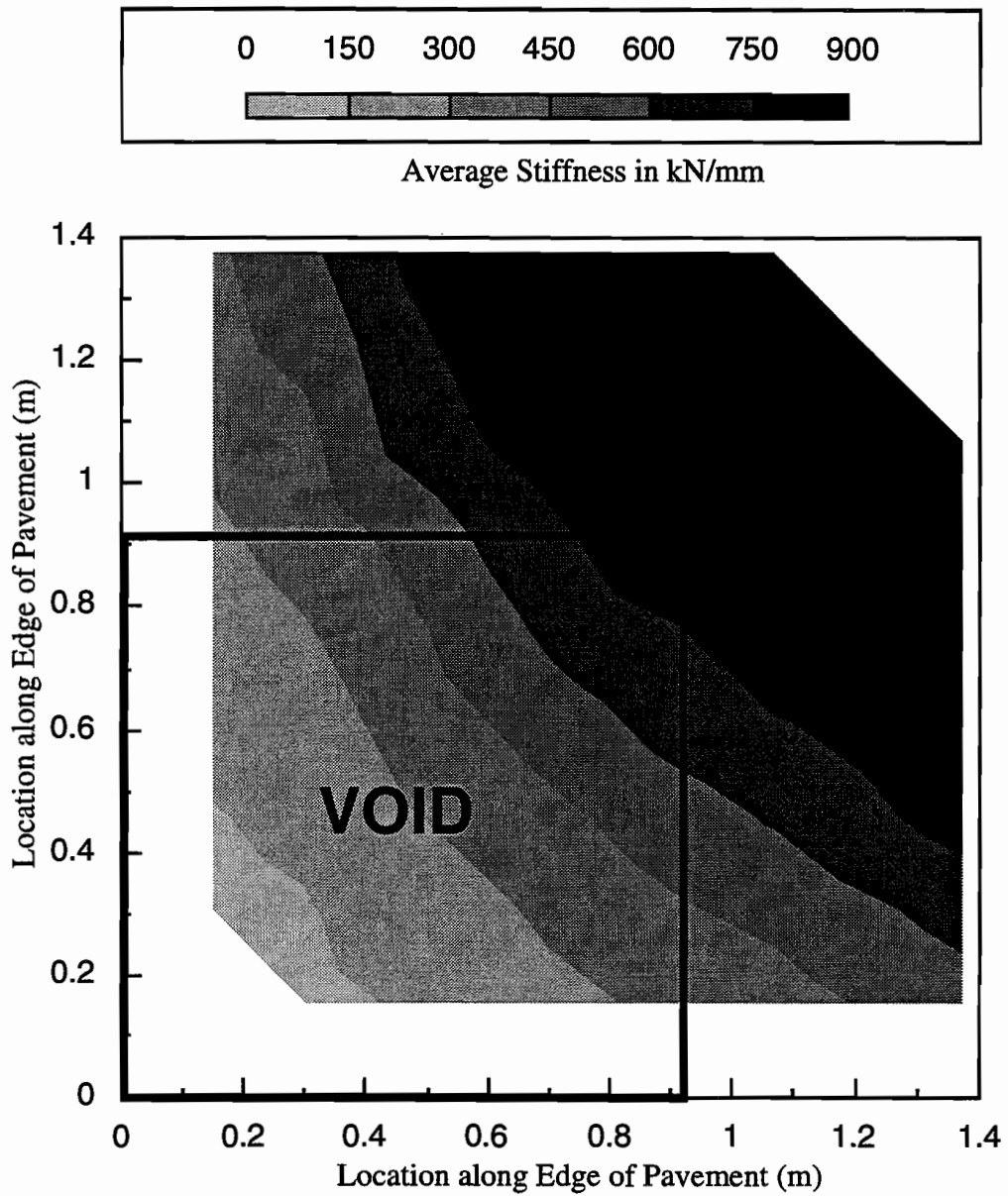


Figure 5.15 Contour Plot of Dynamic Stiffnesses from Impulse-Response Tests over Region 1 (Void) at Site 2

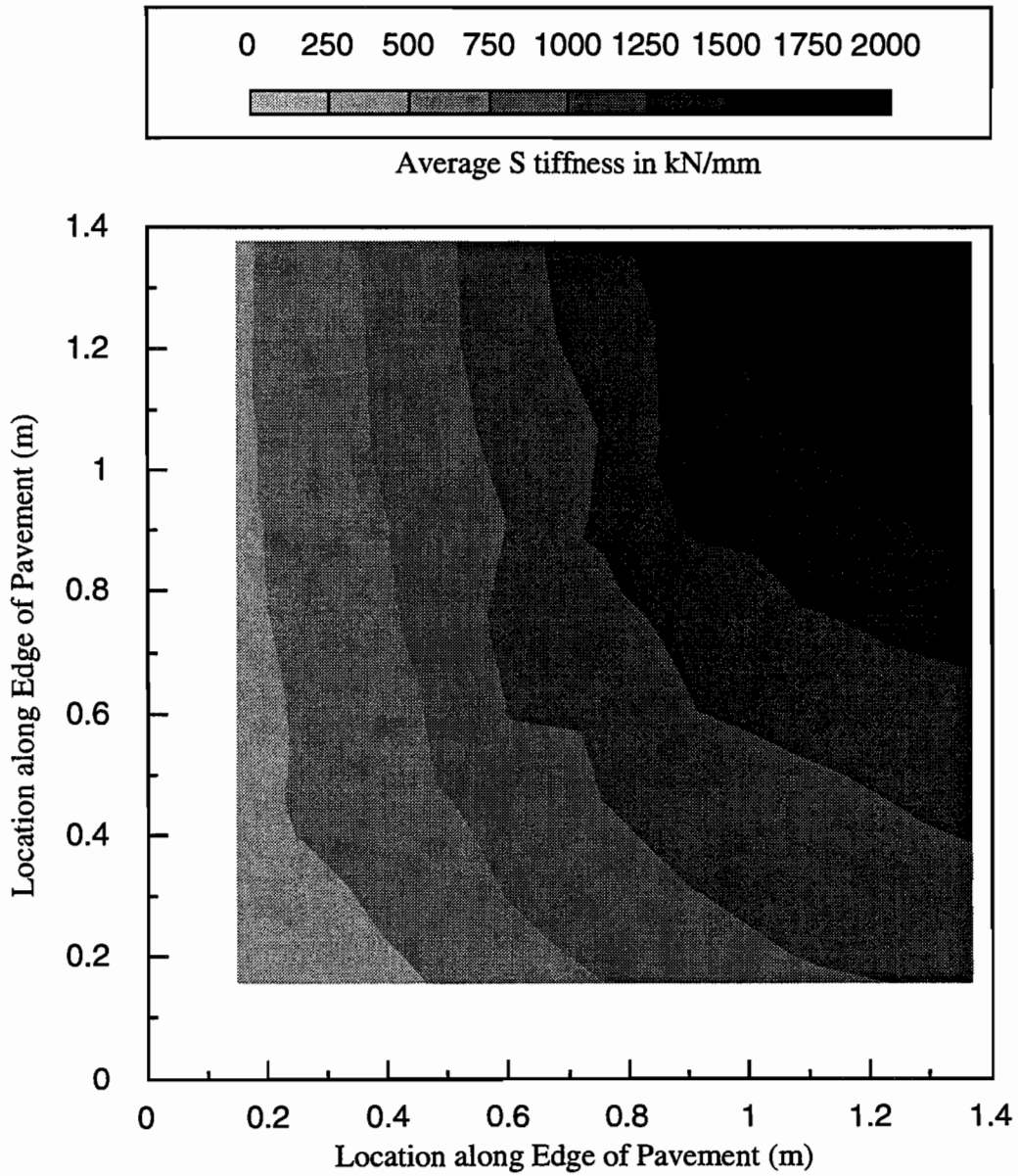
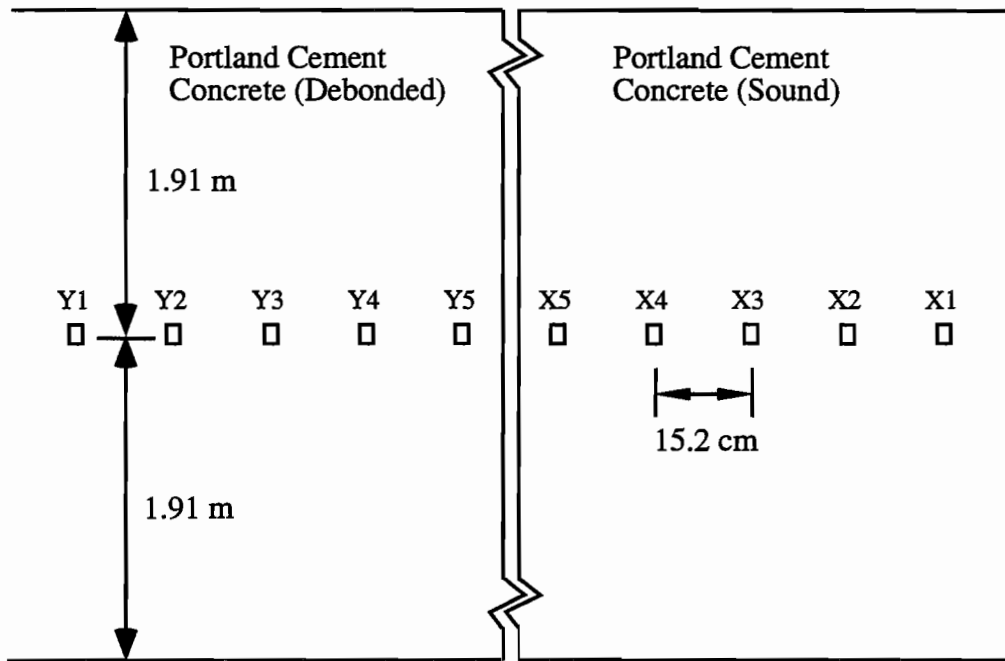
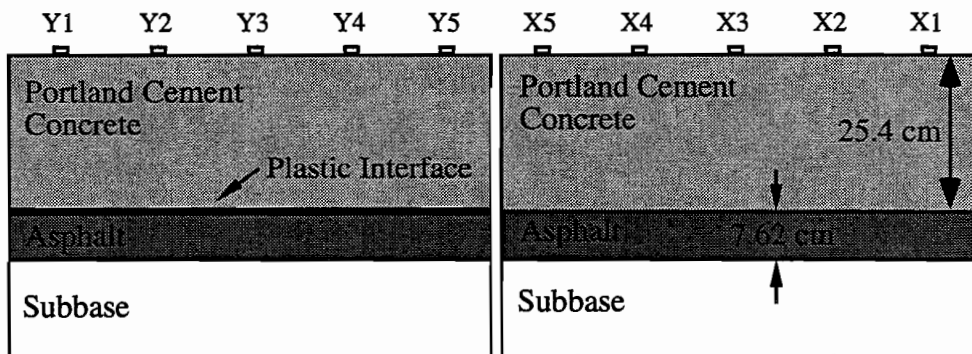


Figure 5.16 Contour Plot of Dynamic Stiffnesses from Impulse-Response Tests over Region 2 (No Void) at Site 2

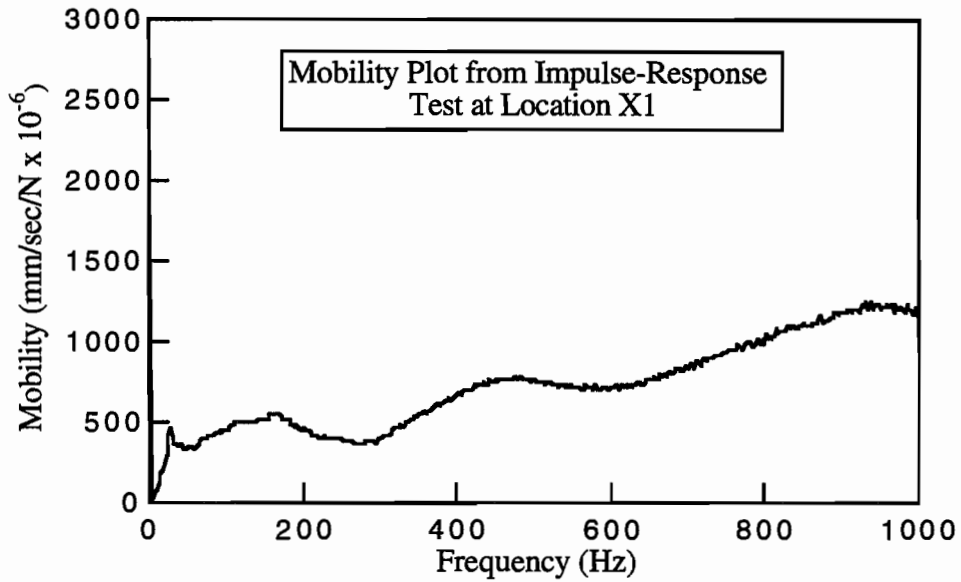


a. Plan View of Test Location Y1-Y5 and X1-X5 at Site 2

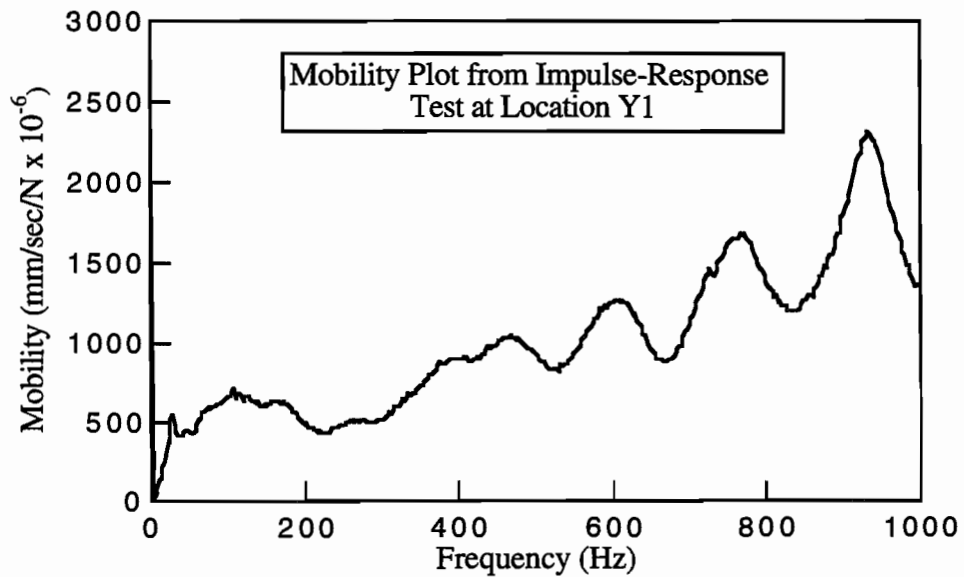


b. Profile View of Test Location Y1-Y5 and X1-X5 at Site 2

Figure 5.17 Plan and Profile Views of Test Locations X1-X5 and Y1-Y5 over Sound and Debonded Pavements at Site 2

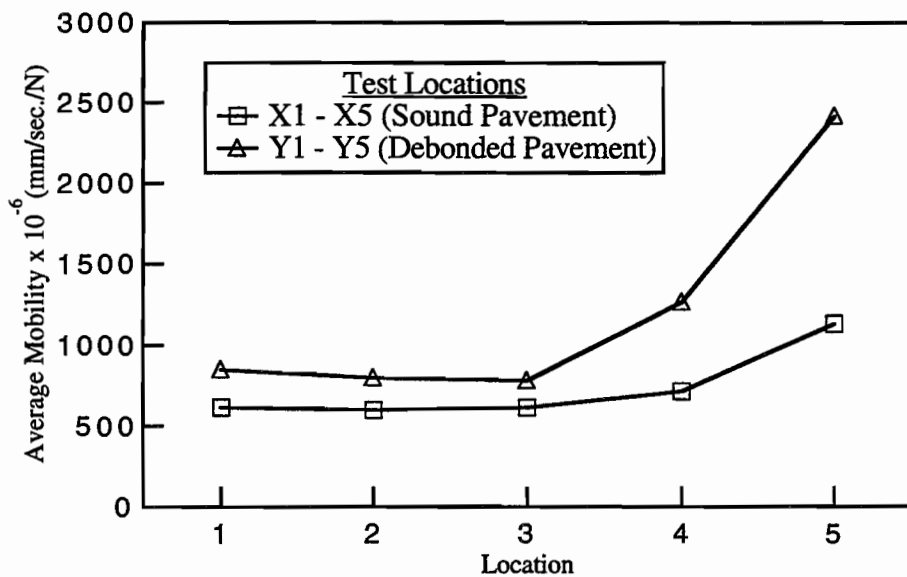


a. Mobility Plot from Test over Sound Pavement at Site 2

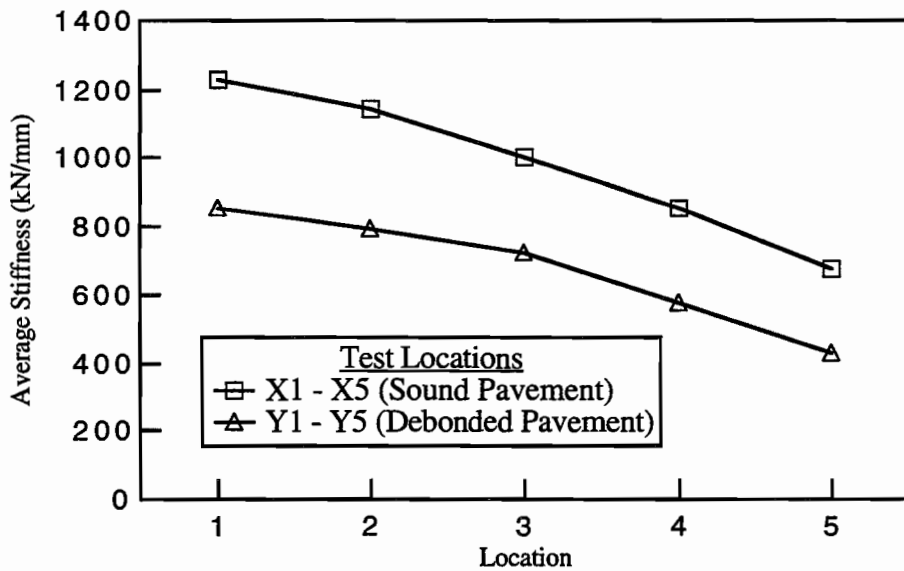


b. Mobility Plot from Test over Debonded Pavement at Site 2

Figure 5.18 Comparison of Mobility Plots from Tests over Sections of Sound Pavement and Debonded Pavement at Site 2



a. Average Mobility Values along Arrays X1 - X5 and Y1-Y5, as shown in Figure 5.17



b. Average Stiffness Values along Arrays X1 - X5 and Y1-Y5, as shown in Figure 5.17

Figure 5.19 Results from Impulse-Response Tests Performed over Sections of Sound Pavement and Debonded Pavement at Site 2

5.6 EXPERIMENTAL RESULTS FROM IMPULSE-RESPONSE TESTS AT SITE 3

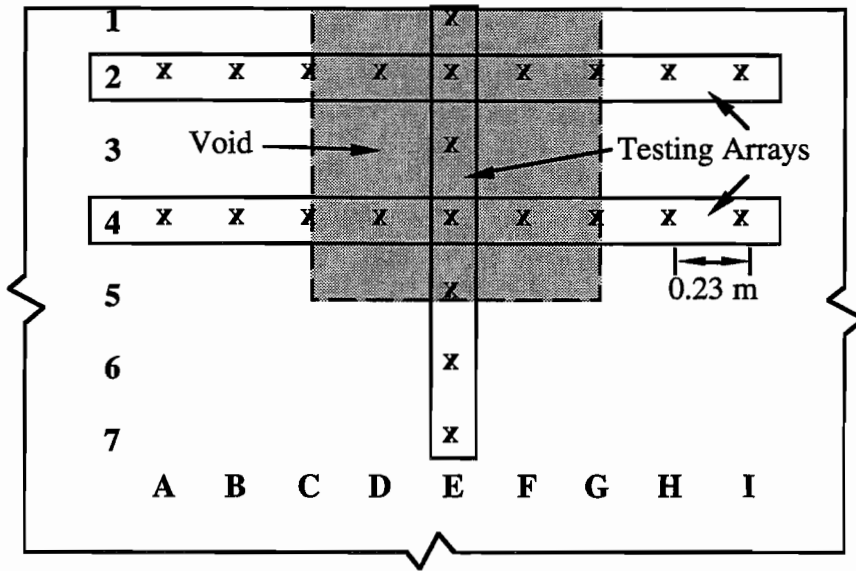
Impulse-response tests were performed on two slabs at Site 3, described in Section 3.4.3. The slabs were 17.8 cm and 30.5 cm thick, as shown in Figures 3.8 and 3.9.

5.6.1 Test Results from 17.8-cm Thick Slab at Site 3

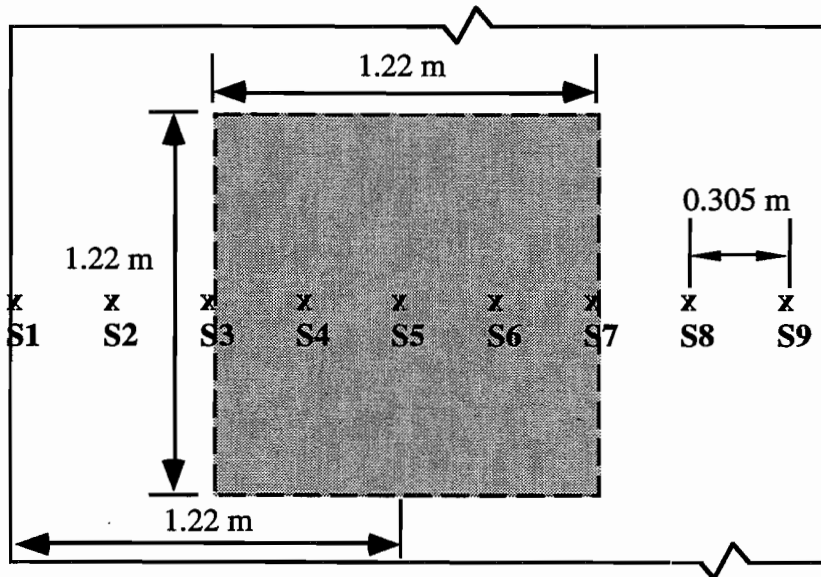
Impulse-response tests were performed over two voids in a 17.8-cm thick concrete pavement at Site 3. Void 1 was located at the edge of the slab about mid-way along the length of the slab. Three arrays were tested that passed over the void location, as shown in Figure 5.20a. Figure 5.21 shows the mobility plots from tests along array A4 to I4. As was observed from tests at Site 2, the void is differentiated from sound pavement by undulating, higher magnitude mobility plots over the void.

Figures 5.22a and 5.22b show a comparison of average mobility values from tests along arrays A2-I2, A4-I4 and E1-E7. Comparison of the average mobility plots along arrays A2-I2 and A4-I4 shows the edge effect on the mobility plots. Array A2-I2 is 22.9 cm from the edge of the slab while array A4-I4 is 45.8 cm from the edge of the slab. When compared to the results along array A4-I4, the average mobility values along A2-I2 are higher due to the effect of the edge of the slab. In both cases, however, the peak average mobility value over the void is approximately twice the value from tests over the pavement with no void. Figure 5.22b shows the edge effect over the void from tests performed along the array E1-E7. The mobility is very high near the edge and over the void, but levels to a value of approximately 1100 mm/sec/N away from the void.

The data from these tests over the 0.915-m square void are also presented in terms of the dynamic stiffness of the slab. Figure 5.23 is a comparison of stiffness profiles along arrays A2-I2, A4-I4, and E1-E7. In this case, it is expected that the stiffness of the slab would decrease over the void. As seen in Figures 5.23a and 5.23b, there is a slight decrease in stiffness over the void for both arrays A2-I2 and A4-I4. The decrease, however, is fairly small and gradual and does not clearly delineate the boundaries of the void. The effect of the edge on the stiffness profiles, however, is clearly seen in these plots. The stiffness along A2-I2 which is 22.9 cm from the edge of the slab is about 200 kN/mm less than the stiffness along array A4-I4 which is 45.7 cm from the edge. Figure 5.23b shows the stiffness profile over the void moving away from the



a. Testing Locations over Edge Void



b. Testing Location over Interior Void

Figure 5.20 Testing Locations over Voids in 17.8-cm Thick Concrete Pavement at Site 3

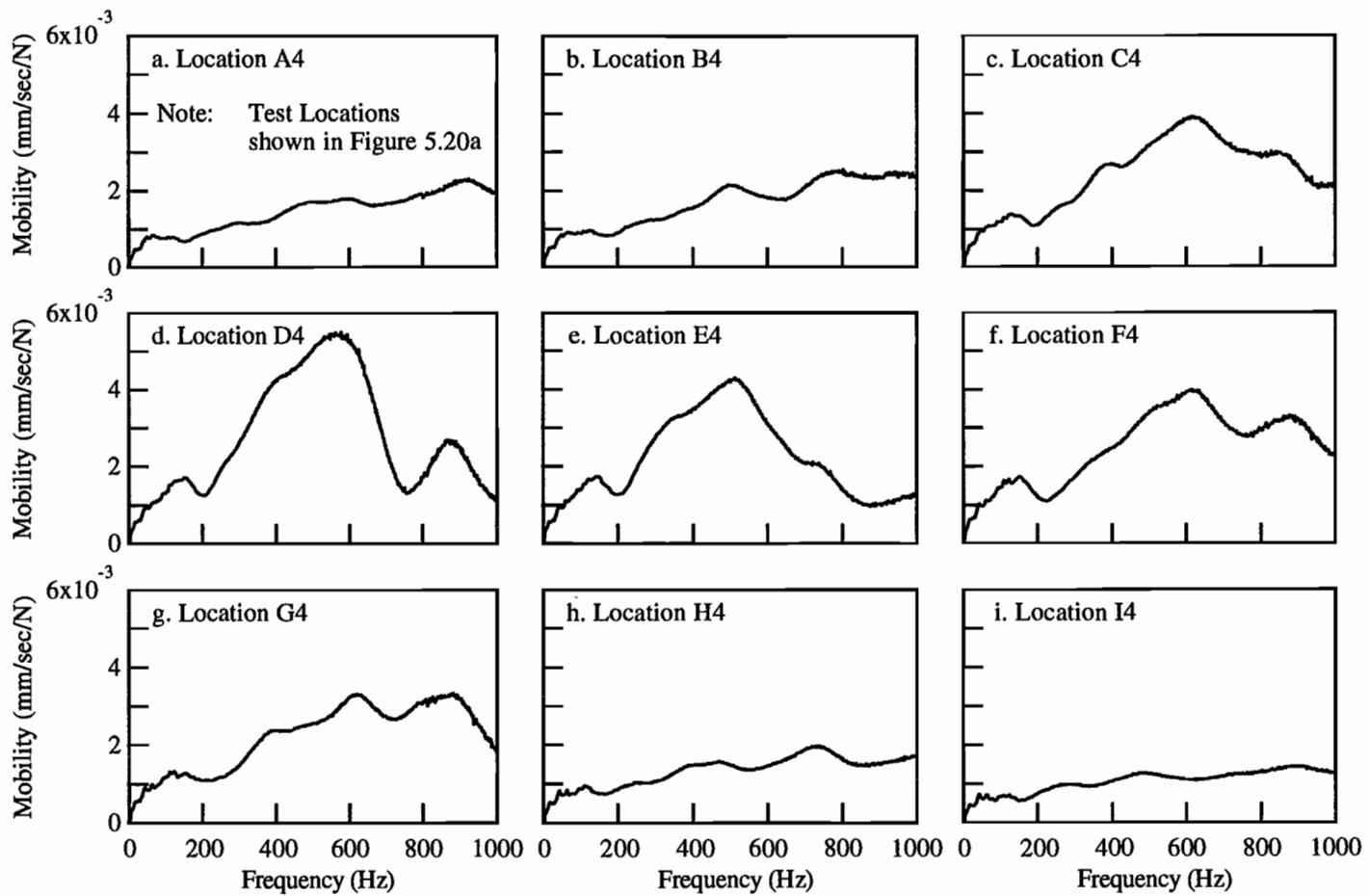
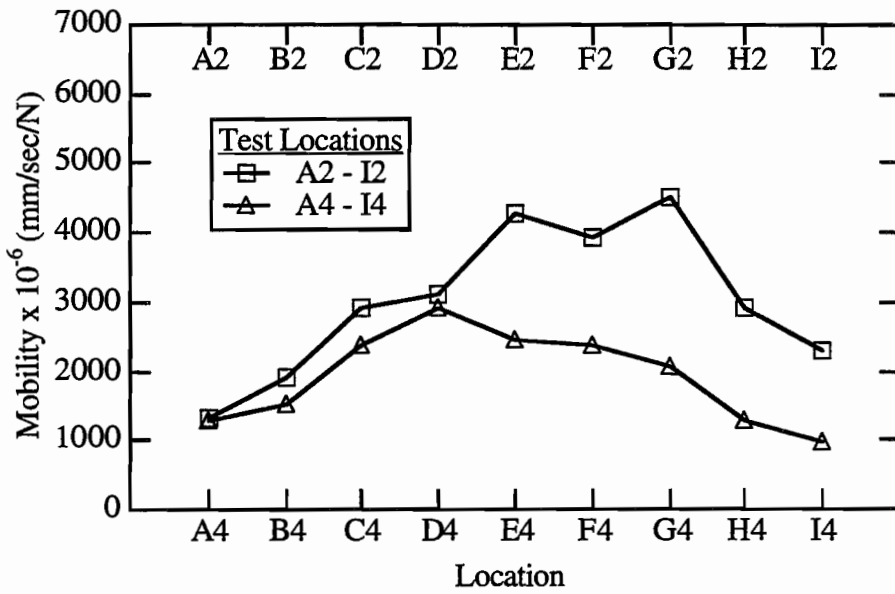
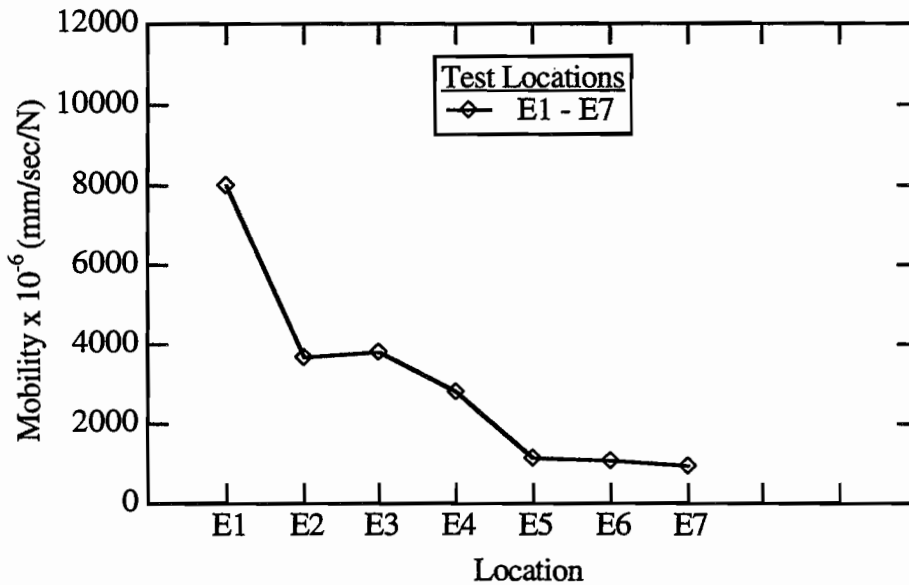


Figure 5.21 Mobility Plots from Impulse-Response Tests Performed along Array A4 - H4 over the 17.8-cm (7-in) Thick Concrete Pavement at Site 3

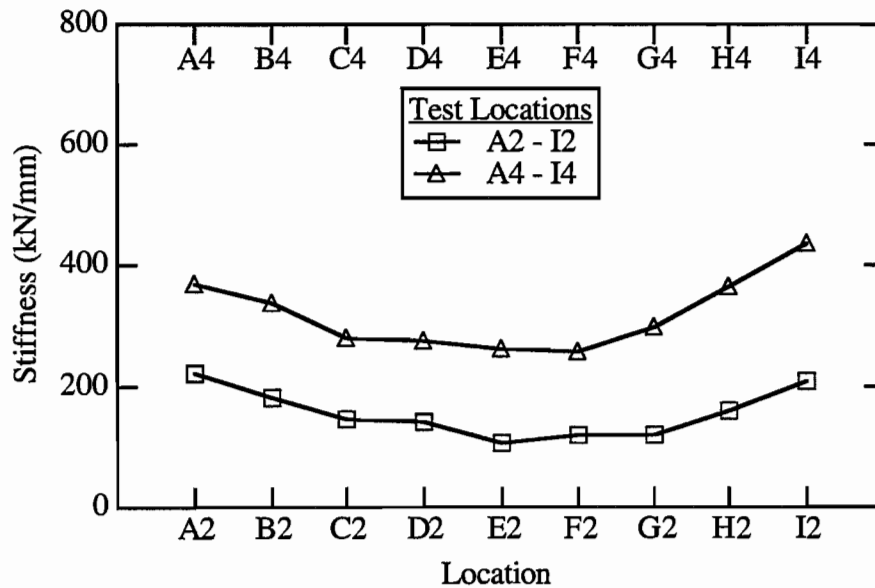


a. Average Mobility Values along arrays A2-I2 and A4-I4, as shown in Figure 5.20a

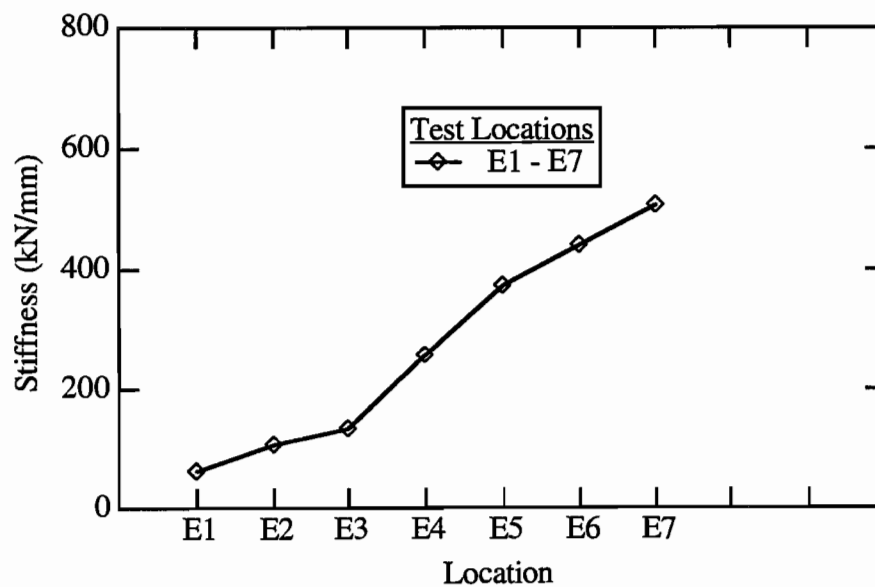


b. Average Mobility Values along array E1-E7, as shown in Figure 5.20a

Figure 5.22 Average Mobility Values from Impulse-Response Tests Performed over a 0.915-m Square Edge Void Beneath a 17.8-cm (7-in.) Thick Concrete Pavement at Site 3



a. Dynamic Stiffness Values along arrays A2-I2 and A4-I4, as shown in Figure 5.20a



b. Dynamic Stiffness Values along array E1-E7, as shown in Figure 5.20a

Figure 5.23 *Dynamic Stiffness Values from Impulse-Response Tests Performed over a 0.915-m Square Edge Void Beneath a 17.8-cm (7-in.) Thick Concrete Pavement at Site 3*

edge. The stiffness increases as the test location is moved further from the edge of the pavement. The lower stiffness values over the void are both a function of the edge location and the effect of the void. Based on the results over A2-I2 and A4-I4, the edge effect appears to be a dominating factor for stiffness values. Based on the stiffness measurements along array E1-E7, the termination point of the void is not apparent, as compared with the mobility measurements shown in Figure 5.22b, where the termination of the void is marked by average mobility values that level out to a fairly constant value.

Tests were next performed along array S1-S9 across a 1.22-m square void with its center located 1.22-m from the edge of the pavement, as shown in Figure 5.20b. In this case, the edges of the concrete over the void were supported on all four sides. Figure 5.24 shows the mobility plots along the array S1-S9. The effect of the void is not as apparent in this case as was the case for the void along the edge of the pavement. When the data is reduced to plots of average mobility, as shown in Figure 5.25a, the effect of the void is somewhat apparent. Over locations S2-S4, on the outer edge of the void, the mobility is fairly constant, over the void (locations S4-S6) the mobility increases slightly, and then decreases to a constant value on the interior side of the void (locations S7-S9). The mobility values are slightly lower over the interior of the slab than over the pavement on the exterior side of the void because of the effect of the edge on mobility values.

When the data from these tests are displayed in terms of stiffness, as shown in Figure 5.25b, the effect of the void is masked by the edge effects of the pavement. The stiffness values over S1-S3 increase fairly linearly due to the increasing distance from the edge of the pavement. At locations S4-S6, where the void is encountered, the combined effect of the distance from the edge and the void below the slab cause a slight disruption in the linear trend. Past the void, at locations S7-S9 on the interior of the pavement, the stiffness values level out to a fairly constant value of about 600 kN/mm. As in the case of the edge void, the average mobility plots appear to provide better information than the dynamic stiffness plots concerning the location and lateral extent of the void.

5.6.2 Test Results from 30.5-cm Thick Slab at Site 3

Impulse-response tests were also performed on a 30.5-cm thick concrete pavement shown in Figure 3.9. Tests were performed along two arrays that passed over the 0.915-m square edge void. The array locations J2-R2 and J4-R4 were mislocated, so the tests on sound pavement were performed on only one side of the void, as shown in Figure 5.26. Figure 5.27 shows the mobility

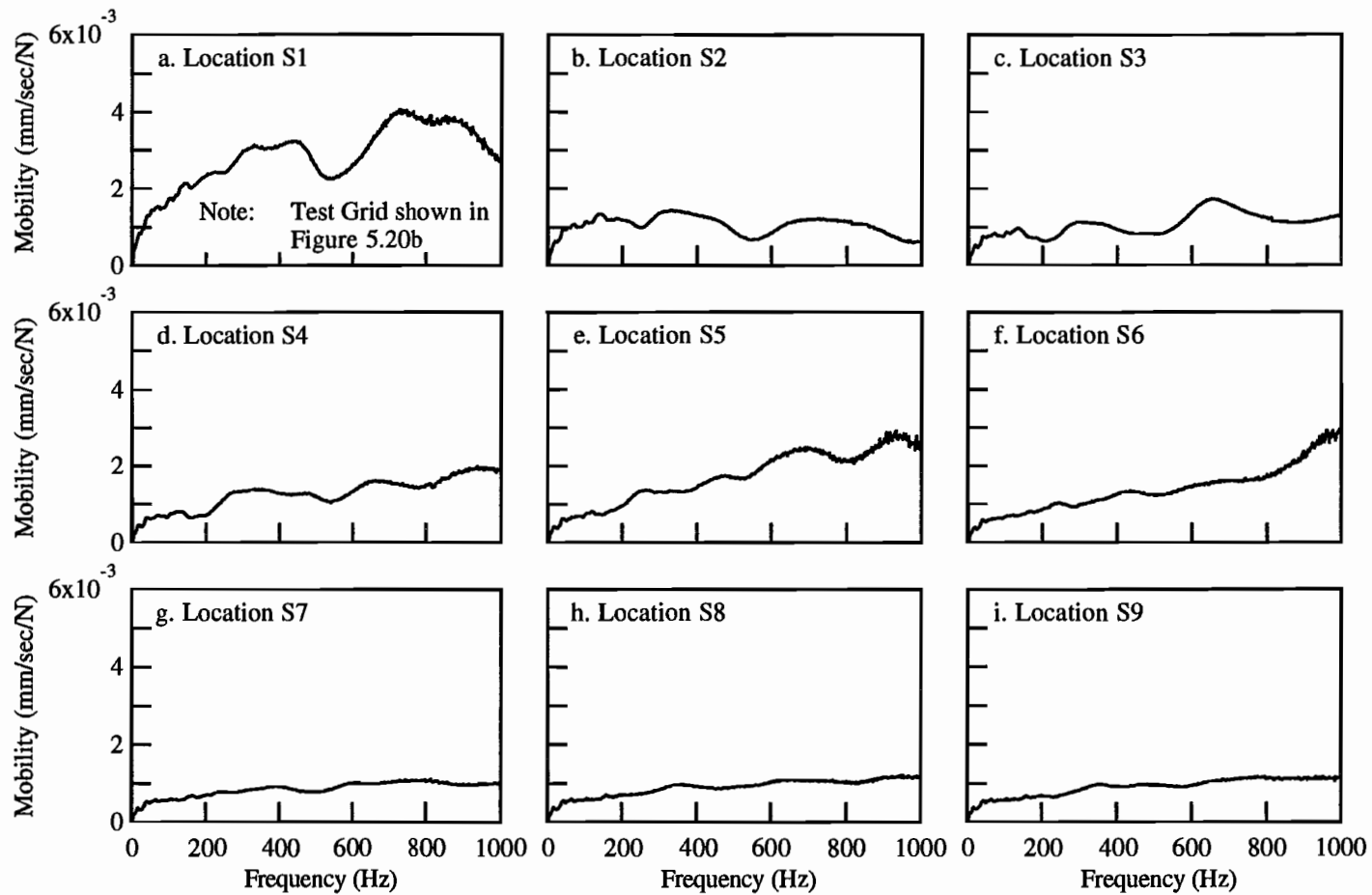
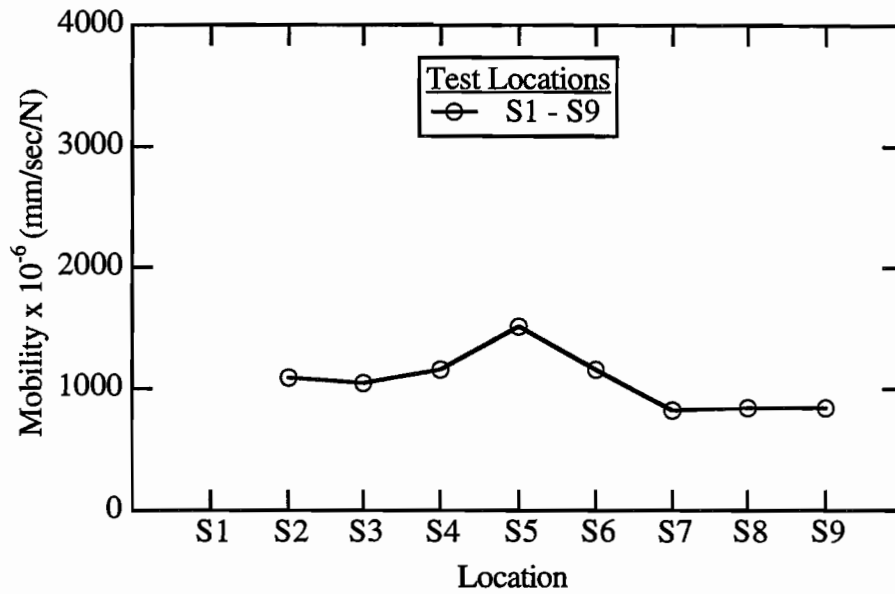
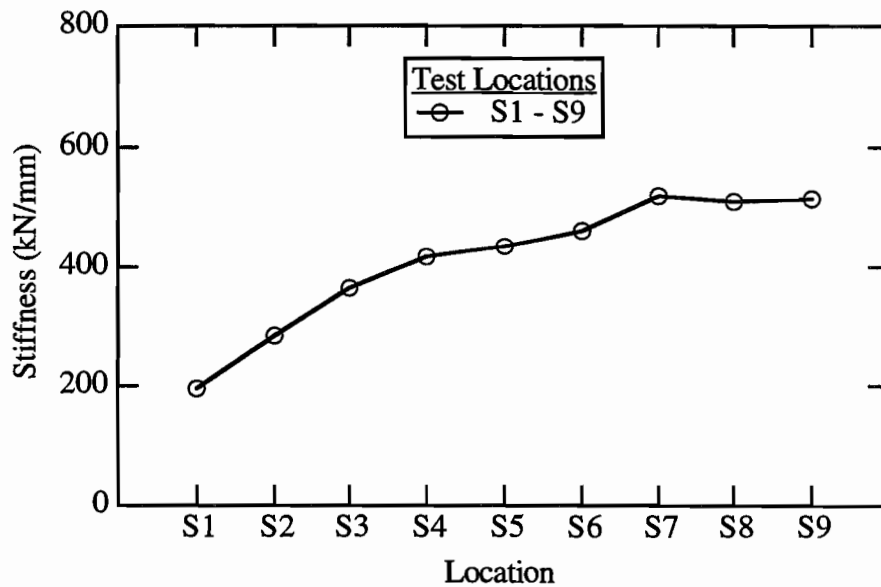


Figure 5.24 Mobility Plots from Impulse-Response Tests Performed along Array S1 - S9 over the 17.8-cm (7-in) Thick Concrete Pavement at Site 3

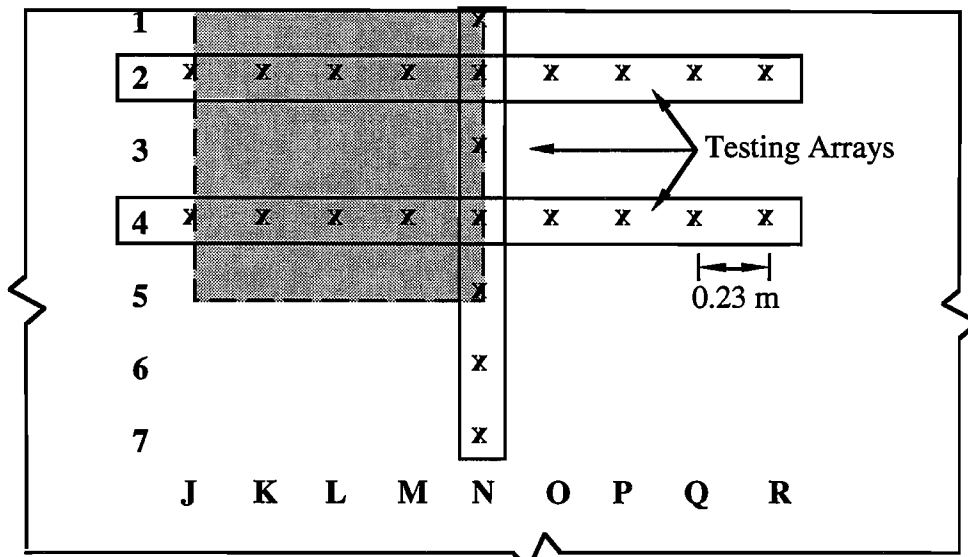


a. Average Mobility Values along Array S1-S9, as shown in Figure 5.20b

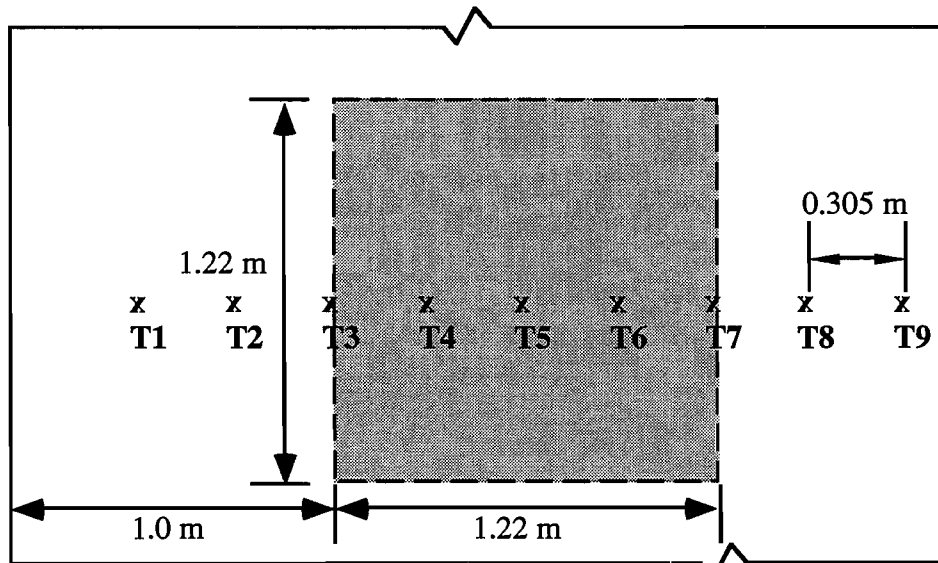


b. Apparent Stiffness Values along Array S1-S9, as shown in Figure 5.20b

Figure 5.25 Results from Impulse-Response Tests Performed over a 1.22-m Square Interior Void Beneath a 17.8-cm (7-in.) Thick Concrete Pavement at Site 3



a. Testing Locations over Edge Void



b. Testing Locations over Interior Void

Figure 5.26 Testing Locations over Voids in 30.5-cm Thick Concrete Pavement at Site 3

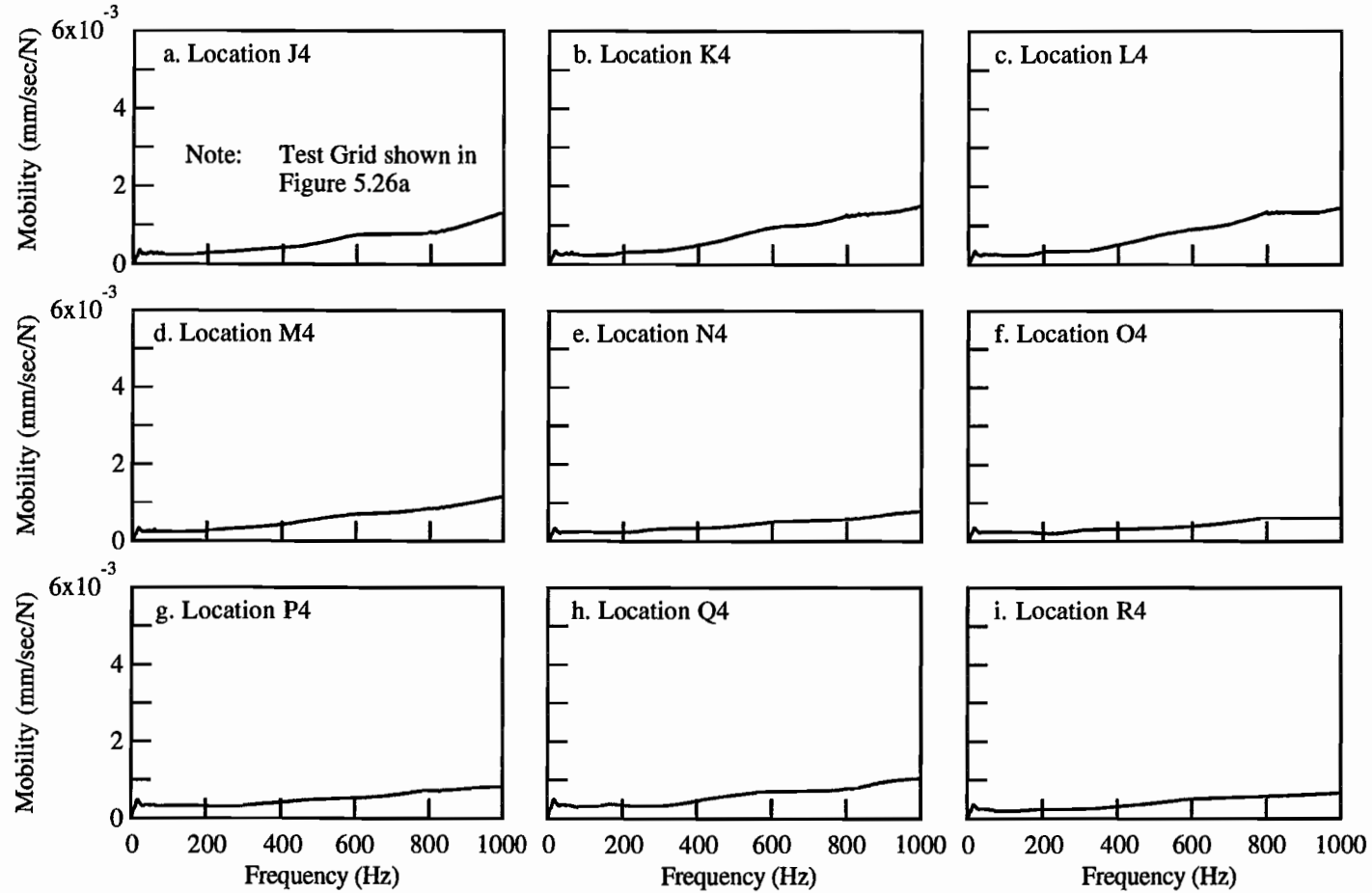


Figure 5.27 Mobility Plots from Impulse-Response Tests Performed along Array J4 - R4 over the 30.5-cm (12-in) Thick Concrete Pavement at Site 3

plots along array J4-R4. The effect of the void is not as readily apparent by inspection as was the case over the 17.8-cm thick concrete slab. In terms of average mobility values, shown in Figure 5.28a, the effect of the void along array J4-R4 is seen by average mobility values that are about 1.5 times greater than those measured away from the void. Results over array J2-R2 are more pronounced due to the closer location to the unsupported edge of the slab. As expected, all mobility values measured over this slab were much less than corresponding values measured over the 17.8-cm thick slab. This difference is due to the greater stiffness of the thicker concrete slab

In terms of dynamic slab stiffness, the void could not be detected along either array J2-R2 or J4-R4, as shown in Figure 5.28b. The increase in stiffness over array J4-R4 is due to the greater distance from the edge of the slab. In all cases the stiffness values were higher than those measured at comparable locations over the 17.8-cm thick pavement, shown in Figure 5.23a.

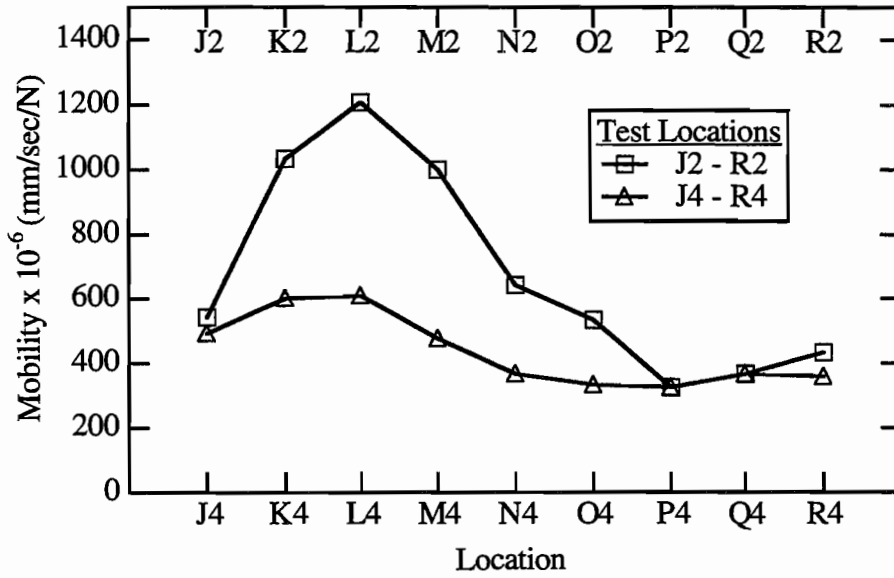
Testing was also performed along array T1-T9, shown in Figure 5.26b, located across a 1.22-m square void. The outer edge of the void was located 1.0 m from the edge of the pavement. Figure 5.29 shows the mobility plots obtained over locations T1-T9. When the data is displayed in terms of average mobility, as shown in Figure 5.30a, the void is detected by a region of higher average mobility values. In this case, the highest value over the void was approximately twice the average values away from the void.

Figure 5.30b is a plot of the dynamic slab stiffness values along array T1-T9. From locations T1-T3, the stiffness increases due to increasing distance from the edge of the pavement. Over the void, at locations T4-T6, the stiffness values decrease slightly. Past the void, the stiffness again continues to increase. The effect of the void, therefore, is detectable, but is overshadowed by the effect of the pavement edge.

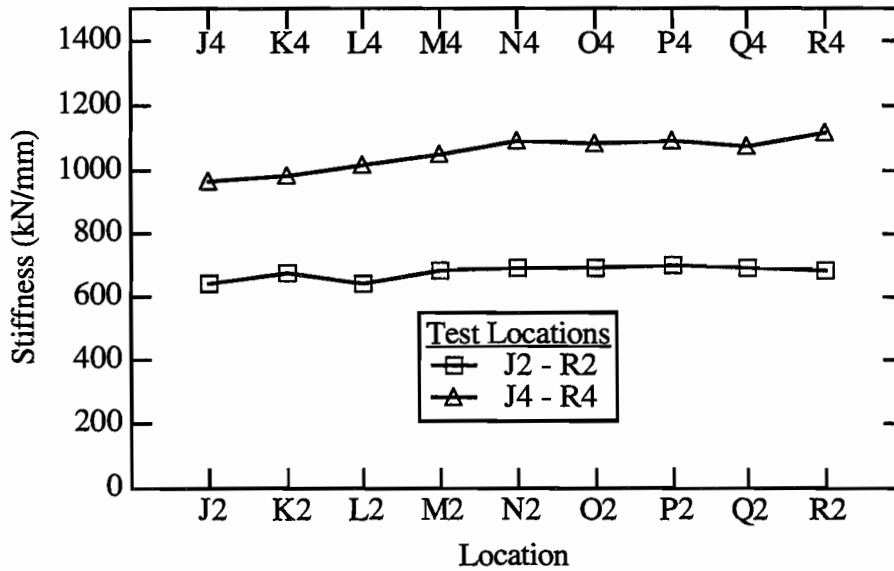
5.7 HIGHER FREQUENCY FLEXURAL RESPONSE

As discussed in Section 5.4, the impulse-response instrumentation is limited to detecting voids that produce flexural vibrations in the low frequency (10 to 1000 Hz) range. Voids that are small or deep, will vibrate in flexure at higher frequencies and, therefore, can not be detected by the impulse-response instrumentation. The higher frequency flexural vibrations, however, can still be of use for detecting the flaws. The instrumentation used for impact-echo testing will respond to vibrations higher than 1000 Hz. Therefore, the high-frequency responses generated by smaller, deeper voids may be detected using this instrumentation.

Testing using impact-echo instrumentation was performed along the east end of the concrete slab at Site 1 passing over the 5.1-cm square "tunnel" with a crown depth of 2.54 cm ,



a. Average Mobility Values along Arrays J2-R2 and J4-R4, as shown in Figure 5.26a



b. Apparent Stiffness Values along Arrays J2-R2 and J4-R4, as shown in Figure 5.26a

Figure 5.28 Results from Impulse-Response Tests Performed over a 0.915-m Square Edge Void Beneath a 25.4-cm (10-in.) Thick Concrete Pavement at Site 3

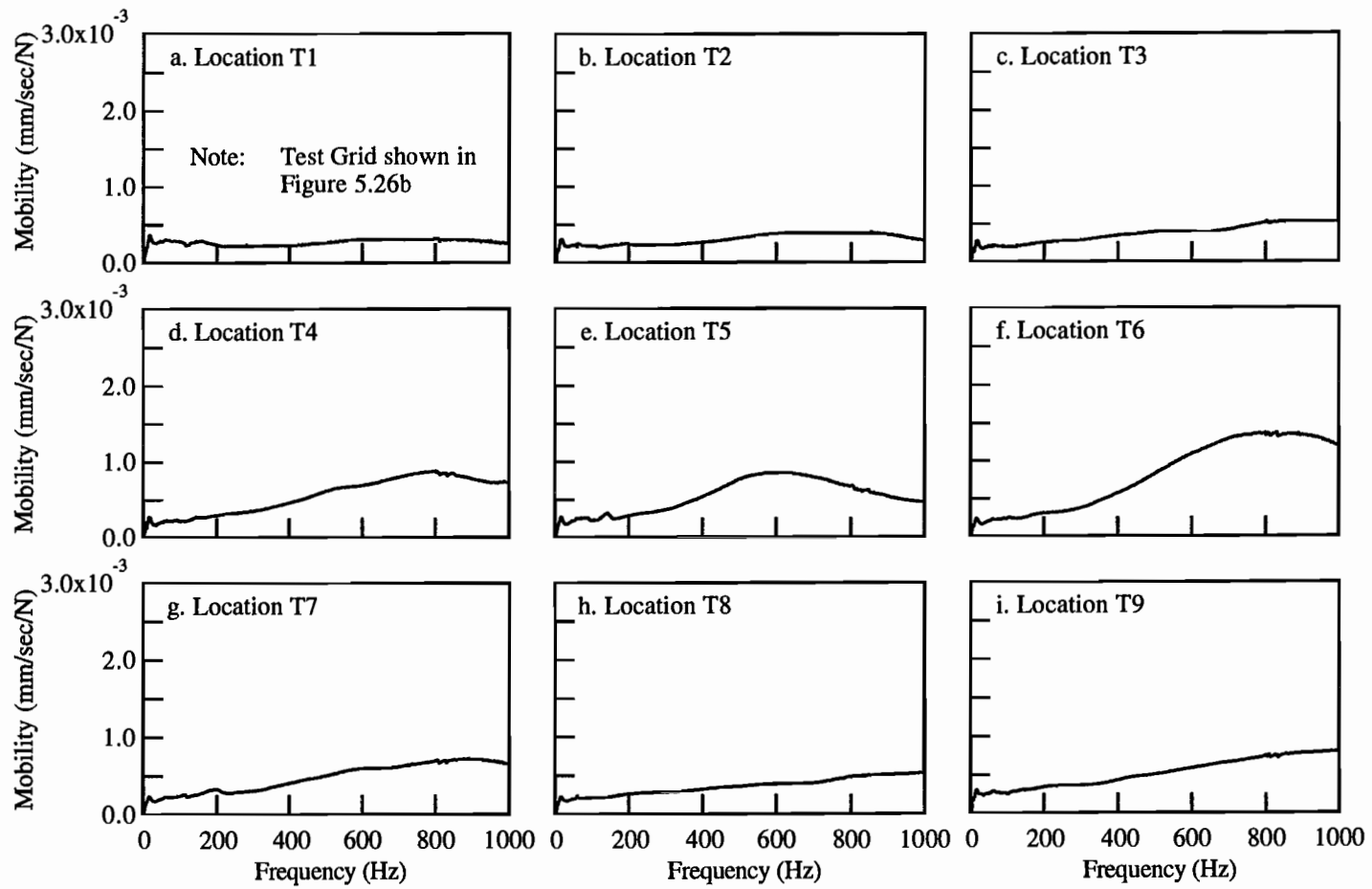
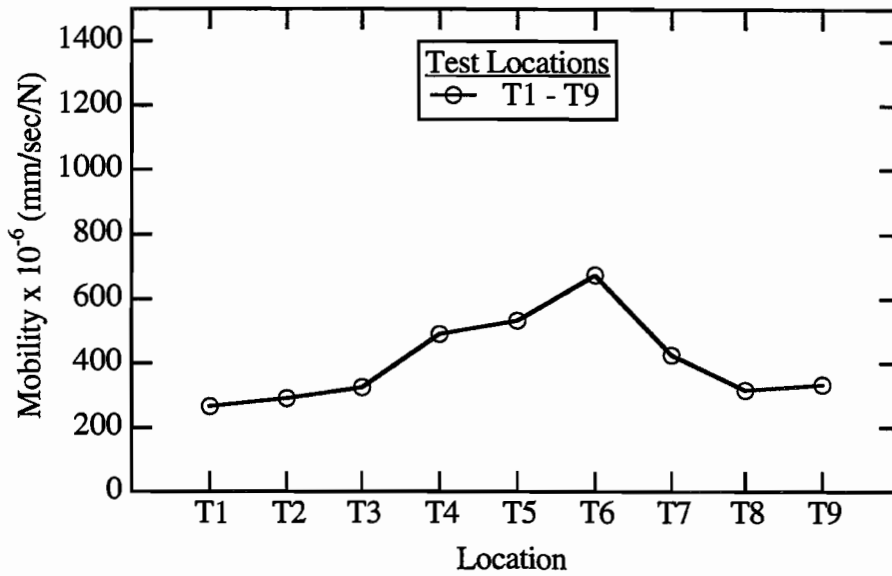
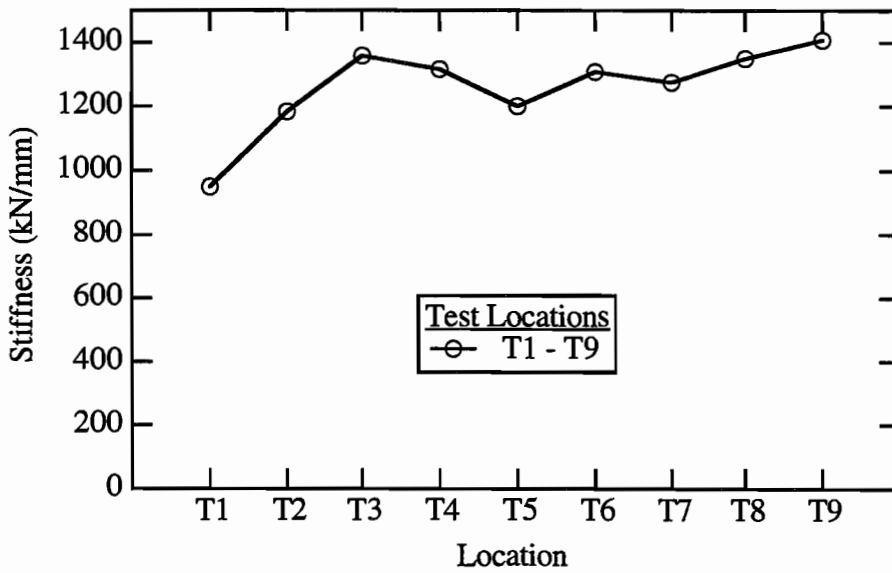


Figure 5.29 Mobility Plots from Impulse-Response Tests Performed along Array T1 - T9 over the 30.5-cm (12-in) Thick Concrete Pavement at Site 3

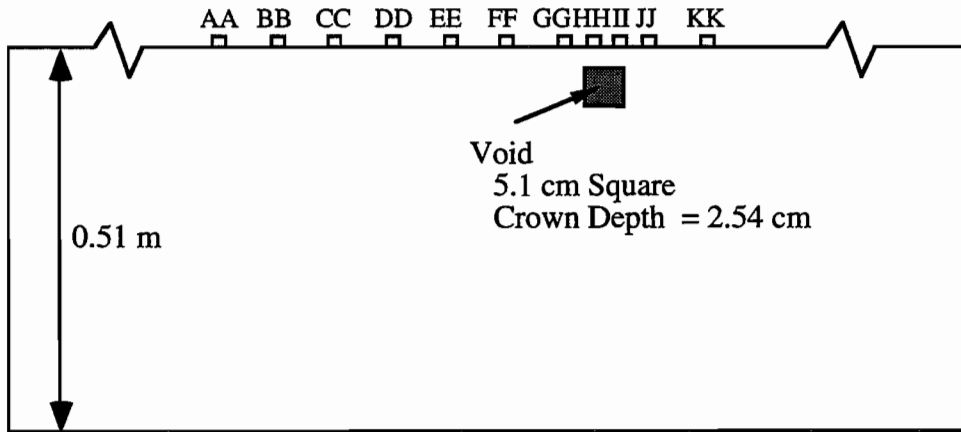


a. Average Mobility Values along Array T1-T9, as shown in Figure 5.26b

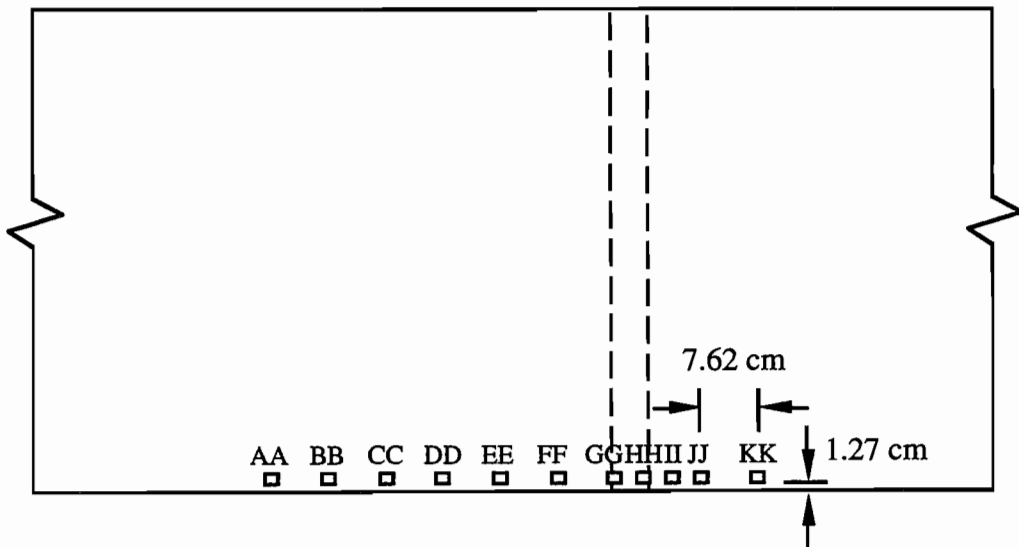


b. Apparent Stiffness Values along Array T1-T9, as shown in Figure 5.26b

Figure 5.30 Results from Impulse-Response Tests Performed over a 1.22-m Square Interior Void Beneath a 25.4-cm (10-in.) Thick Concrete Pavement at Site 3



a. Profile View of Test Locations at Site 1



b. Plan View of Test Locations at Site 1

Figure 5.31 Plan and Profile Views of Test Locations on Concrete Slab at Site 1

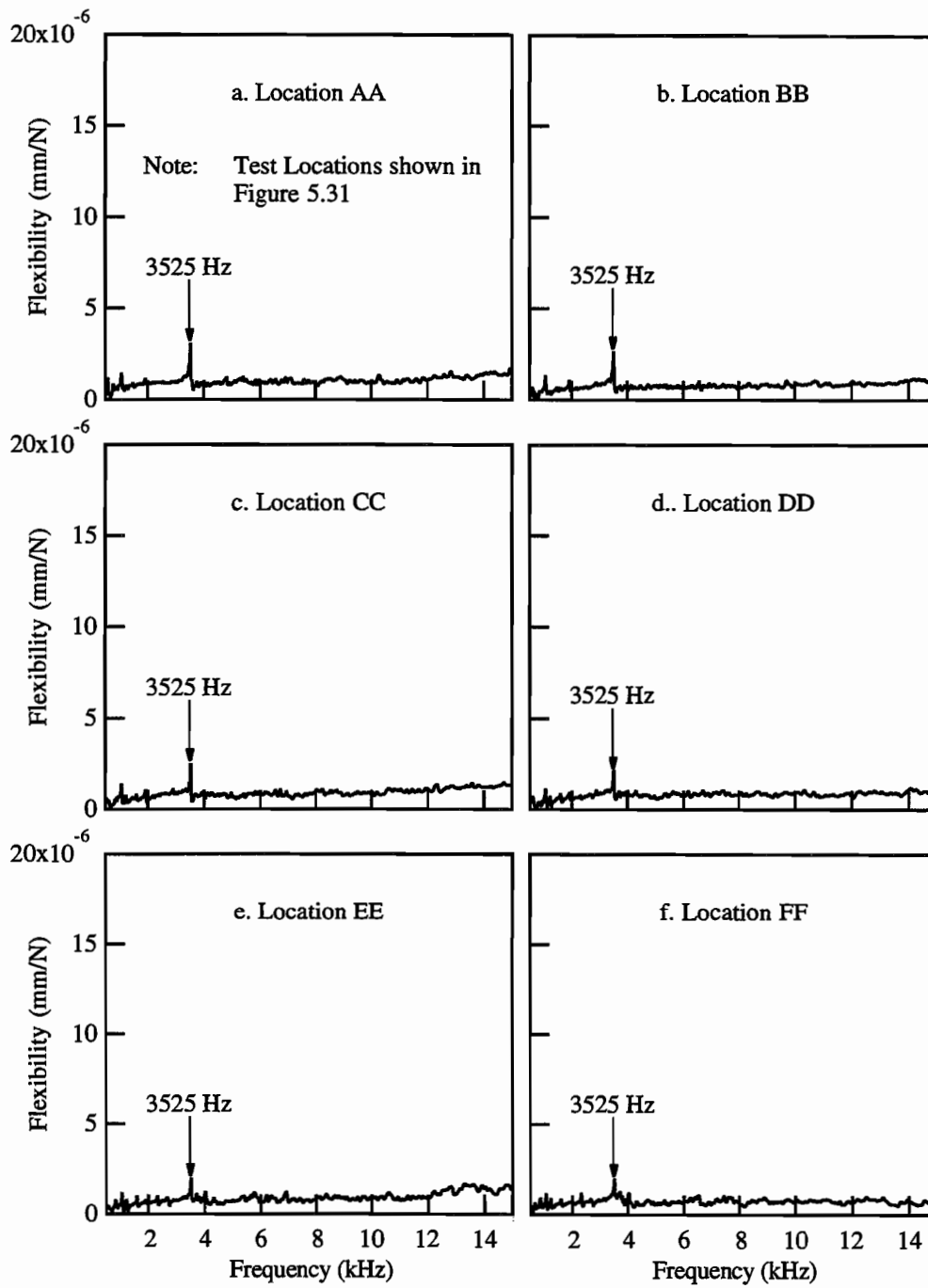


Figure 5.32 Frequency Responses showing Flexural Resonance from Impact-Echo Tests Performed along Array AA-FF at Site 1

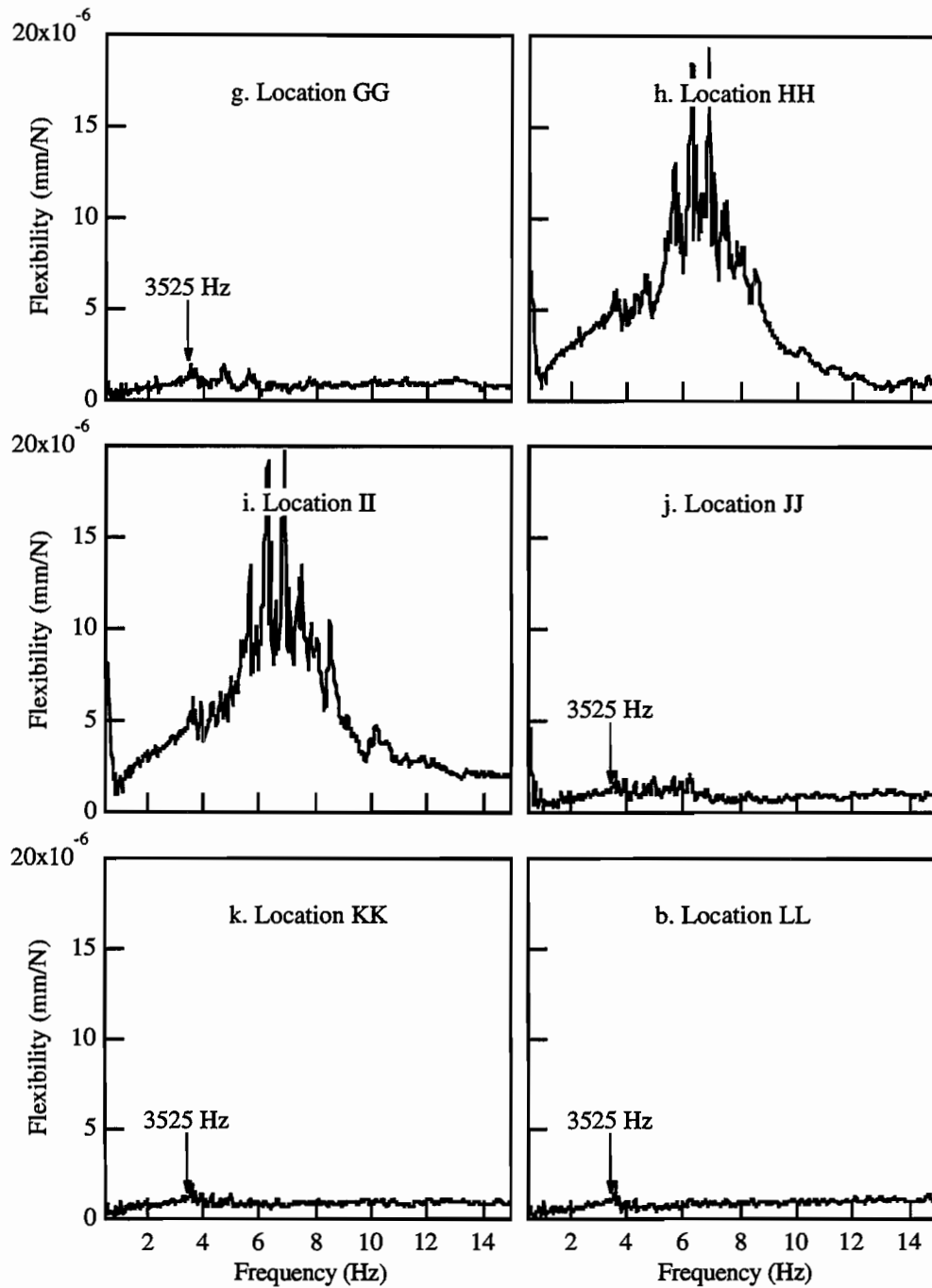


Figure 5.33 Frequency Responses showing Flexural Resonance from Impact-Echo Tests Performed along Array GG-HH at Site 1

shown in Figure 3.6. Figure 5.31 shows the locations AA - KK that were tested along the slab edge. Figures 5.32 and 5.33 contain a series of frequency responses from tests on either side and over the "tunnel" in the slab. The frequency responses over locations AA-FF located before the "tunnel" show a low-magnitude peak at 3.5 kHz, corresponding to the impact-echo compression wave resonance off of the bottom of the 50.8-cm deep slab. Over the "tunnel", which is at a depth of 2.54 cm, the P-wave resonant frequency is expected to be at approximately 75 kHz. This frequency is neither generated nor detected from the instrumentation used. Instead, a high magnitude broad peak is observed at a frequency of approximately 6.8 kHz. This peak corresponds to the flexural response of the concrete beam above the "tunnel". The elongated shape of the "tunnel" and the proximity of the test to the slab edge creates the complex flexural response. Although this measurement can not be used to calculate the depth to the void, it can be used to detect the location of the void in the pavement which could not be easily detected from compressional resonance.

5.8 SUMMARY

The analytical and experimental results presented herein demonstrate some of the advantages and drawbacks of the impulse-response method. The method is effective as a means of detecting void regions that will vibrate at low frequencies. Table 5.1 is a summary of the impulse-response test results comparing the response over various voids to the response over sound pavement. The presentation of the data in terms of average mobility from 10 to 800 Hz appears to be an effective means of locating and delineating regions of concrete pavement with large voids beneath them. When the data is presenting in terms of dynamic slab stiffness, regions with voids appear to be overshadowed by the effects from the pavement edges.

The impulse-response method, however, is an ineffective means of detecting smaller, and deeper voids in the frequency range that was tested. Also, unlike the impact-echo method, the depth to the void can not be determined from impulse-response results. This is an important consideration if detailed contractual estimates of material removal are necessary.

Table 5.1 Summary of Impulse-Response Results

Location	Site	Flaw	Size	Flaw Location	Flaw Depth	Distance from Pavement Edge	Average Mobility	Average Stiffness
			cm square		cm	m	µm/sec/N	kN/mm
C3	2	VOID	0.915	corner	25.4	0.46	1.12	336
N3	2	NONE	N/A	N/A	N/A	0.46	0.65	721
Y1	2	DEBONDED	full pavement	full pavement	25.4	0.69	0.86	855
X1	2	NONE	N/A	N/A	N/A	0.69	0.62	1231
E2	3	VOID	0.915	edge	16.5	0.23	4.29	108
A2	3	NONE	N/A	N/A	N/A	0.23	1.31	220
A4	3	VOID	0.915	edge	16.5	0.69	2.45	263
E4	3	NONE	N/A	N/A	N/A	0.69	1.30	369
S5	3	VOID	1.22	interior	15.2	0.61	1.50	435
S9	3	NONE	N/A	N/A	N/A	1.83	8.45	516
L2	3	VOID	0.915	edge	29.2	0.23	1.21	641
R2	3	NONE	N/A	N/A	N/A	0.23	0.43	680
L4	3	VOID	0.915	edge	29.2	0.69	0.61	1014
R4	3	NONE	N/A	N/A	N/A	0.69	0.36	1118
T5	3	VOID	1.22	interior	28	1.61	0.53	1200
T9	3	NONE	N/A	N/A	N/A	2.83	0.33	1407

CHAPTER 6.

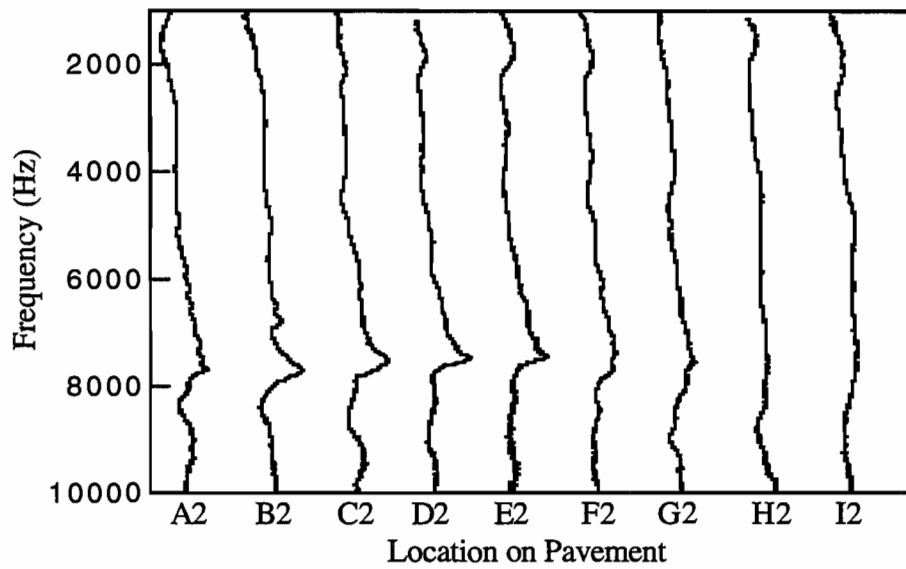
RECEPTION OF HIGH-FREQUENCY ENERGY

WITH A MOBILE RECEIVER

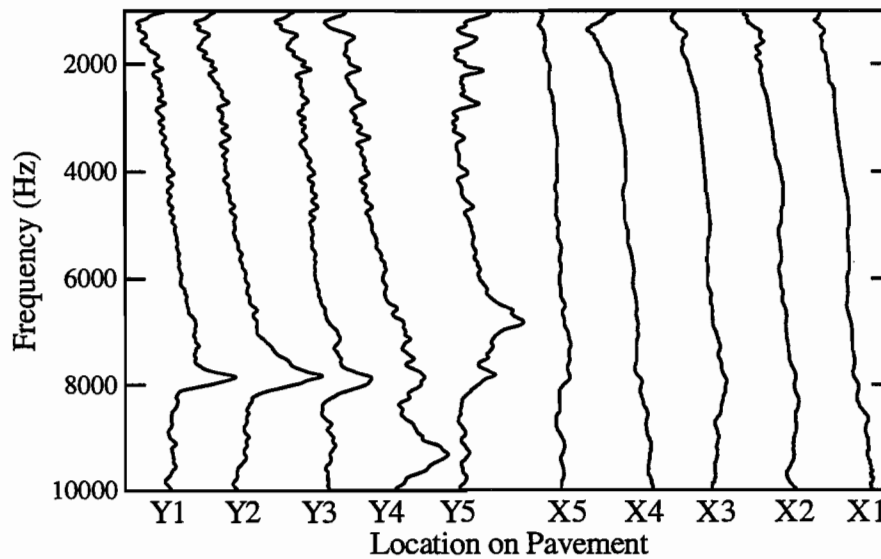
6.1 INTRODUCTION

Based on the results presented in Chapters 4 and 5, both the impact-echo and impulse-response methods can be effectively used to detect certain flaw conditions in pavements. For site specific cases, the impact-echo method is especially effective for detecting many types of flaws in pavements, as long as the quality of the surface impact can be monitored. The impact-echo method, however, requires a broader and higher frequency range for effective use as compared to the impulse-response method. The necessity of generating and receiving this broad range of frequencies while moving is one of the major obstacles to implementing the impact-echo method into a rolling system.

The effectiveness of the impulse-response method, however, is limited by the size and depth of flaws that can be detected. Small, deep voids will not respond in the frequency range of the impulse-response method. Therefore, neither the impact-echo nor the impulse-response method seems well suited for exclusive implementation into a mobile system. However, in many ways the two methods complement one another. For example, the near-surface voids that require high frequencies to detect with the impact-echo method may be detected using the impulse-response method, as was shown in Chapters 4 and 5. Likewise, small deep voids that can not be detected with the impulse-response method may be detected using the impact-echo test. Secondly, the impulse-response and impact-echo methods provide supplemental information about support conditions and depth to the void, respectively. For example, the impact-echo plots from Site 2, shown in Figures 6.1a and 6.1b are from tests over a void and over debonded pavement, respectively. With the exception of the responses over X4 and X5 - which are affected by the pavement edge - the responses are very similar. Both responses show peaks at approximately 7800 Hz which indicates an interface at approximately 25.4 cm below the pavement. They do not, however, indicate the support conditions under the pavement. However, when the impulse-response tests are also used, as shown in Figures 6.2a and 6.2b, the determination of a void or debonded pavement can be made from the average mobility values that are measured. Lastly,

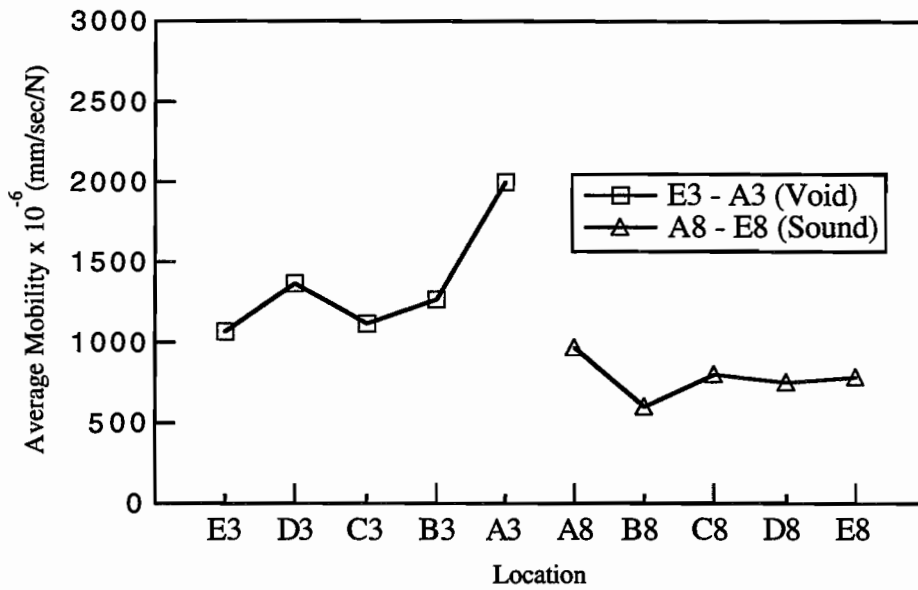


a. Passing over Void (locations A2 - I2 in Figure 5.9b)

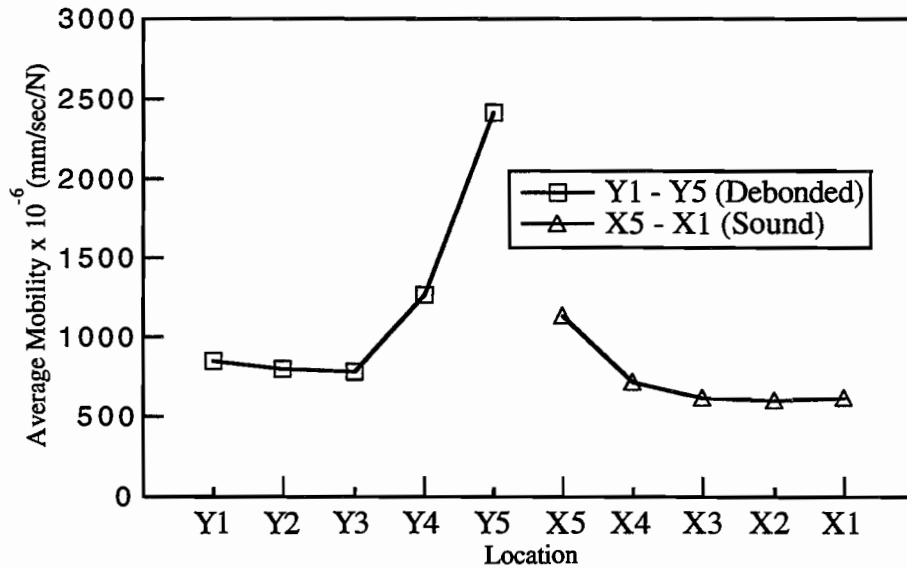


b. Passing over Debonded Pavement
(locations X1 - X5 and Y1-Y5 in Figure 5.17)

Figure 6.1 Comparison of Impact-Echo Results from Tests Passing over a Void and over Debonded Pavement



a. Average Mobility over Locations E3-A3 and A8-E8, shown in Figure 5.9



b. Average Mobility over Locations X1-X5 and Y5-Y1, shown in Figure 5.17

Figure 6.2 Comparison of Impulse-Response Results from Tests Passing over a Void and over Debanded Pavement

many higher frequency flexural vibrations that could not be detected with the impulse-response method could be detected with impact-echo instrumentation, as discussed in Section 5.7. Therefore, a system implementing both the impact-echo and impulse-response methods would provide more information about the condition of the pavement than either test alone.

Based on this reasoning, a frequency range of 10 to 20,000 Hz was set as a design goal for a mobile receiver. The range from 10 to 1000 Hz would be used primarily for impulse-response testing, while the range from 1000-20,000 Hz would be used for impact-echo testing. This frequency range would allow impact-echo detection of voids at depths greater than approximately 7.5 to 10 cm. This chapter presents results from initial testing of mobile receivers for energy reception in the range of 1 to 20 kHz. The mobile receivers tested were wheels which support accelerometers. In these initial tests, all testing was performed with the wheels stationary to evaluate the optimum performance of this system.

6.2 ENERGY RECEPTION USING WHEEL MOUNTED RECEIVERS

Testing was performed to evaluate the feasibility of high frequency (1 to 20 kHz) stress wave energy reception using a wheel-mounted receiver. Several wheel types of different sizes were tested with receivers mounted at various locations to determine the energy reception characteristics through the wheels.

6.2.1 Testing Arrangement and Procedures

Tests were arranged such that the response of a receiver mounted on a wheel could be compared directly to the response with the receiver directly on the concrete. Two PCB 303A12 accelerometers, described in Section 3.3.1, were used to measure the response. Tests were first performed with both accelerometers located directly on the concrete. The accelerometers were located 7.6 cm apart and were coupled to the pavement with super glue, as shown in Figure 6.3a. An impact was applied 5.1 cm along a center line passing through the midpoint between the receivers (see Figure 6.3a). Five impacts were used to get an average response. The output from receiver #1 was passed into channel 1 of the HP 3562A waveform analyzer, and the output from receiver #2 was passed into channel 2 of the analyzer. The frequency response obtained from this test, therefore, is the ratio of the linear spectrum at location 2 to the linear spectrum at location 1. To test the effect of the wheel on the measured vibration response, the wheel to be tested was placed at location 2, and receiver #2 was placed at some location on the wheel, as shown in Figure

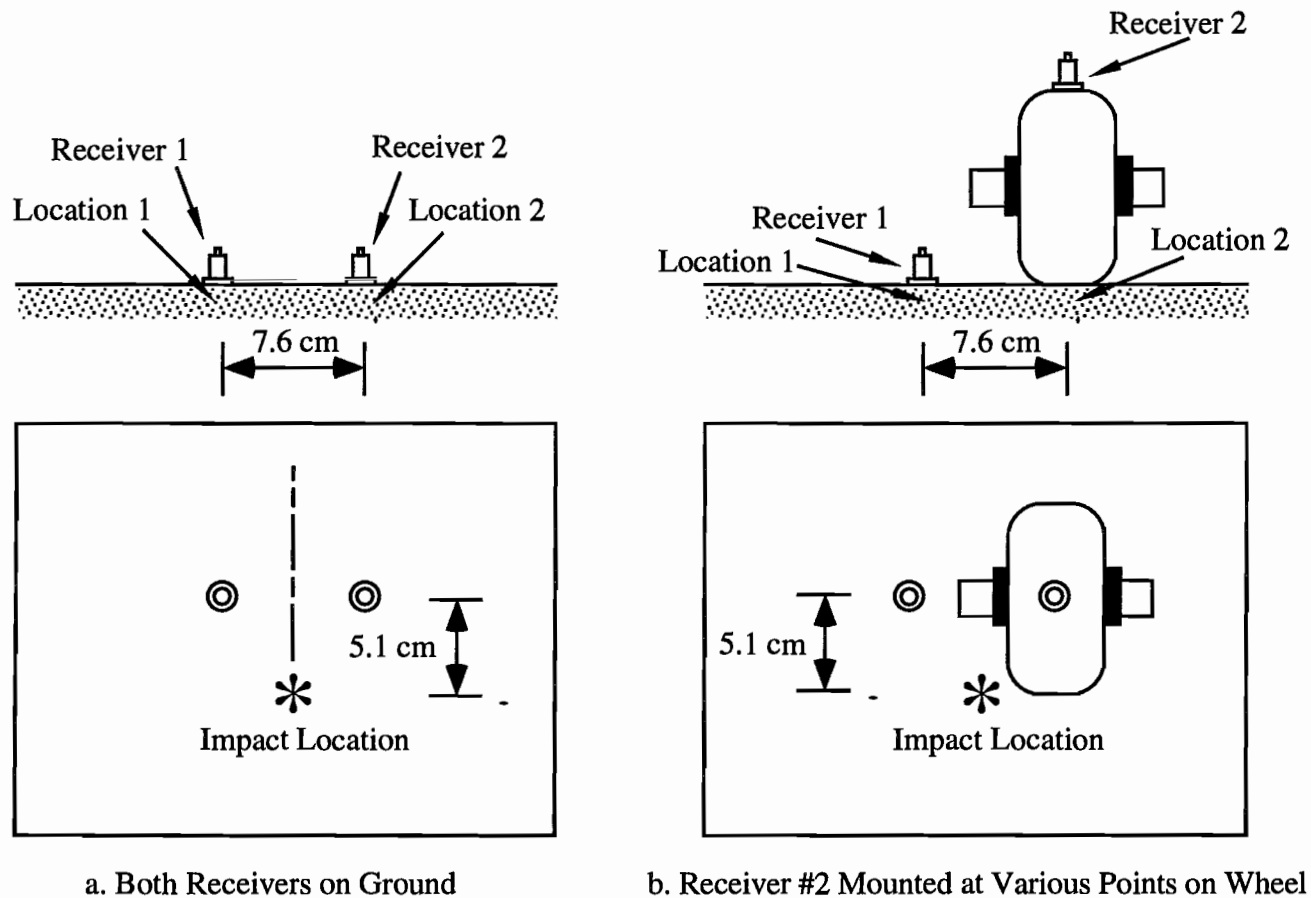


Figure 6.3 Test Arrangement for Evaluation of High-Frequency Energy Propagation Through Stationary Wheels

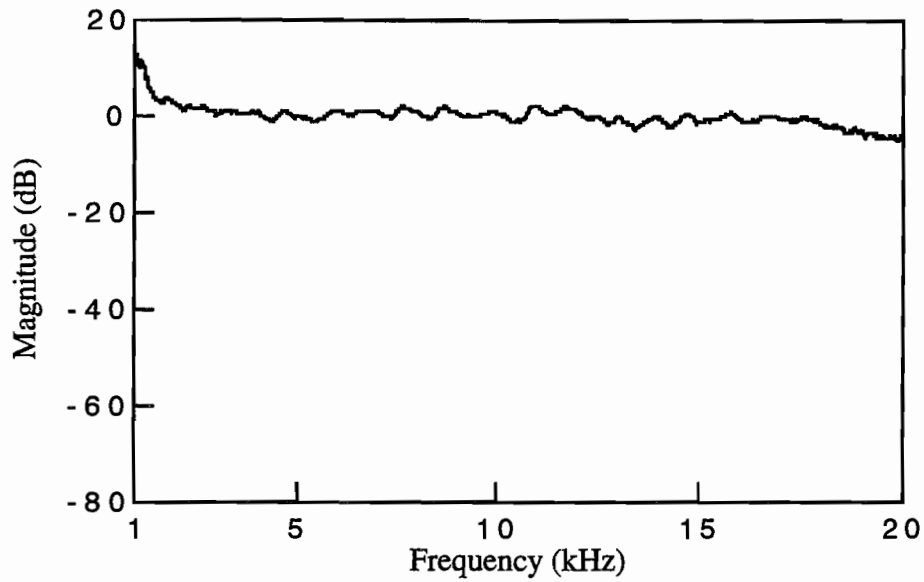
6.3b. The frequency response from this test represents the ratio of the linear spectrum from the receiver on the wheel at location 2, to the linear spectrum of the receiver alone at location 1. To remove the effect of the 7.6 cm receiver spacing from the results, the frequency response obtained from the test with the wheel was divided by the response obtained with both receivers mounted directly on the concrete. The final frequency response obtained, therefore, is the ratio of the linear spectrum of receiver #2 on the wheel located at location 2 to the linear spectrum of receiver #2 located directly on the concrete surface at location 2. Because this ratio involves the same receiver tested over the same location, the frequency response should have a magnitude of 1 (0 dB) at all frequencies. Any deviation from this behavior can be assumed to be the effect of the wheel on the measured pavement vibration.

6.2.2 Energy Reception using a Steel Wheel

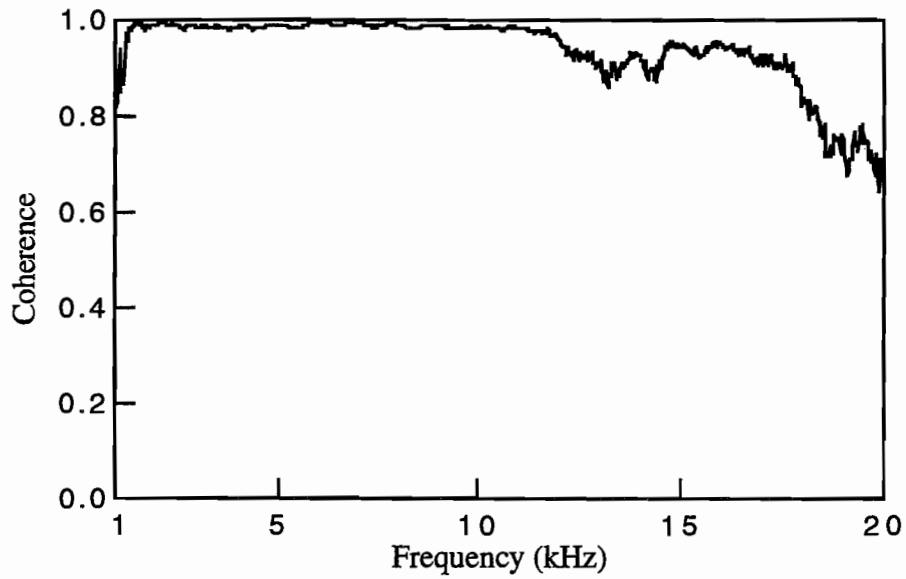
Figure 6.4 shows the frequency response and coherence obtained from tests with both receivers mounted directly on the concrete surface at Site 2. Unless otherwise noted, the frequency responses presented in this section were divided by the response shown in Figure 6.4a. As explained in Section 6.2.1, this removes the effect of using different receivers at different locations.

Testing was performed with receivers mounted at various locations on a stationary wheel system consisting of a steel wheel, a stainless steel axle and a steel wheel stand, in order to measure the stress wave energy propagation through the system. A drawing of the wheel system and the testing locations is shown in Figure 6.5. The steel wheel used in these tests is 10.2 cm in diameter and 5.1 cm in width, with a weight of 3007 g. The axle is 12 cm long with a diameter of 2.5 cm and was passed through a greased 2.5 cm hole in the center of the steel wheel. The wheel stand is 10.5 cm high with a flat 10.2 x 11.4 cm top. For stability, the stand was attached with isolators to an aluminum arm which was attached with a hinge to a support at the other end

The first test involved mounting a receiver (PCB 303A12 accelerometer) on top of the wheel stand, between the top of the stand and the aluminum arm, shown as location A in Figure 6.5. The accelerometer was glued to the top of the wheel stand. The wheel was placed directly on the concrete slab with water coupling between the wheel and the ground, and the control receiver was located 7.6 cm from the wheel mounted receiver as described earlier. The PCB B01 impact hammer (described in Section 3.3.1) was used as the source in this case. The concrete was impacted 5.1 cm from the midpoint between the receivers. If the wheel was to have no effect on the measured motion, it is expected that the frequency response would be flat and have a magnitude



a. Frequency Response



b. Coherence Function

Figure 6.4 Response from Tests with both Receivers Located Directly on the Concrete Surface at Site 2

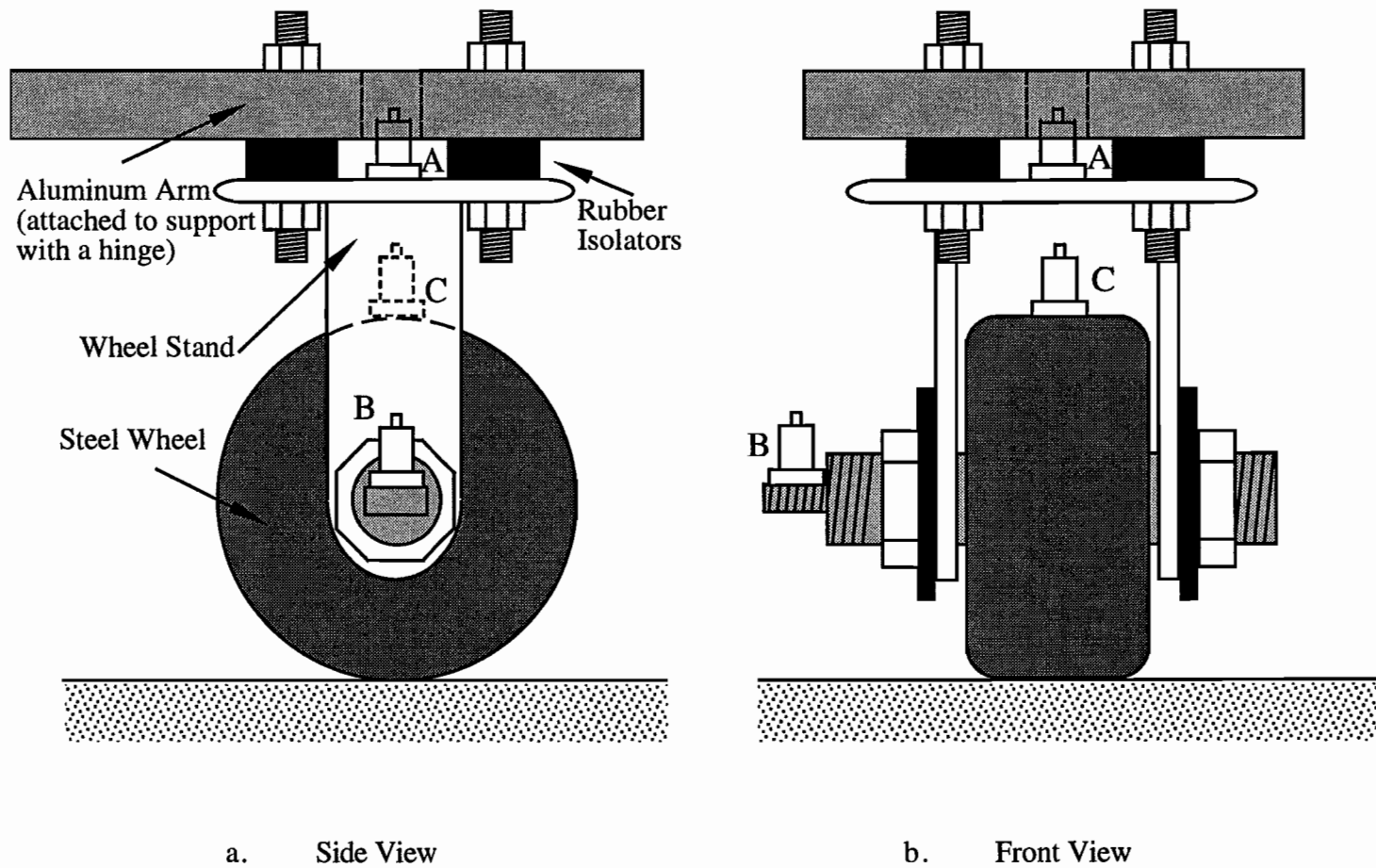


Figure 6.5 Steel Wheel Testing System and Receiver Locations

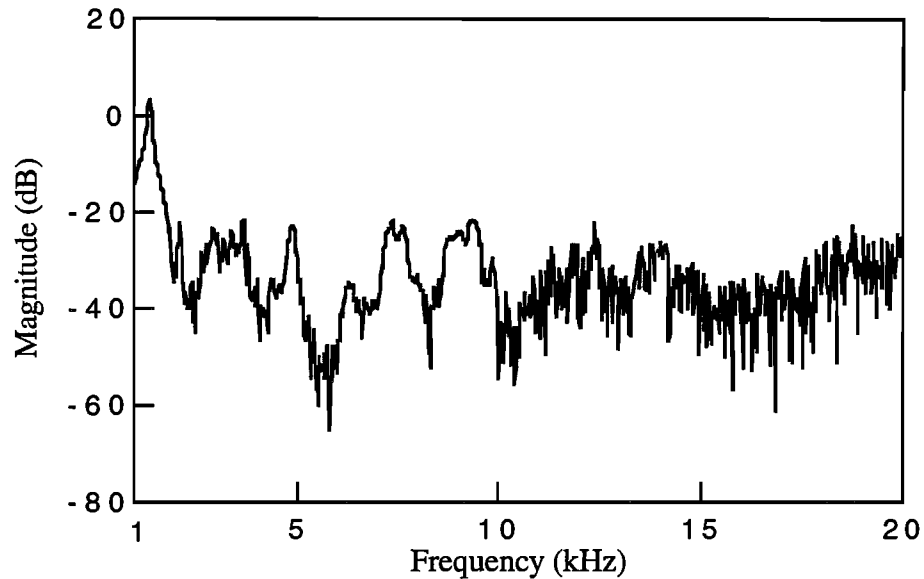
of 1 (0 dB) and the coherence would have a value of 1 throughout the frequency range tested. In this case, however, the wheel greatly affected the measured response, as seen in Figures 6.6a and 6.6b. The coherence plot indicates that by using this arrangement, very little of the impact energy is received by the receiver mounted on the wheel stand. The frequency response is very irregular throughout the frequency range which is due to the many vibration modes of the wheel/axle/stand system. Also, the energy level received on the wheel has an average level of approximately -40 dB relative to the receiver on the ground, which means that the frequencies above about 1500 Hz are reduced by 100 times.

The second test was performed with the identical arrangement described above, except the PCB C80 impact hammer was used as the source. Figures 6.7a and 6.7b show the frequency response and coherence from this test. The smaller and lighter impact hammer generates higher frequencies, but less energy. The response from this test also showed poor coherence and energy reception.

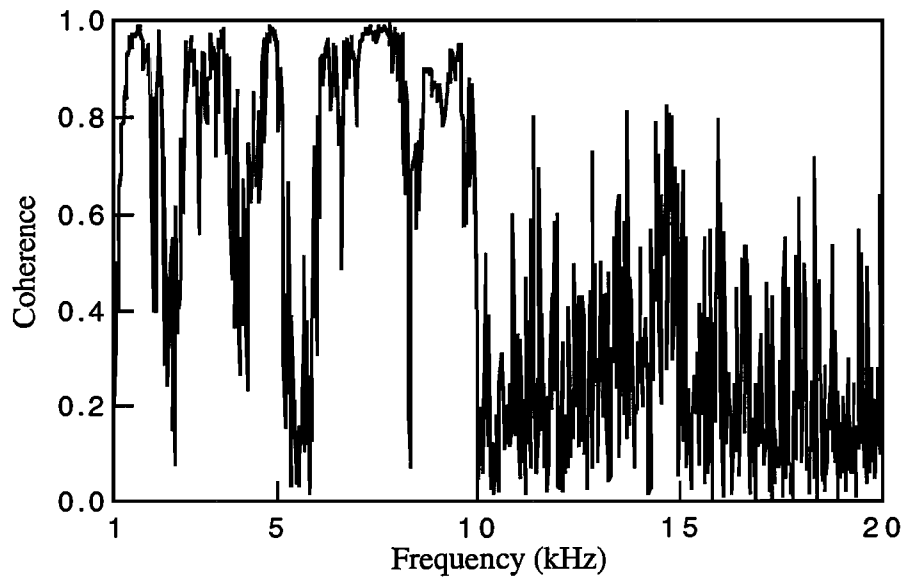
Tests were next performed by mounting the receiver on the outer edge of the axle passing through the wheel, location B in Figure 6.5. The receiver was glued to the axle and the wheel was coupled to the concrete with water. The source used for this test was the PCB B01 impact hammer. The frequency response and coherence from this test are shown in Figures 6.8a and 6.8b, respectively. The results using this arrangement showed little improvement from the previous arrangement. The coherence was slightly improved at lower frequencies, but the frequency response exhibited undulations and significant energy attenuation. The results from the same test using the PCB C80 hammer were also very poor, as shown in Figures 6.9a and 6.9b. Based on these results, it appears that the simple solution of mounting a receiver at a stationary location on the wheel system is not feasible. Tests were next performed to study the energy reception through the wheel itself, without passing through the axle and mounting stand.

6.2.3 Effect of Wheel Type on Energy Transmission

Four wheel types were tested to observe the energy reception of the wheel itself. In this case, the receiver was mounted directly on the top of a stationary wheel, shown as location C in Figure 6.5. The wheel stand, axle, and aluminum support arm were removed so that the response of the wheel alone could be measured. The receivers were attached to the top of the wheels with super glue. The first wheel (CW1) is a 10.2-cm diameter caster wheel with a width of 5.1 cm and a weight of 734.0 g (1.6 lbs). It has a 1.0-cm thick urethane tread, and a webbed aluminum hub. A 1-cm (0.4-in.) axle passes through a greased ball bearing in the center of the wheel. The second

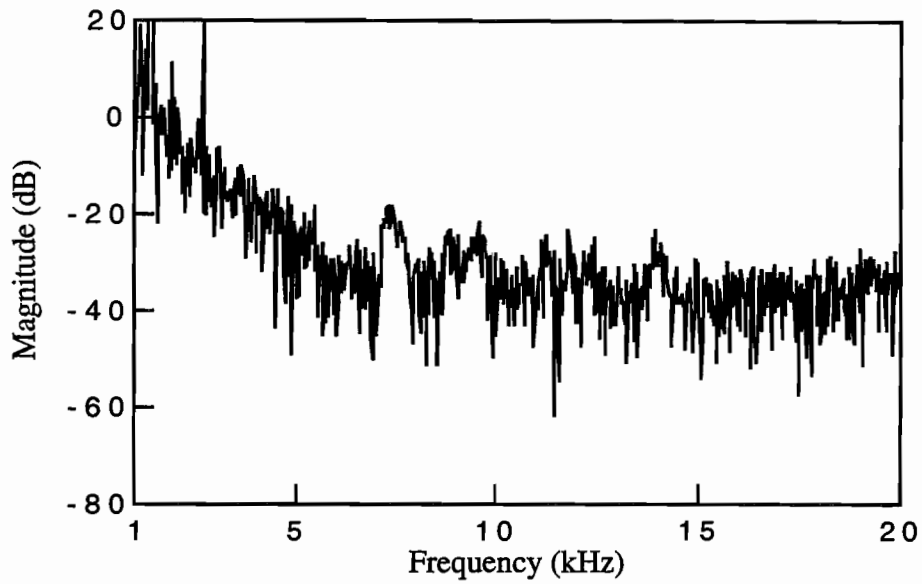


a. Frequency Response

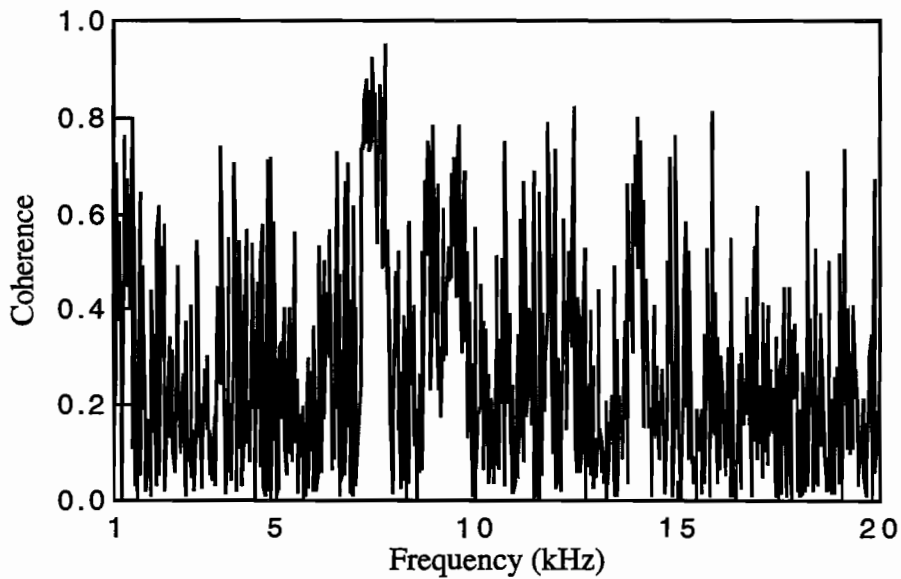


b. Coherence Function

Figure 6.6 Response from Tests with Receiver #2 Located on Top of Wheel Stand (Location A in Figure 6.5); Water Coupling at Wheel / Ground Interface; PCB B01 Source

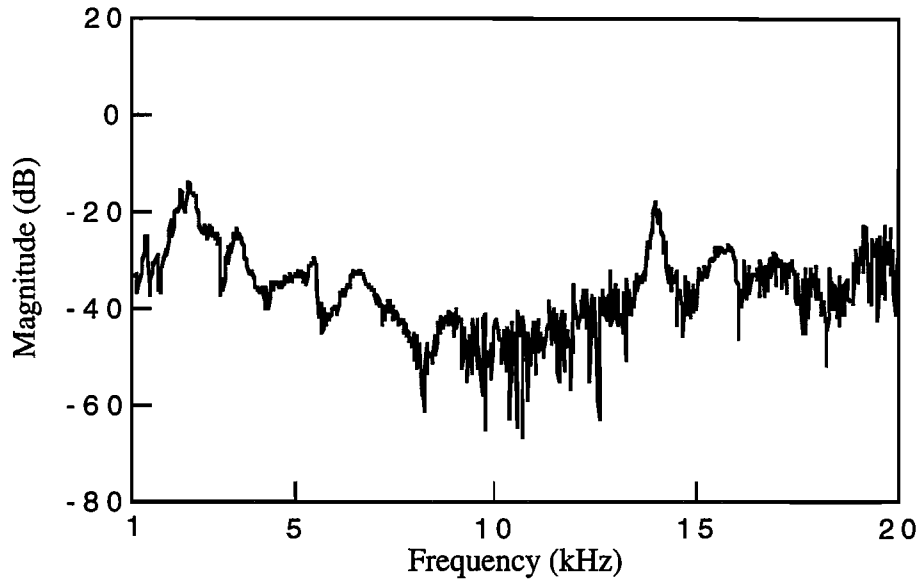


a. Frequency Response

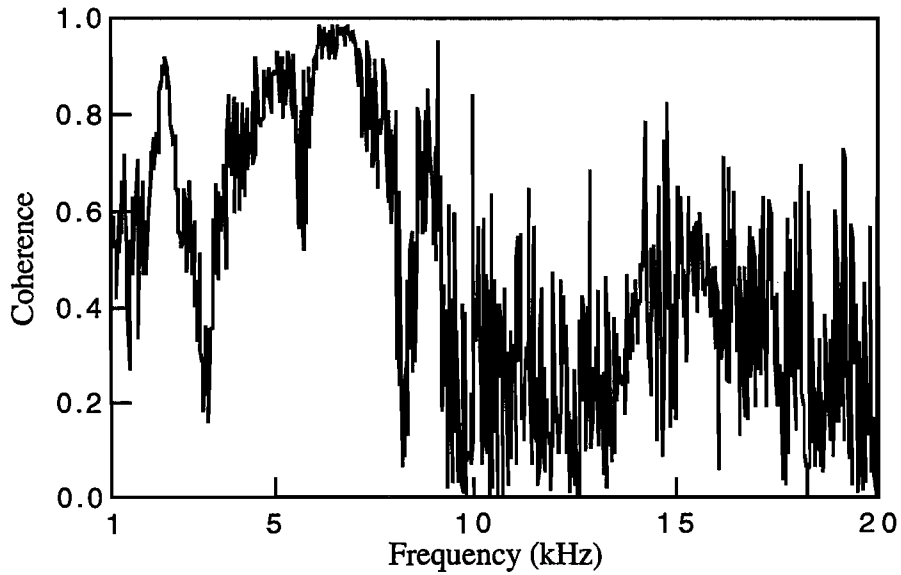


b. Coherence Function

Figure 6.7 Response from Tests with Receiver #2 Located on Top of Wheel Stand (Location A in Figure 6.5); Water Coupling at Wheel / Ground Interface; PCB C80 Source

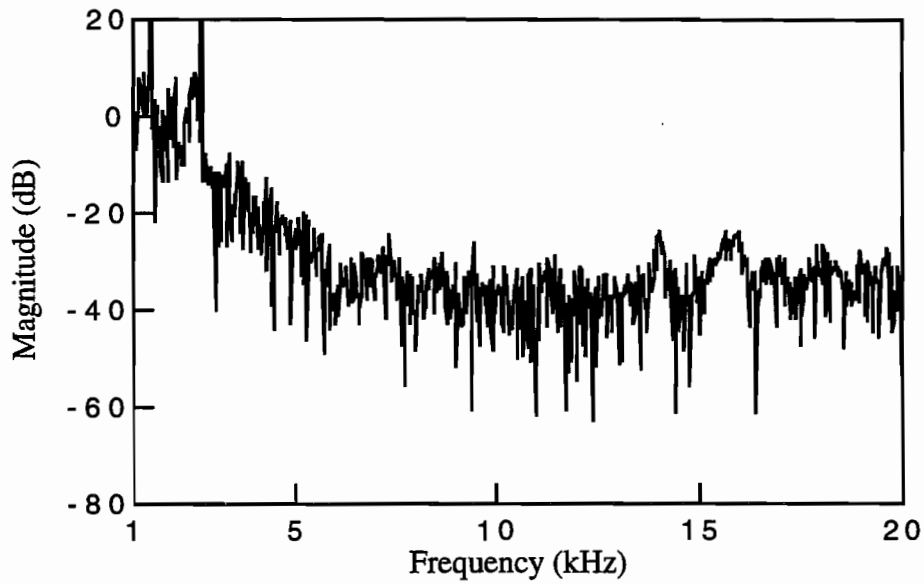


a. Frequency Response

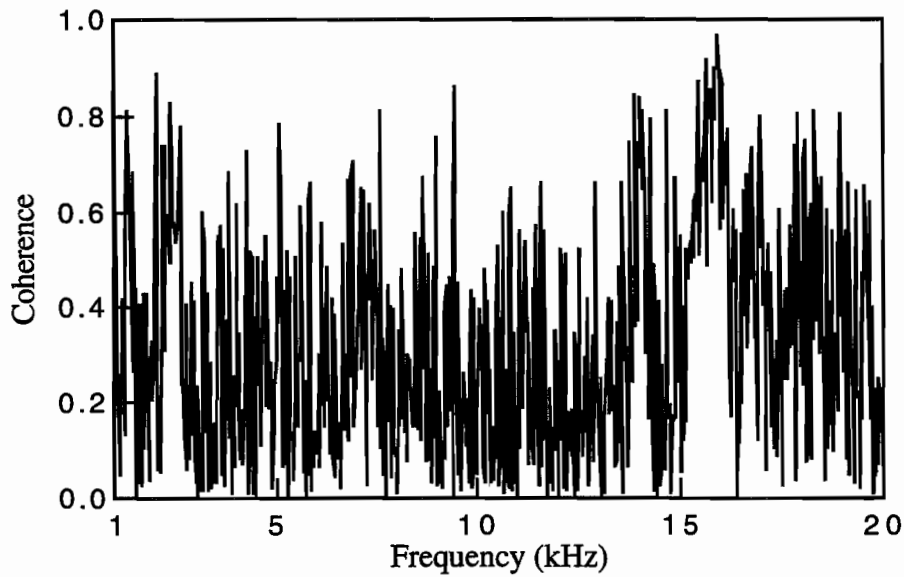


b. Coherence Function

Figure 6.8 Response from Tests with Receiver #2 Located on Outside of Wheel Axle (Location B in Figure 6.5); Water Coupling at Wheel / Ground Interface; PCB B01 Source



a. Frequency Response



b. Coherence Function

Figure 6.9 Response from Tests with Receiver #2 Located on Outside of Wheel Axle (Location B in Figure 6.5); Water Coupling at Wheel / Ground Interface; PCB C80 Source

wheel (SW1) is the steel wheel that is described in Section 6.2.2. The third wheel (AW1) is an aluminum rim with an outside diameter of 10.2 cm, an inside diameter of 9.2 cm, a width of 5.1 cm and a weight of 291 g. The fourth wheel (AW2) is a solid aluminum wheel with a diameter of 10.2 cm, a width of 5.1 cm and a weight of 1012 g. Wheels AW1, AW2, CW1, and SW1 are shown in Figure 6.10. Figure 6.11 shows the testing in progress.

Figures 6.12a through 6.12d show the frequency response and coherence functions from tests with no coupling between the wheels and concrete for CW1, SW1, AW1, and AW2, respectively. The PCB C80 impact hammer was used as the source for these tests. With the exception of wheel AW1, the coherence from each test was very poor. The frequency responses obtained from wheels CW1, SW1, and AW2 were also poor, showing large energy attenuation through the wheels. The coherence from the test using AW1 was fairly good, however, the frequency response was dominated by the many ringing modes of the aluminum rim. The tests were next repeated using the PCB B01 impact hammer. This hammer generates more energy in the frequency range of 1 to 10 kHz as compared to the PCB C80 impact hammer. The frequency responses and coherence values from each test are shown in Figures 6.13a through 6.13d. The use of the larger impact hammer yielded better coherence values in the range of 1 to 10 kHz for tests on wheels CW1, SW1 and AW2. For wheel CW1, the energy received was at approximately -26 dB in the range of good coherence. For wheel SW1, the energy was attenuated to approximately -40 dB (100 times) in the range of 5 to 10 kHz. At a frequency of 17 kHz, the energy was amplified due to the high-frequency ringing of the solid steel wheel. For wheel AW2, the energy was attenuated to approximately -40 dB in the range of 5 to 10 kHz, and was amplified to 3 dB at a frequency of 15.5 kHz. The response of wheel AW1 was again dominated by the multiple resonant peaks due to the ringing of the wheel rim.

The tests discussed above were next repeated with water coupling used between the wheel and the concrete slab. Figures 6.14a through 6.14d show the frequency responses and coherence values from these tests performed with the PCB C80 impact hammer. When compared to the tests with no water coupling, shown in Figure 6.12, in all cases the coherence improved greatly with the addition of water under the wheel. A comparison of Figures 6.12a and 6.14a from tests on wheel CW1 shows the improved coherence values from 3 to 12 kHz. In this frequency range, the received energy increased by approximately 14 dB due to the addition of water under the wheel. Above 12 kHz, however, the coherence and energy reception deteriorated. Tests results on wheel SW1 also improved when water coupling was used. In this case, fair coherence values were measured from 3 to 20 kHz. In this frequency range, the energy reception improved from -40 dB

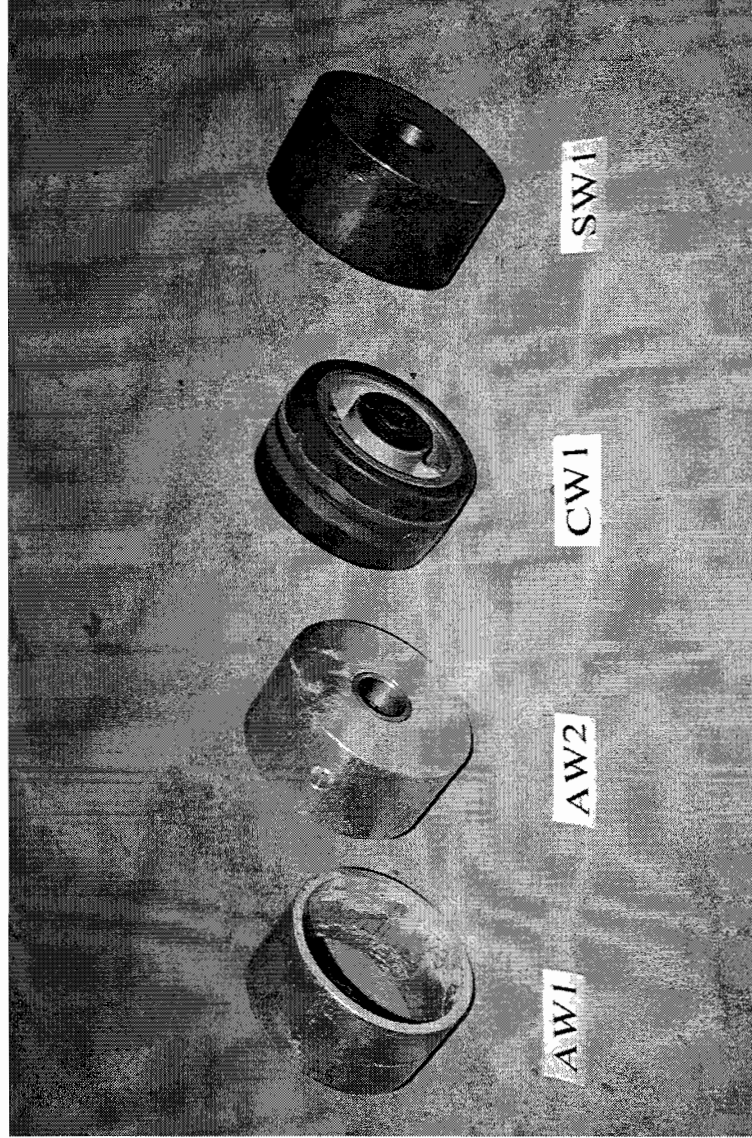


Figure 6.10 Wheels AW1, AW2, CW1, and SW1

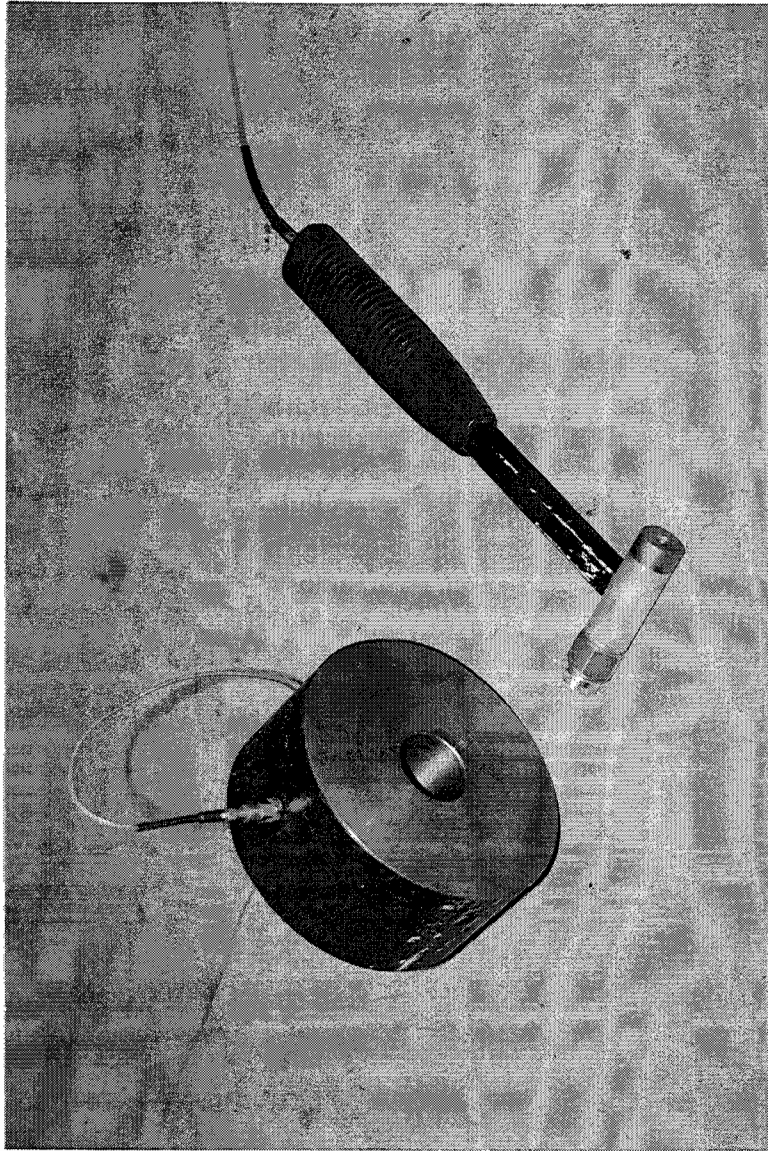


Figure 6.11 Testing Arrangement for Evaluating Energy Propagation through a Wheel

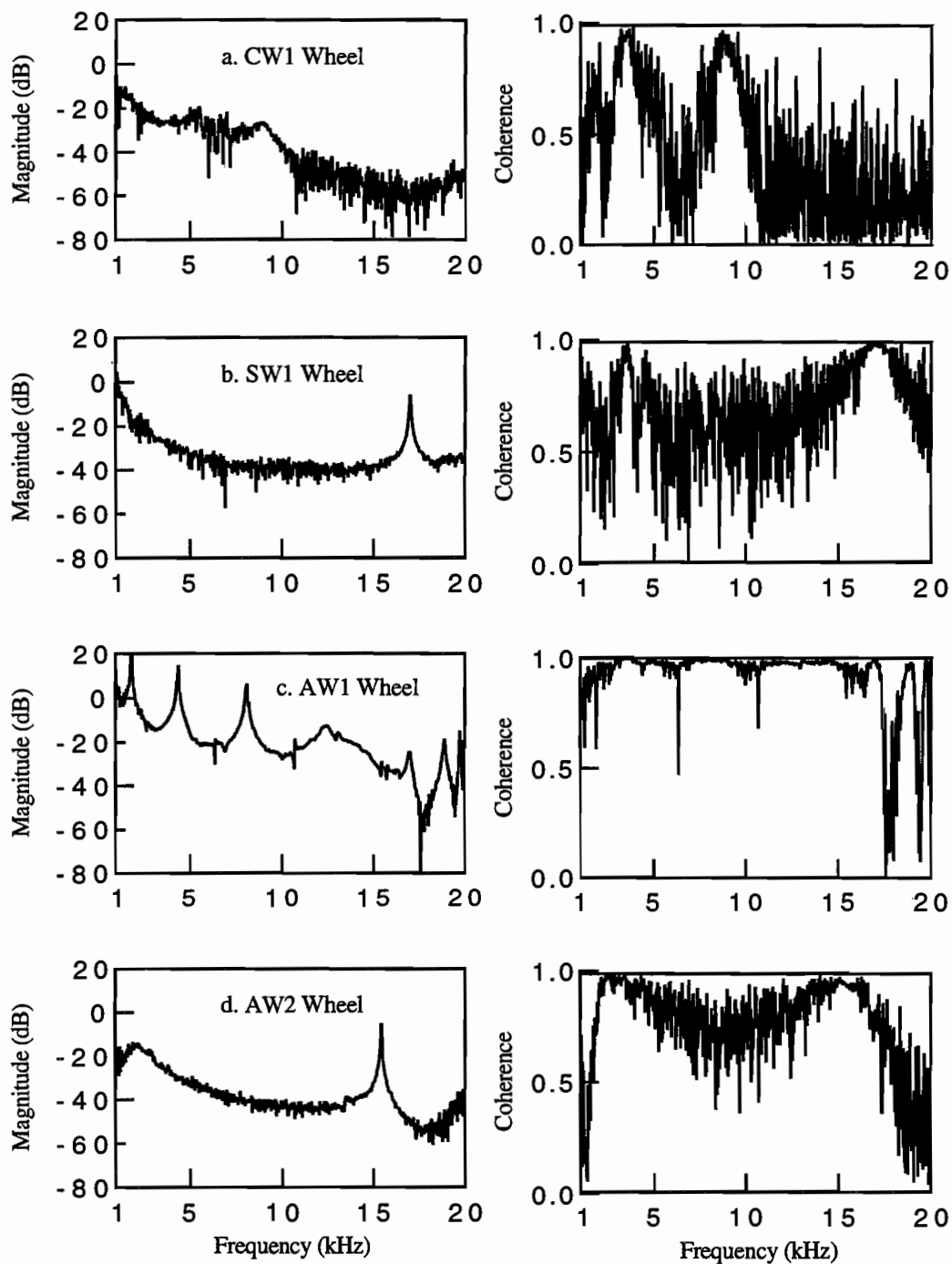


Figure 6.12 High-Frequency Energy Reception from Accelerometer Mounted Directly on Top of Stationary Wheel; No Special Coupling between Wheel and Ground; PCB C80 Source

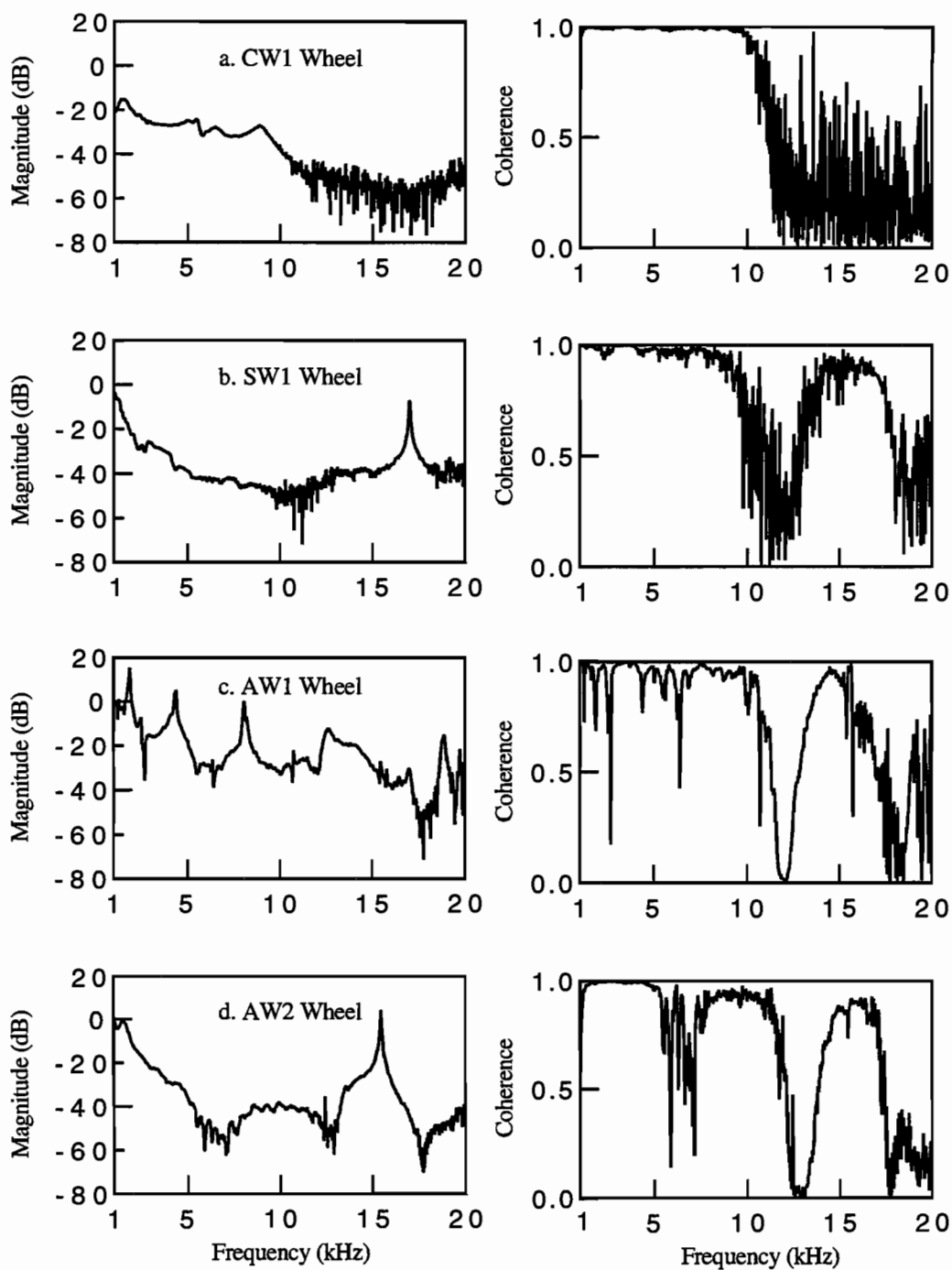


Figure 6.13 *High-Frequency Energy Reception from Accelerometer Mounted Directly on Top of Stationary Wheel; No Special Coupling between Wheel and Ground; PCB B01 Source*

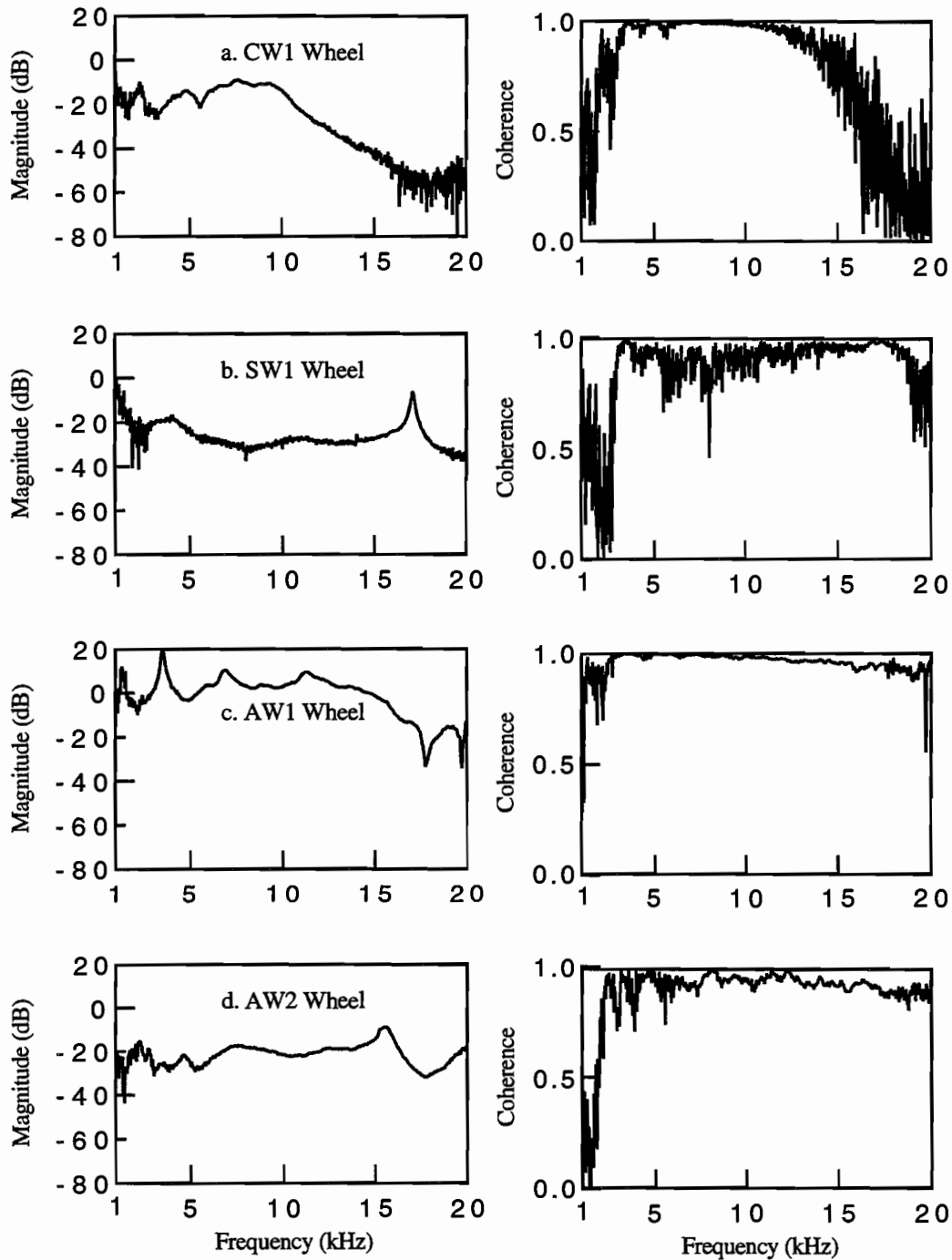


Figure 6.14 High-Frequency Energy Reception from Accelerometer Mounted Directly on Top of Stationary Wheel; Water Coupling between Wheel and Ground; PCB C80 Source

for the case with no water coupling to -28dB for the case with water coupling, as shown in Figure 6.12b and 6.14b, respectively.

For wheel AW1, the coherence and energy reception was improved with the addition of water to couple the wheel. Good coherence was measured in the frequency range of 3 to 20 kHz. The average energy reception was approximately 0 dB between 1 to 15 kHz, indicating small energy loss through the wheel. The addition of the water did appear to dampen some of the ringing in the wheel. The frequency response, however, was still dominated by the internal ringing of the wheel, as seen in Figure 6.14c. Lastly, test results on wheel AW2 were also improved greatly with the addition of water coupling. Good coherence values were measured in the range of 3 to 20 kHz, as shown in Figure 6.14d. Energy reception improved to a level of approximately -20 dB in the range from 5 to 15 kHz.

The same tests using water coupling under the wheel were then repeated using the larger PCB B01 hammer as the impact source. These results are shown in Figures 6.15a through 6.15d. In each case the larger hammer produced better coherence at lower frequencies and poorer coherence at higher frequencies, as compared to the response using the smaller PCB C80 hammer. This is due to the larger energy input at lower frequencies.

In summary, several problems were identified from these initial tests. The addition of the wheel into the measuring system has two major impacts on the measured response. The first is the effect of the wheel on the actual pavement vibration. The weight of the wheel on the pavement will cause the pavement vibration to be altered. The inertial force from the mass of the wheel will tend to decrease the vibration of the pavement. This is especially true at high frequencies where the accelerations and hence inertial forces are large. This effect appears to be confirmed from these simple measurements. The highest level of energy reception and coherence was observed with the receiver mounted on the aluminum rim (291 g). By comparison, the heavier steel wheel (3007 g) showed good coherence, but energy attenuation of approximately -26 dB. The second major effect is the effect of the wheel vibrations on the measured vibrations. The wheel itself will vibrate at one or more resonant frequencies and effect the measured response. Because it is the pavement vibration that is of interest, it is desirable to eliminate these other vibrations. With respect to this problem, the aluminum rim behaved the poorest of the wheels tested. The response shown in Figure 6.12c, for example, shows the many modes of vibration of the aluminum wheel. When water was added to the system, some of these modes were dampened, as shown in Figure 6.14c. However, the frequency response was still very much dominated by the vibration of the wheel rim. In contrast, the steel and aluminum wheels resonate at a single frequency. Below that frequency, the response is fairly flat. Therefore, ideally, the wheel used to

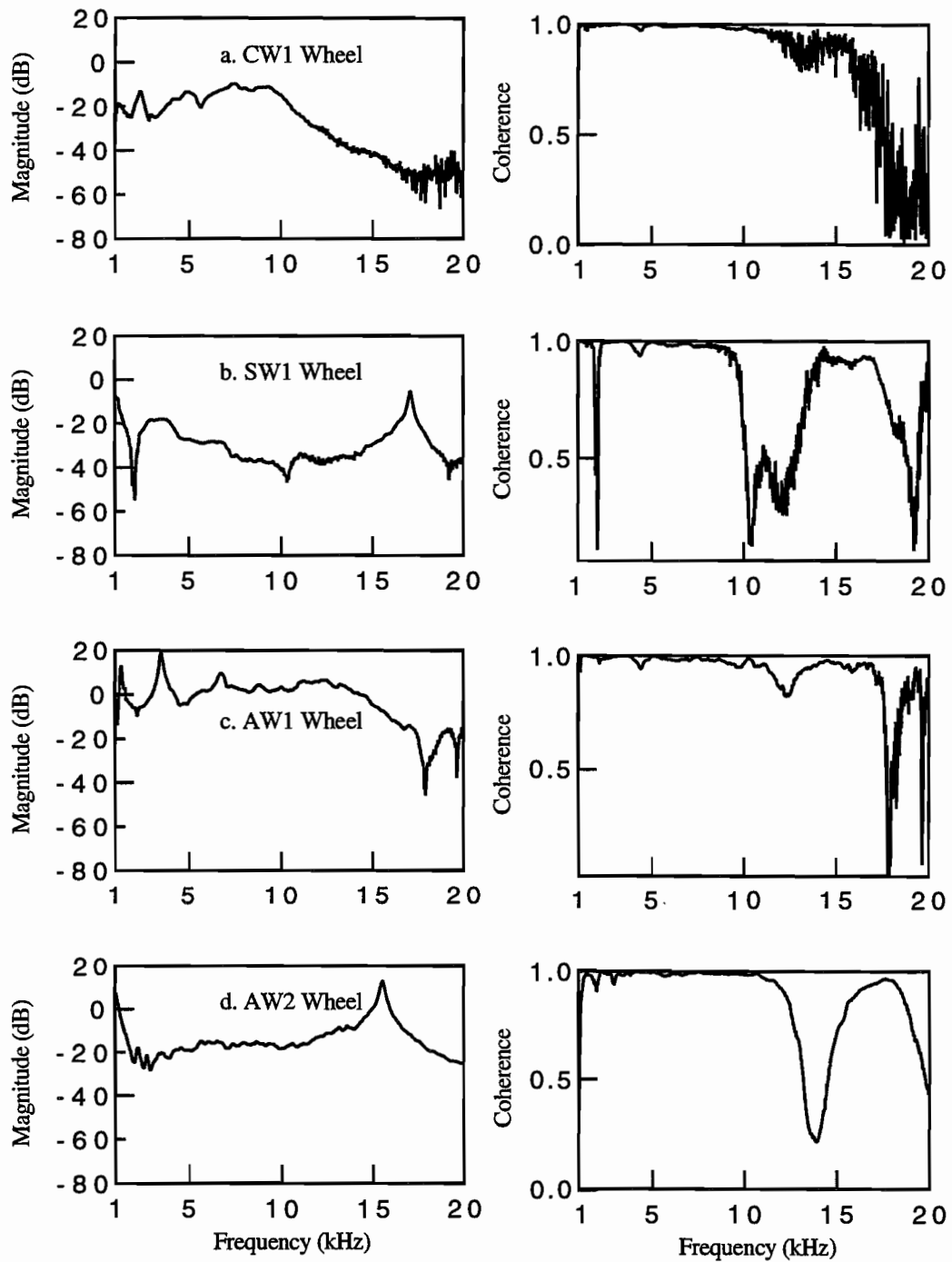


Figure 6.15 High-Frequency Energy Reception from Accelerometer Mounted Directly on Top of Stationary Wheel; Water Coupling between Wheel and Ground; PCB B01 Source

mount a receiver on should be as light as possible and resonate at frequencies outside of the range of 1 to 20 kHz.

6.2.4 Test on Aluminum Wheels

Tests were performed on three aluminum wheels of various shapes and sizes to demonstrate the effect of mass and size on energy reception through the wheels. Wheels AW1, AW2, and AW3 are shown in Figure 6.16.

6.2.4.1 Effect of Wheel Size and Shape: Wheels AW1 and AW3 were used to compare the energy reception characteristics through wheels of different diameters. A 1.28-cm thick epoxy hub was added to the inside of wheel AW1. This was done for two reasons. First, the addition of the epoxy to the aluminum rim (not shown in Fig. 6.16) increased the mass of wheel AW1 to approximately the same value of wheel AW3, thereby eliminating the effect of mass. Secondly, the epoxy was added to try to dampen the ringing of the wheel that dominated the responses, shown in Figure 6.12c. Wheel AW3 is a solid aluminum cylinder with a diameter of 5.1 cm, a width of 5.1 cm, and a mass of 290 g. The tests were performed as described in Section 6.2.1. Figures 6.17a and 6.17b show the frequency responses and coherence plots obtained from tests on these wheels. Because these wheels, have the same mass, any differences in their responses should be due to the difference in size and shape. The first point to be observed from Figure 6.17 is that the addition of the epoxy hub did not greatly reduce the ringing in the aluminum rim. Figure 6.18 is a comparison of the frequency response of the aluminum rim with and without the epoxy hub. The resonant peaks observed in the test without the epoxy were generally still present when the epoxy was added. The frequency and amplitude of the peaks did, however, change. The slight decrease in the overall energy received through the wheel with the epoxy is probably due to the greater mass of the wheel and hence greater inertial effects. Secondly, from Figure 6.17 it is observed that the energy level received by wheel AW1 is greater than that received by wheel AW3. Because these two wheels have the same mass, it is expected that the magnitude of the energy received should be similar. One possible explanation for this is that the contact area of the smaller wheel on the concrete is less than the larger diameter wheel. To investigate this, the smaller wheel was turned on end and the same test was performed. This allows for comparison of the same material with the same mass and the receiver located the same distance above the concrete surface. Figure 6.19 shows the comparison of these results. As expected, the response from the

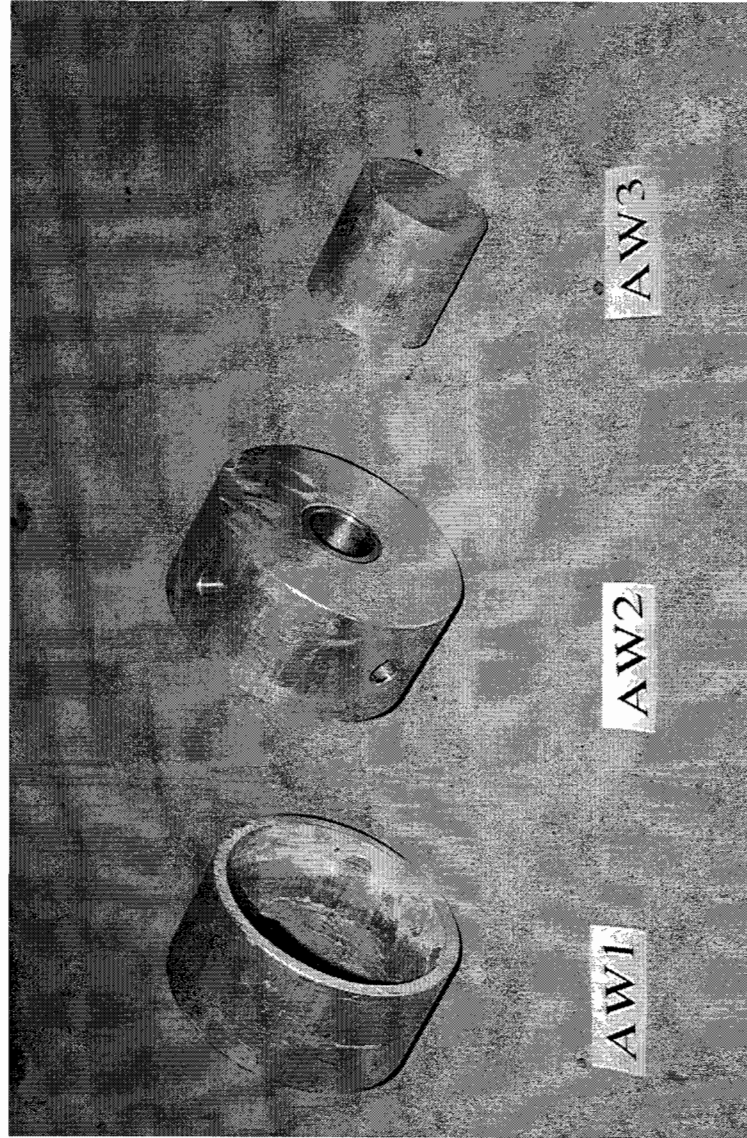


Figure 6.16 Aluminum Wheels AW1, AW2, and AW3

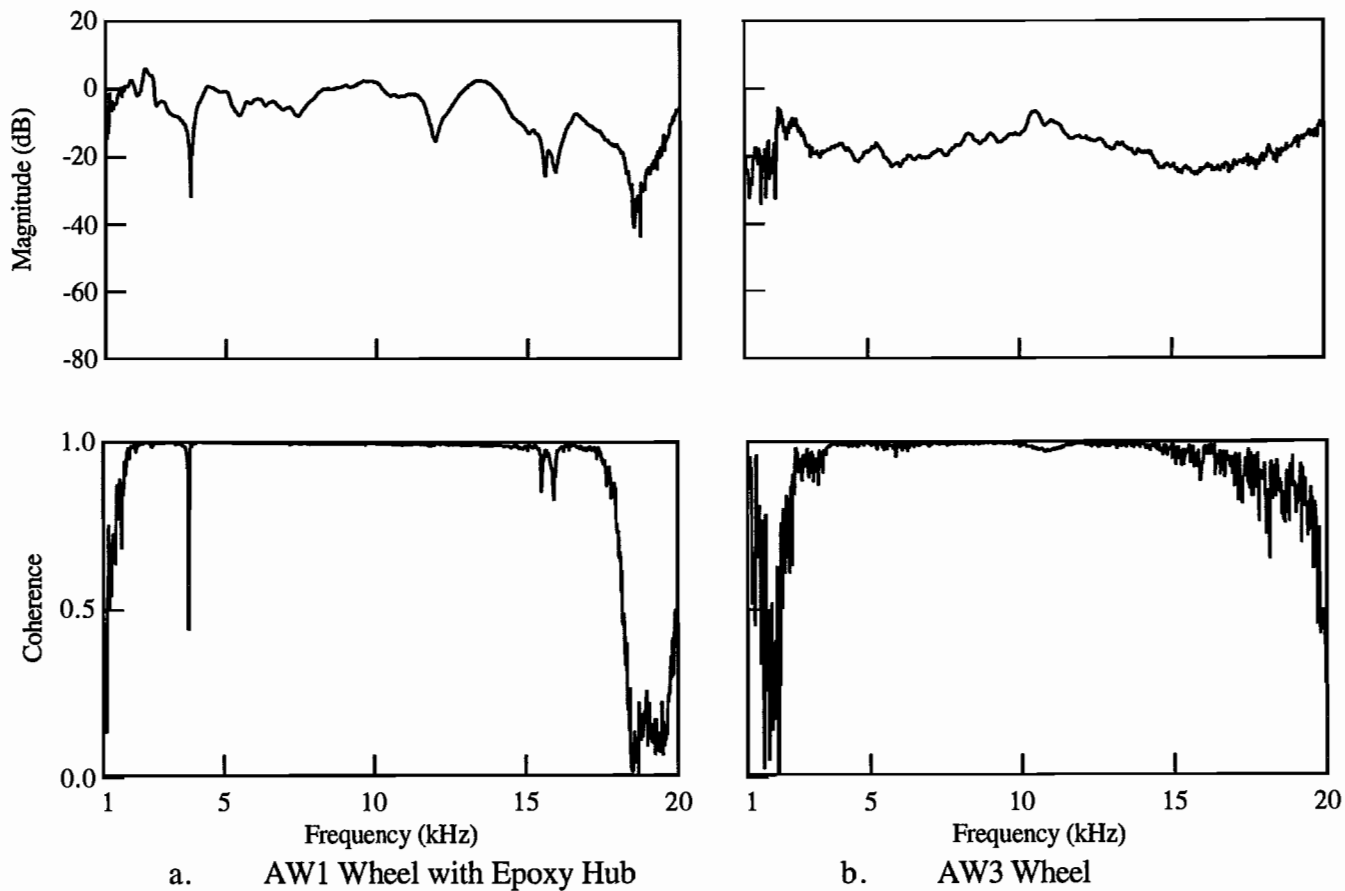


Figure 6.17 High-Frequency Energy Propagation Through Wheels AW1 and AW3

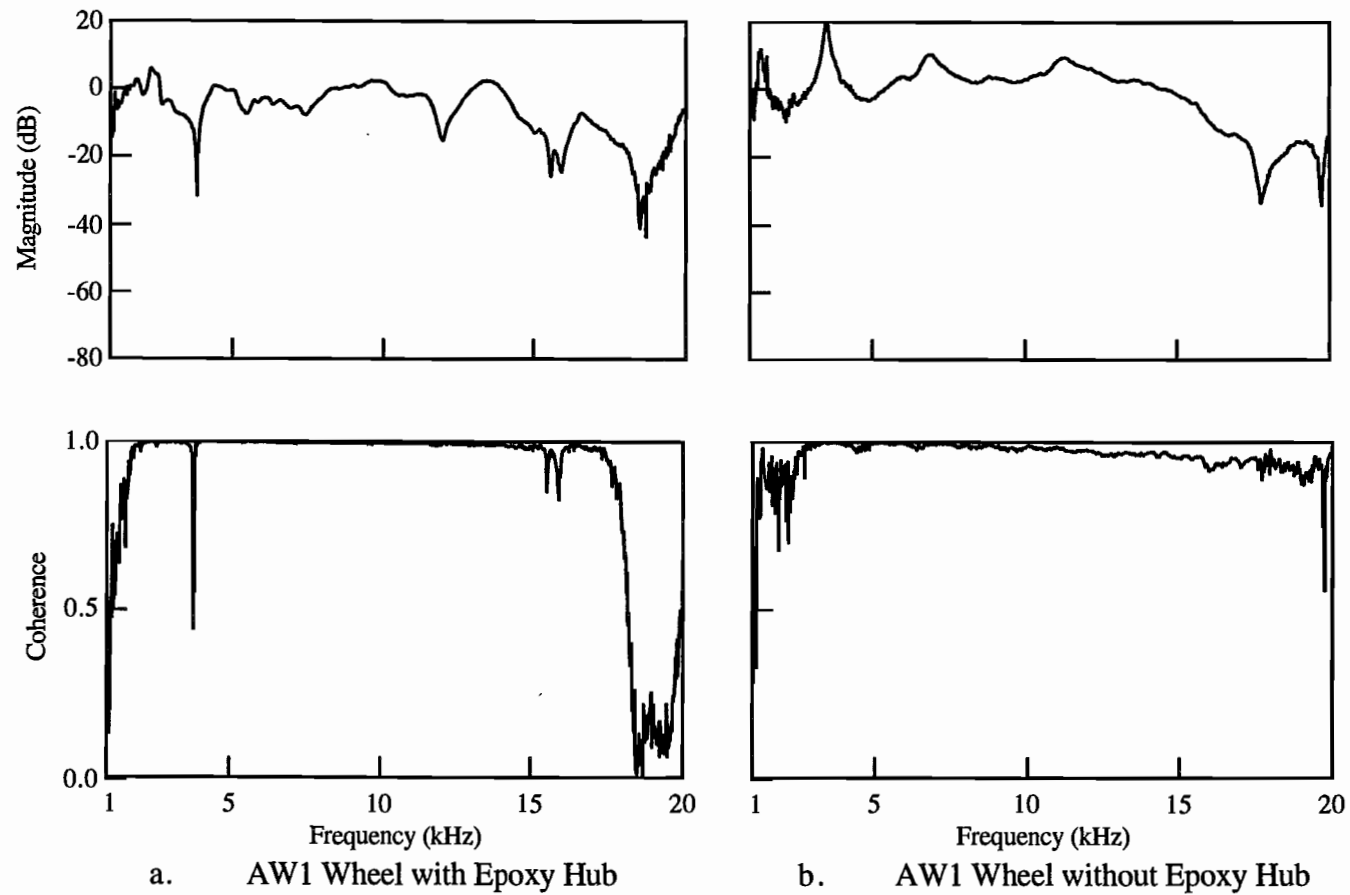


Figure 6.18 High-Frequency Energy Propagation Through AW1 Wheel with and without Epoxy Hub

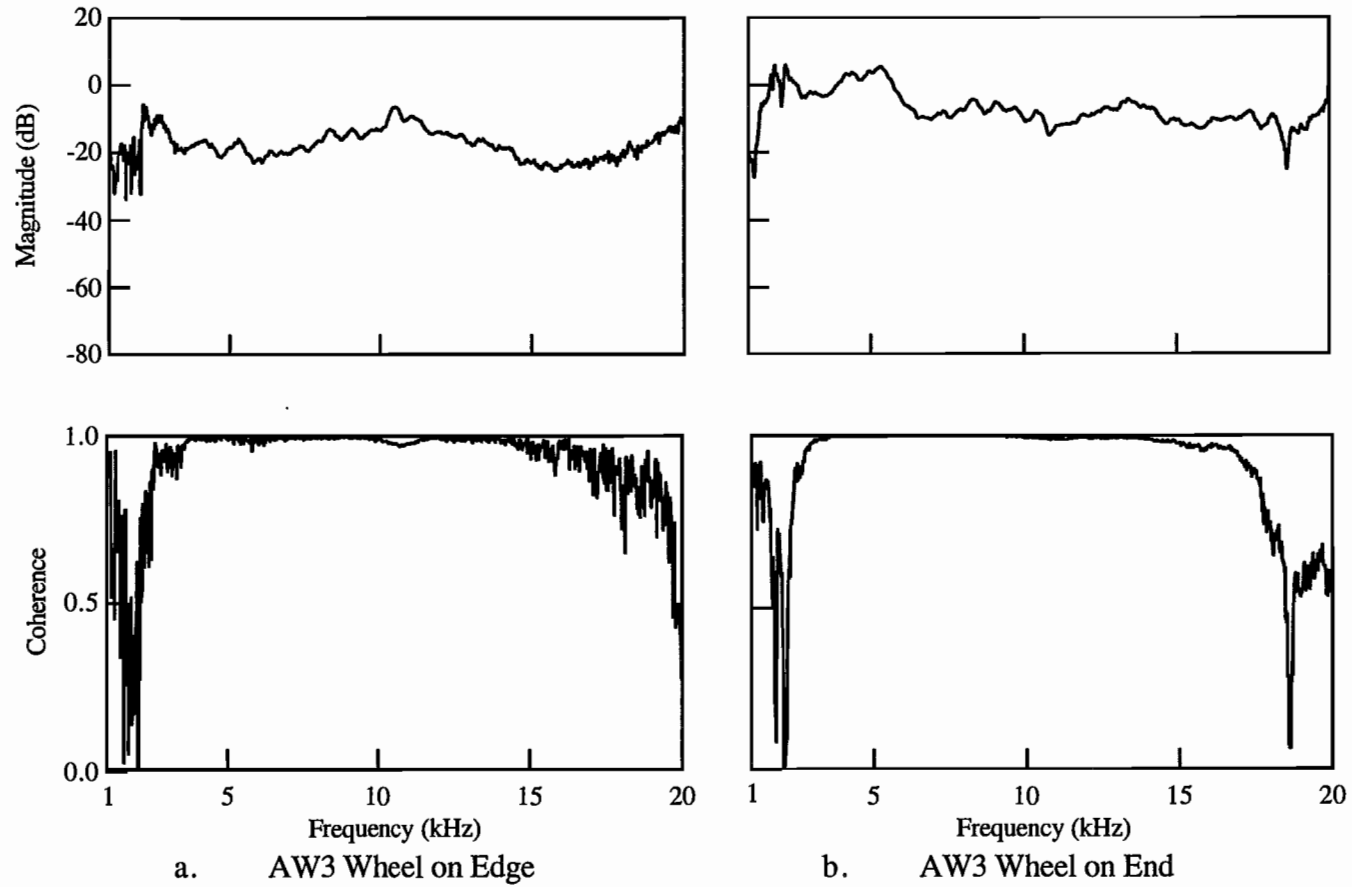


Figure 6.19 Comparison of High-Frequency Energy Reception through AW3 Wheel Oriented on its Edge and on its End

wheel that was turned on end is slightly greater in magnitude. This indicates that the contact area is also an important consideration for design of the rolling receiver.

6.2.4.2 Effect of Tread Material on Energy Reception: Tests were next performed to evaluate how the addition of tread material under the wheel affects the energy transmission through the wheel. Tests were performed as previously described on wheels AW1, AW2, and AW3, except a piece of 1.62 mm thick polyurethane with a durometer of 50A was placed under the wheel. Water was used between the urethane pad and the concrete, and between the wheel and the urethane. Figures 6.20a and 6.20b show the comparison of the frequency response and coherence from tests on wheel AW3 with and without the urethane tread. The addition of the tread material had two effects on the frequency response. First, the response was flattened out to a fairly constant level with no distinct peaks in the frequency range of 1 to 20 kHz. The second effect was that the received energy level decreased with the addition of the urethane tread. For example, in the frequency range of 5 to 20 kHz, the average energy reception decreased from -13 to -26 dB.

The same test was performed using the aluminum rim with the epoxy hub (AW1). The frequency response and coherence comparisons are shown in Figure 6.21. In this case, the tread had little effect on the frequency response. The same general response was observed in both cases except for a reduction in energy level of approximately 5 dB when the urethane was used. Also, the low points in the frequency response were further reduced when the urethane was used.

Lastly, the tests were performed on the solid aluminum wheel (AW2). The comparison of frequency response and coherence for this wheel is shown in Figures 6.22a and 6.22b. In this case, the addition of the urethane pad improved the response. The frequency response was flattened as a result of adding the polyurethane pad without reducing the energy transmission. The frequency response has one dominant peak at 15.5 kHz with a magnitude of 8 dB, which is due to the high frequency ringing of the wheel. In the frequency range of 1 to 10 kHz, however, the response is fairly flat and is attenuated by approximately -21 dB. Figure 6.23 shows the impact-echo results over the debonded and sound pavement at Site 2, shown in Figure 5.17, using this wheel arrangement. In this case, the wheel was completely covered with a polyurethane tread. These results can be compared to those shown in Figure 6.1, which were obtained with the accelerometer mounted directly on the pavement. The responses obtained using the wheel are inferior to those using just the accelerometer, in that the energy reception with the wheel is greatly attenuated. However, the characteristic vibrations of the pavement - in this case the resonant peak at 7900 Hz - is still detected using the wheel arrangement.

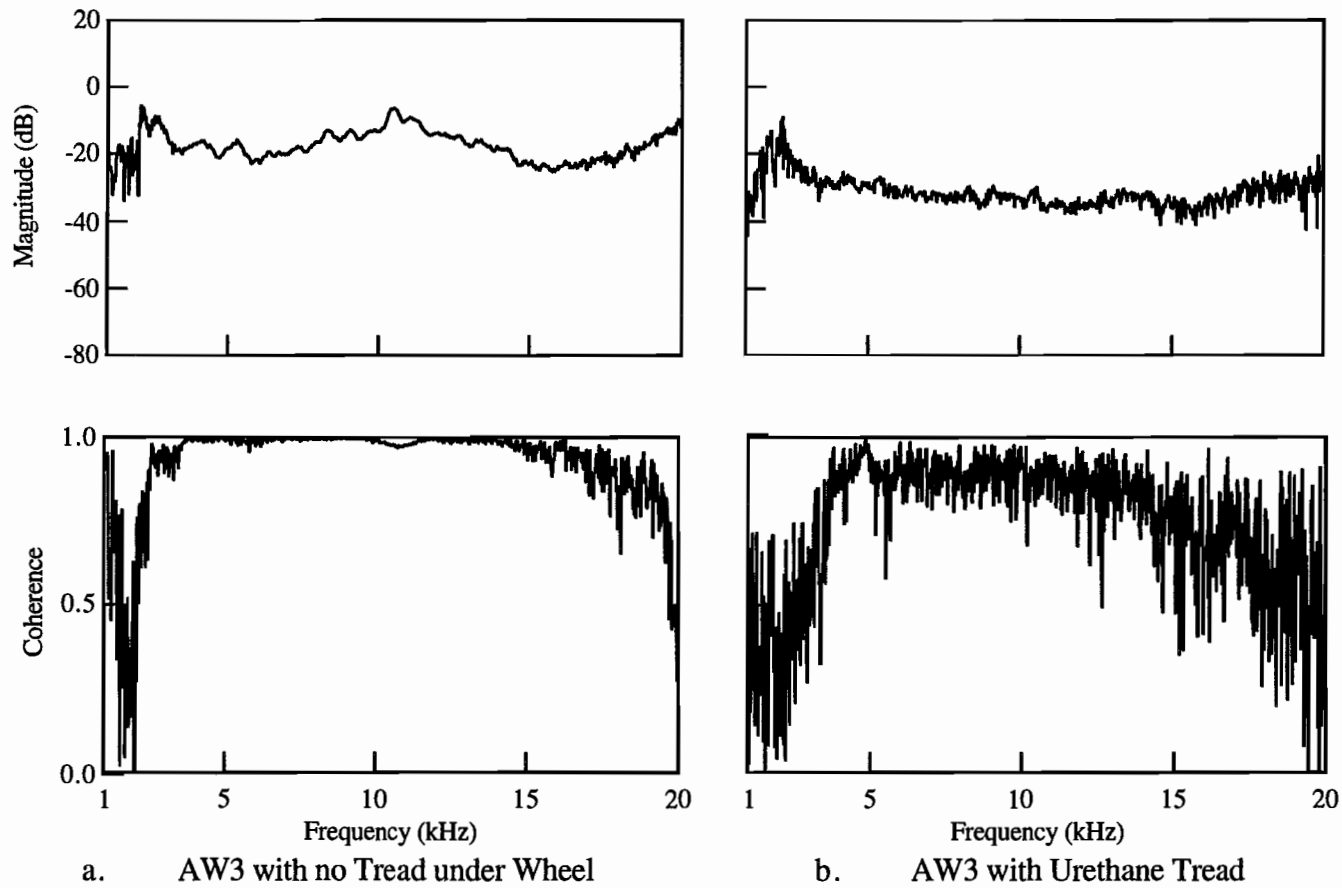


Figure 6.20 High-Frequency Energy Propagation Through AW3 Wheel with and without Urethane Tread (Durameter = 50 A; Thickness = 1.52 mm)

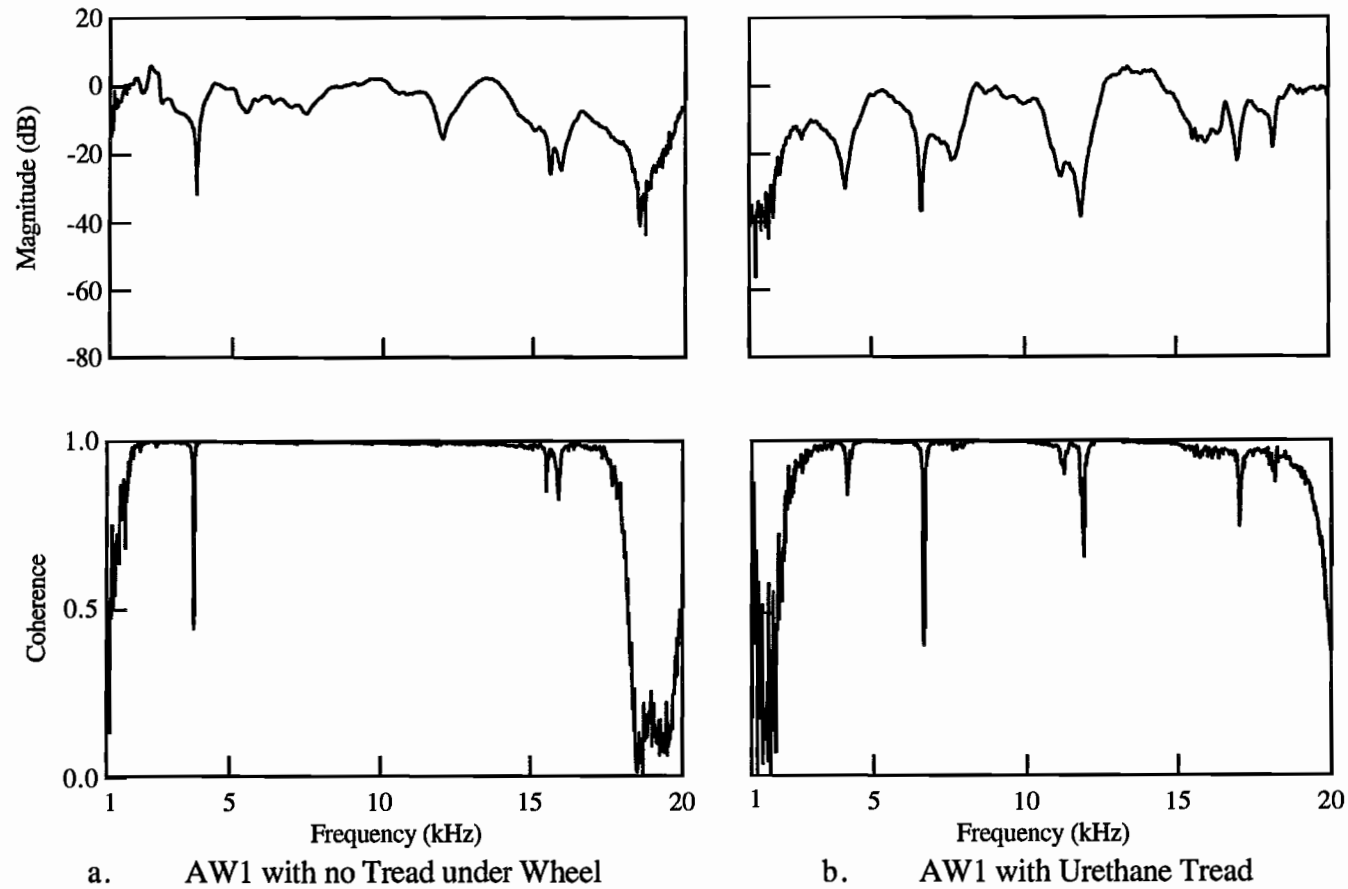


Figure 6.21 High-Frequency Energy Propagation Through AW1 Wheel with and without Urethane Tread (Durameter = 50 A; Thickness = 1.52 mm)

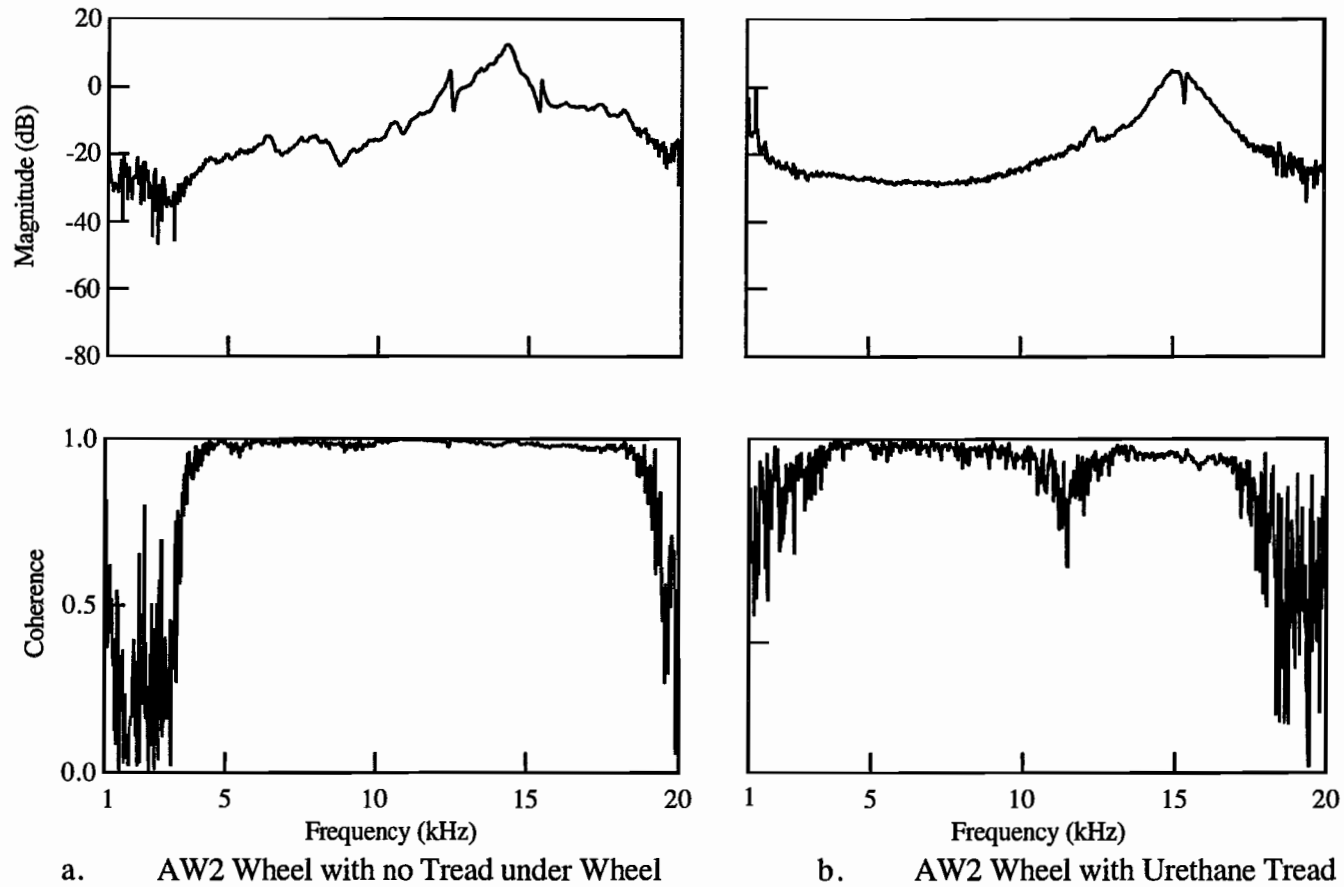
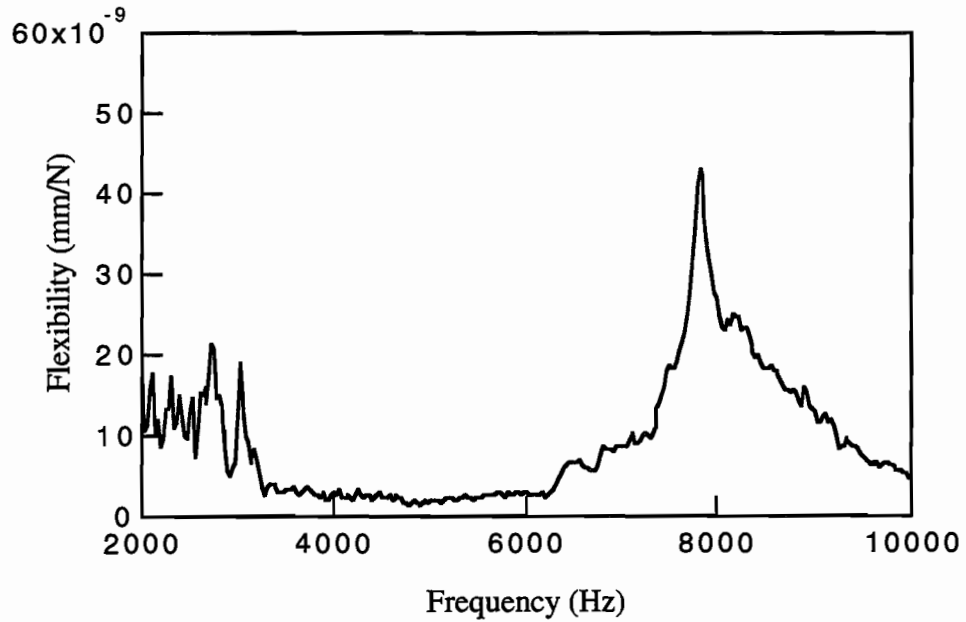
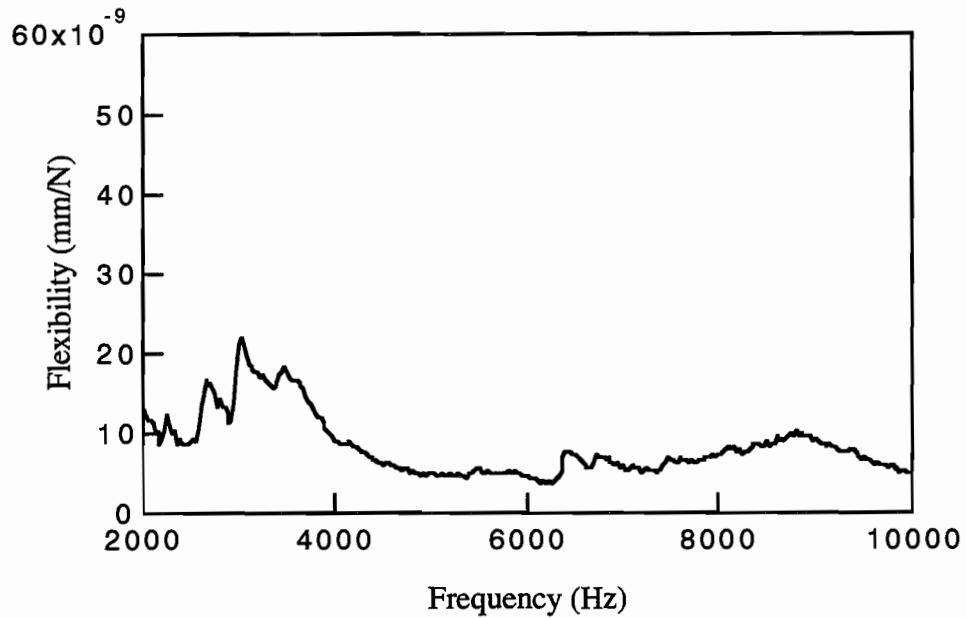


Figure 6.22 High Frequency Energy Propagation Through AW2 Wheel with and without Urethane Tread (Durameter = 50 A; Thickness = 1.52 mm)



a. Impact-Echo Record over Location Y1,
shown in Figure 5.17



b. Impact-Echo Record over Location X1,
shown in Figure 5.17

Figure 6.23 Impact-Echo Results using AW2 Wheel-Mounted Receiver

6.3 SUMMARY OF RESULTS FROM WHEEL MOUNTED RECEIVER TESTS

From these tests on stationary wheels with mounted receivers, it was found that there are several important variables affecting the high frequency (1 to 20 kHz) energy reception through the wheel. The first variable is the location of the receiver on the wheel system. When the receiver was mounted at a stationary location, such as the wheel stand or axle, the energy reception was generally poor. Better reception was achieved when the receiver was mounted directly on top of the wheel. The addition of water under the wheel greatly improved the coherence and frequency response in most cases. Secondly, the size of the wheel is important for multiple reasons. The wheel itself will tend to resonate or "ring" at certain frequencies depending on the size and shape of the wheel. Simple geometries such as solid wheels will tend to vibrate at a single frequency. More complicated geometries may have multiple vibration frequencies. An aluminum rim such as AW1, for example, resonates in many modes in the range of 1 to 20 kHz. On the other hand, a smaller (5.1-cm dia.) solid aluminum wheel such as AW3 will ring at a frequency outside of the range of interest. This is the most desirable result. However, practical limitations for use in the field mandate that the wheel be larger. A larger (10.2-cm. dia.) wheel, such as AW2, will resonate at approximately 15 kHz which interferes with the measured response of the pavement. In the range of 1 to 10 kHz, however, useful measurements could be made with a wheel of this size. Lastly, the tread used around the wheel will affect the measured response of the wheel on the pavement. The tread material will act as a spring under the mass of the wheel. It will, therefore, tend to amplify some frequencies and attenuate others depending on the mass of the wheel and the stiffness of the tread material. The addition of the tread material, therefore, may tend to improve or deteriorate the energy reception of the wheel.

The design of a wheel to receive frequencies in range from 1 to 20 kHz is a complicated problem involving many practical and theoretical limitations. Practically, a wheel to be used to test pavements needs to be fairly large, durable and have a wearing surface. In theory, the wheel should have a low mass and should not resonate in the frequency range of 1 to 20 kHz. Therefore, to have a large wheel that does not resonate in the range of 1 to 20 kHz, special design considerations will be necessary to damp resonant frequencies. Also, a tread material with a stiffness that is compatible with the wheel mass would need to be used. Lastly, if this wheel is built, receivers would need to be mounted in the wheel itself. This would require a slip ring system that is capable of charging the receivers and triggering their response at the appropriate time. The design and construction of such a system is beyond the scope of this research. One

possible alternative is to implement a continuous piezoelectric ceramic ring into the wheel design. This would allow for continuous vibration measurements as discussed below.

6.4 ENERGY RECEPTION WITH PIEZOELECTRIC CERAMIC MATERIALS

Initial testing was performed on small-scale piezoelectric ceramic materials to investigate the feasibility of implementing them into a rolling receiver. A piezoelectric material generates a voltage when a stress is applied, or conversely develops some displacement when a voltage is applied to the material. Quartz is an example of a naturally occurring material with piezoelectric properties. Piezoelectric materials can also be formed using ceramic materials. Two common types of piezoelectric ceramics are lead zirconate titanate and barium titanate. These ceramic materials can be designed for specific needs of sensitivity and stress direction. The EDO Corporation provided various small samples of piezoelectric ceramic materials, shown in Figure 6.24. Three small samples were tested to see if they could conceivably be implemented into a rolling receiver. Two disc shaped ceramic pieces with diameters of 2.5 cm and 3.8 cm and thicknesses of 4.7 mm and 6.4 mm, respectively, were tested. A cylindrical sample with an outside diameter of 2.54 cm, a width of 1.27 cm, and a wall thickness of 2.54 mm was also tested.

6.4.1 Frequency Response of Piezoelectric Ceramic Materials

The three materials shown in Figure 6.24 were tested to measure their response in the frequency range of interest (1 to 20 kHz). The small size of the receivers allowed testing to be performed on a small shake table. The testing arrangement is shown in Figure 6.25. A Wilcoxon 728T accelerometer with a sensitivity of 520 mV/g was used as the control receiver. It was screwed into the bottom of the top plate of a 8.9-cm high cylindrical aluminum stand with a diameter of 7.62 cm. The bottom of the aluminum stand was screwed into the top of a Wilcoxon F8 Piezoelectric Vibration Generator. The vibration generator was driven using a swept sine signal from the HP 3562A waveform analyzer. The signal was passed through a Wilcoxon Model PA8 Power Amplifier into a Wilcoxon Model N8H Matching Network and into the F8 Vibration Generator. The output from the 728T accelerometer was passed through a Wilcoxon P702 Power Unit and into Channel 1 of the HP 3562A waveform analyzer. The ceramic materials to be tested were mounted on top of the aluminum stand with vacuum grease. The output from the ceramic materials was passed through a Neff Model 128 amplifier and into Channel 2 of the HP 3562A waveform analyzer. A log sweep from 100 Hz to 100 kHz was performed on each test sample.

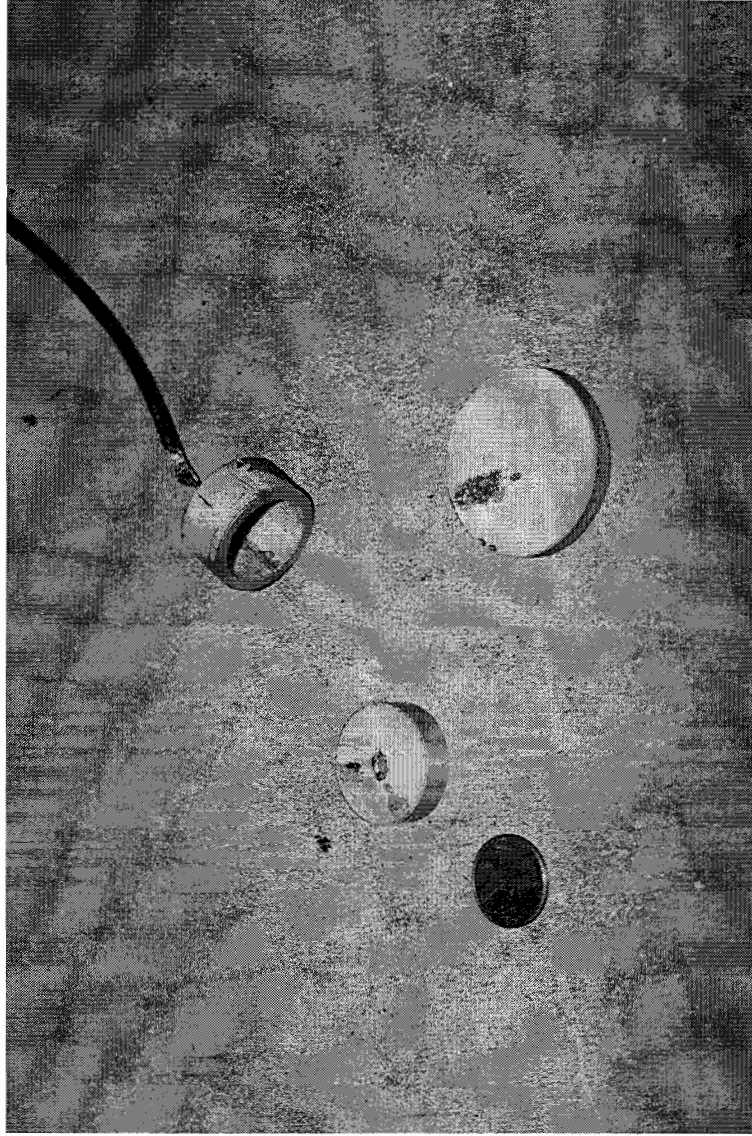


Figure 6.24 Piezoelectric Ceramic Receiver Elements (provided by EDO Corp.)

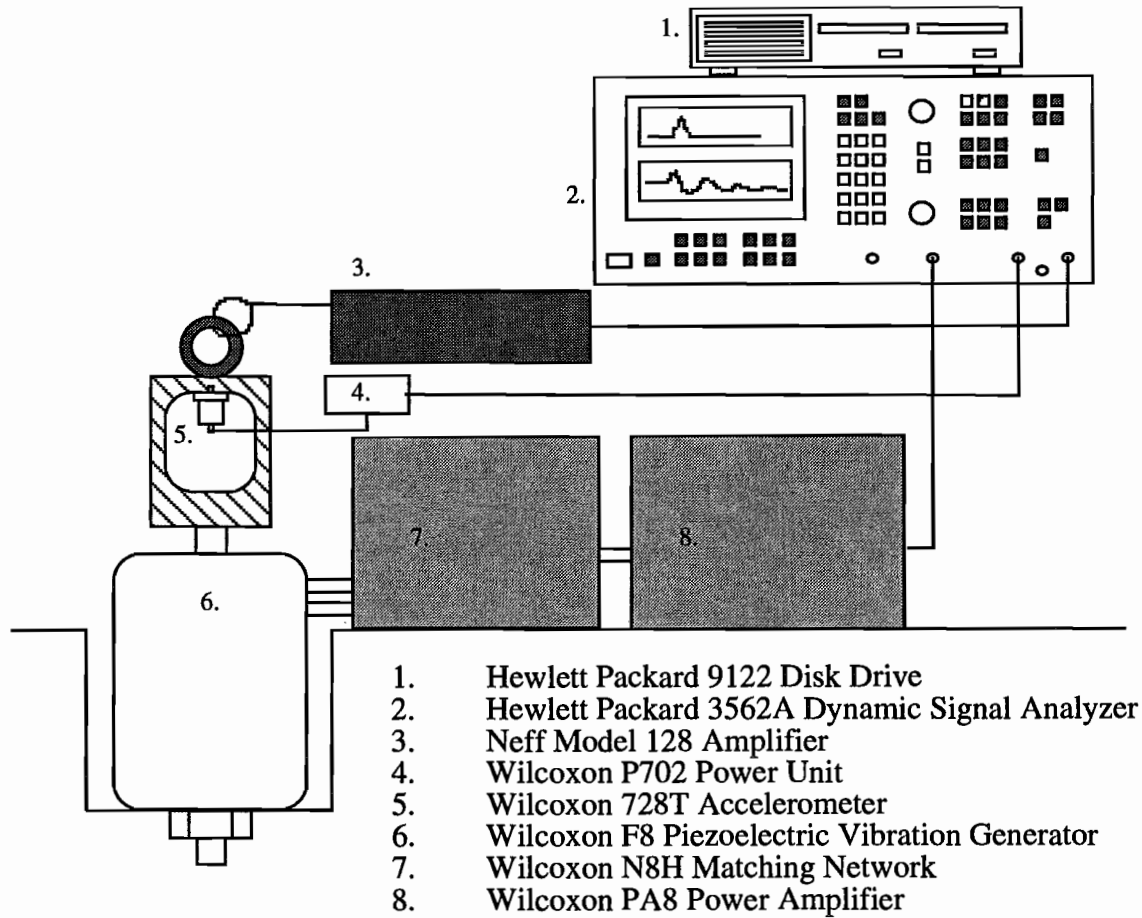


Figure 6.25 Testing Arrangement used to Study Piezoelectric Ceramic Materials for Rolling Receivers

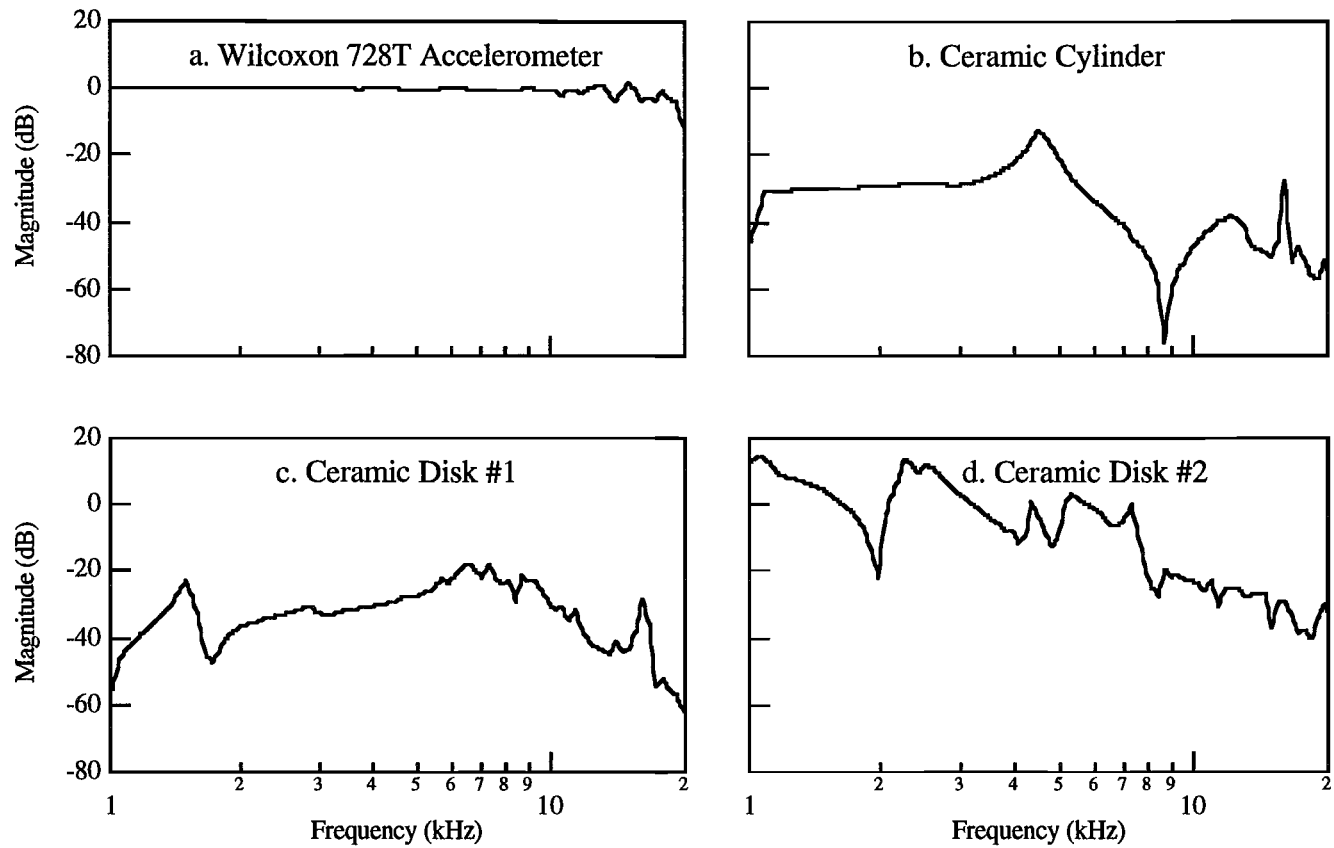


Figure 6.26 Frequency Response Plots from Tests using Piezoelectric Ceramic Receivers, shown in Figure 6.24

Figure 6.26a shows the frequency response and coherence values obtained from tests with a 728T accelerometer mounted on top of the receiver stand. As expected, the frequency response was flat and has a magnitude of approximately 1 (0 dB) from 1 to 20 kHz. Figures 6.26b through 6.26d show frequency response plots from tests performed on the cylindrical ceramic material, and the two ceramic disks. In each case, the frequency response was very irregular in the frequency range of interest (1 to 20 kHz). As discussed previously, it is desirable to have a linear response in the range of interest. Implementing a ceramic cylinder into a rolling wheel would require that a larger piezoelectric ceramic cylinder with a flat frequency response be developed. The cylinder would then be used as the rim of the receiver wheel. Many of the same problems discussed in Section 6.2 would also be of concern for this design. Based on the results from these small piezoelectric ceramic samples, the option of purchasing and testing larger piezoelectric cylinders was not pursued. However, with more extensive investigation and development, this may be a feasible solution.

6.5 SUMMARY

In summary, the tests performed on several stationary wheels indicate that it is difficult to receive stress-wave energy in the frequency range of interest for impact-echo testing. Factors affecting the response include the mass of the wheel, the geometry of the wheel, the wheel material, the wheel size, the contact area of the wheel on the pavement, and the tread material used around the wheel. The addition of water under the wheel helps to improve the energy reception. Energy reception through a wheel was achieved in the frequency range of 1 to 10 kHz. This range, however, is not acceptable for the effective use of the impact-echo method.

Tests were next performed on three small-scale piezoelectric ceramic materials, to study the feasibility of implementing them into a rolling receiver. The frequency responses of these materials were irregular in the range of interest. Therefore, the possibility of using larger piezoelectric ceramic materials was not pursued. The use of piezoelectric ceramic materials as the rim of a rolling receiver, however, may be a possible solution with more study.

CHAPTER 7.

RECEPTION OF LOW-FREQUENCY ENERGY

WITH A MOBILE RECEIVER

7.1 INTRODUCTION

As was discussed in Chapter 6, the problem of receiving energy in a rolling device over the frequency range required for impact-echo testing (1 to 20 kHz) is complicated by the introduction of a wheel into the testing system. The problems encountered are related to the effect of the wheel on the pavement motion and the effect of the wheel on the received signal.

The effective use of the impulse-response method in a rolling system also requires the use of a receiver wheel. However, this method requires that sufficient energy be generated and received in the frequency range of 10 to 1000 Hz. The behavior of the wheel/receiver system over this narrower and lower frequency range differs significantly from the response required for impact-echo testing.

In this chapter, results will be presented from tests with receivers mounted on several different wheels. The effect of wheel type, tread material and receiver location on received energy in the 10 to 1000-Hz frequency range is discussed.

7.2 LOW-FREQUENCY ENERGY RECEPTION USING WHEEL MOUNTED RECEIVERS

7.2.1 Testing Arrangement and Procedures

The testing arrangement used for low frequency testing is very similar to the testing arrangement described in Section 6.2.1. Figure 7.1 shows the testing arrangement used for the test results presented in this chapter. As before, the tests were arranged such that the response of the receiver mounted on the wheel could be compared to the response with the receiver mounted directly on the concrete. Therefore, measurements were first performed with both receivers on the concrete surface spaced 7.6 cm apart. The impact in this case was applied 7.6 cm along a center line passing through the midpoint between the receivers, as shown in Figure 7.1a. The test was

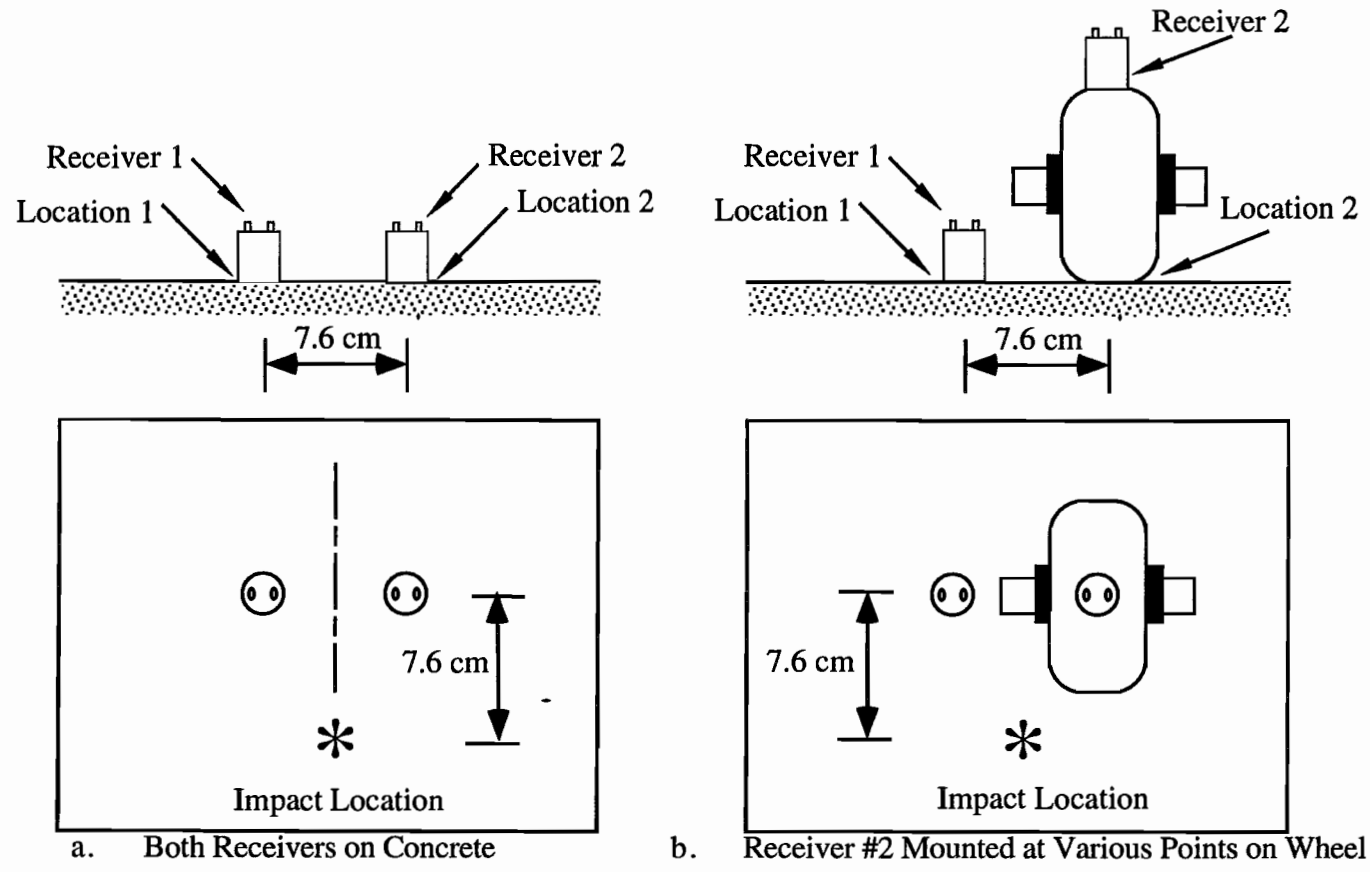


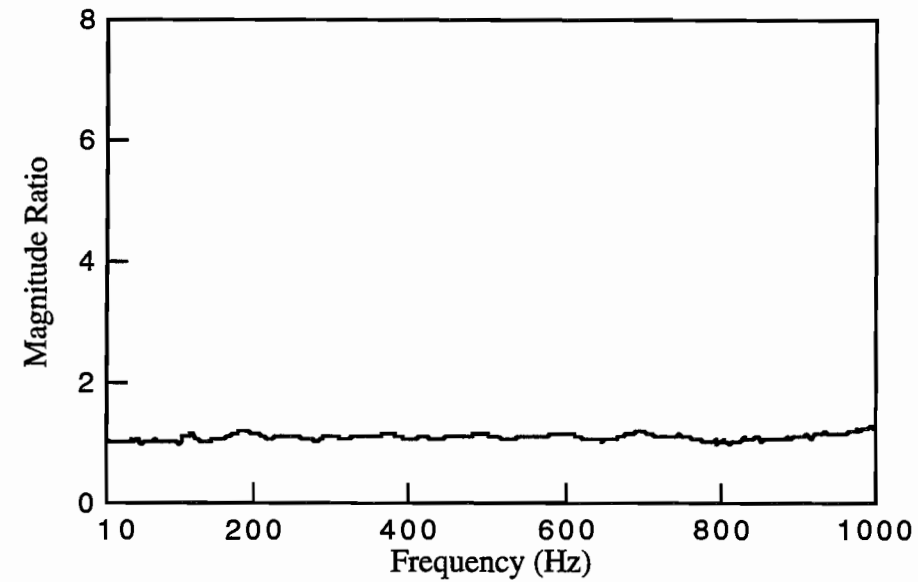
Figure 7.1 Test Arrangement for Evaluation of the Propagation of Low-Frequency Energy Through Wheels

then repeated with Receiver 2 mounted on the wheel at Location 2. The response from this test was then divided by the response from the test with both receivers on the concrete to give the desired frequency response. Due to the low frequencies that were to be measured, geophones were used instead of accelerometers to record the pavement vibrations. Mark Product L-15B geophones were used for these tests. These geophones have a resonant frequency of 4.5 Hz and a sensitivity of approximately 55 V/m/sec at frequencies greater than 7 Hz.

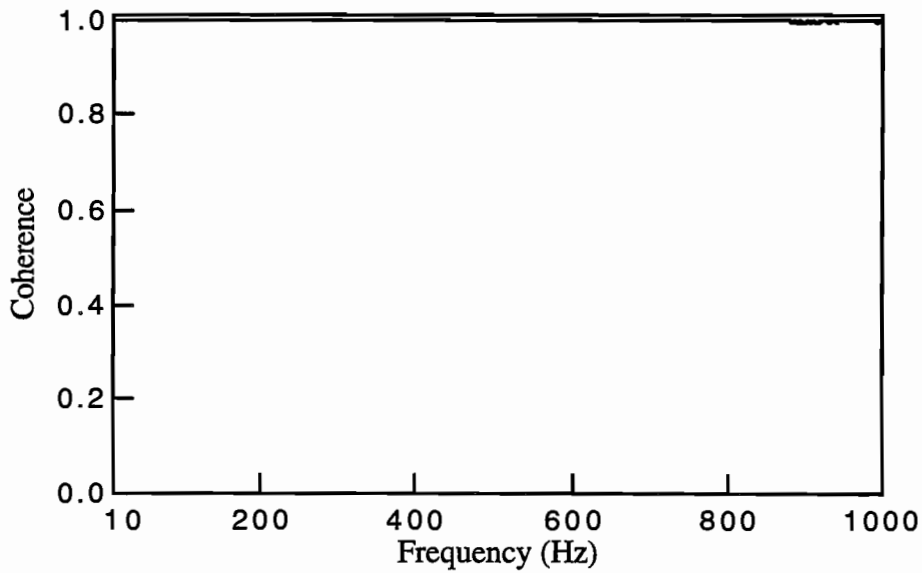
7.2.2 Wheel Mounted Receiver Tests

7.2.2.1 Results from Tests on Wheels of Different Sizes: Tests were first performed on two caster wheels of different sizes and masses. The first wheel (CW1) is a 10.2-cm diameter wheel which is described in detail in Section 6.2.3. The second wheel (CW2) is the same type of wheel as CW1, but is heavier and larger. This wheel has a diameter of 30.5 cm, and a width of 7.6 cm. Both wheels CW1 and CW2 have a stainless steel axle that passes through a ball bearing. A wheel stand was also used in each case. The total system for wheel CW1 weighs 1.88 kg; for CW2, the total mass is 16.6 kg. Tests were performed with the geophone located at various locations in the wheel system, such as on the wheel stand and on the outside of the wheel axle. Figure 7.2 shows the frequency response and coherence with both geophones located on the concrete. As expected, the response is fairly flat, and the coherence is good over the frequency interval of 10 to 1000 Hz. As was discussed in Section 7.2.1, the frequency responses presented herein were divided by Figure 7.2a, to remove the effect of location from the results.

Figure 7.3 shows a comparison of the results from tests on wheels CW1 and CW2 where the geophone was mounted on the top of the wheel stand (location A in Figure 6.5). These tests were performed with no coupling material or water between the wheel and the ground. Although both tests yielded good coherence values, the difference in wheel size and mass affected the response of the wheel in the frequency range of 10 to 1000 Hz. The response from the test on wheel CW1 shows a peak at 270 Hz. Below this peak, in the range from 10 to 100 Hz, the response is flat and has a magnitude of 0 dB, indicating no effect from the wheel. Above the resonant peak, however, the frequency response drops off significantly to a level of approximately -11 dB. The response from wheel CW2 has similar characteristics. In this case, the resonant peak was at a frequency of 80 Hz. At very low frequencies, from 10 to 20 Hz, the response is again flat indicating no effect from the wheel. Above the resonant peak, the energy received drops off significantly, to a level of -42 dB near 1000 Hz. The same test on wheel CW2 was repeated with the receiver mounted directly on the wheel, and on the axle of the wheel. The comparison of the



a. Frequency Response



b. Coherence Function

Figure 7.2 Frequency Response and Coherence from a Test with both Geophones Directly on the Concrete Surface

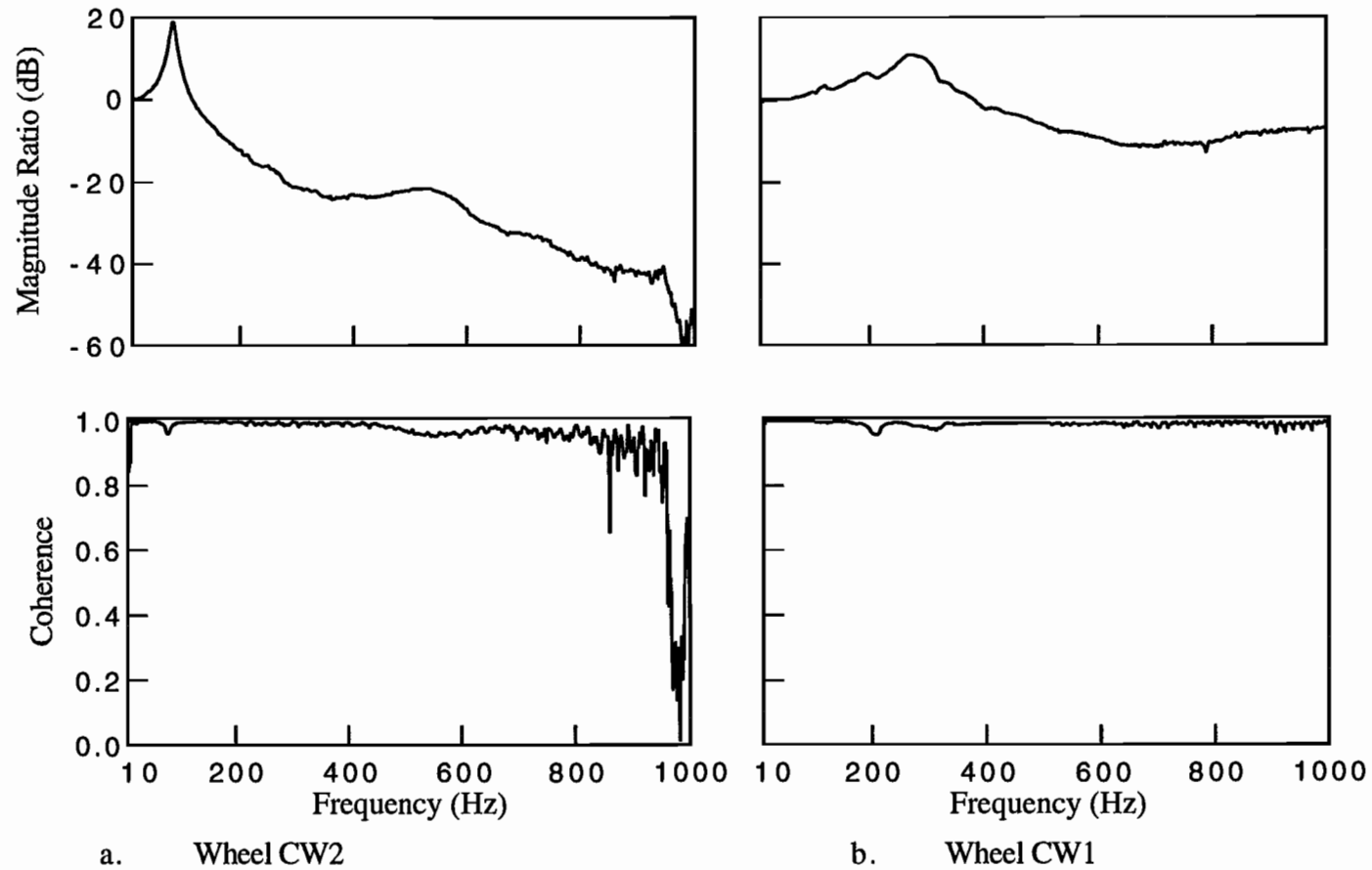


Figure 7.3 Frequency Responses and Coherences from Tests with Receiver Mounted on Wheel Stand of Wheels CW1 and CW2

frequency responses and coherences with the receiver at these locations on the wheel system is shown in Figures 7.4a and 7.4b, respectively. The general shape of the response showing a peak at 85 Hz and energy loss at higher frequencies was the same for each receiver location tested. The coherence was generally good in all cases, with slightly poorer coherence for the case of the axle-mounted receiver.

7.2.2.2 Discussion of Results: Variations in the frequency responses measured from wheel mounted receivers in the frequency range 10 to 1000 Hz are less complicated than those observed in the range of impact-echo testing (1000 to 20000 Hz). Due to the smaller and lower frequency range, problems such as internal resonances of the wheel are not present in the response plot. Also, the longer wavelengths associated with these lower frequencies allow the entire wheel system to move approximately in phase. This is demonstrated by the similar responses measured with the receiver mounted on the wheel stand, wheel, and axle, as shown in Figures 7.3 and 7.4.

The general shape of the frequency responses that were measured in all cases is indicative of a single-degree-of-freedom oscillating system. The low frequency resonant peak is caused by the wheel (mass) vibrating on the wheel tread (spring). Below the resonant frequency and away from the peak, the response is approximately unity. At frequencies above and away from the peak, the response is greatly attenuated. It is desirable, therefore, to operate the wheel in the frequency range below the resonant peak. For the frequency range of interest for impulse-response testing, therefore, the peak must be moved to a frequency greater than 1000 Hz. The following section demonstrates how the wheel can be designed to have a response of unity in the frequency range from 10 to 1000 Hz.

7.2.2.3 Effect of Wheel Mass and Tread Material: The frequency response of the wheel can be altered by changing two parameters. If the wheel is modelled as a single-degree-of-freedom oscillator, the resonant frequency is equal to the square root of the spring stiffness (k) divided by the square root of the mass (m). In this case the mass is the mass of the wheel system, and the spring stiffness is the stiffness of the wheel tread. Therefore, by changing these two parameters - mass and tread stiffness - the frequency response can be altered.

Tests were performed with two solid metal wheels of different masses. Wheel SW1, described in Section 6.2.3, is a steel wheel with a diameter of 10.2 cm and a mass of 3007 g. Wheel AW2 is an aluminum wheel with a diameter of 10.2 cm and a mass of 1012 g. These wheels were tested alone (no wheel stand or axle) and the receiver was mounted on the top of the

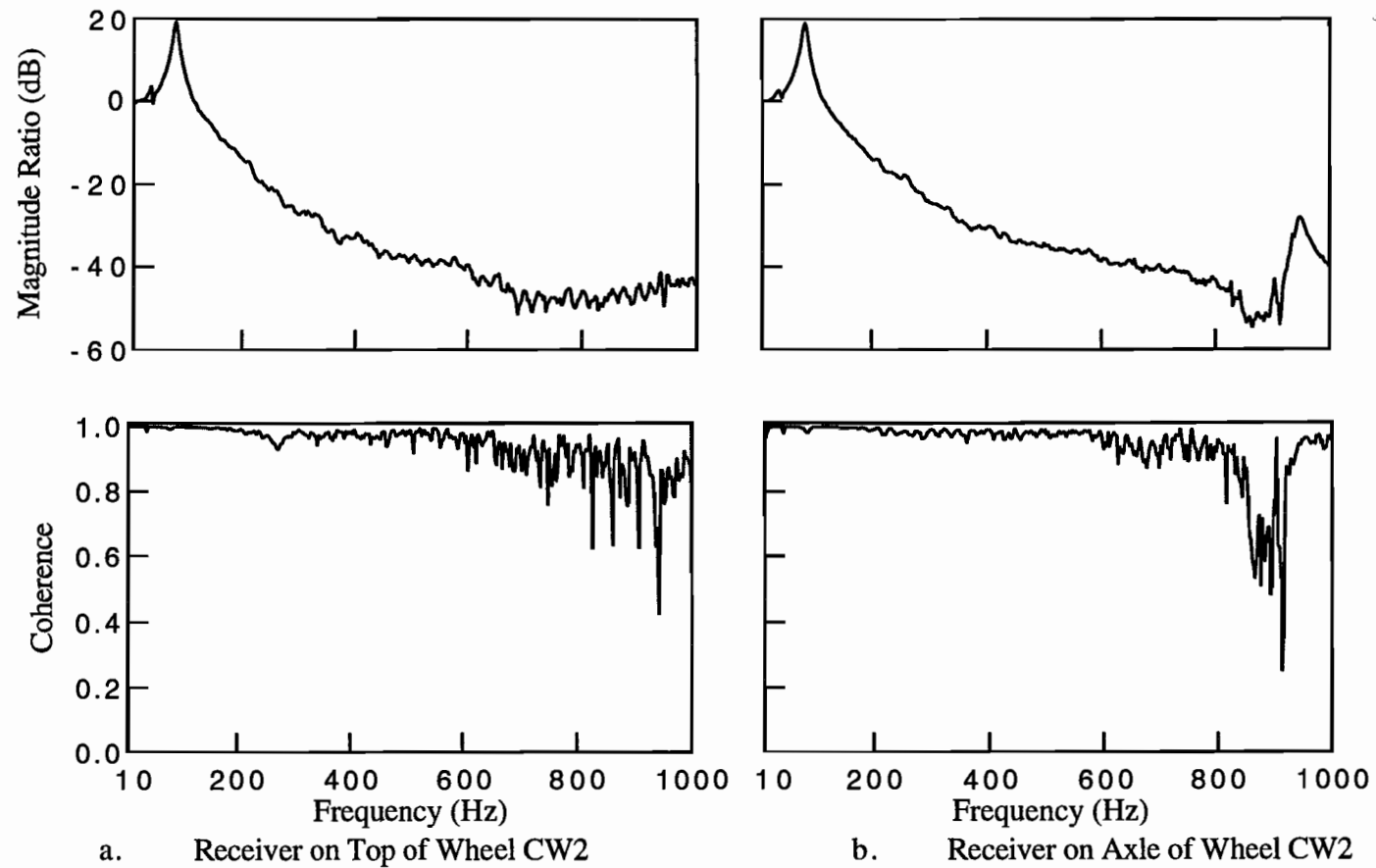


Figure 7.4 Frequency Responses and Coherences from Tests with Receiver Mounted at Different Locations on Wheel CW2

wheel, as illustrated in Figure 7.5. Two different tread materials were tested under the wheels. Tread 1 is a soft polyurethane material with a thickness of 1.5 mm and a durometer value of 90A. Tread 2 is a stiff polyurethane material with a thickness of 1.3 mm and a durometer value of 65D. Square swatches of each material (5.1 cm on a side) were glued to the bottom of the wheels. The wheel was then placed on the concrete surface. The tests were performed as described in Section 7.2.1.

Figures 7.6a and 7.6b show the frequency response and coherence from tests with Tread 1 under SW1. The response is shown on a linear scale to emphasize the resonant peak. As expected, the general single-degree-of-freedom response was measured. In this case, the peak is located at a frequency of 350 Hz. Below this peak, the response approaches unity; above the peak the response attenuates greatly. The test was next performed using the lighter AW2 wheel with Tread 1. The frequency response and coherence from this test are shown in Figures 7.7a and 7.7b. As expected, decreasing the mass of the wheel caused the resonant peak to move to a higher frequency of 562.5 Hz. This produced a near unity frequency response up to approximately 200 Hz. Frequencies were significantly amplified from 300 to 700 Hz, and attenuated between 800 and 1000 Hz.

The next test was performed with wheel SW1 on the stiffer Tread 2 material. The frequency response and coherence from this test is shown in Figures 7.8a and 7.8b. The greater stiffness of Tread 2 caused the peak to move from a frequency of 350 Hz with Tread 1 to a frequency of 813 Hz with Tread 2, as shown in Figures 7.6a and 7.8a, respectively. The frequency response from this case has a near unity value in the range from 10 to 400 Hz. From 400 to 1000 Hz, the response is amplified. The attenuated portion of the response has been moved outside of the frequency range of interest.

Lastly, wheel AW2 was tested with Tread 2 under the wheel. This is the case of the lighter mass on the stiffer tread and should yield the highest frequency peak. The frequency response and coherence for this case are shown in Figures 7.9a and 7.9b, respectively. The resonant peak has now moved outside of the frequency range of interest. Although the leading edge of the resonant peak causes slight amplification of energy at frequencies near 1000 Hz, the response is generally flat throughout the frequency range. This response is clearly more desirable than the others presented in this chapter.

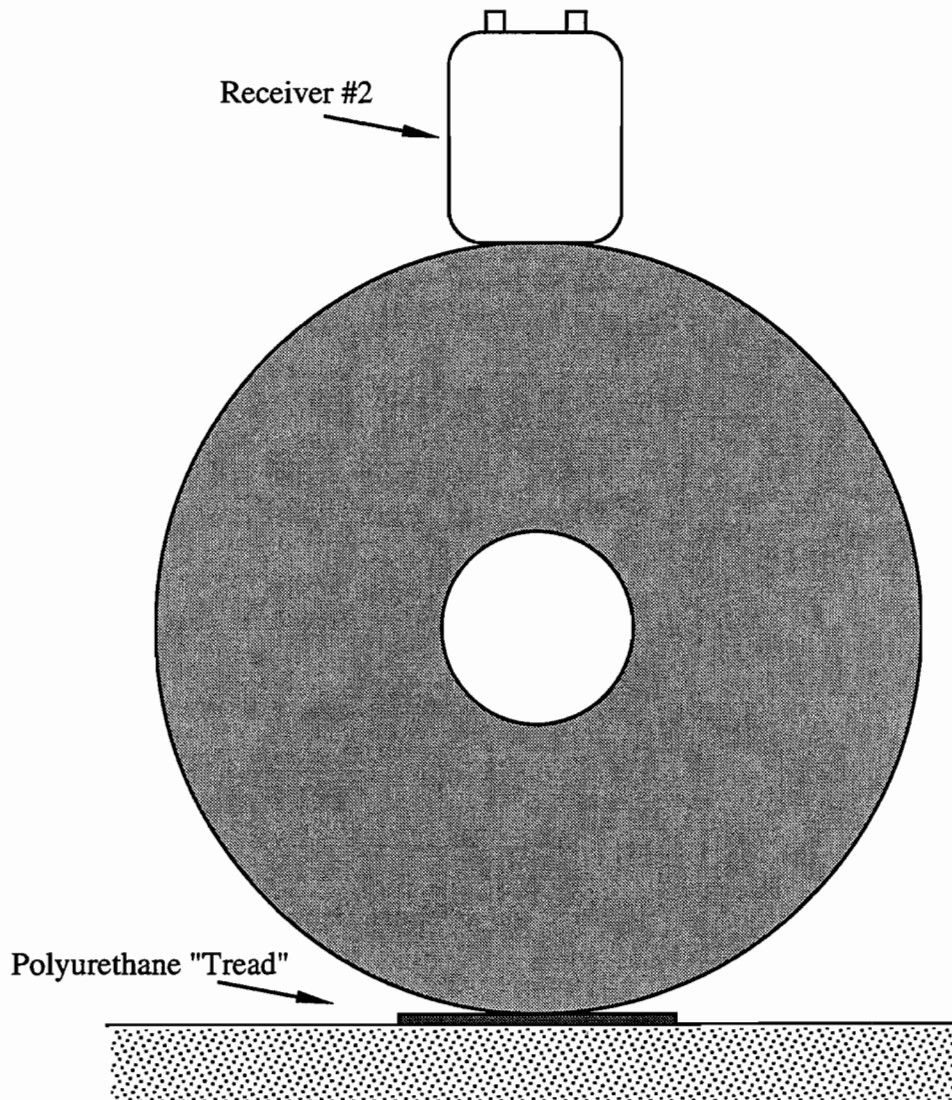
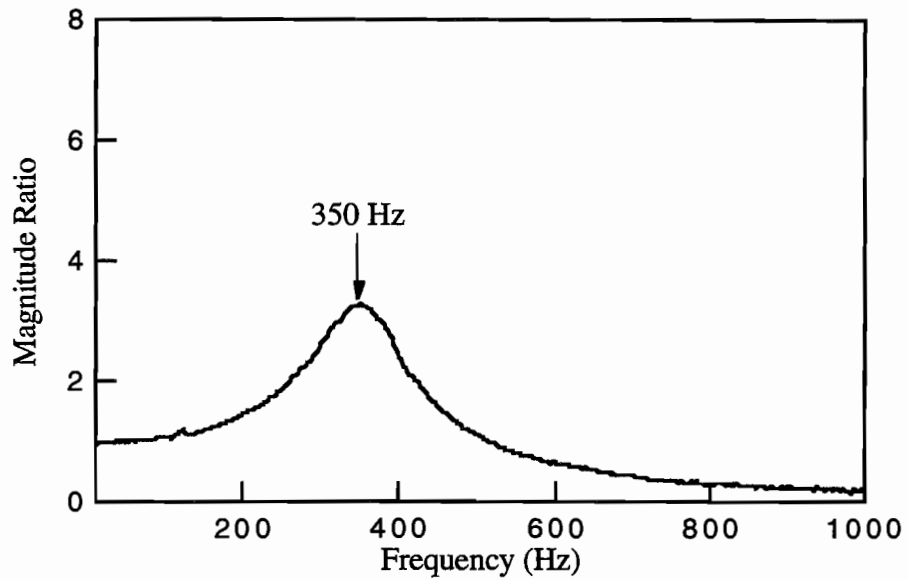
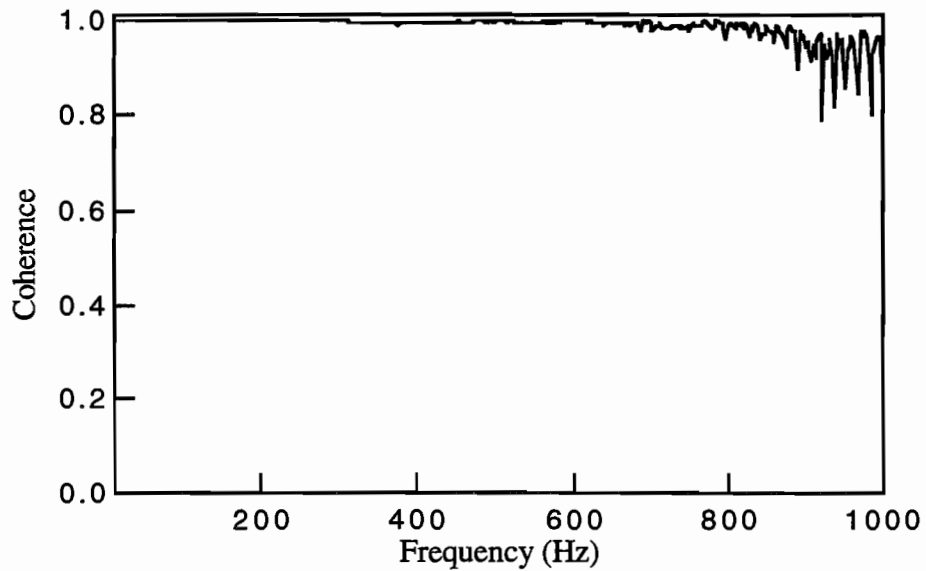


Figure 7.5 Testing Arrangement for Evaluating the Effect of Wheel Mass and Tread Stiffness

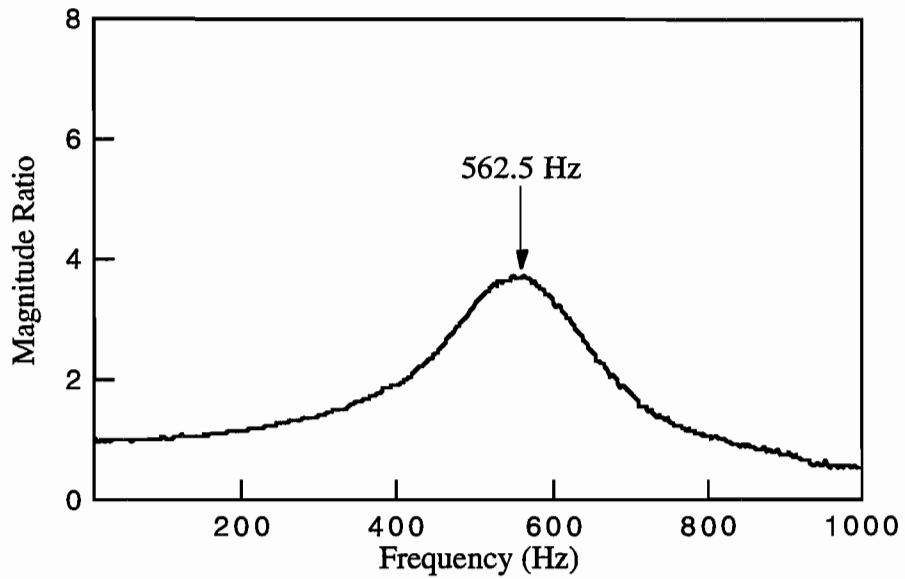


a. Frequency Response

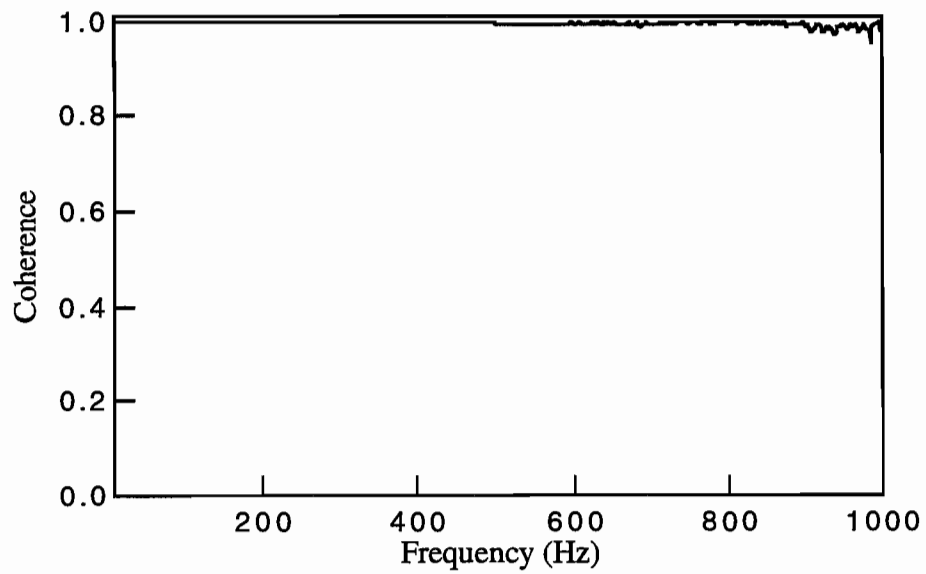


b. Coherence Function

Figure 7.6 Frequency Response and Coherence from Test with Geophone on Wheel SW1 coupled with Tread 1

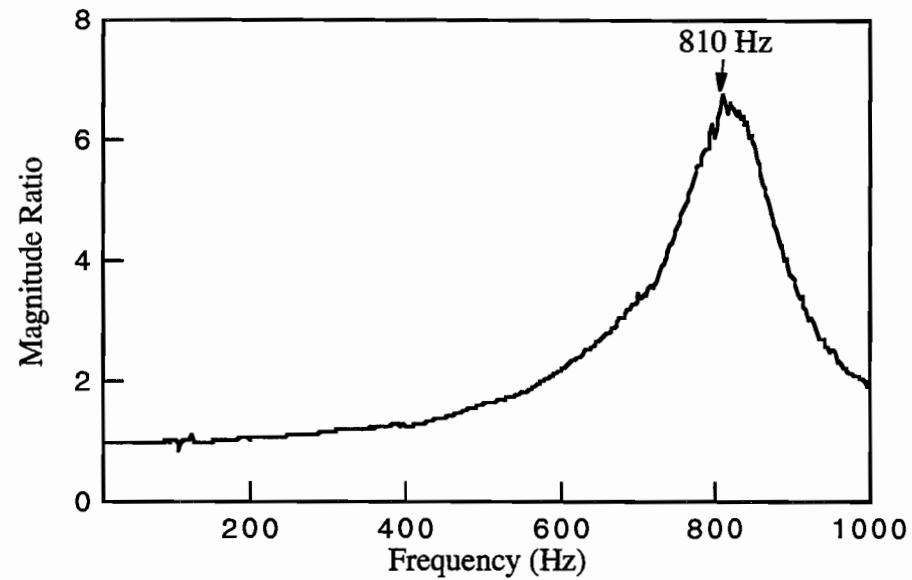


a. Frequency Response

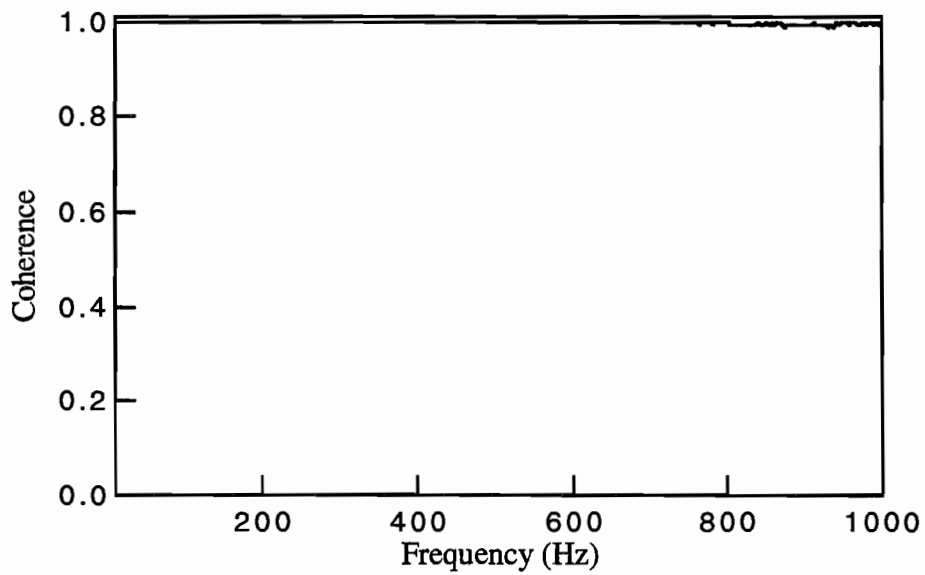


b. Coherence Function

Figure 7.7 Frequency Response and Coherence from Test with Geophone on Wheel AW2 coupled with Tread 1

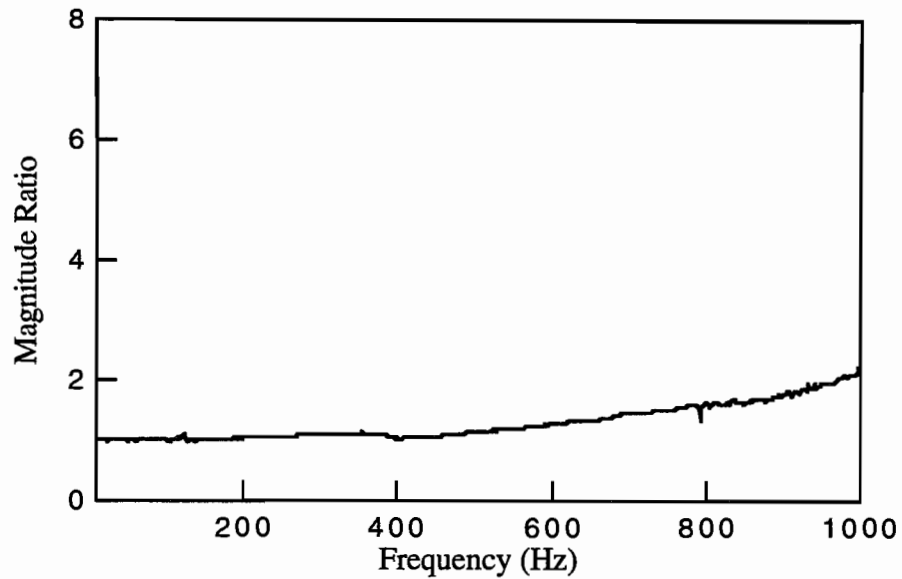


a. Frequency Response

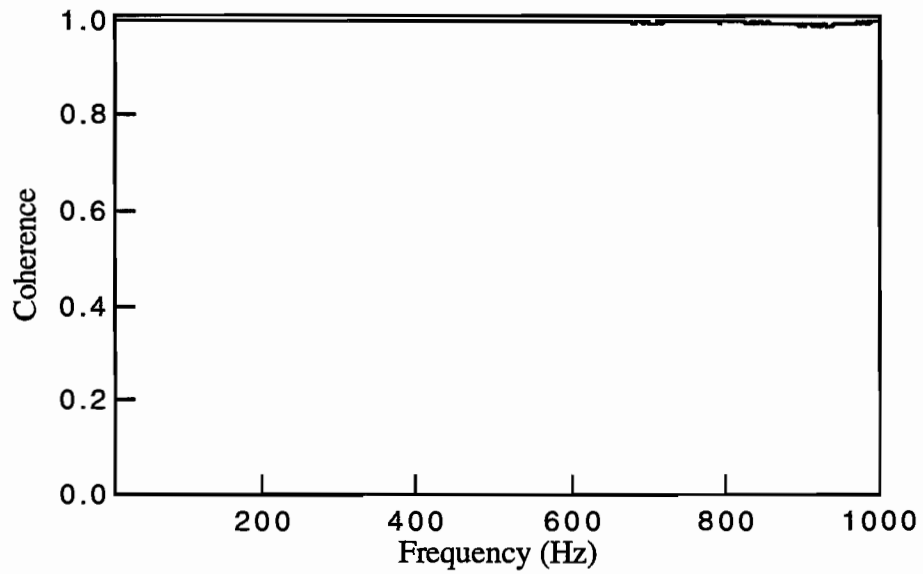


b. Coherence Function

Figure 7.8 Frequency Response and Coherence from Test with Geophone on Wheel SW1 coupled with Tread 2



a. Frequency Response



b. Coherence Function

Figure 7.9 Frequency Response and Coherence from Test with Geophone on Wheel AW2 coupled with Tread 2

7.3 SUMMARY

The results presented in this chapter demonstrate the comparatively easy task of receiving energy for impulse-response testing through a rolling receiver wheel as compared to impact-echo testing. Unlike impact-echo testing, the lower frequency and longer wavelength waves in impulse-response testing allow for good measurements with a receiver mounted at stationary locations on the wheel system. Also, problems such as high frequency ringing of the receiver wheel are not encountered in the frequency range of 10 to 1000 Hz. The dominant feature in the low frequency responses is the "spring-mass" resonance of the wheel. The wheel/tread system behaves as a single-degree-of-freedom oscillator. The frequency responses measured from this system show the characteristic response of amplification at the resonant frequency and attenuation beyond the resonant frequency. By minimizing the mass of the wheel and increasing the stiffness of the wheel tread, the resonant peak can be moved to a frequency outside the range of interest. This creates a fairly flat response with a magnitude near unity throughout the frequency range of impulse-response testing.

The ability to receive the vibration energy with minimal or no signal attenuation is very important for field use of the impulse-response method. Previous noise measurements of IH-35, IH-77, and 26th Street in Austin, TX indicate that the majority of road noise is in the range from 10 to 1000 Hz (Ref 1). Therefore, the signal generated and received must be greater than the ambient road noise for valid results.

Although the prospect of mobile impulse-response testing appears to be very feasible, the use of this method alone would not provide all necessary information concerning subsurface defects in a pavement, as discussed in Chapter 5. The additional information provided from impact-echo testing would be very important in identifying the flaw depths and in locating some of the deeper flaws.

CHAPTER 8.

SUMMARY, CONCLUSIONS, AND RECOMMENDATIONS

8.1 SUMMARY

The development of flaws in pavements can lead to the rapid deterioration of the pavement surface, requiring costly repairs. Often these flaws originate below the pavement surface with no detectable surface manifestation. Two common types of subsurface flaws are voids and delaminations. The ability to detect these flaws before extensive damage results is an important part of any pavement management program. Many nondestructive methods ranging from simple sounding devices to radar and infrared devices have been applied to this problem. No system has yet been developed which is capable of consistent, accurate, and rapid detection of subsurface flaws in pavements. The key requirement is "rapid" because identification methods now exist with which point measurements can successfully be performed with stationary equipment.

In this research, stress-wave based nondestructive testing techniques were examined to determine the feasibility of implementing these methods into a rolling pavement testing system. Several stress wave methods were reviewed. Two methods, the impact-echo and impulse-response methods, were chosen to be studied using both experimental tests and numerical models. The objective was to first examine the effectiveness and limitations of the methods on a site-specific basis, and second, to examine the feasibility of using these methods in a rolling system. Therefore, experimental testing was performed at three test site locations to evaluate the effectiveness of the impact-echo and impulse-response methods for detecting various flaws in rigid pavements. Cases that could not be studied experimentally were studied using results from finite element tests performed by Chine Chung Chiang, as part of Project 1243 (Ref 33). Secondly, experimental tests were performed to study the propagation behavior of stress waves in the frequency range of interest through a receiver wheel. Tests were performed using receivers mounted on wheels of various sizes and composed of various materials. Variables affecting the test results included wheel size, wheel mass, wheel shape, wheel tread material, and receiver location. These tests were performed for both the frequency range of the impact-echo test (1 to 20 kHz) and the impulse-response test (10 to 1000 Hz). From these test results, conclusions were drawn concerning the feasibility of using these stress wave methods in a mobile testing system.

8.2 CONCLUSIONS

The experimental and analytical results from this research indicate that an effective rolling system for evaluating pavements requires that stress-wave energy be generated and received over a broad frequency range. At a minimum, a range from 10 Hz to 20,000 Hz is necessary to detect most of the subsurface pavement flaws of interest. The range from 10 to 1000 Hz would be used for impulse-response testing to detect low-frequency flexural vibrations. The range from 1000 to 20,000 Hz, would be used for impact-echo testing to detect high-frequency compression wave resonance that develops over flaws in the pavement. Assuming that good compression wave velocity values of the concrete were known, the impact-echo results would also provide information about the depth to the void interface.

Ideally, the impact-echo testing method could be used exclusively to detect flaws in the pavement. This would require, however, that stress-wave energy be generated and received at the very high frequencies that are needed for shallow (depths to 5 cm) flaw detection. For site-specific applications, this can often be achieved by using a special displacement transducer and small, ball bearing sources. The location and quality of the source impact can be monitored and repeated if necessary to ensure good results. In a mobile system, a single impact must consistently generate the necessary frequencies in the pavement. This can be difficult if the pavement is very rough or damaged. Therefore, use of an impacting source for a rolling testing system presents several practical problems. Secondly, receiving the high-frequency energy through a mobile receiver presents many practical problems. Tests were performed as part of this research to study the wave propagation behavior of stress waves through various wheels. Good energy reception could only be achieved up to frequencies of approximately 10 kHz. Problems that were encountered included energy attenuation at high frequencies and internal ringing of the wheel system. A frequency range to 10 kHz would only provide effective impact-echo results for detecting voids at depths of approximately 20 cm or greater. This is, therefore, not an acceptable frequency range for thorough evaluation of pavements. Another limitation of the impact-echo method observed from the experimental testing is the difficulty in detecting small, deep flaws in the pavement (flaws that are significantly less in extent than twice their depth).

Impulse-response tests were shown to be effective means of detecting areas of large voids, especially under the edges and corners of rigid pavements. The experimental results indicate that when the data are displayed in terms of average mobility, as opposed to dynamic stiffness, the lateral extent of the void can be delineated fairly well. Also, when impulse-response results are

combined with impact-echo results, debonded pavement can be differentiated from pavement containing a void. Impulse-response results alone, however, do not detect many flaws of interest in the pavement. Small or deep voids that vibrate in flexure at frequencies greater than 1000 Hz will likely not be detected with impulse-response instrumentation. Therefore, the results from this method are best used in conjunction with the impact-echo results. The low and narrow frequency range of the impulse-response method makes it well suited for implementation into a rolling system. Experimental testing has demonstrated the ability to receive energy in the frequency range of 10 to 1000 Hz through a wheel with minimal energy loss or distortion. Furthermore, experimental testing has demonstrated the ability to generate consistent results from individual impacts of the source, even on rough pavements.

8.3 RECOMMENDATIONS

The problem of developing a rolling stress-wave based testing system is difficult due to the necessity of consistently generating and receiving high-frequency energy "on the fly". The results from these experimental tests have demonstrated the difficulties of receiving energy using a wheel mounted receiver. The following recommendations are made concerning future research of this problem.

1. The use of wheel mounted receivers appears to be an inadequate solution to the problem of receiving high-frequency stress wave energy. The use of piezoelectric ceramic materials was investigated briefly as part of this research as a means of mobile energy reception. More detailed research could be performed to develop a wheel with a piezoelectric rim receiving element. Special attention would need to be paid to the durability of the wheel as well as the factors mentioned in this research, including wheel size, mass, and coupling material.

2. It also appears that the development of a source to generate frequencies in the range from 1 to 20 kHz is necessary. An impacting source is unlikely to yield the consistent results that are desirable for impact-echo testing. Therefore, a wheel mounted source that generates band-limited noise in the pavement is a possible solution. It may be necessary to have several sources that each input energy over a fixed frequency range. The use of piezoelectric ceramics is again a possible solution to this problem.

3. If a sufficient source and receiver could be developed, the system could be used for other means of pavement testing. Spectral-Analysis-of-Surface-Waves (SASW) testing to profile the pavement, for example, could be performed with such a device.

REFERENCES

- 1 Cotton, B. E. (1992), "Development of a Trailer-Mounted System to Delineate Irregularities in Rigid Pavements", Thesis submitted in partial fulfillment of the Master of Science Degree, The University of Texas at Austin.
- 2 Van Daveer, J. R. (1975), "Techniques for Evaluating Reinforced Concrete Bridge Decks," *Proceedings*, Journal of the American Concrete Institute, Vol. 72, No. 12, pp. 697-703.
- 3 Torres, F. and McCullough, B. F. (1983), "Void Detection and Grouting Process", Research Report Number 249-3, Implementation of Rigid Pavement Overlay and Design System, Research Project 3-8-79-249, Center for Transportation Research, The University of Texas at Austin, pp. 33-36.
- 4 Uddin, W., Hudson, W. R., Elkins, G. E., and Reilley, K. T. (1987), "Pavement Condition Monitoring Methods and Equipment: Evaluation of Equipment for Measuring Voids Under Pavements", Report Number FH6713, Prepared by ARE Inc. for the Federal Highway Administration, Austin, Texas, 173 pp.
- 5 Birkoff, J. W. and McCullough, B. F. (1979), "Detection of Voids Underneath Continuously Reinforced Concrete Pavements", Research Report Number 177-18, Development and Implementation of the Design, Construction, and Rehabilitation of Rigid Pavements, Research Project 3-8-75-177, Center for Highway Research, The University of Texas at Austin, 52 pp.
- 6 Cantor, T. R. and Kneeter, C. P. (1977), "Radar and Acoustic Emission Applied to the Study of Bridge Decks, Suspension Cables, and a Masonry Tunnel", Report No. 77-13, Port Authority of New York and New Jersey, 1977, pp. 1-12.
- 7 Ransom, R. C. and Kunz, J. T. (1986), "Nondestructive Detection of Voids Beneath Pavements", *Public Works*, Vol. 117, No. 1, January, pp. 52-54.
- 8 Manning, D. G. and Holt, F. B. (1980), "Detecting Delamination in Concrete Bridge Decks", *Concrete International*, Nov., pp. 34-41.
- 9 Holt, F. B., and Eales, J. W. (1987), "Nondestructive Evaluations of Pavements", *Concrete International: Design and Construction*, Vol. 9, No. 6, June, pp. 41-45.
- 10 Clemena, G. G. (1983), "Nondestructive Inspection of Overlaid Bridge Decks with Ground Penetrating Radar", *Transportation Research Record* 899, pp. 21-32.

- 11 Clemena, G. G., Sprinkel, M. M., and Long, R. R. (1986), "Use of Ground Penetrating Radar for Detecting Voids Underneath a Jointed Concrete Pavement", VHTRC 86-R36, Virginia Highway and Transportation Research Council, Virginia, 39 pp.
- 12 Knorr, R. E., Buba, J. M., and Kogut, G. P. (1983), "Bridge Rehabilitation Programming by Using Infrared Techniques", *Transportation Research Record 899*, pp. 32-34
- 13 Manning, D. G. and Holt, F. B. (1983), "Detecting Deterioration in Asphalt-Covered Bridge Decks", *Transportation Research Record 899*, pp. 10-20.
- 14 Manning, D. G. and Ryell, J. (1981), "Decision Criteria for Rehabilitation of Concrete Bridge Decks", *Transportation Research Record 762*, pp. 1-9.
- 15 Chang, D. W., Kang, Y. V., Roesset, J. M., and Stokoe, K. H., II (1992), "Effect of Depth to Bedrock on Deflection Basins Obtained with Dynaflect and FWD Tests", *Transportation Research Record 1355*, pp. 8-16.
- 16 Bay, J. A., Stokoe, K. H., II, and Jackson, J. (1995), "Development and Preliminary Investigation of a Rolling Dynamic Deflectometer", Presented at 1995 Transportation Research Board, accepted for Publication.
- 17 Le Laboratoire Central des Ponts et Chaussees (1983), "Le Collographe", Bull. Liaison Labo. P. et Ch., No. 126, pp. 77-90.
- 18 Moore, W. M., Swift, G., and Milberger, L. J. (1973), "An Instrument for Detecting Delamination in Concrete Bridge Decks", *Highway Research Record 452*, pp. 44-52.
- 19 Alexander, A. M. and Thornton, H. T., Jr. (1988), "Developments in Ultrasonic Pitch-Catch and Pulse-Echo for Measurements in Concrete", *Nondestructive Testing, SP112-2*, American Concrete Institute, Detroit, pp. 21-40.
- 20 Carino, N. J., Sansalone, M., and Hsu, N. N. (1986), "A Point Source-Point Receiver, Pulse-Echo Technique for Flaw Detection in Concrete", *ACI Journal*, No. 83-20, March-April, pp. 199-208.
- 21 Sansalone, M. and Carino, N. J. (1988), "Laboratory and Field Studies of the Impact-Echo Method for Flaw Detection in Concrete", *Nondestructive Testing, SP 112-1*, American Concrete Institute, Detroit, pp. 1-20.

- 22 Sansalone, M. and Carino, N. J. (1989), "Detecting Delaminations in Concrete Slabs with and without Overlays using the Impact-Echo Method", *ACI Materials Journal*, Vol. 86, No. 2, March-April, pp. 175-184.
- 23 Sansalone, M. and Carino, N. J. (1988), "Impact-Echo Method: Detecting Honeycombing, the Depth of Surface-Opening Cracks, and Ungrounded Ducts", *Concrete International: Design and Construction*, Vol. 10, No. 4, April, pp. 38-46.
- 24 Olson, L. D., Wright, C., and Stokoe, K. H., II (1990), "Strides in Nondestructive Testing", *Civil Engineering*, May.
- 25 Peterson, C. M. and Senkowski, L. J. (1985), "Slab Stabilization of PCC Pavements", Report from Research and Development Division of Oklahoma Department of Transportation, August.
- 26 Olson, L. D., and Wright, C. (1990) "Nondestructive Testing for Repair and Rehabilitation", *Concrete International: Design and Construction*, ACI, March, pp. 58-64.
- 27 Aouad, M. F. (1993), "Evaluation of Flexible Pavements and Subgrades using the Spectral-Analysis-of-Surface-Waves Method", Dissertation submitted in partial fulfillment of the Doctor of Philosophy Degree, The University of Texas at Austin.
- 28 Stokoe, K. H., II, Nazarian, S., Rix, G. J., Sanchez-Salinerro, I., Sheu, J. C., and Mok, Y. J. (1988), "In-Situ Seismic Testing of Hard-to-Sample Soils by Surface Wave Method", *Proceedings*, American Society of Civil Engineers, Specialty Conference on Earthquake Engineering and Soil Dynamics II - Recent Advances in Ground Motion Evaluation, Park City, Utah, June.
- 29 Rix, G. J., Bay, J. A., and Stokoe, K. H., II (1990), "Assessing In-Situ Stiffness of Curing Portland Cement Concrete with Seismic Tests," *Transportation Research Record 1022*, Washington, D.C., pp. 7-16.
- 30 Kalinski, M. E. (1994), "Measurement of Intact and Cracked Concrete Structural Elements by the SASW Method", Thesis submitted in partial fulfillment of the Master of Science Degree, The University of Texas at Austin.
- 31 Proctor, T. M., Jr. (1982), "Some Details on the NBS Conical Transducer", *Journal of Acoustic Emission*, Vol. 1, No. 3, pp. 173-178.

- 32 White, R., Hudson, R. W., Meyer, A. H., and Stokoe, K. H., II (1984), "Design and Construction of a Rigid Pavement Research Facility", Research Report 355-1, Construction of a Multipurpose Rigid Pavement Research Facility, Research Project 3-8-83-355, Center for Transportation Research, Bureau of Engineering Research, University of Texas, Austin, Texas, 108 pp.
- 33 Chiang, C. C. (1994), "Effects of Irregularities on the Dynamic Response of Pavements in Non-Destructive Testing", Dissertation submitted in partial fulfillment of the Doctor of Philosophy Degree, The University of Texas at Austin.
- 34 Pratt, D. and Sansalone, M. (1992), "Impact-Echo Signal Interpretation Using Artificial Intelligence", ACI Materials Journal, Vol. 89, No. 2, March-April, pp. 178-187.
- 35 Masliwec, T. (1990), "Optimizing Infrared Detection for Bridge Deck Deterioration", ME-88-10, Ontario Ministry of Transportation, Research and Development Branch, Downsview, Ontario, 58 pp.
- 36 Uddin, W., Torres-Verdin, V., Hudson, R. W., Meyer, A. H., and McCullough, F. B. (1983), "Dynalect Testing for Rigid Pavement Evaluation", Research Report Number 256-6F, The Study of New Technologies for Pavement Evaluation, Research Project 3-8-80-256, Center for Transportation Research, Bureau of Engineering Research, The University of Texas at Austin, 102 pp.
- 37 Sansalone, M., Carino, N. J., and Hsu, N. N. (1987), "A Finite Element Study of Transient Wave Propagation in Plates", Journal of Research of the National Bureau of Standards, Vol. 92, No. 4, July-August.